AREA QUALITÀ,
PROGRAMMAZIONE E
SUPPORTO STRATEGICO
SETTORE STRATEGIA PER LA
RICERCA
U. O. DOTTORATI

Dottorato di Ricerca in:
SISTEMI AGRO-ALIMENTARI E FORESTALI MEDITERRANEI
Dipartimento di Scienze Agrarie, Alimentari e Forestali
Settore Scientifico Disciplinare – AGR-04/A Idraulica agraria e sistemazioni idraulico-forestali

HYDRAULIC CHARACTERIZATION OF SOILS AND MODELLING OF WATER REQUIREMENTS OF A MANDARIN ORCHARD

LA DOTTORESSA
MARIACHIARA FUSCO

IL COORDINATORE
PROF. VINCENZO BAGARELLO

IL TUTOR
PROF. VINCENZO BAGARELLO

CO TUTOR
DOTT. VINCENZO ALAGNA

CICLO XXXVII-INPS
ANNO 2026

TABLE OF CONTENTS

CHAPTER 1: General Introduction

I. Definition of the Problems

Globally, there is a delicate balance between increasing food production to support a growing population and safeguarding natural resources, including soil and water. Agricultural systems are approaching critical thresholds, constrained by intensive farming, climate variability, and competition for limited resources (FAO, 2021).

Agriculture accounts for approximately 70% of global freshwater withdrawals (IPCC, 2022), making it both a leading cause of water scarcity and land degradation, and one of the sectors most severely affected by these issues. These challenges are particularly acute in Mediterranean regions, where semi-arid climates, unpredictable rainfall patterns, and frequent droughts severely constrain both crop productivity and water availability. Under these conditions, irrigation becomes essential, especially for water-demanding species like citrus, making effective water management crucial for both conservation and agricultural productivity (Fereres & Soriano, 2007).

Citrus is a key economic crop in Mediterranean environments, representing both the potential and the challenges of agriculture in water-scarce regions. Widely distributed across Mediterranean-climate areas (Spain, Italy, Greece, Turkey, Egypt, and Morocco), these orchards characterize extensive landscapes, significantly contributing to the identity and economy of many regions, particularly within the European Union (Schimmenti et al., 2013; Duru et al., 2022).

However, as one of the most widely cultivated and water-intensive crops, its substantial water footprint has spurred growing interest in optimizing irrigation to improve water-use efficiency and sustain profitability (Provenzano et al., 2013; Rallo et al., 2017). Addressing these issues requires developing resilient agricultural systems that can withstand climate change while ensuring food security, especially in water-limited regions (Kumari et al., 2025).

Enhancing water productivity is therefore a central goal, which entails not only technological upgrades but also a systemic shift in agronomic planning. Achieving this objective, reconciling citrus productivity with water resource conservation, requires an integrated scientific approach that combines innovations in precision agriculture, remote sensing, real-time monitoring of the Soil-Plant-Atmosphere continuum (SPAc), and agro-hydrological models within Decision Support Systems (DSS). Their effective implementation in the field, however, depends on intuitive design, the ability to adapt to local contexts, and the active farmer engagement (Ara et al., 2021). Only a holistic understanding of these interdependent elements, grounded in in-depth studies of soil hydraulic characterization and continuous SPAc monitoring, can provide the knowledge base for precision irrigation strategies capable of maximizing water-use efficiency.

Central to developing effective solutions is obtaining accurate knowledge of soil hydrostatic and hydrodynamic properties. These proprieties are essential for agronomic, engineering, and environmental projects that address drought risks under evolving climatic conditions. Models of saturated and unsaturated flow rely on reliable data for soil water retention *θ(h)* and hydraulic conductivity *K(h)*. These properties govern water transport and storage mechanisms within the SPAc and are particularly critical in water-scarce regions such as the Mediterranean, where they support optimized irrigation strategies that reduce non-productive water losses while maintaining crop yields. As climate change intensifies weather extremes, soil hydraulic properties become key indicators of drought resilience and flood mitigation capacity. They serve as essential inputs for the precision agriculture technologies and decision support systems needed to achieve sustainable intensification, allowing for data-driven irrigation management that minimizes water waste and energy use. Furthermore, monitoring these properties helps to contain land degradation by identifying compacted or salinized soils needing remediation.

In fact, soil hydraulic properties determine the efficiency of water exchanges and directly influence critical processes such as infiltration, water redistribution through the soil profile, drainage, and water availability for crops. In particular, the hydraulic conductivity function *K(θ)*or *K(h)*, describing how the soil's water transmission capacity changes with water content, provides the conceptual basis for modeling water flow under both saturated and unsaturated conditions, thus representing a unifying element for understanding water dynamics in the soil porous system.

Within this framework, saturated hydraulic conductivity (K_s) emerges as a specific yet highly significant parameter of the more general *K(θ)* function, corresponding to the maximum conductivity value achieved when all pores are water-filled. While *K(θ)* describes the soil's hydraulic behaviour across the entire moisture range, K_s represents a limiting condition of practical relevance for various applications, including irrigation design, runoff prediction, water dynamics modelling, and solute transport simulation.

The determination of K_s can be carried out through infiltrometer tests conducted either in the field or in the laboratory, each with its specific advantages and limitations. Field measurements enable the direct assessment of K_s in situ, preserving the soil’s natural structure, which remains connected to the surrounding mass and incorporates real environmental conditions, such as the presence of macropores, surface crusts, and existing moisture (Bouma, 1983; Beven & Germann, 1982; Bagarello et al., 2004; Bagarello & David, 2020). These undisturbed conditions are particularly valuable for studying macropore flow dynamics, landscape hydrology, and in situ soil behaviour. Moreover, even carefully collected undisturbed samples may experience structural changes during extraction, potentially altering pore space geometry and bulk density, particularly with certain coring methods

(Spliethoff et al., 2020; Carr et al., 2020). Field methods are essential for farm-scale assessments and hydrological model calibration, though they require extensive replication due to natural spatial variability and present logistical challenges in standardization, especially in heterogeneous soils (Nielsen et al., 1973; Amoozegar & Warrick, 1986; Nimmo et al., 2009; Zhang et al., 2020).

Laboratory-based testing provides a critical advantage by enabling precise control over experimental variables, including temperature, hydraulic gradients, and sample dimensions, while effectively minimizing external sources of variability (Klute, 1965; Rodríguez-Juárez et al., 2018). This high degree of control ensures exceptional repeatability and standardization, making laboratory methods indispensable for isolating and analyzing specific factors under consistent and reproducible conditions. Such controlled environments are particularly valuable for evaluating the impacts of soil amendments (e.g., organic matter, compost, or biochar) on hydraulic properties (Bondì et al., 2024; Castellini et al., 2025), validating theoretical models (Reynolds & Elrick, 1987), or establishing quantitative relationships between saturated (K_s) or near-saturated (K) hydraulic conductivity and the bulk soil physical properties (Assouline, 2006). By eliminating field-scale heterogeneity, laboratory testing allows researchers to establish clear cause-effect relationships, refine predictive models, and develop standardized guidelines for soil management practices.

However, laboratory determinations are not without limitations that can significantly affect the accuracy and representativeness of results compared to real soil conditions. A critical aspect concerns the alteration of the soil's natural structure during sample preparation: operations such as sieving or compaction modify macropore continuity, leading to K_s values potentially different from in situ conditions (Reynolds et al., 2002). Furthermore, sample history plays a fundamental role, as repeated wetting-drying cycles or reuse of the same sample can progressively alter its texture and porosity, resulting in systematic variations in K_s (Bagarello et al., 2024). Furthermore, the small volume of soil typically used in laboratory tests may fail to capture the spatial heterogeneity and structural complexity of the field, thereby limiting the scalability of the results to the agronomic level (Almeida et al., 2024).

The choice of the most appropriate methodology for determining K_s and K, therefore, depends on variables such as the scale of the investigation, soil characteristics, and the study's objectives. In many practical contexts, integrating both field and laboratory measurements have proven to be the most effective strategy to obtain reliable and representative estimates of K_s and K (Reynolds et al., 2000). For this reason, the critical comparison of different K_s and K estimation techniques remains a central topic in soil hydrological research.

Accurate determination of saturated soil hydraulic conductivity is essential for designing efficient irrigation systems that ensure uniform water distribution while minimizing water and nutrient losses due to leaching (Bagarello et al., 2014; Basile et al., 2020). This is particularly relevant in Mediterranean environments, where localized irrigation systems, such as drip and subsurface drip irrigation, are increasingly adopted due to their high water-use efficiency. These systems deliver water directly to the root zone, significantly reducing evaporation and runoff losses.

However, the use of efficient irrigation systems alone is insufficient to guarantee significant water savings; they must be combined with advanced strategies such as deficit irrigation, which intentionally supplies less water than the crop's full evapotranspiration demand.

Advanced irrigation strategies, such as deficit irrigation (DI), partial root-zone drying (PRD), and regulated deficit irrigation (RDI), when combined with surface or subsurface drip systems, offer strong potential for improving water productivity in citrus cultivation. The key lies in strategically applying water deficits during phenological stages with lower stress sensitivity, such as pit hardening and fruit maturation. Although deficit irrigation can result in slight yield reductions, research indicates that it substantially improves water productivity, making it a viable strategy for sustainable water management in agriculture (Yetik and Candoğan, 2022). Several research evidence underscores this potential: in Navelina oranges, DI increased water productivity by 24% while reducing water use by over 30%, provided the deficit was carefully aligned with the crop's phenological stages (García-Tejero et al., 2010); in Nagpur mandarin, a 50% irrigation reduction led to a 75% increase in water productivity (Panigrahi, 2023); and in Washington Navel oranges, a PRD-50% strategy applied during fruit maturation increased water productivity by 26.5% without compromising yield or fruit quality (Belkher et al., 2025). These findings unequivocally demonstrate that the effectiveness of irrigation strategies is determined not only by the severity of water stress, but crucially by its timing within the crop's phenological cycle (García-Tejero et al., 2010).

The implementation of deficit irrigation strategies requires comprehensive understanding of the SPAc to prevent water deficit from compromising crop productivity. Continuous monitoring of SPAc is indispensable for effectively guiding these strategies, enabling precise assessment of plant water status and atmospheric demand, and allowing stress application during less critical phenological stages.

Puig-Sirera et al. (2021) highlight the importance of monitoring the SPAc system to establish accurate thresholds of allowable soil water depletion. This research is critical because it is ultimately unfeasible for every individual farmer to possess specialized knowledge, resources, and equipment for such comprehensive monitoring. Instead, the role of research is to translate these complex data into simple, actionable guidelines, such as specific soil moisture thresholds or crop water stress indicators, that can be easily adopted using affordable technology.

By simultaneously measuring soil moisture, plant water status, and atmospheric conditions at a research level, it becomes possible to determine and validate optimal irrigation timing based on specific crop physiological needs and growth stages. This data-driven approach provides the scientific basis for developing precise irrigation management protocols, maximizing water use efficiency by reducing waste while maintaining yield and quality.

Monitoring the SPAc involves a range of techniques to assess water status across all components of the continuum, with increasing complexity depending on the level of precision required.

Soil water status can be measured using direct or indirect methods. The gravimetric method, considered the gold standard for determining soil water content, provides accurate measurements by weighing the sample before and after drying, but it is destructive, labor-intensive, and unsuitable for continuous monitoring. To overcome these limitations, indirect methods are used that measure physical properties correlated with the soil moisture, such as Time Domain Reflectometry (TDR) and Frequency Domain Reflectometry (FDR), which allow estimation of volumetric water content with high temporal resolution (Ferré and Topp, 2002).

The evapotranspiration component of the SPAc system can be characterized using both direct and indirect methods. Among direct methods, the weighing lysimeter is the most widely used to measure actual crop evapotranspiration (ETc) by detecting weight changes of an isolated soil-plant volume (Anapalli et al., 2016; Fenner et al., 2019). Indirect methods estimate reference evapotranspiration (ETo) from climatic data recorded by automatic weather stations, applying empirical equations such as the FAO Penman-Monteith (FAO-56 model).

Although estimates of soil moisture and atmospheric demand provide essential information for irrigation scheduling, the application of deficit irrigation strategies requires precise knowledge of the plant's water status. Plant-based indicators treat the plant as an integrated biosensor reflecting soil water status, atmospheric demand, and dynamic physiological responses to water stress (Fernández, 2017). Therefore, accurate monitoring of plant water status and defining specific thresholds for each phenological phase are essential for implementing controlled water stress strategies that optimize water use efficiency without compromising crop productivity.

The plant water potential represents the standard measurement of plant water status, and its determination is performed using a Scholander pressure chamber. Although this technique is well-established, it does not allow for continuous monitoring and is subject to operator-related variability, such as sample selection and measurement reading. Continuous monitoring of plant water status can be achieved using advanced technologies that overcome the limitations of traditional point measurements (Chai et al., 2021; Carella et al., 2024). Among these, the sap flow technique enables the estimation of transpiration flow, providing valuable physiological data for optimizing irrigation management. The collected data allow for real-time assessment of the plant's physiological response to environmental conditions (Steppe et al., 2008; Fernández, 2017). Recent studies have confirmed its reliability under field conditions, especially when integrated with other sensors such as microtensiometers and weather stations (Villalobos et al., 2024; Blanco & Kalcsits, 2024).

The introduction of microtensiometers, such as FloraPulse sensors, has enabled continuous measurement of plant water potential directly from the trunk or branches, providing highly accurate data. These devices have so far been used mainly on woody crops like apples, grapevines, and almonds under both experimental and field conditions (Lakso, 2019; 2022). In pear (Blanco and Kalcsits, 2021), daily fluctuations in trunk water potential recorded by microtensiometers showed strong correlations with stem water potential measured by the Scholander chamber, confirming their reliability. Further validation was provided by Conesa et al. (2023), who demonstrated the effectiveness of trunk water potential as a robust, continuous plant-based indicator of water status in drip-irrigated nectarine trees.

Despite these positive results, the use of microtensiometers under field conditions has not yet been adequately tested in citrus crops. The physiological and phenological specificities of citrus require dedicated studies to define water stress thresholds and optimal operational parameters (Jamshidi et al., 2021). This lack of experimental evidence represents a major limitation to the widespread adoption of such technologies in the citrus sector, constraining the development of sustainable irrigation strategies based on direct plant-based measurement.

Therefore, further field experiments integrating deficit irrigation strategies with real-time monitoring using microtensiometers in citrus orchards need to be promoted. These studies should aim to assess the productive, qualitative, and physiological responses of citrus to different irrigation regimes. Robust scientific validation will be essential to support the development and implementation of precise and sustainable irrigation management systems, capable of improving water productivity in citrus cultivation while addressing the growing challenges of water scarcity and climate change.

The integration of soil hydraulic characterization and continuous monitoring of soil and plant water status provides a robust empirical basis for estimating crop water requirements. Such monitoring is essential for the scientific development of agro-hydrological models, enabling their calibration, validation, and eventual transformation into reliable operational tools for farmers. However, large-scale implementation of these monitoring systems can be limited by practical and economic constraints. Plant-based sensors are often fragile and require annual replacement, while the installation and maintenance of complete sensor networks demand technical expertise and financial resources. These limitations are particularly relevant for small and medium-sized farms, which may lack the capacity to sustain complex infrastructures.

In this context, agro-hydrological models offer a strategic complement; once properly calibrated with empirical data, they can accurately simulate the SPAc, support irrigation management, and optimize water use efficiency. Models such as FAO-56, AquaCrop, and SIMDualKc integrate real-time soil and climate data, crop-specific parameters, and meteorological forecasts to provide actionable irrigation schedules while minimizing water losses as demonstrated by several authors.

For example, Heng et al. (2009) evaluated the performance of the AquaCrop model for maize using data from three studies conducted under diverse environmental conditions. Rallo et al. (2017) successfully validated the performance of the FAO-56 model in identifying the temporal dynamics of soil and crop water status in citrus orchards under different irrigation strategies, demonstrating its utility for precision water management. Ramos et al. (2023) conducted a comprehensive evaluation of the SIMDualKc model's performance in estimating crop evapotranspiration across nine commercial Mediterranean orchards (almonds, olives, citrus, and pomegranates). However, many of these models rely on the theoretical "big leaf" approximation, which represents the entire vegetation canopy as a single homogeneous leaf surface. This simplification introduces limitations when applied to sparse crops such as citrus, where discontinuous canopy coverage, non-uniform root distribution and variable soil evaporation contribute to spatially diverse microclimatic and hydrological conditions (Friend, 2001; Knauer et al., 2018; Bonan et al., 2021).

The limitations of traditional models become particularly evident under localized irrigation conditions, where complex soil moisture patterns develop and wet and dry zones often coexist within the same root system. This spatial heterogeneity, combined with the non-uniform water distribution typical of localized irrigation systems, makes the application of models designed for continuous vegetation cover and uniform irrigation particularly challenging. Beyond these specific issues, existing agro-hydrological models present additional limitations, including substantial input data requirements that can limit their operational implementation, complex parameterization procedures requiring specialized expertise, and insufficient validation across diverse pedoclimatic conditions and management scenarios (Paredes et al., 2017; Sandhu and Irmak, 2019; Er-Raki et al., 2021). These constraints particularly affect model transferability and may introduce uncertainties in water flux simulations.

To overcome these limitations, AquaCitrus (Boubakri et al., 2023) has been recently introduced as an innovative agro-hydrological model specifically developed for citrus irrigation. This model represents a significant advancement by integrating novel features that directly address the challenges posed by localized irrigation in sparse crops. The structure of AquaCitrus incorporates key innovations such as separate estimation of plant transpiration and soil evaporation, a dual soil module that accurately reproduces the heterogeneous moisture patterns characteristic of localized irrigation, and the integration of citrus-specific physiological traits. Designed for practical use, AquaCitrus requires minimal input data, adapts to the non-uniform canopy and root conditions typical of citrus plantations, and features a user-friendly interface, making it an effective tool for sustainable irrigation management under real-world conditions. Unlike traditional models based on the big leaf approximation, AquaCitrus offers a targeted approach that accounts for vegetation canopy discontinuity and non-uniform water distribution in the soil. By bridging advanced scientific modelling with on-farm decision-making, it enhances water productivity and supports precision irrigation in Mediterranean citrus orchards. Its implementation represents the final phase of comprehensive approaches that combine detailed soil hydraulic characterization and continuous plant monitoring water status, within a Decision Support System framework for precision agricultural. However, it should be noted that AquaCitrus has not yet been tested for subsurface drip irrigation systems, and its performance under such conditions remains to be evaluated.

II. Thesis Objectives

Sustainable water management in Mediterranean agriculture is a crucial challenge due to water scarcity and climate variability. To increase irrigation efficiency and water productivity, it is essential to integrate precision agriculture technologies, real-time monitoring systems of the SPAc, and agro-hydrological models calibrated with accurate data on soil hydraulic properties. The general objective of this PhD thesis was to investigate the hydraulic characterization of soils and to model the water requirements of a mandarin orchard, pursued through the following research lines:

1. Comparative analysis of laboratory and field methods for estimating the hydrodynamic properties of the sandy loam soil that supports the mandarin orchard in Villabate.
2. Evaluation of methodologies for determining saturated hydraulic conductivity (K_s), comparing the classical single ring infiltrometer method (PI, Pressure Infiltrometer) with the automated SATURO technique.
3. Assessment of the performance of FloraPulse microtensiometers for continuous monitoring of plant water potential in the experimental mandarin orchard of Villabate under varying irrigation regimes.
4. Preliminary application of the AquaCitrus agro-hydrological model to simulate soil water content dynamics in the Villabate experimental mandarin orchard under subsurface drip irrigation.

The hydraulic characterization of soil in a laboratory, for instance to test the hydrological effectiveness of an amendment, often requires the preparation of repacked soil samples to ensure controlled and reproducible experimental conditions. The preparation procedures themselves, including compaction methods and soil handling techniques, can introduce significant artefacts, altering the physical and hydraulic properties intended to be measured. This methodological variability represents a critical source of uncertainty, potentially compromising the reliability and comparability of the obtained data, especially for fundamental parameters such as saturated hydraulic conductivity. However, to the best of my knowledge, the available literature does not address these issues; therefore, to quantify and standardize these procedures, an appendix of the thesis was focused on two further complementary objectives:

- Measurement of saturated hydraulic conductivity on sieved and compacted soil samples, including the design, implementation, and testing of a new soil compaction apparatus (Soil Compaction Apparatus - SCA).
- Investigation of how different preparation procedures for soil columns, such as sieving duration and the scraping of surfaces between layers, influence the measurement of saturated hydraulic conductivity using the Simplified Falling Head (SFH) technique (Bagarello et al., 2004).

III. Structure of the thesis

This thesis is organized into three interconnected parts, each representing a fundamental pillar of the research journey undertaken during these years of PhD study. Each part begins with a general paragraph reviewing the state of the art in its respective field, providing the necessary theoretical foundation and scientific context for the experimental work that follows. The work progresses from methodological advancements in soil characterization to real-time field monitoring and culminates in the application of agro-hydrological models for irrigation optimization in citrus orchards.

Chapter 2 focuses on determining soil hydrodynamic properties through both laboratory and field methods. A description is initially presented for several techniques adopted (chapter **2.1**), including:

- Constant-head permeameter (CHP)
- Mini Disk Infiltrometer (MDI)
- Beerkan Estimation of Soil Transfer Parameters (BEST)
- Pressure Infiltrometer (PI)
- SATURO Infiltrometer (SATURO)

The first manuscript, *"Comparing mini-disk infiltrometer, BEST method and soil core estimates of hydraulic conductivity of a sandy-loam soil"* (chapter **2.2**), published in Soil & Tillage Research

(2024), compares K_s and K, obtained by comparing field measurements, using the BEST method and the unconfined mini-disk infiltrometer, with laboratory measurements carried out using the confined mini-disk infiltrometer and the constant-head permeameter (CHP).

The second manuscript *"Comparison of the single-ring pressure infiltrometer and SATURO methods for determination of field-saturated soil hydraulic conductivity*" (chapter **2.3**) published in Vadose Zone Journal (2025), compares the classical pressure infiltrometer method and the automated SATURO device for measuring K_s.

Chapter 3 focuses on monitoring the Soil-Plant-Atmosphere system. The first manuscript, *"The open-Lab vision of Prof. Provenzano at the Villabate site: integration of novel technologies for sensor-driven irrigation management"* (chapter **3.1**), published in Quaderni di Idronomia Montana (2024) reports the methodological and experimental approach adopted by Professor Provenzano, highlighting how the integration of new technologies and management strategies can serve as a replicable model to improve irrigation efficiency in agricultural contexts characterized by limited water availability.

The subsequent sections then detail the specific monitoring methodologies developed for this site (**3.2**): reference evapotranspiration (chapter **3.2.1**), soil water status (chapter **3.2.2**), and plant water status (chapter **3.2.3**). It provides a real-time, holistic view of water dynamics in the mandarin orchard. The application of this integrated monitoring framework and its comprehensive results are presented in chapter **3.3**. Finally, the second manuscript, *"Assessing microtensiometers for monitoring stem water potential in mandarin (Citrus reticulata Blanco) orchard under different irrigation regimes* (chapter **3.4**)*"*, was published in Agriculture Water Management in 2025. This paper assessed the effectiveness of FloraPulse microtensiometers as a viable alternative to the traditional Scholander pressure chamber for continuous monitoring of stem water potential in a mandarin orchard, considering two different irrigation regimes: a high-frequency irrigation regime using a subsurface drip irrigation (SDI) system, and a low-frequency regime employing a micro-sprinkler (SPR) system.

Chapter 4 analyzes agro-hydrological models, including the FAO-56 (chapter **4.1**) and AquaCitrus (chapter **4.2**) models, emphasizing the inherent limitations of the conventional approach and the key innovations proposed by the new model to address them. Chapter **4.3** describes the parameterization of both models using field-derived soil hydrological properties, meteorological data, and irrigation records from the Villabate experimental site. Chapter **4.4** presents the statistical indicators (RMSE, Bias, PBias, NSE, R^2) adopted for model performance evaluation. Finally, Chapter **4.5** presents preliminary findings from the application of the AquaCitrus model for irrigation management in Mediterranean citrus orchards under subsurface drip irrigation system, focusing on its performance in simulating soil water status and providing a comparison with the FAO-56 model.

Chapter 5 presents the main conclusions of the thesis, integrating the findings from soil hydraulic characterization, SPAc monitoring, and agro-hydrological modelling. The chapter also discusses limitations and future perspectives.

Appendix A examines the impact of repacked soil column preparation methods on soil hydraulic properties, with a particular focus on saturated hydraulic conductivity. Appendix **A.1** describes the Simplified Falling-Head Technique (SFH), which is the measurement method adopted in both experimental studies presented in the following sections (**A.2** and **A.3**). The manuscript "*Investigating Soil Compaction and Its Impact on Physical and Hydraulic Properties Using a Simple Testing Apparatus*" (appendix **A.2**), published in Water (2025), analyzed the effect of controlled mechanical compaction, using a soil compaction apparatus (SCA), to assess the impact of compaction energy on the K_s across three soil types. The manuscript "*Determining saturated hydraulic conductivity of a repacked loam soil by the simplified falling-head technique: Impact of sieving duration and scraping of exposed surfaces*" (appendix **A.3**), published in Soil & Water Research (2024) examines the effect of sieving duration and surface scraping between compacted layers, highlighting how these practices influence hydraulic conductivity.

Together, these studies aim to provide optimized and validated laboratory protocols, contributing to improved accuracy and reliability in the soil hydraulic characterization for subsequent applications in agro-hydrological modeling. In the final chapter, the main conclusions of the thesis are summarized.

REFERENCES

Almeida, B., da Silva Santos, E. M., Freire, F. J., Duarte Guedes Cabral de Almeida, C., dos Santos Silva, T. H., Telles Lima, A. L., & Anunciato Mota, J. C., 2024. Validation of Double Constant and Falling Head Permeameter for Determination of Hydraulic Conductivity of Soils in the Laboratory. Revista Brasileira De Geografia Física, 17(6), 4744–4760.

Amoozegar, A., & Warrick, A. W., 1986. Hydraulic conductivity of saturated soils: field methods. Methods of Soil Analysis: Part 1 Physical and Mineralogical Methods, 5, 735-770.

Anapalli, S. S., Ahuja, L. R., Gowda, P. H., Ma, L., Marek, G., Evett, S. R., & Howell, T. A., 2016. Simulation of crop evapotranspiration and crop coefficients with data in weighing lysimeters. Agricultural Water Management, 177, 274-283.

Ara, I., Turner, L., Harrison, M. T., Monjardino, M., DeVoil, P., & Rodriguez, D., 2021. Application, adoption and opportunities for improving decision support systems in irrigated agriculture: A review. Agricultural Water Management, 257, 107161.

Bagarello, V., & David, S. M., 2020. Run duration effects on the hydrodynamic properties of a loam soil estimated by steady-state infiltration methods. Journal of Agricultural Engineering, 51(4), 229-238.

Bagarello, V., Baiamonte, G., Castellini, M., Di Prima, S., & Iovino, M., 2014. A comparison between the single ring pressure infiltrometer and simplified falling head techniques. Hydrological Processes, 28(18), 4843-4853.

Bagarello, V., Caltabellotta, G., & Iovino, M., 2024. Soil reuse effects on determination of saturated hydraulic conductivity of different loamy soils. European Journal of Soil Science, 75(1), e13454.

Bagarello, V., Iovino, M., & Elrick, D., 2004. A simplified falling-head technique for rapid determination of field-saturated hydraulic conductivity. Soil Science Society of America Journal, 68(1), 66-73.

Basile, A., Albrizio, R., Autovino, D., Bonfante, A., De Mascellis, R., Terribile, F., & Giorio, P., 2020. A modelling approach to discriminate contributions of soil hydrological properties and slope gradient to water stress in Mediterranean vineyards. Agricultural Water Management, 241, 106338.

Belkher, S., Latrech, B., Rezig, M., Bouhlal, R., Bekri, W., Markwordt, F., ... & Ben Abdallah, M. A., 2025. Effects of partial root-zone drying and deficit irrigation on yield, quality and water productivity of Washington Naval orange. Journal of Ecological Engineering, 26(6).

Beven, K., & Germann, P., 1982. Macropores and water flow in soils. Water resources research, 18(5), 1311-1325.

Blanco, V., & Kalcsits, L., 2021. Microtensiometers accurately measure stem water potential in woody perennials. Plants, 10(12), 2780.

Blanco, V., & Kalcsits, L., 2024. Relating microtensiometer-based trunk water potential with sap flow, canopy temperature, and trunk and fruit diameter variations for irrigated 'Honeycrisp'apple. Frontiers in Plant Science, 15, 1393028.

Bondì, C., Castellini, M., Iovino, M., 2024. Temporal variability of physical quality of a sandy loam soil amended with compost. Biologia. https://doi.org/10.1007/s11756-024-01637-1

Bonan, G. B., Patton, E. G., Finnigan, J. J., Baldocchi, D. D., & Harman, I. N., 2021. Moving beyond the incorrect but useful paradigm: reevaluating big-leaf and multilayer plant canopies to model biosphere-atmosphere fluxes–a review. *Agricultural and Forest Meteorology*, *306*, 108435.

Boubakri, N., Garcia-Prats, A., & Pulido-Velázquez, M., 2023. AquaCitrus: Soil water balance model for irrigation management in citrus orchards. In EGU General Assembly Conference Abstracts (pp. EGU-13408).

Bouma, J., 1983. Use of soil survey data to select measurement techniques for hydraulic conductivity. Agricultural Water Management, 6(2-3), 177-190.

Carella, A., Bulacio Fischer, P. T., Massenti, R., & Lo Bianco, R., 2024. Continuous plant-based and remote sensing for determination of fruit tree water status. Horticulturae, 10(5), 516.

Carr, S. J., Diggens, L. M., & Spencer, K. L., 2020. There is no such thing as ‘undisturbed’soil and sediment sampling: sampler-induced deformation of salt marsh sediments revealed by 3D X-ray computed tomography. Journal of Soils and Sediments, 20(7), 2960-2976.

Castellini, M., Bondì, C., Leogrande, R., Giglio, L., Vitti, C., Mastrangelo, M., Bagarello, V., 2025. Evaluating the Effects of Compost, Vermicompost, and Biochar on Physical Quality of Sandy-Loam Soils. Applied Sciences 15, 3392. Chai, Y., Chen, C., Luo, X., Zhan, S., Kim, J., Luo, J., ... & Liu, X., 2021. Cohabiting plant-wearable sensor in situ monitors water transport in plant. Advanced Science, 8(10), 2003642.

Clarke Topp, G., & Ferré, P. A., 2002. 3.1 Water Content. Methods of soil analysis: part 4 physical methods, 5, 417-545.

Conesa, M. R., Conejero, W., Vera, J., & Ruiz-Sánchez, M. C., 2023. Assessment of trunk microtensiometer as a novel biosensor to continuously monitor plant water status in nectarine trees. Frontiers in Plant Science, 14, 1123045.

Duru, S., Hayran, S., & Gül, A., 2022. The analysis of competitiveness of Mediterranean countries in the world citrus trade. *Mediterranean Agricultural Sciences*, *35*(1), 21-26.

Er-Raki, S., Bouras, E., Rodriguez, J. C., Watts, C. J., Lizarraga-Celaya, C., & Chehbouni, A., 2021. Parameterization of the AquaCrop model for simulating table grapes growth and water productivity in an arid region of Mexico. Agricultural Water Management, 245, 106585.

FAO., 2021. The state of the world’s land and water resources for food and agriculture – Systems at breaking point. Synthesis report 2021. Rome.

Faybishenko, B., 1997. Comparison of laboratory and field methods for determining the quasi-saturated hydraulic conductivity of soils.

Fenner, W., Dallacort, R., Faria, C. A., Freitas, P. S. D., Queiroz, T. M. D., & Santi, A., 2019. Development, calibration and validation of weighing lysimeters for measurement of evapotranspiration of crops. Revista Brasileira de Engenharia Agrícola e Ambiental, 23(4), 297-302.

Fereres, E., Soriano, M.A., 2006. Deficit irrigation for reducing agricultural water use. J. Exp. Bot. 58, 147–159. https://doi.org/10.1093/jxb/erl165

Fernández, J. E., 2017. Plant-based methods for irrigation scheduling of woody crops. Horticulturae, 3(2), 35.

Ferré, P. A., & Topp, G. C., 2002. Time domain reflectometry. Methods of soil analysis. Part, 4, 434-445.

Friend, A. D., 2001. Modelling canopy CO2 fluxes: are ‘big-leaf ’simplifications justified? *Global Ecology and Biogeography*, *10*(6), 603-619.

García-Tejero, I., Romero-Vicente, R., Jiménez-Bocanegra, J. A., Martínez-García, G., Durán-Zuazo, V. H., & Muriel-Fernández, J. L., 2010. Response of citrus trees to deficit irrigation during different phenological periods in relation to yield, fruit quality, and water productivity. Agricultural Water Management, 97(5), 689-699.

Heng, L. K., Hsiao, T., Evett, S., Howell, T., & Steduto, P., 2009. Validating the FAO AquaCrop model for irrigated and water deficient field maize. Agronomy journal, 101(3), 488-498.

IPCC, 2022. IPCC, 2022: Climate Change 2022: Impacts, Adaptation, and Vulnerability. Contribution of Working Group II to the Sixth Assessment Report of the Intergovernmental Panel on Climate Change. Cambridge, UK and New York, NY, USA.

Jamshidi, S., Zand-Parsa, S., & Niyogi, D., 2021. Physiological responses of orange trees subject to regulated deficit irrigation and partial root drying. Irrigation Science, 39(4), 441-455.

Klute, A., 1965. Laboratory measurement of hydraulic conductivity of saturated soil. Methods of Soil Analysis: Part 1 Physical and Mineralogical Properties, Including Statistics of Measurement and Sampling, 9, 210-221.

Knauer, J., El-Madany, T. S., Zaehle, S., & Migliavacca, M., 2018. Bigleaf—An R package for the calculation of physical and physiological ecosystem properties from eddy covariance data. *PloS one*, *13*(8), e0201114.

Kumari, V. V., KA, G., Chandran MA, S., Shankar, A. K., S, S., Kumar, M., ... & Singh, V. K., 2025. Diversified legume-oilseed cropping system for synergistic enhancement of yield and water use efficiency in rainfed areas of semi-arid tropics. PloS one, 20(2), e0317373.

Lakso, A. N., Santiago, M., & Stroock, A. D., 2022. Monitoring stem water potential with an embedded microtensiometer to inform irrigation scheduling in fruit crops. Horticulturae, 8(12), 1207.

Lakso, A. N., Zhu, S., Santiago, M., Shackel, K., Volkov, V., & Stroock, A. D., 2019. A microtensiometer sensor to continuously monitor stem water potentials in woody plants design and field testing. In IX International Symposium on Irrigation of Horticultural Crops 1335 (pp. 317-324).

Nielsen, D. R., Biggar, J. W., & Erh, K. T., 1973. Spatial variability of field-measured soil-water properties.

Nimmo, J. R., Schmidt, K. M., Perkins, K. S., & Stock, J. D., 2009. Rapid measurement of field-saturated hydraulic conductivity for areal characterization. Vadose Zone Journal, 8(1), 142-149.

Panigrahi, P., 2023. Impact of deficit irrigation on citrus production under a sub-humid climate: a case study. Water Supply, 23(3), 1177-1188.

Paredes, P., Pereira, L. S., Rodrigues, G. C., Botelho, N., & Torres, M. O., 2017. Using the FAO dual crop coefficient approach to model water use and productivity of processing pea (Pisum sativum L.) as influenced by irrigation strategies. Agricultural Water Management, 189, 5-18.

Provenzano G., Tarquis A. M., Rodriguez-Sinobas L., 2013. Soil and irrigation sustainability practices. Agricultural water management, 120, 1-4.

Puig-Sirera, À., Provenzano, G., González-Altozano, P., Intrigliolo, D. S., & Rallo, G., 2021. Irrigation water saving strategies in Citrus orchards: Analysis of the combined effects of timing and severity of soil water deficit. Agricultural Water Management, 248, 106773.

Rallo G., González-Altozano P., Manzano-Juárez J., Provenzano G., 2017. Using field measurements and FAO-56 model to assess the eco-physiological response of citrus orchards under regulated deficit irrigation. Agricultural water management, 180, 136-147.

Ramos, T. B., Darouich, H., Oliveira, A. R., Farzamian, M., Monteiro, T., Castanheira, N., ... & Pereira, L. S., 2023. Water use and soil water balance of Mediterranean tree crops assessed with the SIMDualKc model in orchards of southern Portugal. Agricultural Water Management, 279, 108209.

Reynolds, W. D., Bowman, B. T., Brunke, R. R., Drury, C. F., & Tan, C. S., 2000. Comparison of tension infiltrometer, pressure infiltrometer, and soil core estimates of saturated hydraulic conductivity. Soil Science Society of America Journal, 64(2), 478-484.

Reynolds, W. D., Elrick, D. E., Youngs, E. G., Booltink, H. W. G., & Bouma, J. 2002. 3.4. 2 Laboratory Methods. Methods of soil analysis: part 4 physical methods, 5, 802-816.

Rodríguez-Juárez, P., Júnez-Ferreira, H. E., González Trinidad, J., Zavala, M., Burnes-Rudecino, S., & Bautista-Capetillo, C., 2018. Automated laboratory infiltrometer to estimate saturated hydraulic conductivity using an arduino microcontroller board. Water, 10(12), 1867.

Sandhu, R., & Irmak, S., 2019. Assessment of AquaCrop model in simulating maize canopy cover, soil-water, evapotranspiration, yield, and water productivity for different planting dates and densities under irrigated and rainfed conditions. Agricultural Water Management, 224, 105753.

Schimmenti, E., Borsellino, V., & Galati, A., 2013. Growth of citrus production among the Euro-Mediterranean countries: Political implications and empirical findings. *Spanish Journal of Agricultural Research*, *11*(3), 561-577.

Spliethoff, J., Rampim, L., Pott, C. A., Vidigal, J. C. B., & Neto, E. G., 2022. Development and validation of a hydraulic sampler for collection of undisturbed soil samples. Archives of Agronomy and Soil Science, 68(4), 431-446.

Steppe, K., De Pauw, D. J., & Lemeur, R., 2008. A step towards new irrigation scheduling strategies using plant-based measurements and mathematical modelling. Irrigation Science, 26(6), 505-517.

Villalobos, F. J., Testi, L., García-Tejera, O., López-Bernal, Á., Tejado, I., & Vinagre, B. M., 2024. Measuring the Diurnal Variation of Root Conductance in Olive Trees Using Microtensiometers and Sap Flow Sensors. Plant and Soil, 1-14.

Yetik, A. K., & Candoğan, B. N., 2022. Optimisation of irrigation strategy in sugar beet farming based on yield, quality and water productivity. Plant, Soil & Environment, 68(8).

Zhang, X., Wendroth, O., Matocha, C., Zhu, J., & Reyes, J., 2020. Assessing field-scale variability of soil hydraulic conductivity at and near saturation. Catena, 187, 104335.

CHAPTER 2: Soil Hydraulic Characterization

Background

Soil hydraulic characterization is essential for agro-environmental applications, including the optimization of water use efficiency in cropping systems (Rallo et al., 2018), modelling water and solute dynamics (Autovino et al., 2018; Basile et al., 2020), and studying key processes such as infiltration, runoff, drainage, and erosion (Hillel, 2003; Grismer, 2016). However, obtaining an accurate determination of these parameters presents a multi-layered challenge. First and foremost, soil hydraulic properties are an intrinsically variable property, exhibiting significant heterogeneity across spatial scales, temporal fluctuations, and a strong dependence on the sampled soil volume (Lauren et al., 1988; Prieksat, et al., 1994; Logsdon & Jaynes, 1996). Second, a critical layer of complexity arises from methodological choices, as measured values are strongly dependent on the specific technique employed (Jarvis and Messing, 1995; Bagarello et al., 2000; Soulis et al., 2020). This dependence derives from the fact that different techniques are based upon distinct physical and operational principles. The conceptual and operational diversity among methods used to determine soil hydraulic properties, particularly soil hydrodynamic parameters, often results in markedly divergent estimates, as consistently demonstrated by comparative studies reporting differences by several orders of magnitude (Fodor et al., 2011; Alagna et al., 2016). These disparities are not random; rather, they systematically reflect intrinsic methodological factors. The challenge of obtaining a reliable soil hydraulic characterization persists even after a general methodological framework has been selected. Within a single experimental technique, the choice of analytical protocol, inversion algorithm, or data-interpretation scheme can profoundly influence the resulting parameter estimates (Vienken and Dietrich, 2011; Bagarello et al., 2014). Consequently, the selection of an 'appropriate' method is further complicated by the proliferation of analytical variants within each experimental approach.

Considering the foregoing, methodological selection constitutes a true decision cascade, beginning with the choice of operating domain (field versus laboratory), proceeding through the selection of a specific instrument, and culminating in the adoption of a data-inversion algorithm or calculation procedure. Each step in this sequence introduces additional sources of variability that directly affect the reliability and comparability of the resulting hydraulic parameter estimates. Addressing this methodological complexity through targeted research is therefore imperative. Within this framework, saturated (K_s) and near-saturated (K) hydraulic conductivity are pivotal parameters, as they directly govern subsurface hydrological fluxes (Bagarello et al., 2019; Usowicz and Lipiec, 2021; Mozaffari et al., 2024). The methodological spectrum for determining soil hydraulic conductivity is notably broad, ranging from rigorously controlled laboratory permeameters (e.g., the Constant-Head

Permeameter, CHP) to various field-based approaches (e.g., the Mini Disk Infiltrometer, MDI; the Beerkan Estimation of Soil Transfer parameters, BEST; the Pressure Infiltrometer, PI; and automated devices like the SATURO).

These methods differ fundamentally in aspects such as induced flow geometry (e.g., one-dimensional, 1D, vs. three-dimensional, 3D flow), boundary conditions, representative scale (sample size), and the type of data utilized, whether derived from transient infiltration, steady-state flow, or a combination thereof (Lee et al., 1985; Bagarello et al., 2000; Ibrahim, 2016). Systematic differences between estimates reflect, for example, the scale and type of soil sample considered, such as small potentially disturbed laboratory cores vs larger in-situ volumes (Mohanty et al., 1994; Bagarello et al., 2019), and the specific flow dynamics induced by the experimental setup (Reynolds et al., 2000).). For example, using Beerkan infiltration data, Di Prima et al. (2019) and Castellini et al. (2024) reported K_s estimates that differed by several orders of magnitude when different algorithms were applied. Similarly, Bát'ková et al. (2020) showed that alternative analyses of MDI and Hood Infiltrometer data on a silty-clay loam yielded hydraulic parameters differing in order of magnitude solely as a function of the adopted analytical protocol. Addressing this methodological complexity through targeted research is therefore imperative, particularly in Mediterranean environments, where soils are often well structured, spatially heterogeneous, and subject to pronounced climatic seasonality, yet where this issue remains largely underexplored.

To address these knowledge gaps, Chapter **2** develops two specific and interrelated lines of research.

The first focuses on the validation of a method that determines soil hydraulic conductivity indirectly, i.e. through mathematical inversion of infiltration data. Specifically, for the widely used BEST algorithm, a central concern is the accuracy of the inferred hydraulic functions, particularly in the critical near-saturation range. Empirical evidence indicates that conductivity curves derived from BEST often fail to reproduce direct *K* measurements obtained with established methods such as the MDI and CHP, thereby casting doubt on their reliability for predictive modelling (Fernández-Gálvez et al., 2019; Castellini et al., 2021). Accordingly, Chapter **2** undertakes controlled comparative experiments that not only quantify these discrepancies but also try to disentangle their causes, from physical artefacts (e.g., air entrapment, surface disturbance) to intrinsic limitations of the underlying hydraulic models and inversion algorithms.

The second line of research addresses the evaluation of technological innovation in field infiltration testing. The advent of automated “smart” infiltrometers, such as SATURO, promises to standardize procedures and reduce operator work; however, their adoption requires a critical assessment of whether the embedded automation and validation algorithms ensure a level of physical robustness and consistency comparable to that of well-established, operator-controlled manual protocols (e.g., the PI). This issue is particularly salient when such instruments are deployed in complex, structured soils that may challenge predefined analytical assumptions (Concialdi et al., 2020; Rauber et al., 2024; Baqerkhani et al., 2025).

Chapter **2** is organized as follows. Chapter **2.1** lists the principal approaches to soil hydraulic characterization used in the present thesis, offering a concise synthesis of their physical foundations, operational procedures, and typical application domains. By juxtaposing these techniques, the section provides an immediate comparative perspective that clarifies key contrasts in flow geometry, boundary conditions, investigation scale, and data demands. In doing so, it establishes a shared conceptual framework for the thesis and a coherent basis for interpreting the experimental work that follows.

Chapter **2.2**, based on the paper *"Comparing mini-disk infiltrometer, BEST method and soil core estimates of hydraulic conductivity of a sandy-loam soil"* published in *Soil & Tillage Research* (Fusco et al., 2024), addresses the validation gap for direct and indirect methods, by executing a focused comparison between the K_s and K values of a sandy-loam soil obtained, in the field, with the BEST method and an unconfined MDI experiment and, in the laboratory, with a confined MDI experiment and the CHP method. The analysis is designed to quantify discrepancies in the near-saturation range and systematically investigate their potential causes, such as the impact of using soil porosity versus measured saturated soil water status in BEST calculations, the effects of flow geometry (3D vs. 1D), and artefacts like air entrapment. The aim is to clarify the specific contexts in which indirect methods like BEST provide reliable estimates for hydrological modelling.

Finally, Chapter **2.3**, based on the paper *"Comparison of the single-ring pressure infiltrometer and SATURO methods for determination of field-saturated soil hydraulic conductivity"* published in *Vadose Zone Journal* (Autovino et al., 2025), addresses the evaluation gap for technological innovation by conducting a comprehensive comparison between field K_s measured with the automated SATURO infiltrometer and the manual standard of the PI, on soils of contrasting texture and structure. This study critically assesses not only the agreement in derived soil hydraulic parameters but also the practical implications of automation on data quality, operational feasibility, and the ability to capture representative hydrological processes in the field.

The unifying purpose of these experimental studies is to contribute to evolving soil hydraulic characterization from a practice often heterogeneous and guided by convenience toward a more robust approach informed by comparative evidence. Through the critical evaluation conducted in Chapters **2.2** and **2.3** on the reliability, physical consistency, and operational pragmatism of prominent techniques, this experimental work aims to provide empirically grounded guidance for methodological selection in Mediterranean contexts.

The comparative evidence gathered in these chapters can offer valuable insights for parameterizing agro-hydrological models, helping reduce uncertainties in hydraulic inputs and improve simulation reliability. Specifically, understanding the sources of divergence between methods, investigated in Chapter **2.2**, and evaluating the operational reliability of the automated device, conducted in Chapter **2.3**, provides concrete elements for a more informed choice of characterization techniques. This translates into a more robust foundation for generating the input data required for modelling, thereby advancing basic hydrological research and meeting the needs of sustainable agronomic and environmental management.

2.1. Saturated, field-saturated and near-saturated soil hydraulic conductivity:

Laboratory Methods:

Constant-head permeameter (CHP)

The constant-head permeameter (CHP, **Fig.1**) is a laboratory instrument used to measure K_s by applying Darcy's Law under steady-state flow conditions.

According to this fundamental law, formulated by Henry Darcy in 1856, water flow through a saturated porous medium is proportional to the applied hydraulic gradient, a relationship valid as long as the flow regime remains laminar. It is important to emphasize that Darcy's Law, and consequently the constant-head permeameter method, applies specifically to saturated soils, where all pores are filled with water and therefore, they all contribute to the infiltration process. The CHP method involves applying a constant hydraulic head to the surface of a saturated soil sample, typically contained in a cylinder, and measuring the volume of water passing through it over a known time interval. The water flow can be applied in two directions: from top to bottom or vice versa, depending on the experimental requirements.

In the case of top feeding, the soil sample, with a height "L" and a volume equal to the internal volume of the sampling cylinder, is placed on a fine-mesh synthetic fabric and a metal screen, both secured to the sampler with a clamp. These supports, which offer negligible resistance to flow, serve to hold the sample and prevent the detachment of soil particles, thereby preserving the sample's integrity and representativeness. An empty cylinder, open at both ends and with the same diameter as the sampler, is placed on top of the sample to establish and maintain the constant hydraulic head on the sample's surface.

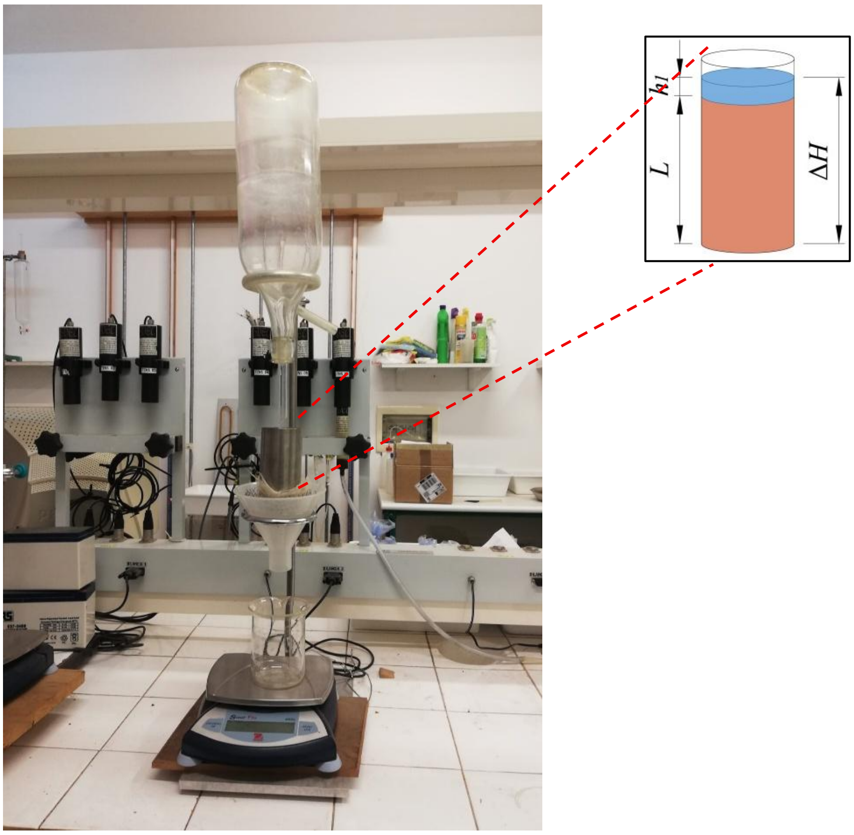

Fig. 1 Constant-head permeameter (CHP)

After saturating the sample using standard procedures, a pre-established water layer thickness (h_1, **Fig. 1**) is maintained on its upper surface throughout the test using devices such as a Mariotte bottle or a siphon. The water passing through the sample is collected in a container and weighed at predetermined time intervals, which are long enough to ensure the collection of a measurable volume with accuracy. The flow density q (L T^{-1}) is calculated using the relation:

$$q = \frac{V}{(A \times \Delta t)} \tag{1.0}$$

Where V (L^3) is the volume of water collected, A (L^2) is the cross-sectional area of the sample, and Δt (T) is the time interval considered.

The test continues until steady-state conditions are reached, meaning the flow density measured in several consecutive readings shows no appreciable variations. Alternatively, the steady-state value of q can be estimated by determining the slope of the linear section of the relationship between the cumulative height of filtered water vs time. Once the steady-state flow density is obtained, K_s is calculated by applying Darcy's law in the form:

$$K_s = q \frac{L}{\Delta H} \tag{1.1}$$

Where $\Delta H = h_1 + L$ represents the total hydraulic head difference between the inlet and outlet of the sample (**Fig. 2**).

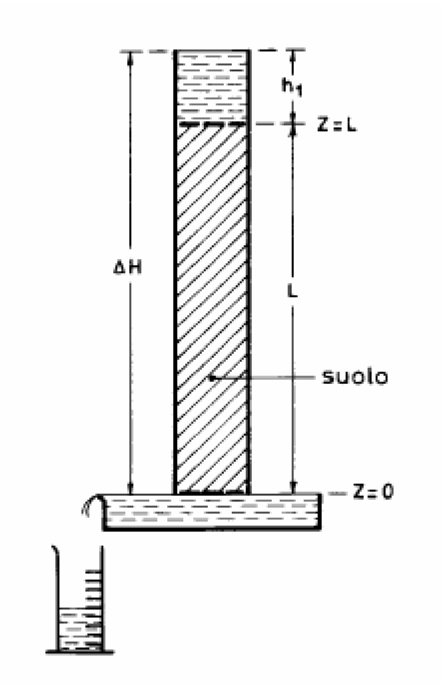

Fig. 2 Schematic of water flow in a saturated soil column under top-feeding conditions (from Hillel, 1998, modified)

This method is particularly suitable for medium to high permeability soils. For more conductive materials, bottom feeding may be preferable, as it allows for a reduction in the hydraulic gradient and minimizes the risk of non-linear flow. In any case, the quality of the measurement depends on the proper saturation of the sample and the maintenance of steady-state flow conditions.

Field Methods:

Minidisk Infiltrometer (MDI)

The Mini Disk Infiltrometer (MDI) (Decagon Devices Inc., 2014) is a compact tension infiltrometer designed for measuring soil hydrodynamic parameters, such as hydraulic conductivity (K, L T^{-1}) and sorptivity (S, L $T^{-1/2}$) under near-saturated conditions. Its versatility allows for use in both field and laboratory settings, facilitating comparative studies and standardized measurements. The instrument is simple, economical, portable, and requires only 135 mL of water for operation. The MDI consists of a transparent polycarbonate tube (3.1 cm in diameter, 32.7 cm in length) divided into two chambers by a rubber septum (**Fig. 3**).

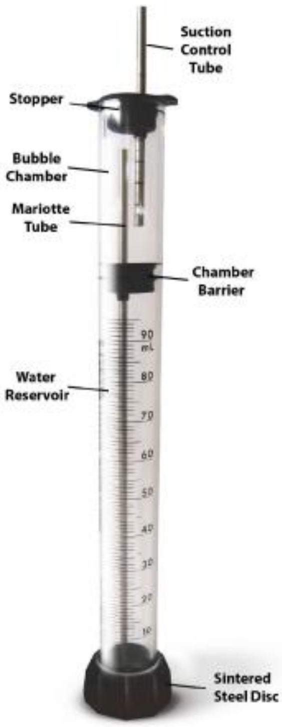

Fig. 3 Scheme of Minidisk infiltrometer

The upper chamber (bubble chamber) regulates the pressure potential through an adjustable suction control tube, while the lower chamber (reservoir) acts as a graduated cylinder containing approximately 95 mL of water. This water infiltrates the soil through a sintered stainless-steel porous disk (4.5 cm in diameter, 0.3 cm thick) located at the base of the infiltrometer, maintaining the selected pressure potential (h_0, L). This porous sintered stainless-steel disk does not allow water to leak in open air. To ensure good hydraulic contact between the disk and the soil, a contact material layer is often placed beneath the infiltrometer. The suction control tube allows pressure potentials ranging from -0.5 to -7 cm, determined by the difference in height between the water level in the bubble chamber and the bottom end of the suction control tube. Once the MDI is placed on the soil surface, the infiltration test begins when the first air bubble rises into the reservoir. Initially, the infiltration rate (i, L T^{-1}) decreases during a transient phase before reaching a steady-state infiltration rate (i_s, L T^{-1}). The water infiltration rate is monitored by reading the water level on the graduated scale of the reservoir, with frequent readings recommended, especially at the start of the experiment, to capture rapid changes in infiltration dynamics.

Soil hydraulic conductivity is closely related to the soil water potential and water content; in fact, it decreases as the soil dries because air begins to occupy the spaces previously filled by water. Several methods in the literature can be used to determine soil hydraulic conductivity from MDI measurements. Among these is the method proposed by Zhang (1997), which involves fitting cumulative infiltration data with the following equation:

$$I = C_1\sqrt{t} + C_2 t \tag{1.2}$$

The parameter C_1 (L $T^{-1/2}$) is related to sorptivity, while the parameter C_2 (L T^{-1}) is related to hydraulic conductivity. K (L T^{-1}) is then given by the following equation:

$$K = \frac{C_2}{A} \tag{1.3}$$

Where A is a value that relates the van Genuchten parameters for a given soil type to the suction rate and the disk radius of the MDI.

$$A = \frac{11.65(n^{0.1} - 1)\exp[2.92(n - 1.9)\alpha h_0]}{(\alpha r_0)^{0.91}} \quad n \geq 1.9 \tag{1.4}$$

$$A = \frac{11.65(n^{0.1} - 1)\exp[7.5(n - 1.9)\alpha h_0]}{(\alpha r_0)^{0.91}} \quad n < 1.9 \tag{1.5}$$

Where n and α (L^{-1}) are the van Genuchten parameters for the soil, r_0 (L) is the disk radius, and h_0 (L) is the suction applied to the surface of the porous disk.

Beerkan Estimation of Soil Transfer Parameters (BEST)

The BEST methodology (**Fig. 4**), as described by Lassabatère et al. (2006), allows for the simultaneous determination of both the water retention curve and the hydraulic conductivity function through a limited number of field and laboratory tests. To apply this method, the initial and final water contents of the soil, the dry bulk density, particle size distribution, and a simple field infiltration test must be known.

Fig. 4 Equipment needed for a Beerkan Estimation of Soil Transfer Parameters (BEST) experiment

The methodology assumes that the water retention and hydraulic conductivity functions can be represented by the van Genuchten (1980) model, incorporating Burdine's (1953) and Brooks and Corey's (1964) conditions. The van Genuchten equation for the water retention curve is:

$$\frac{\theta - \theta_r}{\theta_s - \theta_r} = \left(1 + \left(\frac{h}{h_g}\right)^n\right)^{-m} \tag{1.6}$$

$$m = 1 - \frac{2}{n} \tag{1.7}$$

where θ ($L^3\ L^{-3}$) is the soil volumetric water content, θ_r ($L^3\ L^{-3}$) is the soil residual volumetric water, θ_s ($L^3\ L^{-3}$) is the soil saturated water content, h (L) is the matrix potential of soil water, and n, m, and h_g are parameters. The hydraulic conductivity function (Brooks and Corey's, 1964) is given by:

$$\frac{K(\theta)}{K_s} = \left(\frac{\theta - \theta_r}{\theta_s - \theta_r}\right)^{\eta} \tag{1.8}$$

where $K(\theta)$ (L T^{-1}) is the hydraulic conductivity, K_s (L T^{-1}) is the saturated hydraulic conductivity, and η is a parameter. The conductivity shape parameter η can be estimated from the capillary model (Haverkamp et al., 1999):

$$\eta = \frac{2}{m \times n} + 2 + p \tag{1.9}$$

where the tortuosity parameter p is assumed equal to 1 in BEST (Burdine, 1953). The shape parameters n, m, and η depend on the soil texture and are estimated through particle size analysis of the fine fraction (< 2 mm). The scale parameters h_g, θ_s, θ_r, and K_s depend on the structure of the porous medium and can be measured directly or derived from the infiltration test, except for θ_r, which is assumed to be zero in this method.

The BEST methodology can be applied both to infiltration rate and cumulative infiltration. The three-dimensional infiltration process in homogeneous soil, with an initial water content θ_i (L^3 L^{-3}) and a circular infiltration area of radius r (L), can be described using the following equations from Haverkamp et al. (1994):

$$I(t) = S\sqrt{t} + (AS^2 + BK_s)t \tag{2.0}$$

$$i_s = AS^2 + K_s \tag{2.1}$$

where I (L) is the cumulative infiltration, t (T) is time, S (L T$^{-1/2}$) is the sorptivity, i_s (L T^{-1}) is the steady-state infiltration rate, and A (L^{-1}) and B are coefficients defined by the following relations, using the Brooks and Corey relationship for $K(\theta)$:

$$A = \frac{\gamma}{r(\theta_s - \theta_i)} \tag{2.2}$$

$$B = \frac{2-\beta}{3}\left[1 - \left(\frac{\theta_i}{\theta_s}\right)^{\eta}\right] + \left(\frac{\theta_i}{\theta_s}\right)^{\eta} \tag{2.3}$$

where β and γ are coefficients that, for $\theta_i < 0.25\ \theta_s$, are set at 0.6 and 0.75, respectively.

The link between sorptivity and the scale parameters is given by:

$$S^2(\theta_i, \theta_s) = -c_p \theta_s K_s h_g \left(1 - \frac{\theta_i}{\theta_s}\right)\left[1 - \left(\frac{\theta_i}{\theta_s}\right)^{\eta}\right] \tag{2.4}$$

where:

$$c_p = \Gamma\left(1 + \frac{1}{n}\right)\left\{\frac{\Gamma\left(m\eta - \frac{1}{n}\right)}{\Gamma(m\eta)} + \frac{\Gamma\left(m\eta + m - \frac{1}{n}\right)}{\Gamma(m\eta + m)}\right\} \tag{2.5}$$

Γ is the gamma function. The BEST method first estimates the shape parameters from the particle size information and then evaluates the scale parameters from the infiltration experiment by fitting the equation for cumulative infiltration (2.0) to the transient phase of the infiltration data. The steady-state infiltration rate is determined experimentally, and K_s is estimated using equation (2.1). Finally, the scale parameter h_g is derived from equation (2.4).

Cumulative infiltration curves are obtained by applying the Beerkan technique in the field, where a cylinder is inserted into the soil to a depth of about 0.01 m. A series of pre-established water volumes are added sequentially, to maintain a water depth of about 0.01 m on the soil surface, and the infiltration time is measured for each volume until the water has completely infiltrated (Lassabatère et al., 2006). For the experimental investigations conducted in this thesis, during beerkan runs, and as required by the research protocol, to determine gravimetric soil water content and bulk density, undisturbed soil samples were collected during field campaigns using cylindrical cores of known volume (0.05 m in diameter and 0.05 m in height) at two depths (0-5 and 5-10 cm).

Various algorithms, such as the BEST-Slope algorithm (Lassabatère et al., 2006), BEST-Intercept (Yilmaz et al., 2010), and BEST-Steady (Bagarello et al., 2014), are used for the application of the BEST methodology. In this thesis, the BEST-Steady algorithm proposed by Bagarello et al. (2014) was employed. This algorithm allows for the estimation of soil sorptivity S (L $T^{-1/2}$) and saturated hydraulic conductivity K_s (L T^{-1}) using the intercept b_s (L) and slope is (L T^{-1}) of the line representing the steady-state phase of the infiltration process:

$$S = \sqrt{\frac{i_s}{A + \frac{C}{b_s}}} \tag{2.6}$$

$$K_s = \frac{C\, i_s}{A\, b_s + C} \tag{2.7}$$

where A (L^{-1}) is calculated using equation (2.3), and C is a constant given by:

$$C \approx \frac{1}{2(1-\beta)} \ln\left(\frac{1}{\beta}\right) \tag{2.8}$$

in which β and γ are coefficients equal to 0.6 and 0.75 respectively.

According to White and Sully (1987), the macroscopic capillary length λ_c (L), which indicates the relative importance of capillarity in comparison to gravity during water movement in unsaturated soils, is given by:

$$\lambda_c = \frac{bS^2}{\Delta\theta \Delta K} \tag{2.9}$$

where b is a dimensionless constant (0.55), and ΔK is the difference between K_s and the initial hydraulic conductivity K_i. Low values of λ_c (between 0 mm and 100 mm) suggest that gravity dominates over capillarity, typical of coarse or highly structured porous media, while high values of λ_c (greater than 1000 mm) indicate capillarity dominance, typical of fine-textured or minimally structured soils (Reynolds et al., 2002). According to Di Prima et al. (2020), λ_c can be calculated during the steady-state phase of the Beerkan test as follows:

$$\lambda_c = 0.861 \frac{b_s}{\Delta\theta} \quad (3.0)$$

Pressure Infiltrometer (PI) and SATURO Infiltrometer

The Pressure Infiltrometer (PI) and an automated one, using the SATURO Infiltrometer, are based on the analytical equation of Reynolds and Elrick (1990), which describes the three-dimensional steady-state flow from an inserted ring in a homogeneous, isotropic and initially unsaturated porous medium:

$$Q_s = \frac{r}{G}(K_s H + \phi_m) + \pi r^2 K_s \quad (3.1)$$

where Q_s (L^3 T^{-1}) is the steady-state flow rate, r (L) is the ring radius, K_s (L T^{-1}) is the saturated soil hydraulic conductivity, H (L) is the ponded head of water on the infiltration surface, ϕ_m (L^2 T^{-1}) is the matric flux potential and G is a dimensionless shape factor expressing the complex interactions between ring radius, depth of ring insertion, d (L), depth of ponding in the ring, soil capillarity and gravity. The value of G can be estimated empirically as a function of the ratio between insertion depth and ring radius according to:

$$G_e = 0.316 \frac{d}{r} + 0.184 \quad (3.2)$$

which is strictly valid for $0.03 \leq d \leq 0.05$ m, $0.05 \leq r \leq 0.10$ m and $0.05 \leq H \leq 0.25$ m.

The shared analysis methodology for both instruments can employ two approaches. The primary one is the Two-Ponding-Depth (TPD) approach (Reynolds and Elrick, 1990), approach, also known as the Two-Head-Analysis (Reynolds and Elrick, 2002). This method enables the simultaneous determination of K_s and ϕ_m. It requires measuring the steady-state flow rates, Q_{s1} and Q_{s2}, corresponding to two ponding depths of water, H_1 and H_2 ($H_2 > H_1$), consecutively established on the infiltrating surface without the occurrence of a drainage phase in the passage from H_1 to H_2. The following relationships yield K_s and ϕ_m:

$$K_s = \frac{G_e}{r}\left(\frac{Q_{s2} - Q_{s1}}{H_2 - H_1}\right) \quad (3.3)$$

$$\phi_m = \frac{G_e}{r}\left(\frac{H_2 Q_{s1} - H_1 Q_{s2}}{H_2 - H_1} - \pi r G_e \frac{Q_{s2} - Q_{s1}}{H_2 - H_1}\right) \quad (3.4)$$

Simultaneous calculation of K_s and ϕ_m also yields an estimate of the so-called α^* (L^{-1}) parameter (Reynolds and Elrick, 2002):

$$\alpha^* = \frac{K_s}{\phi_m} \tag{3.5}$$

When the TPD approach yields a negative result for either K_s or ϕ_m or an α^* value that falls substantially outside the realistic range of $1 \leq \alpha^* \leq 100$ m^{-1}, both K_s and ϕ_m calculations must be discarded (Reynolds and Elrick, 2002; Angulo-Jaramillo et al., 2016). In this case, the One-Ponding-Depth (OPD) approach (Reynolds and Elrick, 1990), also named Single-Head-Analysis, should be applied to each H value and the resulting K_s and ϕ_m values averaged (Reynolds and Elrick, 2002). With the OPD approach, an estimate of K_s is obtained from a single Q_s value by the following relationship:

$$K_s = \frac{\alpha^* G_e Q_s}{r(\alpha^* H + 1) + G_e \alpha^* \pi r^2} \tag{3.6}$$

in which α^* can be estimated from a field evaluation of soil textural and structural characteristics or an a-priori knowledge of a field representative value of α^* (Elrick and Reynolds, 1992a, b; Reynolds et al., 2002).

Pressure Infiltrometer (PI)

The Pressure Infiltrometer employed in this thesis (**Fig. 5**) follows the design specifications established by Ciollaro and Lamaddalena (1998). The apparatus consists of a stainless-steel infiltration ring with a radius of 7.5 cm that is inserted to a depth of 5 cm into the unsaturated soil. A Mariotte bottle maintains a constant hydraulic head during infiltration experiments. The steady-state infiltration rate is determined by monitoring the water level decrease in the Mariotte bottle over time. The experimental procedure involves establishing two successive ponding heads on the soil surface within the ring: an initial head (H_1) of 5 cm followed by a higher head (H_2) of 10 cm, with immediate transition between the two pressure stages.

Fig. 5 Pressure Infiltrometer (PI)

The test duration is site-specific, depending on the soil's hydraulic properties and initial moisture conditions, which determine the time required to reach steady-state flow conditions.

SATURO

The SATURO infiltrometer (**Fig. 6**) is an automated Pressure Infiltrometer that enables fully automated determination of K_s without the need of post-processing the infiltration data. The device includes two insertion rings, each with r = 7.5 cm and options for insertion depths of 10 or 5 cm. The ring is inserted into the soil using a driving plate and a hammer.

Fig. 6 SATURO infiltrometer

The infiltrometer head, comprising an airtight chamber, connects to the ring via a quick-release mechanism. A control unit within the infiltrometer head pumps water to maintain a ponded water depth of approximately 5 cm on the soil surface and applies air pressure to establish the required pressure head. Infiltration rates are measured and logged at 1-minute intervals throughout each test. The procedure begins with an initial soaking phase of 25 minutes, during which the infiltrometer applies water to saturate the soil while maintaining a pressure head of approximately 5 cm. After soaking, the infiltrometer performs a series of infiltration cycles alternating between two different pressure heads. Each cycle includes a high-pressure head (H_2 = 10 cm) applied for 15 min, followed by a low-pressure head (H_1 = 5 cm) for another 15 min. These cycles ensure that steady-state infiltration rates are achieved. The control unit calculates K_s by averaging the infiltration rates at the two different pressure heads during the last pressure cycle.

REFERENCES

Alagna, V., Bagarello, V., Di Prima, S., & Iovino, M., 2016. Determining hydraulic properties of a loam soil by alternative infiltrometer techniques. *Hydrological Processes*, *30*(2), 263-275.

Angulo-Jaramillo, R., Bagarello, V., Iovino, M., Lassabatère, L., 2016. Infiltration measurements for soil hydraulic characterization, Infiltration Measurements for Soil Hydraulic Characterization. https://doi.org/10.1007/978-3-319-31788-5

Autovino, D., Rallo, G., & Provenzano, G., 2018. Predicting soil and plant water status dynamic in olive orchards under different irrigation systems with Hydrus-2D: Model performance and scenario analysis. *Agricultural water management*, *203*, 225-235.

Bagarello, V., Baiamonte, G., & Caia, C., 2019. Variability of near-surface saturated hydraulic conductivity for the clay soils of a small Sicilian basin. *Geoderma*, *340*, 133-145.

Bagarello, V., Di Prima, S., Iovino, M., 2014. Comparison of alternative algorithms to analyze the beerkan infiltration experiment. Suolo Sci. Soc. Am. J., 78, 724-736. doi:10.2136/sssaj2013.06.0231.

Bagarello, V., Iovino, M., & Tusa, G., 2000. Factors affecting measurement of the near-saturated soil hydraulic conductivity. *Soil Science Society of America Journal*, *64*(4), 1203-1210.

Baqerkhani, A., Zare Abyaneh, H., Bahmani, O., & Nozari, H., 2025. Estimating the saturated hydraulic conductivity of the vadose zone with an automatic infiltration data logger for the BEST algorithm. *Irrigation and Drainage*, *74*(1), 128-138.

Basile, A., Albrizio, R., Autovino, D., Bonfante, A., De Mascellis, R., Terribile, F., & Giorio, P., 2020. A modelling approach to discriminate contributions of soil hydrological properties and slope gradient to water stress in Mediterranean vineyards. *Agricultural Water Management*, *241*, 106338.

Báťková, K., Miháliková, M., & Matula, S., 2020. Hydraulic properties of a cultivated soil in temperate continental climate determined by mini disk infiltrometer. *Water*, *12*(3), 843.

Brooks, R.H. and Corey, A.T., 1964. Hydraulic Properties of Porous Media. Hydrology Paper, Vol. 3, Colorado State University, Fort Collins.

Burdine, N.T., 1953. Relative Permeability Calculations from Pore Size Distribution Data. Journal of Petroleum Technology, 5, 71-78.

Castellini, M., Di Prima, S., Moret-Fernández, D., & Lassabatere, L., 2021. Rapid and accurate measurement methods for determining soil hydraulic properties: A review. *Journal of Hydrology and Hydromechanics*, *69*(2), 121-139.

Castellini, M., Prima, S. D., Giglio, L., Leogrande, R., Alagna, V., Autovino, D., ... & Iovino, M., 2024. Applying a Comprehensive Model for Single-Ring Infiltration: Assessment of Temporal Changes in Saturated Hydraulic Conductivity and Physical Soil Properties. *Water*, *16*(20), 2950.

Ciollaro, G., and N. Lamaddalena, 1998. Effect of tillage on the hydraulic properties of a vertic soil. Journal of Agricultural and Engineering Research, 71(2), 147-155, doi: 10.1006/jaer.1998.0312.

Concialdi, P., Di Prima, S., Bhanderi, H. M., Stewart, R. D., Abou Najm, M. R., Gaur, M. L., ... & Lassabatere, L., 2020. An open-source instrumentation package for intensive soil hydraulic characterization. *Journal of Hydrology*, *582*, 124492.

Decagon, 2014. Minidisk Infiltrometer User's Manual. Decagon Devices, Inc., Pullman, USA, 24.

Di Prima, S., Castellini, M., Abou Najm, M. R., Stewart, R. D., Angulo-Jaramillo, R., Winiarski, T., & Lassabatere, L., 2019. Experimental assessment of a new comprehensive model for single ring infiltration data. *Journal of Hydrology*, *573*, 937-951.

Di Prima, S., Stewart, R.D., Castellini, M., Bagarello, V., Abou Najm, M.R., Pirastru, M., Giadrossich, F., Iovino, M., Angulo-Jaramillo, R., Lassabatere, L., 2020. Estimation of macroscopic capillary length from Beerkan infiltration experiments and its impact on hydraulic conductivity predictions of saturated soil. J. Hydrol., 589, 125159, 11 pp. doi: 10.1016/j.jhydrol.2020.125159.

Elrick, D. E., & Reynolds, W. D., 1992. Infiltration from constant-head well permeameters and infiltrometers. *Advances in measurement of soil physical properties: Bringing theory into practice*, *30*, 1-24.

Elrick, D.E., Reynolds, W.D., 1992. Methods for Analyzing Constant-Head Well Permeameter Data. Soil Science Society of America Journal 56. https://doi.org/10.2136/sssaj1992.03615995005600010052x

Fernández-Gálvez, J., Pollacco, J. A. P., Lassabatere, L., Angulo-Jaramillo, R., & Carrick, S., 2019. A general Beerkan Estimation of Soil Transfer parameters method predicting hydraulic parameters of any unimodal water retention and hydraulic conductivity curves: Application to the Kosugi soil hydraulic model without using particle size distribution data. *Advances in Water Resources*, *129*, 118-130.

Fodor, N., Sándor, R., Orfanus, T., Lichner, L., & Rajkai, K., 2011. Evaluation method dependency of measured saturated hydraulic conductivity. *Geoderma*, *165*(1), 60-68.

Grismer, M. E., 2016. Determination of watershed infiltration and erosion parameters from field rainfall simulation analyses. *Hydrology*, *3*(3), 23.

Haverkamp, R., Bouraoui, F., Zammit, C., Angulo-Jaramillo, R., & Delleur, J. W., 1999. Soil properties and moisture movement in the unsaturated zone. *Handbook of groundwater engineering*, *5*, 1-47.

Haverkamp, R., Ross, P. J., Smettem, K. R. J., & Parlange, J. Y., 1994. Three-dimensional analysis of infiltration from the disc infiltrometer: 2. Physically based infiltration equation. *Water Resources Research*, *30*(11), 2931-2935.

Hillel, D., 2003. *Introduction to environmental soil physics*. Elsevier.

Jarvis, N. J., & Messing, I., 1995. Near-saturated hydraulic conductivity in soils of contrasting texture measured by tension infiltrometers. *Soil Science Society of America Journal*, *59*(1), 27-34.

Lassabatere L., Angulo-Jaramillo R., Soria Ugalde J.M., Cuenca R., Braud I., Haverkamp R., 2006. Beerkan estimation of soil transfer parameters through infiltration experiments – BEST. Soil Science Society of America Journal 70: 521-532, doi: 10.2136/sssaj2005.0026.

Lauren, J.G., Wagnet, R.J., Bouma, J., Wosten, J.H.M., 1988. Variability of saturated hydraulic conductivity in a glossaquic hapludalf with macropores. Soil Sci 145. https://doi.org/10.1097/00010694-198801000-00003

Lee, D. M., Elrick, D. E., Reynolds, W. D., & Clothier, B. E., 1985. A comparison of three field methods for measuring saturated hydraulic conductivity. *Canadian journal of soil science*, *65*(3), 563-573.

Logsdon, S. D., & Jaynes, D. B., 1996. Spatial variability of hydraulic conductivity in a cultivated field at different times. *Soil Science Society of America Journal*, *60*(3), 703-709.

MM Ibrahim, J. A., 2016. Comparison of Methods for saturated hydraulic conductivity determination: field, laboratory and empirical measurements (A Pre-view). *British Journal of Applied Science & Technology*, *15*(3).

Mohanty, B. P., Kanwar, R. S., & Everts, C. J., 1994. Comparison of saturated hydraulic conductivity measurement methods for a glacial-till soil. *Soil Science Society of America Journal*, *58*(3), 672-677.

Mozaffari, H., Moosavi, A. A., & Nematollahi, M. A., 2024. Predicting saturated and near-saturated hydraulic conductivity using artificial neural networks and multiple linear regression in calcareous soils. *Plos one*, *19*(1), e0296933.

Prieksat, M. A., Kaspar, T. C., & Ankeny, M. D., 1994. Positional and temporal changes in ponded infiltration in a corn field. *Soil Science Society of America Journal*, *58*(1), 181-184.

Rallo, G., Provenzano, G., Castellini, M., & Sirera, À. P., 2018. Application of EMI and FDR sensors to assess the fraction of transpirable soil water over an olive grove. *Water*, *10*(2), 168.

Rauber, L. R., Mallman, M. S., Reinert, D. J., Pires, F. S., Vargas, F. D., & Gubiani, P. I., 2024. Automatic measurement of water infiltration into the soil. *Revista Brasileira de Ciência do Solo*, *48*, e0230078.

Reynolds W.D., Elrick D.E., 1990. Ponded infiltration from a single ring: I. Analysis of steady flow. Soil Science Society of America Journal, 54: 1233-1241.

Reynolds, W.D., and D.E. Elrick., 2002. Pressure infiltrometer. In: Dane, J.H. and Topp, G.C., editors, Methods of Soil Analysis, Part 4, Physical Methods, Number 5. Book Series, Inc., Madison, WI, USA. pp. 826–836.

Reynolds, W.D., Bowman, B.T., Brunke, R.R., Drury, C.F., Tan, C.S., 2000. Comparison of Tension Infiltrometer, Pressure Infiltrometer, and Soil Core Estimates of Saturated Hydraulic Conductivity. Soil Science Society of America Journal 64, 478–484. https://doi.org/10.2136/sssaj2000.642478x

Reynolds, W.D., Bowman, B.T., Drury, C.F., Tan, C.S., Lu, X., 2002. Indicators of good soil physical quality: Density and storage parameters. Geoderma 110. https://doi.org/10.1016/S0016-662 7061(02)00228-8.

Soulis, K. X., Londra, P. A., & Kargas, G., 2020. Characterizing surface soil layer saturated hydraulic conductivity in a Mediterranean natural watershed. *Hydrological Sciences Journal*, *65*(15), 2616-2629.

Usowicz, B., & Lipiec, J., 2021. Spatial variability of saturated hydraulic conductivity and its links with other soil properties at the regional scale. *Scientific Reports*, *11*(1), 8293.

Van Genuchten, M. T., 1980. A closed-form equation for predicting the hydraulic conductivity of unsaturated soils. *Soil science society of America journal*, *44*(5), 892-898.

Vienken, T., & Dietrich, P., 2011. Field evaluation of methods for determining hydraulic conductivity from grain size data. *Journal of hydrology*, *400*(1-2), 58-71.

White, I., & Sully, M. J., 1987. Macroscopic and microscopic capillary length and time scales from field infiltration. *Water Resources Research*, *23*(8), 1514-1522.

Yilmaz, D., Lassabatere, L., Angulo-Jaramillo, R., Deneele, D., Legret, M., 2010. Hydrodynamic Characterization of Basic Oxygen Furnace Slag through an Adapted BEST Method. Vadose Zone J. 9, 107

Zhang, R., 1997. Infiltration models for the disk infiltrometer. *Soil Science Society of America Journal*, *61*(6), 1597-1603.

2.2 Comparing mini-disk infiltrometer, BEST method and soil core estimates of hydraulic conductivity of a sandy-loam soil

M. Fusco[1], V. Alagna[1], D. Autovino[1], G. Caltabellotta[1], M. Iovino[1], G. Vaccaro[1], V. Bagarello[1]

[1]Dipartimento di Scienze Agrarie, Alimentari e Forestali, Università di Palermo, dario.autovino@unipa.it

Abstract

Saturated, K_s, and near-saturated, K, soil hydraulic conductivity control many hydrological processes but they are difficult to measure. Comparing methods to determine K_s and K is a means to establish how and why these soil hydrodynamic properties vary with the applied method. A comparison was established between the K_s and K values of a sandy-loam soil obtained, in the field, with the BEST (Beerkan Estimation of Soil Transfer parameters) method of soil hydraulic characterization and an unconfined MDI (mini-disk infiltrometer) experiment and, in the laboratory, with a confined MDI experiment and the CHP (constant-head permeameter) method. Using for the BEST calculations the soil porosity instead of the saturated soil water content yielded 1.4 to 1.1 times higher estimates of K_s and K, depending on the pressure head, and differences decreased in more unsaturated soil conditions. The confined MDI experiment yielded 22% - 77% higher K values than the unconfined MDI experiment, depending on the established pressure head, h_0, and differences were not significant for h_0 = -1 cm. In the close to saturation region, the soil hydraulic conductivity function predicted with BEST did not generally agree well with the K_s and K values obtained in the laboratory by a direct application of the Darcy's law. In particular, BEST yielded a 5.6 times smaller K_s value than the CHP method and up to an 8.1 times higher K value than the MDI. Overall, i) the two application methods of the MDI yielded relatively similar results, especially close to saturation, and ii) there was not a satisfactory agreement between the field (BEST) and the laboratory (MDI plus CHP) determination of soil hydraulic conductivity close to saturation, unless a comparison was made with the same soil water content. The detected differences were probably attributable to soil spatial variability, overestimation of K_s in the laboratory due to preferential flow phenomena, underestimation of K_s in the field due to air entrapment in the soil and infiltration surface disturbance, inability of BEST to describe the actual soil hydraulic conductivity function at the sampled field site. Testing BEST predictions of K_s and K in other soils appears advisable and combining the MDI and CHP methods appears a rather simple means to make these checks. These additional investigations could improve interpretation of the differences between methods, which is an important step for properly selecting a method yielding K_s and K data appropriate for an intended use.

Keywords: Soil hydraulic conductivity; Field methods; Laboratory methods; Mini-disk infiltrometer; Constant-head permeameter; BEST methods of soil hydraulic characterization.

2.2.1 INTRODUCTION

Knowledge of the hydrodynamic soil properties is essential for understanding water flow and solute transport processes in the soil-plant system (Autovino et al., 2018; Basile et al., 2020; Farzamian et al., 2021). Hydraulic conductivity of saturated, K_s, and near-saturated, K, soil are particularly important since flow and solute transport processes occur at the highest possible rates at or close to saturation. Saturated and near-saturated hydraulic conductivity can be determined by many methods (Carter and Gregorich, 2007; Dane et al., 2018; Angulo-Jaramillo et al., 2016), differing for various aspects such as the application ambit (laboratory, field), the established flow field (one-, 1D, or three-, 3D, dimensional), the information used to determine K_s or K (transient, steady-state, both transient and steady-state).

The choice of a method over another can be expected to have appreciable effects on determination of K_s and K, which raises the problem of choosing an appropriate measurement method in relation to the specific purpose of the sampling campaign and considering the advantages and disadvantages of the possibly usable methods (Alagna et al., 2016; Paige and Hillel, 1993; Reynolds et al., 2000). For example, laboratory methods are relatively comfortable to apply and they can guarantee highly controlled conditions which positively affect the reliability of the individual measurement. However, soil compaction and alteration of pore connectivity represent two of the possible adverse consequences of using a presumably undisturbed sample in the laboratory (Bouma, 1982; Lauren et al., 1988; Lee et al., 1985). Soil disturbance can be controlled to some extent when measurements are performed in the field, which also implies maintaining the connection between the sampled soil volume and the surrounding soil. However, field experiments are generally more tiring and also less accurate than the laboratory ones since they have to be performed in environmental conditions that are not always fully favorable for carrying out measurement activities. In addition, many potential limitations of several field methods can be identified such as relatively small sample size, possible edge flow along the ring wall, disturbance of the exposed soil surface due to water application, difficulty to guarantee a correspondence between theory and practice (Bagarello and David, 2020; Reynolds et al., 2008; Xu et al., 2012). In this complex context, one of the few sources of information from which practitioners can choose the appropriate methods for their specific circumstances is provided by comparisons between alternative methods for measuring K_s or K (Ghosh et al., 2019; Reynolds et al., 2000). These comparisons are important also because, especially on large areas, K_s or K data can be collected by applying different methods. According to Braud et al. (2017), in this particular case it is necessary to develop appropriate methodologies for creating an equivalent set of hydraulic conductivity data from data obtained with different methods. Therefore, the comparison between K_s and K determination methods continues to remain a central aspect of soil hydrology research.

Simple methods to determine soil hydraulic conductivity include BEST (Beerkan Estimation of Soil Transfer parameters) methods (Angulo-Jaramillo et al., 2019, 2016; Bagarello et al., 2014; Lassabatère et al., 2006; Yilmaz et al., 2010), the mini-disk infiltrometer (MDI; Dohnal et al., 2010; METER Group, 2021) and the constant-head permeameter (CHP) method (Reynolds and Elrick, 2002).

With BEST, a 3D field infiltration run under a nearly null ponded depth of water yields an estimate of K_s and the η parameter of the Brooks and Corey (1964) hydraulic conductivity function. Therefore, a given function is assumed to describe the relationship between K and the volumetric soil water content, θ, and the methodology produces an estimate of the parameters of this function.

The MDI is a miniaturized tension infiltrometer that allows simple and rapid determination of the soil hydraulic conductivity corresponding to fixed pressure head values, h, in the range from -0.5 cm to -6 cm. Typically, the device is used in the field to establish a 3D infiltration process at an established h value (Alagna et al., 2013; Fodor et al., 2011; Gonzalez-Sosa et al., 2010), but it was also applied to anthropic soils and green infrastructures substrates (Bondì et al., 2023; Gadi et al., 2017; Radinja et al., 2019). The corresponding K value is then obtained according to Zhang (1997) and Dohnal et al. (2010). However, the MDI has also been used in the laboratory on soil columns to establish 1D infiltration processes (Assouline and Narkis, 2011; Kargas et al., 2018). Using the unit hydraulic gradient (UHG) method (Klute and Dirksen, 1986) with the MDI, a given sample can be equilibrated at fixed, and high (close to zero), h values to obtain points of the hydraulic conductivity curve close to saturation (Bagarello et al., 2007).

The CHP represents the standard method for determining K_s in the laboratory and it is often used as a benchmark for evaluating other methods (Reynolds et al., 2000). A 1D flow process is established under a constant hydraulic head on an initially saturated soil sample (Madsen et al., 2008). Knowledge of the hydraulic head gradient and measurement of volumetric flow rate yields the K_s value by direct application of the Darcy's law.

Considering BEST, the MDI and the CHP, alone or in some combination among them, as possible methods to obtain K_s or K data leads to recognize that there are at least three issues that require investigation and development.

According to the original BEST application procedure (Lassabatère et al., 2006), the saturated soil has to be sampled at the end of an infiltration run to determine the saturated gravimetric water content which is then transformed into a volumetric value, θ_s, by considering the dry soil bulk density. With another simpler and largely applied approach, θ_s is assumed to coincide with soil porosity, ϕ (Bagarello et al., 2011; Di Prima, 2015; Mubarak et al., 2009a; Xu et al., 2009; Yilmaz et al., 2010).

The effect of the θ_s estimating method on the BEST prediction of soil hydraulic properties has been tested with somewhat contrasting results. For example, Alagna et al. (2016) suggested that sampling the soil confined by the ring at the end of the beerkan run to obtain an experimental value of θ_s could be expected to yield a more reliable estimation of soil hydraulic properties in comparison with that obtained by assuming a coincidence between θ_s and ϕ. Instead, the conclusion by Di Prima et al. (2017) was that the assumed coincidence between θ_s and ϕ as an alternative approach to the direct measurement of θ_s could be expected not to have a strong effect on estimation of K_s. Therefore, it does not seem clear to what extent ϕ represents a valid alternative to the direct measurement of θ_s.

For a fixed pressure head, *h,* the mean *K* value of the undisturbed soil in an area of interest can be obtained by field or laboratory MDI runs. The dependence of *K* on the MDI application method is unknown since the MDI has rarely been applied to establish both 3D and 1D infiltration processes. An exception is the investigation by Kargas et al. (2018), whose objective however was to determine the infiltration shape parameter, γ, of the infiltration model by Haverkamp et al. (1994). Consequently, the unconfined 3D and confined 1D MDI runs were carried out in the laboratory on repacked soil samples. The outcome of a comparison between field and laboratory determinations of *K* on undisturbed soil is difficult to predict *a-priori*. On the one hand, a certain similarity can be expected since the size of the sample, that can be expected to affect *K* determination (Reynolds et al., 2000), does not vary much between a field and a laboratory experiment. On the other hand, however, several other factors could induce a difference between field and laboratory determination of *K* with the MDI. For example, differences in the established flow field (3D in the field and 1D in the laboratory) could determine differences in *K* estimation since flow is not forced to follow a pre-established direction only in the first case (Reynolds and Elrick, 1985). Soil spatial variability (Logsdon and Jaynes, 1996) can affect a comparison between 3D and 1D MDI experiments. A reason is that, in the laboratory, all *K* values can be determined on a single sample regardless of the established *h* values whereas, in the field, each *K(h)* data point is obtained at a different sampling point. Further, differences can also be expected as a consequence of the applied method to analyze the data, that is the Darcy law in the laboratory (Klute and Dirksen, 1986) and an infiltration model in the field (Dohnal et al., 2010; Zhang, 1997).

BEST (Lassabatère et al., 2006) allows a field determination of the unsaturated hydraulic conductivity function according to the Brooks and Corey (1964) model. An independent estimation of near-saturated *K* values can be obtained by collecting an undisturbed soil sample in the field and using it in the laboratory for a sequence of 1D MDI runs followed by a CHP run. In the former case, the experiment is very simple but it is assumed that *K* decreases for smaller (more negative) pressure heads according to a pre-established law. In the latter case, the experiment is longer and it only yields some discrete K values, depending on the number of applied pressure heads. Comparing these two methods to obtain hydraulic conductivity is advisable. A reason is that BEST methods have been largely applied in many circumstances (Angulo-Jaramillo et al., 2019) but their predictions have been compared with soil hydraulic properties obtained with independent methods only in an overall limited number of investigations, not always with unequivocal results (Alagna et al., 2016; Bagarello and Iovino, 2012; Castellini et al., 2018). Supporting the usability of BEST methods could open new perspectives of practical interest. For example, BEST can potentially be used to also obtain an estimate of the macroscopic capillary length (Di Prima et al., 2020; White and Sully, 1987) and this soil parameter allows estimating bulb geometric variables for both buried and surface infiltration point sources (Baiamonte et al., 2024; Philip, 1984). Therefore, BEST experiments could be suggested for designing point irrigation systems taking into account spatial variability of soil hydraulic properties, with implications in terms of water saving and efficiency of water distribution.

The general objective of this investigation was to compare saturated and near-saturated hydraulic conductivity of a sandy-loam soil obtained with BEST, MDI and CHP methods. The specific objectives were to: i) compare soil hydraulic conductivity obtained with BEST when two different methods for estimating the saturated volumetric water content are used; ii) compare, for fixed pressure head values, the soil hydraulic conductivity obtained with field and laboratory application of the MDI; and iii) compare the soil hydraulic conductivity relationship obtained with BEST with that determined by using 1D MDI and CHP runs for the close to saturation region.

2.2.2 MATERIALS AND METHODS

2.2.2.1 Field site

The experimental site is located near Palermo (Western Sicily, Italy), in the area formerly known as Conca d'Oro (Golden Basin), where the soil is fertile and there is a good supply of freshwater (38°04'53.1" N and 13°25'08.4" E). In the field, there is a 30-year-old mandarin orchard planted with a spacing of 5 m × 5 m. The soil is not tilled and only mechanical weed control is performed. The altitude is 35 m a.s.l. and the surface is flat. The soil is a typic Rhodoxeralf with a depth of nearly 1 m and a moderate gravel content. According to the USDA classification, the soil texture, determined on two replicate soil samples, is sandy-loam with percentages of clay, cl = 16.6%, silt, si = 20.2% and sand, sa = 63.2%. The sampled area was of about 50 m^2.

At the beginning of the field campaign, disturbed soil samples were collected at three randomly chosen points within the sampling area and at two depths (0-5 and 5-10 cm) for each point. This soil was used to determine the gravimetric soil water content, w (kg/kg). The mean of these six w values was assumed to represent the antecedent gravimetric soil water content, w_i (kg/kg), at the field site since the sampled area was small and all field runs were carried out in a short time, that is in two consecutive days.

2.2.3 Experimental methods

2.2.3.1 *Beerkan infiltration experiments*

Small diameter (D = 0.08 m) rings were inserted on the soil surface to a depth of 0.01 m for the beerkan infiltration runs (Lassabatère et al., 2006). Rings were inserted manually or by gently using a rubber hammer and ensuring that the upper rim of the ring remained horizontal during insertion. The rings were relatively small since the soil surface layer was moderately stony and the small size of the ring simplified finding appropriate surfaces for soil sampling (**Fig. 1a**). A total of 15 infiltration runs were carried out in a single day at randomly selected locations. For each run, 20 water volumes, each of 57 mL, were successively poured in nearly 3 s for each volume on the confined infiltration surface. Therefore, with each volume, the initial ponded depth of water was equal to 11.3 mm. For each water volume (1^{st}, 2^{nd}, …, 20^{th}), the infiltration time was measured from water application to disappearance of all water, when the subsequent water volume was poured on the infiltration surface (Bagarello et al., 2021; Lassabatère et al., 2006).

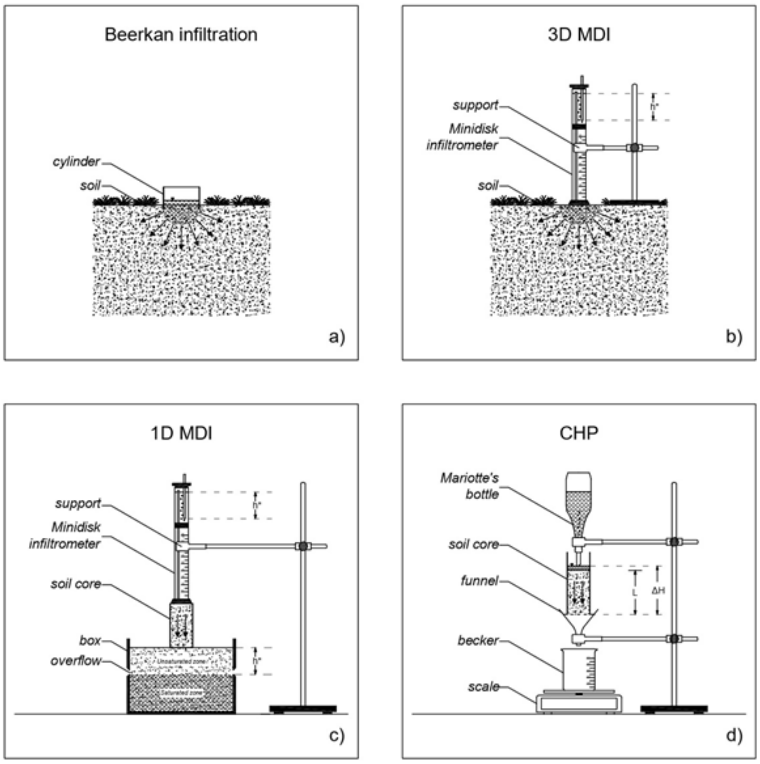

Fig. 1. Experimental setup for the field experiments with a) beerkan infiltration runs and b) three-dimensional mini-disk infiltrometer (3D MDI) and for the laboratory experiments with c) one-dimensional mini-disk infiltrometer (1D MDI) and d) constant-head permeameter (CHP)

Energy of the applied water was dissipated on the fingers of the hand in an attempt to minimize soil disturbance due to water application. A cumulative infiltration, I (mm), vs. time, t (h), curve, comprising 20 data points, was therefore obtained at each sampling point.

2.2.3.2 *Mini-disk field infiltration experiments*

Mini-disk infiltrometers (MDI; METER Group, 2021), having a disk diameter of 4.5 cm, were used to perform three-dimensional (3D) infiltration experiments in the field. In particular, the MDI was used to obtain 3D infiltration data for established pressure heads, h_0, equal to -6, -3 and -1 cm. Each individual infiltration process for an established h_0 value was carried out at a different sampling point, so that all infiltration curves were obtained under similar initial soil water content conditions. For a given h_0 value, the experiment was replicated at 15 different, randomly chosen, sampling points, for a total of 45 MDI infiltration runs in the field. The soil surface at a sampling point was gently leveled with a trowel and small amounts of loose soil were used when necessary to improve the contact between the device and the infiltration surface (**Fig. 1b)**. The MDI was fixed to a support to keep it still during the run and infiltration was measured until the reservoir emptied. Readings were taken visually at ≤1 min, during the first stage of the run, to 5 min intervals in the most advanced stages of the infiltration process. A cumulative infiltration curve, $I(t)$, was obtained at each sampling point.

2.2.3.3 *Mini-disk laboratory infiltration experiments*

Mini-disk infiltrometers were also used to perform 1D infiltration experiments in the laboratory. At this aim, undisturbed soil cores were collected at 15 randomly chosen points of the soil surface, after scraping out the first cm of soil, in 5-cm-inner diameter by 10-cm-high stainless-steel cylinders to determine unsaturated soil hydraulic conductivity, K (mm/h), in the laboratory. Each cylinder was inserted vertically into the soil by hammering gently on the top of the cylinder with a rubber hammer and progressively removing the surrounding soil up to the established depth to reduce disturbance during sampling. A nylon guard cloth was attached to the base of the core to prevent soil loss from the bottom of the sample. To improve the contact between the MDI and the soil, its surface was gently leveled in the laboratory with a sharp knife and, when necessary, small amounts of loose soil were applied to the top of the sample.

To establish a given h_0 value at the base of a soil core, a plastic box of 38 (length) × 17 (width) × 13 (height) cm^3 was filled with a bed of sand and several small holes (diameter = 1 cm) were made on the walls of the box at a downward distance $h^* = h_0$ (L) from the surface of the sand bed (**Fig. 1c**). A metal net was glued to each hole to prevent sand from escaping. Water was added to the box to form a saturated zone below the holes and an unsaturated zone above them. At hydrostatic equilibrium, the soil water pressure head at the surface of the sand bed was assumed to be equal to h_0. Different boxes were prepared, depending on the considered h_0 value (h_0 = -6, -3, -1 cm). The first established pressure head was h_0 = -6 cm. The soil cores were placed on the surface of the sand box and left to equilibrate for 24-48 hours. During this period, small volumes of water were periodically added to the box to maintain a constant h_0 value at the surface of the sand bed. Then, the MDI, set at this h_0 value, was placed on the soil surface by gently pressing the device and using a support to maintain it in place (**Fig. 1c**) and infiltration was measured. The small space between the walls of the cylinder and the porous plate of the device (5 mm) was not sealed to enable air to freely escape from the soil core during the run. After the run, the soil sample was left to freely drain for nearly 12 hours. Then, the same core was equilibrated for 48 hours at -3 cm and the MDI run at h_0 = -3 cm was carried out. Finally, after another 12 hours of free drainage, the core was equilibrated for 48 hours at -1 cm and the last MDI run at h_0 = -1 cm was performed. Generally, each individual run continued until the reservoir of the device emptied. For particularly slow runs, infiltration was stopped after 6 hours. Readings were taken visually at 1 to 5 min time intervals, with shorter intervals in the early stages of the run and for the higher (closer to zero) pressure heads. A run with a given h_0 value was replicated on 14 soil cores since a soil core broke during laboratory treatment. Immediately after each run with a given h_0 value, the soil columns were weighed to later determine the final gravimetric, w (kg/kg), soil water content.

2.2.3.4 *Laboratory constant-head permeameter experiments*

After the 1D MDI experiment at h_0 = -1 cm, the soil cores were left exposed to the air for a few days and then they were used for measuring the saturated soil hydraulic conductivity, K_s (mm/h), with the constant-head laboratory permeameter (CHP) method. Preliminary, these cores were saturated from the bottom according to Booltink and Bouma (2002). The saturation procedure lasted a total of 24 hours, during which, specifically, the soil cores were placed inside a plastic box and the water level was raised five times in 2 cm increments. A funnel was used to support the sample and to collect percolating water (**Fig. 1d**). A Mariotte bottle was used to establish the constant head of about 1 cm above the soil surface. The amount of water passing through the sample was measured by weighing the collected water volume at fixed intervals of 1 min. A Scout Pro portable electronic balance 4000 g connected to a CR1000 datalogger was used to automate the measurements. The average value of the flux density was calculated for a fixed time interval. The experiment was considered concluded when the flow approached a steady-state condition characterized by a near constant steady-state value, i.e. when the flux density appear nearly stable in 10 consecutive time intervals. At the end of the run, the soil was dried in an oven at 105° C for 48 h and the dry soil bulk density, ρ_b (g/cm^3), was determined from the oven-dry soil mass and the bulk soil volume.

2.2.4 Calculations

An estimate of the antecedent volumetric soil water content, θ_i (m^3/m^3), that is, the soil water content at the beginning of the field campaign of measurements and sampling, was obtained by the product between w_i and the mean of the 14 ρ_b values obtained after the CHP experiment.

The volumetric soil water content, θ (m^3/m^3), at the end of a 1D run with the MDI set at a given pressure head (h_0 = -6, -3 or -1 cm) was calculated from the gravimetric soil water content and the dry soil bulk density of the considered soil core.

The BEST-steady algorithm (Bagarello et al., 2014) was applied to estimate the soil water retention curve (van Genuchten, 1980) and the hydraulic conductivity function (Brooks and Corey, 1964) from the experimentally determined intercept, b_s (mm), and slope, i_s (mm/h), of the straight line fitted to the last three (I, t) data points describing steady-state conditions on the cumulative infiltration plot. The shape parameters of the retention and hydraulic conductivity curves were obtained from the particle-size distribution data (Lassabatère et al., 2006). BEST-steady requires antecedent, θ_i (m^3/m^3), and saturated, θ_s (m^3/m^3), volumetric soil water content that, in this investigation, were assumed not to change from point to point, since the sampled area was small and the beerkan runs were carried out in a single day. The value of θ_i was obtained from the w_i determination. To determine θ_s, it was considered that field-saturated soil water content is generally lower than porosity, ϕ (m^3/m^3), due to the presence of entrapped air (Reynolds and Elrick, 2002; Reynolds and Topp, 2008). According to several investigations, θ_s/ϕ can vary from 0.70 to 0.95 (Alagna et al., 2016; Dane and Hopmans, 2002; Gonzalez-Sosa et al., 2010; Mubarak et al., 2009a; Somaratne and Smettem, 1993; Verbist et al., 2013). Therefore, in this investigation, θ_s was estimated from the fitted line to the $\theta(h)$ values that were determined after the 1D MDI runs. The results of BEST application obtained with this estimate of θ_s were indicated as BEST_R (R indicating the use of water retention data) calculations. However, in practical application of BEST methods, θ_s is often set equal to the porosity, that is easily determined from the ρ_b measurements (Auteri et al., 2020; Bagarello et al., 2023; Mubarak et al., 2009b). Therefore, this approach was also applied for comparative purposes and these results were indicated as BEST_P (P indicating porosity).

For each MDI infiltration run in the field, the two-parameter infiltration model (Philip, 1957) was fitted to the cumulative infiltration, I (mm), vs. time, t (h), data by minimizing the sum of the squared residuals between the measured and the predicted I values (Lassabatère et al., 2006) to simultaneously estimate the C_1 (mm/h$^{1/2}$) and C_2 (mm/h) parameters of the model. The soil hydraulic conductivity value corresponding to a given pressure head was then calculated according to Zhang (1997) and Dohnal et al. (2010). The required soil water retention parameters for calculating K were taken from Castellini et al. (2018), who applied the evaporation method to characterize this field site in a previous investigation.

The 1D MDI measurements were made applying the same pressure head at the two ends of the soil core. Therefore, the assumption was that, at steady-state, a unit hydraulic gradient was established, i.e. the pressure head was the same throughout the soil core. Consequently, steady-state flux density was equivalent to the unsaturated soil hydraulic conductivity corresponding to the imposed pressure head, i.e. K_{-6}, K_{-3} or K_{-1} (mm/h), depending on the run.

Finally, the Darcy's law was applied to calculate K_s from the CHP laboratory data.

2.2.5 Data analysis

Three sets of K_s values (BEST_P, BEST_R, CHP method) and, for each negative pressure head, four sets of K values (BEST_P, BEST_R, 1D MDI, 3D MDI) were overall obtained. For each of these 15 datasets, the hypothesis that the data were normally distributed was never rejected according to the Lilliefors (1967) test at $P = 0.05$. Consequently, the arithmetic mean and the associated coefficient of variation, CV (%), were used to summarize each dataset.

Three different comparisons were carried out.

A comparison was established between the soil hydraulic conductivity values obtained with BEST_R and BEST_P. At this aim, a two-tailed paired t test at $P = 0.05$ was applied for K_s, K_{-1}, K_{-3} and K_{-6}. This comparison was made since i) field-saturated soil water content can be expected to be smaller than soil porosity (e.g., Reynolds and Elrick, 2002), ii) the BEST protocol assumes that θ_s is directly measured (Lassabatère et al., 2006), but iii) in many practical applications of BEST, θ_s is assumed to coincide with soil porosity (Bagarello et al., 2011; Mubarak et al., 2009b; Xu et al., 2009; Yilmaz et al., 2010).

The K values obtained with the 1D, and 3D MDI experiments were compared with each other. An F test and a two-tailed t test at $P = 0.05$ were applied for each h_0 value and hence for K_{-1}, K_{-3} and K_{-6}. Moreover, the cumulative empirical frequency distributions (CFDs) of the laboratory and field data were compared to succinctly visualize all the data for a given pressure head. This comparison was made because, to our knowledge, little is known about what to expect when exactly the same device, that is the MDI, is used to determine the unsaturated hydraulic conductivity of an undisturbed soil with methods which differ by the established infiltration process (3D, 1D) and the method of data analysis for determining K (fitting an infiltration model to the data, directly using the Darcy's law).

Finally, the K values obtained with BEST-steady were compared with those obtained by the CHP method (K_s) and the 1D MDI experiments (K_{-1}, K_{-3} and K_{-6}). Also in this case, F and two-tailed t tests at P = 0.05 were applied for each considered variable. The objective of this comparison was to evaluate differences between a direct measurement of hydraulic conductivity values at and near saturation using undisturbed soil samples and the Darcy's law with a field estimate of these values. This comparison was made since there is much practical interest for BEST methods (Angulo-Jaramillo et al., 2019) but the predicted soil hydraulic properties with this methodology have been compared with those obtained with other methods only in a few investigations.

2.2.6 RESULTS

2.2.6.1 Dry soil bulk density and soil water content

The mean dry soil bulk density, ρ_b, was equal to 1.329 g/cm^3 (coefficient of variation, CV = 4.0%; sample size, N = 14) and the mean antecedent gravimetric soil water content, w_i, was equal to 0.094 kg/kg (CV = 11.0%; N = 6). Consequently, the mean antecedent volumetric soil water content, θ_i, was of 0.125 m^3/m^3.

The relationship between θ and h was approximately linear in the $-6 \leq h \leq -1$ cm range with a coefficient of determination, R^2, of 0.69 (**Fig. 2**).

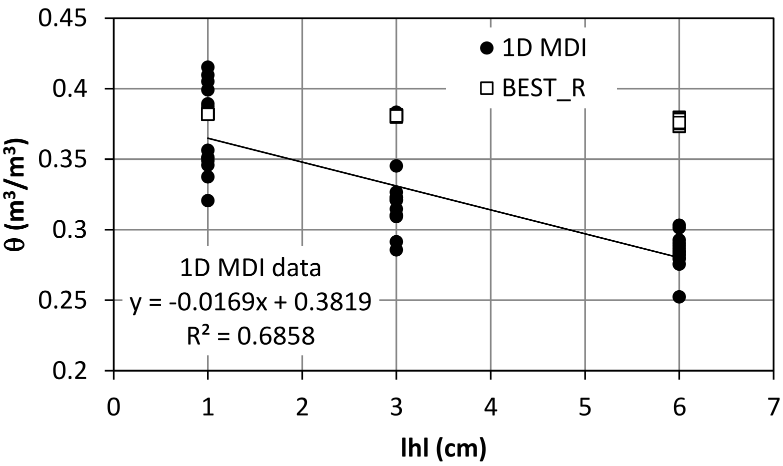

Fig. 2. Volumetric soil water content, θ, vs. pressure head, h, values i) obtained after the one-dimensional mini-disk infiltrometer (1D MDI) runs and ii) estimated with the BEST_R algorithm

The θ vs. h data were described a little better (R^2 = 0.73) by a power relationship but this relationship was not considered since it was not usable to estimate the θ value corresponding to a null pressure head. According to the fitted linear regression line, $\theta(0) = \theta_s$ was equal to 0.382 m^3/m^3. Therefore, θ_s = 0.382 m^3/m^3 was considered for the BEST_R calculations. The soil porosity, ϕ, obtained from the mean ρ_b value and assuming a soil particle density of 2.65 g/cm^3, was equal to 0.499 m^3/m^3. Therefore, θ_s = 0.499 m^3/m^3 was considered for the BEST_P calculations. The θ_s/ϕ ratio, equal to 0.77, was rather small but it appears plausible since it fell in the range of the θ_s/ϕ values found in the literature (Alagna et al., 2016; Dane and Hopmans, 2002; Gonzalez-Sosa et al., 2010; Mubarak et al., 2009a; Somaratne and Smettem, 1993; Verbist et al., 2013).

The θ_i/θ_s and θ_i/ϕ ratios were equal to 0.33 and 0.25, respectively. The θ_i/θ_s ratio was a little higher than the threshold of 0.25 recommended by Lassabatère et al. (2006) for applying BEST. However, wetter conditions can occur in practice (Xu et al., 2012) and Di Prima et al. (2016) showed that, with BEST-steady, the estimated soil hydrodynamic parameters can be expected to be accurate even in initially relatively wet conditions for many soils. Therefore, a θ_i/θ_s ratio of 0.33 was considered not to impede application of BEST in this investigation.

2.2.6.2 Infiltration and soil hydrodynamic parameters

Generally, the established beerkan infiltration processes appeared consistent with theory since the concavity of the *I* vs. *t* curves was faced downwards, denoting that the infiltration rates initially decreased during the run, and the *I* vs. *t* relationship assumed a nearly linear shape at longer times. Consequently, soil hydraulic conductivity data were obtained at each sampling point with both BEST_R and BEST_P (**Table 1**). Also in the case of the field MDI experiments, infiltration appeared consistent with theory since infiltration rates initially decreased during the run and they stabilized at longer times. The method by Zhang (1997) and Dohnal et al. (2010) was successfully applied to calculate K_{-1}, K_{-3} and K_{-6} at each sampling point (**Table 1**).

For the majority of the 1D laboratory runs with the MDI, the *I* vs. *t* relationship was nearly linear from the early stages of the infiltration process or it appeared to some extent concave upwards (**Fig. 3**).

Table 1. Summary statistics of the soil hydraulic conductivity values at saturation (K_s) and at pressure heads of -1 cm (K_{-1}), -3 cm (K_{-3}) and -6 cm (K_{-6}) obtained with two alternative BEST-steady algorithms (BEST_P; BEST_R), the constant-head permeameter (CHP) method, one-dimensional mini-disk infiltrometer runs in the laboratory (1D MDI) and three-dimensional mini-disk infiltrometer runs in the field (3D MDI)

Variable	Statistic	BEST_P	BEST_R	CHP	1D MDI	3D MDI
K_s (mm/h)	Min	19.8	14.3	167.9	-	-
	Max	172.5	124.1	686.2	-	-
	Mean	100.0 (a)	73.1 (a)(b)	406.1 (b)	-	-
	CV (%)	48.2	47.9	41.8	-	-
K_{-1} (mm/h)	Min	19.7	14.3	-	31.5	43.0
	Max	171.8	123.9	-	267.1	172.0
	Mean	99.2 (a)	72.8 (a)(b)	-	122.6 (b)c	100.8 c
	CV (%)	48.4	47.9	-	62.1	35.0
K_{-3} (mm/h)	Min	18.7	13.9	-	9.6	4.5
	Max	164.8	121.8	-	36.7	23.4
	Mean	90.9 (a)	70.1 (a)(b)	-	20.5 (b)(c)	15.2 (c)
	CV (%)	49.8	48.5	-	31.7	37.3
K_{-6} (mm/h)	Min	15.0	12.6	-	3.1	0.08
	Max	137.6	112.5	-	12.5	10.0
	Mean	64.5 (a)	59.6 (a)(b)	-	7.3 (b)(c)	4.1 (c)
	CV (%)	56.4	51.3	-	33.1	59.2

Sample size, N = 14 for the 1D MDI and CHP data and N = 15 for the BEST_R, BEST_P and 3D MDI data. *Min* = minimum value; *Max* = maximum value; *CV* = coefficient of variation. For a given variable, a comparison was established between two means followed by the same lower case letter. Values followed by the same letter not enclosed in parenthesis were not significantly different. Values followed by the same letter enclosed in parenthesis were significantly different. A two-tailed paired t test at P = 0.05 was applied for the BEST_R vs. BEST_P comparison. An F test and a two-tailed t test at P = 0.05 were applied for the following comparisons: i) BEST_R vs. CHP; ii) BEST_R vs. 1D MDI; and iii) 1D MDI vs. 3D MDI.

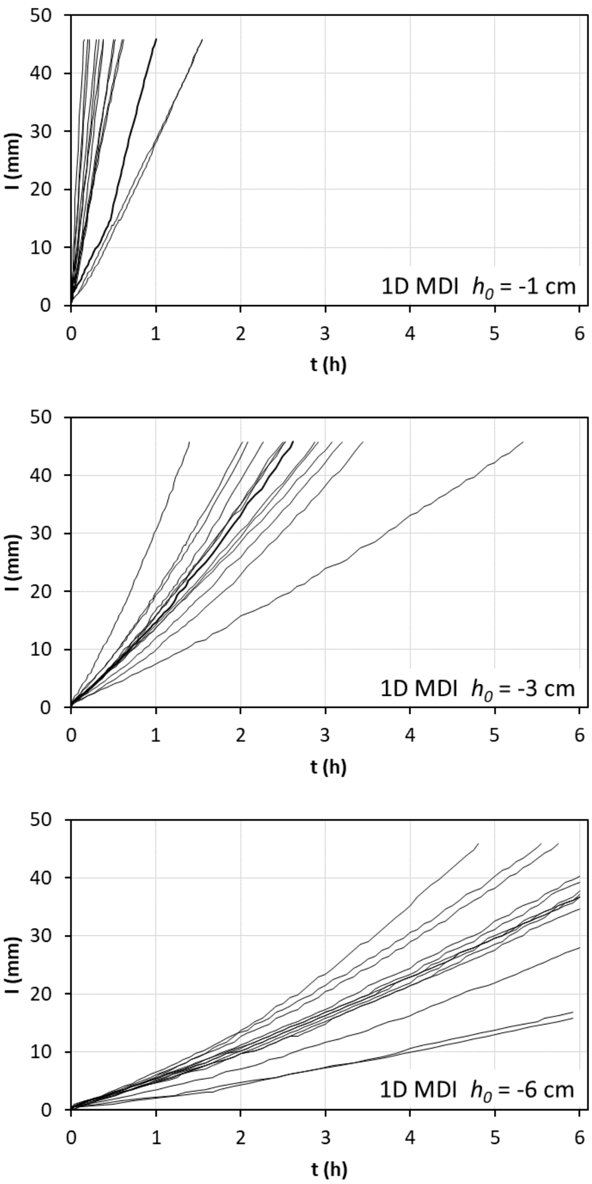

Fig. 3. Cumulative infiltration curves (I vs. t) obtained with the laboratory one-dimensional mini-disk infiltrometer runs (1D MDI) for the three values of the imposed pressure head (h_0 = -1, -3 and -6 cm)

Therefore, infiltrations rates, ir (L/T), were nearly stable during the run or they stabilized after a phase of increasing values. For each run, the stabilized ir value obtained by linear regression of the last I vs. t data points, ir_s, was compared with the slope of the linear regression line fitted to all I vs. t data and forced to pass through the origin of the axes, sl. A similarity between ir_s and sl was expected when the I vs. t relationship was nearly linear for the entire infiltration process whereas $ir_s > sl$ denoted an upwards concavity of this relationship (Bondì et al., 2023). On average, ir_s and sl differed by 1.12, 1.22 and 1.27 times for h_0 = -1, -3 and -6 cm respectively. Moreover, a linear regression analysis between sl and ir_s was carried out (**Fig. 4**).

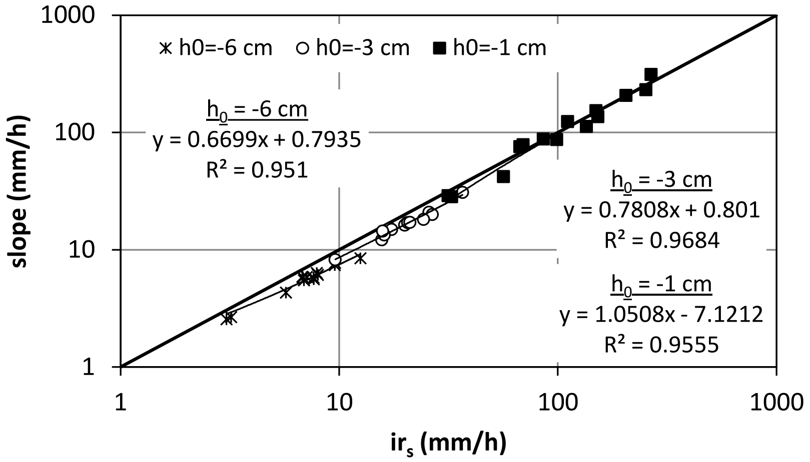

Fig. 4. Comparison between the *sl* and ir_s estimates of the steady-state infiltration rate (*sl* = slope of the linear regression line fitted to all the cumulative infiltration, *I*, vs. time, *t*, data points and forced to pass through the origin of the axes; ir_s = stabilized infiltration rate obtained by linear regression of the last *I* vs. *t* data points) for the 1D MDI runs and the three values of the established pressure head (h_0 = -6, -3 and -1 cm)

According to the calculated 95% confidence intervals for the intercept and the slope, the linear regression line between these two variables did not differ from the identity line by jointly considering all pressure heads (-7.42 – 0.42 and 0.98 – 1.07, respectively) and also for h_0 = -1 cm (-27.5 – 13.2 and 0.91 – 1.19). However, it differed from the identity line for both h_0 = -3 cm (-1.10 – 2.70 and 0.69 – 0.87) and h_0 = -6 cm (0.06 – 1.53 and 0.57 – 0.77). Therefore, a smaller h_0 value produced a greater upwards concavity. However, taking into account that the estimate of the steady-state infiltration rate coincides with the estimate of *K* for the 1D MDI experiment and that an error of 25% can be considered negligible even in more stringent conditions, that is when the data are free of any experimental error (Reynolds, 2013), the detected concavity did not introduce any relevant uncertainty on estimation of *K*. Therefore, all infiltration runs were included in the developed *K* dataset for each established pressure head and, for each run, *K* was assumed to coincide with ir_s (**Table 1**).

All CHP experiments were successful and they yielded a K_s value for each sampling point (**Table 1**).

2.2.7 Comparisons

2.2.7.1 *BEST-R vs. BEST-P*

Regardless of h, higher K values were obtained with BEST_P as compared with BEST_R (**Table 1**) but differences decreased monotonically as the pressure head became smaller (more negative). In particular, two corresponding estimates of K differed by 1.37, 1.36, 1.30 and 1.08 times for h = 0, -1, -3 and -6 cm, respectively. Relative variability of the K values was nearly independent of the saturated soil water content estimation approach.

In the following, the BEST_R calculations were considered for the comparison with other estimates of K for the following reasons: i) air is usually entrapped in a porous medium when it is saturated by downward infiltrating water under ponded conditions (e.g., Reynolds and Elrick, 2002), such as in the case of the beerkan infiltration runs, ii) use of θ_s is conceptually more consistent with the original BEST method (Lassabatère et al., 2006), and iii) using BEST with a saturated soil water content smaller than ϕ can be expected to represent the best choice to satisfactorily reproduce laboratory measured soil water retention values (Alagna et al., 2016).

2.2.7.2 *Field vs. laboratory MDI experiments*

The 1D MDI experiment yielded higher K values than the 3D one by 22% for h_0 = -1 cm, 35% for h_0 = -3 cm and 77% for h_0 = -6 cm (**Table 1**). Differences between two corresponding datasets were statistically significant for the two lowest pressure heads but not for the highest h_0 value. In the field, the highest relative variability of the data was detected for the smallest pressure head. Instead, in the laboratory, relative variability was highest for the highest pressure head. Consequently, the 1D MDI K values were 1.8 times more variable than the 3D MDI ones for h_0 = -1 cm (high, for the 1D data, vs. medium, for the 3D data, variation) (Warrick, 1998) and 1.8 times less variable for h_0 = -6 cm (medium vs. high variation). Relative variability of the two estimates of K was similar, and medium, for h_0 = -3 cm (CV = 32-37%). For both h_0 = -6 and -3 cm, the cumulative empirical frequency distribution (CFD) of the field K values was entirely located to the left of the one corresponding to the laboratory values (**Fig. 5**). For h_0 = -1 cm, the two CFDs intersected with each other since the laboratory method yielded both the highest and the lowest of the overall determined K values.

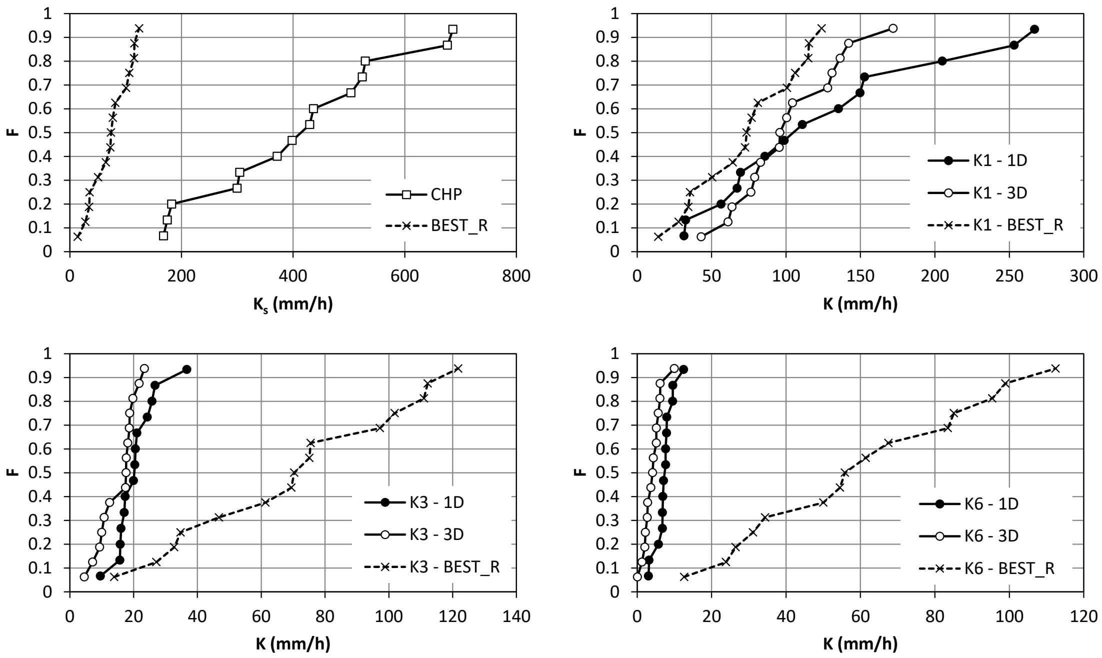

Fig. 5. Cumulative empirical frequency distribution of the saturated, K_s, and near-saturated, $K1$ (corresponding to a pressure head, h = -1 cm), $K3$ (h = -3 cm) and $K6$ (h = -6 cm), soil hydraulic conductivity values obtained with different methods (BEST_R; CHP: constant-head laboratory permeameter; 1D: laboratory mini-disk infiltrometer; 3D: field mini-disk infiltrometer)

2.2.7.3 *BEST_R vs. CHP and 1D MDI experiments*

Regardless of the considered variable (K_s, K_{-1}, K_{-3}, K_{-6}), the differences between the field (BEST_R) and the laboratory (CHP and 1D MDI) estimates of K were statistically significant (**Table 1**). The CHP method yielded a 5.6 times higher K_s value than BEST_R and the lowest laboratory value of K_s was 1.4 times larger than the highest K_s value obtained in the field (**Fig. 5**). The 1D MDI estimates of K_{-1} were 1.7 times larger than those obtained with BEST_R. For K_{-3} and K_{-6}, BEST_R yielded higher estimates than the 1D MDI by 3.4 and 8.1 times, respectively. In both cases, K increased monotonically as the pressure head became less negative (**Table 1**), but at a very different rate for the two tested methods (**Fig. 6**). In particular, the K_s/K_{-6} ratio was equal to 1.23 with BEST_R and 55.4 with the laboratory soil cores. Therefore, BEST_R predicted a nearly flat soil hydraulic conductivity curve for $h \geq$ -6 cm. This shape was not consistent with the K data obtained in the laboratory that instead suggested that even a small variation of h induced large changes of K. The BEST_R $K(h)$ curves intersected the data obtained in the laboratory (**Fig. 6**).

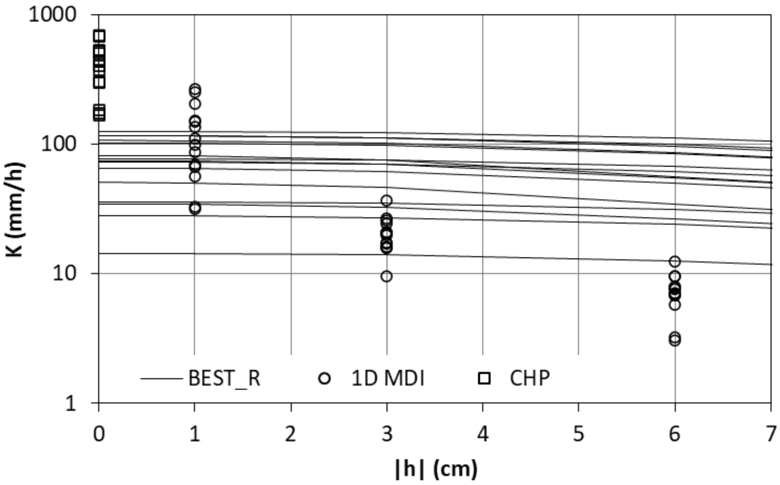

Fig. 6. Soil hydraulic conductivity curves, *K(h)*, estimated by the BEST_R algorithm, saturated soil hydraulic conductivity, K_s, obtained with the constant-head permeameter (CHP) method, and *K* values for the -6, -3 and -1 cm pressure head, *h*, values obtained with the 1D MDI runs

In particular, the former curves were positioned below the laboratory *K* data for $h = 0$ and above them for $h \leq -3$ cm. A certain overlap between the curves obtained with BEST_R and the *K* values measured in the laboratory was detected for $h = -1$ cm. Relative variability of K_s did not differ appreciably between BEST_R and the CHP method and it was medium in both cases (**Table 1**). In unsaturated conditions, BEST_R predicted nearly constant *CV* values that instead decreased, although not exactly monotonically, from high to low pressure heads with the 1D MDI experiments. According to Warrick (1998), relative variability of the unsaturated *K* values was generally medium, with two exceptions (BEST_R, $h = -6$ cm; 1D MDI, $h = -1$ cm), in which variation was high. Even in this case, however, the *CV* values were not appreciably greater than the value that discriminates between a medium and a high variation ($CV = 50\%$).

2.2.8 DISCUSSION

2.2.8.1 Estimating saturated soil water content for the BEST calculations

The choice of the θ_s value to be used for the BEST calculations is expected to be important to recognize a correspondence between estimated and independently measured water retention values (Alagna et al., 2016) but it seems that the same cannot be said with reference to soil hydraulic conductivity. The reason is that the estimates of K_s with BEST_P and BEST_R differed by 1.4 times (**Table 1**) which can be considered a rather small difference (Elrick and Reynolds, 1992). Moreover, for another sandy-loam soil, Di Prima et al. (2017) reported that changing the estimate of θ_s (porosity instead of the field measured value) implied that the K_s estimates differed by only 1.2 times. Probably, the effect was smaller than that detected in this investigation since our θ_s/ϕ value was equal to 0.77 whereas it was 0.85 (i.e., closer to one) in the study by Di Prima et al. (2017).

This investigation also demonstrated that the effect of the used approach for estimating θ_s decreased for more negative pressure heads. To explain this last result, that apparently was not discussed so far, it has to be noted that, with the applied BEST-steady algorithm, K_s and K are given by (Bagarello et al., 2014):

$$K_s = \frac{C\, i_s}{\frac{\gamma\, b_s}{r(\theta_s - \theta_i)} + C} \tag{1a}$$

$$K(\theta) = K_s \left(\frac{\theta}{\theta_s}\right)^{\eta} \tag{1b}$$

where i_s (L/T) and b_s (L) are the slope and the intercept, respectively, of the linear regression line fitted to last data points that describe steady-state conditions on the I vs. t plot, C is a constant that, for an initial soil hydraulic conductivity, $K_i << K_s$, does not depend on the soil water content, θ, and is equal to 0.639, γ is a parameter for geometrical correction of the infiltration front shape, usually assumed to be equal to 0.75, r (L) is the radius of the source and η is a shape parameter. An increase of θ_s (e.g., using ϕ instead of $\theta_s < \phi$) implies a smaller denominator in eq.(1a) and hence a higher estimate of K_s (Di Prima et al., 2017). According to eq.(1b), the increase of K_s is partially compensated by a decrease of θ/θ_s, which explains why the estimate of θ_s had a smaller impact on the K calculations for more negative pressure head values.

In any case, when $\theta_s < \phi$, the BEST_P calculations appear conceptually less reliable than the BEST_R ones since, in the former case, infiltration parameters (i_s, b_s) obtained in a soil that contains air are treated as if they had been obtained in a completely saturated porous medium.

2.2.8.2 Upwards concavity of cumulative infiltration for the laboratory mini-disk runs

An attempt to explain the unexpected upwards concavity of the $I(t)$ curves obtained in the laboratory with the 1D MDI runs (**Fig. 3**) was made and at least three possible reasons were identified.

A possible reason was that the contact between the device and the infiltration surface improved during the run, notwithstanding that this surface appeared leveled and smoothed before firmly putting the MDI in place. In other terms, the actual infiltration surface was smaller than expected at the beginning of the run and then it became larger. Non-uniform wetting even under controlled laboratory conditions on repacked soil columns was reported by Close et al. (1998). These authors also concluded that contact problems can be particularly noticeable in the case of low established pressure heads. There was agreement between this suggestion and our results since a smaller h_0 value produced a greater upwards concavity.

An upwards concave cumulative infiltration curve can be obtained when the soil is initially water repellent but water repellency decreases during infiltration (Alagna et al., 2019). Water repellency should not have a strong effect on infiltration in initially wet soil conditions (de Jonge et al., 1999; Dekker et al., 2001) that were those of this experiment given that, at the beginning of a run, the base of a soil core was equilibrated at not less than -6 cm of water, However, this interpretation was not excluded because other authors also signaled water repellency phenomena in initially relatively wet soil conditions (Carrick et al., 2011).

According to Faybishenko (1995), air can initially be entrapped in the smallest soil pores but, under the influence of capillary forces, water is drawn into these pores so that the entrapped air is displaced into the largest pores. Therefore, another possible interpretation was that some air was entrapped in the smallest soil pores at the beginning of the infiltration run and then it escaped. Infiltration rates increased during the run with the smallest pressure head because the hydraulically active pores were small and they initially contained some entrapped air. This entrapped air did not affect appreciably infiltration rates at the highest pressure head since, in this case, the hydraulically active pores were large enough not to be blocked by air escaping from the smallest pores.

Of course, a less uncertain interpretation of the detected concavity would likely require additional experimental investigations that should particularly be carried out for small pressure heads. However, it does not seem that these investigations constitute a priority in a practical perspective since the detected concavities were not so appreciable as generating great doubts on the reliability of the K estimates.

An upward concavity was not observed in the field since, in this case, infiltration rates tended to stabilize after a transient decreasing stage. Therefore, it appeared plausible to believe that: i) the contact between the device and the soil was better in the field, probably because the leveling of the contact surface was easier in the absence of any confinement of the infiltration surface; ii) in the field, possible soil water repellency effects were masked by lateral capillarity forces that were not active in the laboratory; and/or iii) entrapped air effects were less noticeable in the field since air could escape more easily due to the lack of any confinement of the sampled soil volume. Moreover, infiltration occurred under larger pressure head gradients in the field than in the laboratory. Perhaps, even this difference contributed to determine a different shape of the experimental I vs. t relationship.

2.2.8.3 Comparing mini-disk experiments

With reference to saturated hydraulic conductivity of undisturbed soils, differences from a reference value by nearly 60% (Yilmaz et al., 2023) or by a factor of two or three (Elrick and Reynolds, 1992) could be considered negligible, at least for some practical purposes. Assuming that these suggestions also apply to the case of the near-saturated soil hydraulic conductivity, it could be suggested that the 1D and 3D MDI experiments overall yielded similar results, particularly close to saturation (**Table 1**). However, another interpretation was that the 1D experiment tended to generally yield higher *K* values than the 3D experiment, more noticeably for the smallest pressure heads.

Obtaining a larger *K* value with a 1D experiment than a 3D one could be due to a significant contribution to total flow of macropores extending from the surface to the bottom of the soil sample (Bagarello et al., 2007) or to an overestimation of the steady-state 1D flow rate (Bagarello et al., 2010). However, explaining the differences between the 1D and 3D data as a consequence of preferential flow phenomena did not appear convincing since the largest discrepancies were detected with the lowest established pressure head, which did not activate the largest voids in the sample.

Instead, it can be supposed that 1D K > 3D K was obtained since ir_s (slope of the stabilized part of the I vs. t relationship) was used instead of sl (slope of the linear regression line fitted to all the I vs. t data points) for calculating 1D K and $ir_s > sl$ was obtained for the smallest pressure heads (**Fig. 4**). Although this interpretation could find a numerical support, there were physical reasons for using ir_s instead of sl. The assumption that K coincides with the steady-state infiltration rate can only be made if the flow process is stable. The last part of each infiltration run appeared clearly linear in all cases (**Fig. 3**) denoting that, starting from a certain point, the process stabilized. Instead, considering a not perfectly stable process as if it was stable, i.e. using sl for the K calculations, would have made the reliability of the estimated slopes more questionable in the perspective to determine K.

It was also deemed unlikely that differences were attributable to soil compaction during sampling since, in this case, the opposite result (3D K > 1D K) would have been expected.

An effect of the methods used to determine *K* from the MDI infiltration data was not completely excluded since a dependence of the *K* values on the applied calculation method is documented in the literature (Dohnal et al., 2010; Jacques et al., 2002; Logsdon and Jaynes, 1993). Nor can it be ruled out that differences occurred as a consequence of spatial variability of soil hydrodynamic properties at the field site, given that different points were sampled with the 3D and 1D MDI runs. Moreover, it could also be considered that the 1D data were expressive of a vertical infiltration process whereas the 3D data were representative of a combined vertical and lateral flow process. Therefore, forcing water to move vertically perhaps reduced the overall tortuosity of the flow paths, especially with reference to the smallest active pores given that the differences between the 1D and 3D results increased as h_0 decreased.

2.2.8.4 Field vs. laboratory determination of soil hydraulic conductivity

According to the BEST_R, CHP and 1D MDI data (**Table 1** and **Fig. 6**), the laboratory prediction of K_s was appreciably larger than the field one, that is by 5.6 times. For unsaturated soil conditions, the K estimates were nearly independent of h with BEST_R but they decreased appreciably with smaller pressure heads according to the MDI data. Consequently, the two approaches yielded relatively similar results for h = -1 cm (difference by 1.7 times) but BEST_R predicted appreciably higher K values than the MDI in more unsaturated conditions (by 3.4 and 8.1 times for h = -3 and -6 cm, respectively).

A possible reason of the differences between the laboratory and the field determination of K_s was that the laboratory experiment actually yielded excessively high K_s values. It would not be the first time that soil cores yield higher (even by orders of magnitude) K_s values than those obtained by establishing in the field an infiltration process on an initially unsaturated soil (e.g., Bagarello and Provenzano, 1996; Jačka et al., 2014; Paige and Hillel, 1993; Reynolds et al., 2000). High K_s values could depend on rapid pipe flow through worm holes, old root channels and cracks that extended through the core (Reynolds et al., 2000) or on cracks and fissures created during the collection procedure (Jačka et al., 2014). According to Paige and Hillel (1993), discontinuous macropores in the field can become continuous in a particular soil sample. It cannot be said without any doubt that pipe flow phenomena occurred in this investigation since the length of the soil cores (10 cm) was appreciably greater than that considered in other investigations (e.g. 3 cm in Paige and Hillel, 1993) and continuity of large pores between the upper and the bottom ends of the soil sample appears less probable with a longer sample. On the other hand, it could also be suspected that these cavities may have formed during the experiment given that K_s was measured after three previous K determinations with the MDI, that is, after an intense use of the sample albeit with all possible precautions.

On the other hand, it cannot ever be ruled out that the K_s values obtained with the field experiment were too low. In this investigation, there were some signs that this circumstance occurred even if these signs were not unequivocal. In particular, the 1D MDI experiments (but also the 3D MDI ones) yielded $K_{-1} > K_s$ (**Table 1**), which is physically impossible. This result did not necessarily represent a proof that the field K_s values were too low since it could also be a consequence of spatial variability of soil hydrodynamic properties (e.g., Logsdon and Jaynes, 1996; Prieksat et al., 1994). In other words, these differences occurred because the points sampled with the beerkan runs were inherently less permeable than those sampled for the MDI runs. However, a rather large number of runs were carried out with each method on an overall small area, according to existing guidelines (Reynolds et al., 2002), and this circumstance induced to be cautious in proposing an interpretation exclusively based on spatial variability considerations. Instead, the conclusion that $K_{-1} > K_s$ signaled that BEST_R yielded too low K_s values appeared more convincing than, or at least as plausible as, the suggestion that particularly low permeability points were sampled with the beerkan runs but not with the MDI experiments.

One of the possible reasons why field K_s values were too low was that some air was entrapped in the soil during the ponding infiltration runs (Lee et al., 1985; Mohanty et al., 1994). Indeed, there were many opportunities to induce some air entrapment in the sampled soil volume since the beerkan run was performed in accordance with Lassabatère et al. (2006) and hence by adding a new water volume when the previous water volume had completely infiltrated and the infiltration surface was entirely exposed to air (Bagarello et al., 2021). Field-saturated soil hydraulic conductivity values can be expected to be two or even more times smaller than completely saturated soil values (Gupta et al., 1993; Jačka et al., 2014; Reynolds and Elrick, 1987). Moreover, the results of this investigation were consistent with the conclusion by Sakaguchi et al. (2005) that the saturated hydraulic conductivity measured on a soil containing entrapped air can be smaller than the unsaturated hydraulic conductivity close to saturation.

Another possible reason why the field K_s values were too small was that repeatedly pouring water on an initially unsaturated soil altered the upper soil layer that became progressively less conductive. Mechanical impact of the applied water volumes was minimized by applying water close to the infiltration surface and dissipating the energy of the water on the fingers of the hand. However, some slaking perhaps occurred in the early stages of the run since water was suddenly applied on an initially unsaturated soil (Le Bissonnais, 1996). Consequently, pore sizes decreased and flow paths became perhaps more tortuous. Slaking did not occur in the laboratory experiments since, in this case, the soil was initially wetted slowly from the bottom.

Finally, another possible explanation for low K_s values was that soil structure collapsed to some extent during ring insertion. However, this explanation appeared rather unrealistic since the ring was inserted to a very short depth in the soil (1 cm) and with great caution.

With reference to the unsaturated soil hydraulic conductivity, a similar result to that of this investigation was obtained by Alagna et al. (2016) in a comparison, for a loam soil, between BEST and the classical tension infiltrometer (TI). In particular, differences between corresponding K values were relatively small (by 1.2-3.0 times, depending on the BEST algorithm) for h = -1 cm but BEST yielded 9 to 35 times higher K values than the TI for $-12 \leq h \leq -3$ cm. According to these authors, this difference occurred because the assumed hydraulic conductivity function in BEST did not reproduce satisfactorily the changes in the soil pore system for h < -1 cm. In other words, representation of the soil as a single permeability system was responsible of the poor matching between the two tested methods.

Even in this investigation, differences between the predicted and the measured K values for a given pressure head appeared to depend on the inability of BEST to describe the soil hydraulic properties close to saturation. In particular, the experimental θ values decreased appreciably as h decreased from -1 to -6 cm (from 0.371 to 0.284 m^3/m^3) but the BEST_R predictions of θ varied only minimally in this range of h values (from 0.382 to 0.377 m^3/m^3; **Fig. 2**). The experimental and modelled θ values were rather similar for h = -1 cm and an approximate similarity was also detected with reference to the corresponding estimates of K (**Table 1** and **Fig. 6**). Moreover, plotting K against θ (**Fig. 7**) showed that i) regardless of the imposed h_0 value, the 1D MDI experiment yielded increasing K values with θ, as expected; and ii) the K values predicted with BEST_R fell in a zone of the figure which indicated a certain correspondence between the laboratory and the field K data for similar θ values.

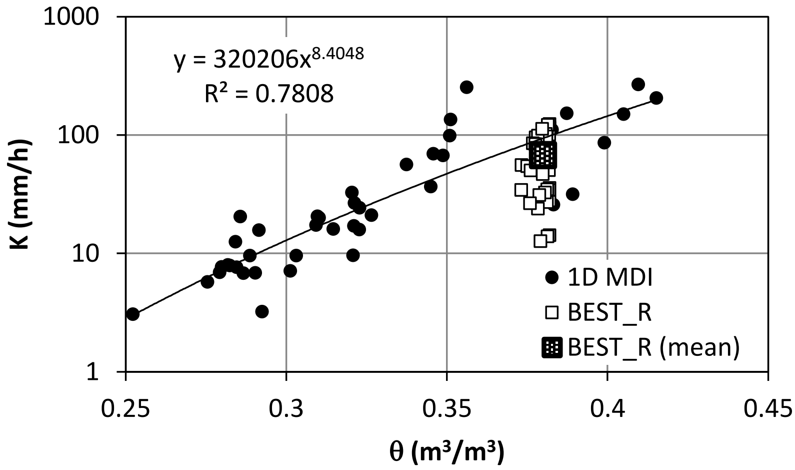

Fig. 7. Relationships between soil hydraulic conductivity, K, and volumetric soil water, θ

In particular, with BEST_R, the means of θ and K were equal to 0.380 m^3/m^3 and 67.5 mm/h, respectively. According to the fitted regression line to the K(1D MDI) vs. θ data, $K_{\theta=0.38}$ was equal to 94.0 mm/h, that is larger than the BEST_R prediction by 39.3%. This difference was rather small (Elrick and Reynolds, 1992; Yilmaz et al., 2023) and it suggested that the BEST_R predictions of K and the 1D MDI values were of the same order of magnitude when the soil water content was the same. In other words, BEST_R overestimated K at small pressure heads since it was unable to predict the same decrease in θ that was detected experimentally. This result reinforces the need to define the setup of BEST-2K, that extends the existing BEST methods for use in dual-permeability soils (Lassabatère et al., 2014, 2019).

In this investigation, standard approaches were applied to determine K with the different devices and experimental methodologies, meaning that different representations of the $K(h)$ relationship were considered. For example, the Brooks and Corey (1964) model was assumed for BEST whereas no assumptions were made with the 1D MDI since individual data points (i.e., a K value for a pre-established h value) were obtained by direct application of the Darcy law. Moreover, a specific BEST algorithm was used to analyze the infiltration data collected by the beerkan runs but other algorithms are available in the literature (Lassabatère et al., 2006; Yilmaz et al., 2010). Future developments of this investigation should also explore these methodological issues taking into account that soil hydraulic conductivity may be expected to vary with the adopted model (Lenhard et al., 1989; Mubarak et al., 2009a; Valiantzas, 2011) and different BEST algorithms could yield different estimates of the soil hydrodynamic properties, depending on the specific circumstances (Angulo-Jaramillo et al., 2016, 2019).

2.2.9 CONCLUSIONS

This investigation contributed to expand, for a sandy-loam soil, our knowledge on different simple field and laboratory methods usable to determine the saturated and near-saturated soil hydraulic conductivity.

Using, for the BEST (Beerkan Estimation of Soil Transfer parameters) calculations, the soil porosity, ϕ, instead of the true saturated soil water content, θ_s, yields higher estimates of soil hydraulic conductivity but differences decrease in more unsaturated soil conditions. It is recommended to make use of θ_s since the established beerkan infiltration process will likely give rise to air entrapment in the soil. In practice, however, using ϕ instead of θ_s could be expected not to introduce large uncertainties in soil hydraulic conductivity estimation.

Pooling the data from the unconfined MDI (mini-disk infiltrometer) infiltration measurements performed in the field and the confined MDI measurements performed in the laboratory appears a possible way to proceed in the perspective to obtain a mean K value for close to saturation soil with reference to an area of interest. The validity of this conclusion becomes weaker in more unsaturated conditions but even in this case it can be expected that only a moderate noise will be introduced in the estimate of K.

In the close to saturation region, the soil hydraulic conductivity function predicted with BEST does not generally reproduce direct measurements of K obtained in the laboratory at different pressure heads by a direct application of the Darcy's law with the MDI and the CHP (constant-head permeameter) method. In particular, the expectation could be that BEST will yield a too small K_s value and too high K values for the more unsaturated conditions. However, a satisfactory correspondence between BEST and laboratory determination of K can be expected for the same soil water content.

Supporting these conclusions with other comparisons is of course necessary. Based on the experience gained in this study, improving the organization of the experiment could be advisable even if delineating these improvements is not easy. For example, spatial variability of soil hydrodynamic properties was suggested to perhaps influencing to some degree some of the established comparisons. In principle, spatial variability effects could be prevented or appreciably reduced by applying all measurement methods at a single sampling point according for example to the sequence i) 3D MDI, ii) beerkan run, iii) collection of the undisturbed soil core, iv) 1D MDI and, finally, v) CHP application. In this case, all measurements refer to nearly the same soil volume. However, it cannot be said that this is the best choice, since the experiment will become unavoidably longer, for example because the soil needs to dry out after the 3D MDI run and before performing the beerkan run. Moreover, repeated solicitations on exactly the same soil volume could promote soil structure alterations having an impact that would be difficult to detect. Therefore, a possible alternative could be to reduce uncertainties attributable to soil spatial variability by performing more runs for each applied measurement method. However, interpreting differences between methods does not solve any problem since the most appropriate measurement method for an intended use of the data has to be chosen. A way to reach this objective could be comparing a monitored soil hydrological process with the corresponding one predicted by a mechanistic model and the measured soil hydrodynamic properties.

REFERECES

Alagna, V., Bagarello, V., Di Prima, S., Giordano, G., Iovino, M., 2013. A simple field method to measure the hydrodynamic properties of soil surface crust. Journal of Agricultural Engineering 44. https://doi.org/10.4081/jae.2013.(s1):e14

Alagna, V., Bagarello, V., Di Prima, S., Iovino, M., 2016. Determining hydraulic properties of a loam soil by alternative infiltrometer techniques. Hydrol Process 30. https://doi.org/10.1002/hyp.10607

Alagna, V., Iovino, M., Bagarello, V., Mataix-Solera, J., Lichner, L., 2019. Alternative analysis of transient infiltration experiment to estimate soil water repellency. Hydrol Process 33. https://doi.org/10.1002/hyp.13352

Angulo-Jaramillo, R., Bagarello, V., Di Prima, S., Gosset, A., Iovino, M., Lassabatère, L., 2019. Beerkan Estimation of Soil Transfer parameters (BEST) across soils and scales. J Hydrol (Amst). https://doi.org/10.1016/j.jhydrol.2019.06.007

Angulo-Jaramillo, R., Bagarello, V., Iovino, M., Lassabatère, L., 2016. Infiltration measurements for soil hydraulic characterization, Infiltration Measurements for Soil Hydraulic Characterization. https://doi.org/10.1007/978-3-319-31788-5

Assouline, S., Narkis, K., 2011. Effects of long-term irrigation with treated wastewater on the hydraulic properties of a clayey soil. Water Resour Res 47. https://doi.org/10.1029/2011WR010498

Auteri, N., Bagarello, V., Concialdi, P., Iovino, M., 2020. Testing an adapted beerkan infiltration run for a hydrologically relevant soil hydraulic characterization. J Hydrol (Amst) 584. https://doi.org/10.1016/j.jhydrol.2020.124697

Autovino, D., Rallo, G., Provenzano, G., 2018. Predicting soil and plant water status dynamic in olive orchards under different irrigation systems with Hydrus-2D: Model performance and scenario analysis. Agric Water Manag 203. https://doi.org/10.1016/j.agwat.2018.03.015

Bagarello, V., Caltabellotta, G., Concialdi, P., Iovino, M., 2023. Comparing two methods to perform a beerkan infiltration run in a loam soil at different dates. J Hydrol (Amst) 617. https://doi.org/10.1016/j.jhydrol.2023.129095

Bagarello, V., Caltabellotta, G., Iovino, M., 2021. Water transmission properties of a sandy-loam soil estimated with Beerkan runs differing by the infiltration time criterion. Journal of Hydrology and Hydromechanics 69. https://doi.org/10.2478/johh-2021-0010

Bagarello, V., Castellini, M., Iovino, M., 2007. Comparison of unconfined and confined unsaturated hydraulic conductivity. Geoderma 137, 394–400. https://doi.org/10.1016/j.geoderma.2006.08.031

Bagarello, V., Castellini, M., Iovino, M., Sgroi, A., 2010. Testing the concentric-disk tension infiltrometer for field measurement of soil hydraulic conductivity. Geoderma 158, 427–435. https://doi.org/10.1016/j.geoderma.2010.06.018

Bagarello, V., David, S.M., 2020. Run duration effects on the hydrodynamic properties of a loam soil estimated by steady-state infiltration methods. Journal of Agricultural Engineering 51. https://doi.org/10.4081/jae.2020.1075

Bagarello, V., Di Prima, S., Iovino, M., 2014. Comparing Alternative Algorithms to Analyze the Beerkan Infiltration Experiment. Soil Science Society of America Journal 78. https://doi.org/10.2136/sssaj2013.06.0231

Bagarello, V., Di Prima, S., Iovino, M., Provenzano, G., Sgroi, A., 2011. Testing different approaches to characterize Burundian soils by the BEST procedure. Geoderma 162. https://doi.org/10.1016/j.geoderma.2011.01.014

Bagarello, V., Iovino, M., 2012. Testing the BEST procedure to estimate the soil water retention curve. Geoderma 187–188. https://doi.org/10.1016/j.geoderma.2012.04.006

Bagarello, V., Provenzano, G., 1996. Factors affecting field and laboratory measurement of saturated hydraulic conductivity. Transactions of the American Society of Agricultural Engineers 39. https://doi.org/10.13031/2013.27493

Baiamonte, G., Alagna, V., Autovino, D., Iovino, M., Palermo, S., Vaccaro, G., Bagarello, V., 2024. Influence of soil hydraulic parameters on bulb size for surface and buried emitters. Agric Water Manag 295, 108756. https://doi.org/10.1016/J.AGWAT.2024.108756

Basile, A., Albrizio, R., Autovino, D., Bonfante, A., De Mascellis, R., Terribile, F., Giorio, P., 2020. A modelling approach to discriminate contributions of soil hydrological properties and slope gradient to water stress in Mediterranean vineyards. Agric Water Manag 241. https://doi.org/10.1016/j.agwat.2020.106338

Bondì, C., Concialdi, P., Iovino, M., Bagarello, V., 2023. Assessing short- and long-term modifications of steady-state water infiltration rate in an extensive Mediterranean green roof. Heliyon 9. https://doi.org/10.1016/j.heliyon.2023.e16829

Booltink, H.W.G., Bouma, J., 2002. Steady flow soil column method., in: Dane, J.H., Topp, G.C. (Eds.), Methods of Soil Analysis. Part 4. Physical Methods. SSSA, Madison, WI, pp. 812–815.

Bouma, J., 1982. Measuring the Hydraulic Conductivity of Soil Horizons with Continuous Macropores. Soil Science Society of America Journal 46. https://doi.org/10.2136/sssaj1982.03615995004600020047x

Braud, I., Desprats, J.F., Ayral, P.A., Bouvier, C., Vandervaere, J.P., 2017. Mapping topsoil field-saturated hydraulic conductivity from point measurements using different methods. Journal of Hydrology and Hydromechanics 65. https://doi.org/10.1515/johh-2017-0017

Brooks, R., Corey, A., 1964. Hydraulic properties of porous media. Hydrology Papers, Colorado State University 3.

Carrick, S., Buchan, G., Almond, P., Smith, N., 2011. Atypical early-time infiltration into a structured soil near field capacity: The dynamic interplay between sorptivity, hydrophobicity, and air encapsulation. Geoderma 160. https://doi.org/10.1016/j.geoderma.2010.11.006

Carter, M.R., Gregorich, E.G., 2007. Soil Sampling and Methods of Analysis: Second Edition, Soil Sampling and Methods of Analysis: Second Edition.

Castellini, M., Di Prima, S., Iovino, M., 2018. An assessment of the BEST procedure to estimate the soil water retention curve: A comparison with the evaporation method. Geoderma 320, 82–94. https://doi.org/10.1016/j.geoderma.2018.01.014

Close, K.R., Frasier, G., Dunn, G.H., Loftis, J.C., 1998. Tension infiltrometer contact interface evaluation by use of a potassium iodide tracer. Transactions of the American Society of Agricultural Engineers 41. https://doi.org/10.13031/2013.17272

Dane, J.H., Hopmans, J.W., 2002. Pressure plate extractor, in: Dane, J.H., Topp, G.C. (Eds.), Methods of Soil Analysis, Part 4, Physical Methods. Soil Science Society of America, Inc., Madison, USA, pp. 680–683.

Dane, J.H., Topp, G.C., Campbell, G.S., Horton, R., Jury, W.A., Nielsen, D.R., van Es, H.M., Wierenga, P.J., Al-Amoodi, L., Dick, W.A., 2018. Methods of Soil Analysis: Part 4 Physical Methods, Methods of Soil Analysis, Part 4: Physical Methods. https://doi.org/10.2136/sssabookser5.4

de Jonge, L.W., Jacobsen, O.H., Moldrup, P., 1999. Soil Water Repellency: Effects of Water Content, Temperature, and Particle Size. Soil Science Society of America Journal 63. https://doi.org/10.2136/sssaj1999.03615995006300030003x

Dekker, L.W., Doerr, S.H., Oostindie, K., Ziogas, A.K., Ritsema, C.J., 2001. Water Repellency and Critical Soil Water Content in a Dune Sand. Soil Science Society of America Journal 65. https://doi.org/10.2136/sssaj2001.1667

Di Prima, S., 2015. Automated single ring infiltrometer with a low-cost microcontroller circuit. Comput Electron Agric 118. https://doi.org/10.1016/j.compag.2015.09.022

Di Prima, S., Bagarello, V., Lassabatère, L., Angulo-Jaramillo, R., Bautista, I., Burguet, M., Cerdà, A., Iovino, M., Prosdocimi, M., 2017. Comparing Beerkan infiltration tests with rainfall simulation experiments for hydraulic characterization of a sandy-loam soil. Hydrol Process 31. https://doi.org/10.1002/hyp.11273

Di Prima, S., Lassabatère, L., Bagarello, V., Iovino, M., Angulo-Jaramillo, R., 2016. Testing a new automated single ring infiltrometer for Beerkan infiltration experiments. Geoderma 262, 20–34. https://doi.org/10.1016/j.geoderma.2015.08.006

Di Prima, S., Stewart, R.D., Castellini, M., Bagarello, V., Abou Najm, M.R., Pirastru, M., Giadrossich, F., Iovino, M., Angulo-Jaramillo, R., Lassabatère, L., 2020. Estimating the macroscopic capillary length from Beerkan infiltration experiments and its impact on saturated soil hydraulic conductivity predictions. J Hydrol (Amst) 589. https://doi.org/10.1016/j.jhydrol.2020.125159

Dohnal, M., Dusek, J., Vogel, T., 2010. Improving Hydraulic Conductivity Estimates from Minidisk Infiltrometer Measurements for Soils with Wide Pore-Size Distributions. Soil Science Society of America Journal 74. https://doi.org/10.2136/sssaj2009.0099

Elrick, D.E., Reynolds, W.D., 1992. Methods for Analyzing Constant-Head Well Permeameter Data. Soil Science Society of America Journal 56. https://doi.org/10.2136/sssaj1992.03615995005600010052x

Farzamian, M., Autovino, D., Basile, A., De Mascellis, R., Dragonetti, G., Monteiro Santos, F., Binley, A., Coppola, A., 2021. Assessing the dynamics of soil salinity with time-lapse inversion of electromagnetic data guided by hydrological modelling. Hydrol Earth Syst Sci 25. https://doi.org/10.5194/hess-25-1509-2021

Faybishenko, B.A., 1995. Hydraulic Behavior of Quasi-Saturated Soils in the Presence of Entrapped Air: Laboratory Experiments. Water Resour Res 31. https://doi.org/10.1029/95WR01654

Fodor, N., Sándor, R., Orfanus, T., Lichner, L., Rajkai, K., 2011. Evaluation method dependency of measured saturated hydraulic conductivity. Geoderma 165. https://doi.org/10.1016/j.geoderma.2011.07.004

Gadi, V.K., Tang, Y.R., Das, A., Monga, C., Garg, A., Berretta, C., Sahoo, L., 2017. Spatial and temporal variation of hydraulic conductivity and vegetation growth in green infrastructures using infiltrometer and visual technique. Catena (Amst) 155, 20–29. https://doi.org/10.1016/J.CATENA.2017.02.024

Ghosh, B., Pekkat, S., Yamsani, S.K., 2019. Evaluation of infiltrometers and permeameters for measuring hydraulic conductivity. Adv Civ Eng Mater 8, 308–321. https://doi.org/10.1520/ACEM20180056

Gonzalez-Sosa, E., Braud, I., Dehotin, J., Lassabatère, L., Angulo-Jaramillo, R., Lagouy, M., Branger, F., Jacqueminet, C., Kermadi, S., Michel, K., 2010. Impact of land use on the hydraulic properties of the topsoil in a small French catchment. Hydrol Process 24. https://doi.org/10.1002/hyp.7640

Gupta, R.K., Rudra, R.P., Dickinson, W.T., Patni, N.K., Wall, G.J., 1993. Comparison of saturated hydraulic conductivity measured by various field methods. Transactions - American Society of Agricultural Engineers 36. https://doi.org/10.13031/2013.28313

Haverkamp, R., Ross, P.J., Smettem, K.R.J., Parlange, J.Y., 1994. Three-dimensional analysis of infiltration from the disc infiltrometer: 2. Physically based infiltration equation. Water Resour Res 30. https://doi.org/10.1029/94WR01788

Jačka, L., Pavlásek, J., Kuráž, V., Pech, P., 2014. A comparison of three measuring methods for estimating the saturated hydraulic conductivity in the shallow subsurface layer of mountain podzols. Geoderma 219–220, 82–88. https://doi.org/10.1016/j.geoderma.2013.12.027

Jacques, D., Mohanty, B.P., Feyen, J., 2002. Comparison of alternative methods for deriving hydraulic properties and scaling factors from single-disc tension infiltrometer measurements. Water Resour Res 38. https://doi.org/10.1029/2001wr000595

Kargas, G., Londra, P., Anastasiou, K., Kerkides, P., 2018. A note on one- and three-dimensional infiltration analysis from a mini disc infiltrometer. Water (Switzerland) 10. https://doi.org/10.3390/w10121783

Klute, A., Dirksen, C., 1986. Hydraulic conductivity and diffusivity: Laboratory methods, in: Methods of Soil Analysis, Part 1: Physical and Mineralogical Methods. American Society of Agronomy, Madison, WI, pp. 687–734. https://doi.org/10.2136/sssabookser5.1.2ed.c28

Lassabatère, L., Angulo-Jaramillo, R., Soria Ugalde, J.M., Cuenca, R., Braud, I., Haverkamp, R., 2006. Beerkan Estimation of Soil Transfer Parameters through Infiltration Experiments-BEST. Soil Science Society of America Journal 70. https://doi.org/10.2136/sssaj2005.0026

Lassabatère, L., Yilmaz, D., Peyrard, X., Peyenau, P.E., Lenoir, T., Šimůnek, J., Angulo-Jaramillo, R., 2014. New Analytical Model for Cumulative Infiltration into Dual-Permeability Soils. Vadose Zone Journal. https://doi.org/10.2136/vzj2013.10.0181

Lassabatère, L., Di Prima, S., Angulo-Jaramillo, R., Keesstra S., Salesa D., 2019. Beerkan multi-runs for characterizing water infiltration and spatial variability of soil hydraulic properties across scales, Hydrological Sciences Journal, 64:2, 165-178, https://doi.org/10.1080/02626667.2018.1560448

Lauren, J.G., Wagnet, R.J., Bouma, J., Wosten, J.H.M., 1988. Variability of saturated hydraulic conductivity in a glossaquic hapludalf with macropores. Soil Sci 145. https://doi.org/10.1097/00010694-198801000-00003

Le Bissonnais, Y., 1996. Aggregate stability and assessment of soil crustability and erodibility: I. Theory and methodology. Eur J Soil Sci 47. https://doi.org/10.1111/j.1365-2389.1996.tb01843.x

Lee, D.M., Reynolds, W.D., Elrick, D.W., Clothier, B.E., 1985. A comparison of three field methods for measuring saturated hydraulic conductivity. Can J Soil Sci 65. https://doi.org/10.4141/cjss85-060

Lenhard, R.J., Mishra, S., 1989. On the Correspondence between Brooks-Corey and van Genuchten Models. Journal of Irrigation and Drainage Engineering 115(4): 744-751. https://doi.org/10.1061/(ASCE)0733-9437(1989)115:4(744)

Lilliefors, H.W., 1967. On the Kolmogorov-Smirnov Test for Normality with Mean and Variance Unknown. J Am Stat Assoc 62. https://doi.org/10.1080/01621459.1967.10482916

Logsdon, S.D., Jaynes, D.B., 1996. Spatial Variability of Hydraulic Conductivity in a Cultivated Field at Different Times. Soil Science Society of America Journal 60. https://doi.org/10.2136/sssaj1996.03615995006000030003x

Logsdon, S.D., Jaynes, D.B., 1993. Methodology for Determining Hydraulic Conductivity with Tension Infiltrometers. Soil Science Society of America Journal 57. https://doi.org/10.2136/sssaj1993.03615995005700060005x

Madsen, M.D., Chandler, D.G., Reynolds, W.D., 2008. Accounting for Bias and Boundary Condition Effects on Measurements of Saturated Core Hydraulic Conductivity. Soil Science Society of America Journal 72. https://doi.org/10.2136/sssaj2007.0254

METER Group, 2021. Mini Disk Infiltrometer Manual. METER Group, Pullman, WA.

Mohanty, B.P., Ankeny, M.D., Horton, R., Kanwar, R.S., 1994. Spatial analysis of hydraulic conductivity measured using disc infiltrometers. Water Resour Res 30. https://doi.org/10.1029/94WR01052

Mubarak, I., Mailhol, J.C., Angulo-Jaramillo, R., Bouarfa, S., Ruelle, P., 2009a. Effect of temporal variability in soil hydraulic properties on simulated water transfer under high-frequency drip irrigation. Agric Water Manag 96, 1547–1559. https://doi.org/10.1016/j.agwat.2009.06.011

Mubarak, I., Mailhol, J.C., Angulo-Jaramillo, R., Ruelle, P., Boivin, P., Khaledian, M., 2009b. Temporal variability in soil hydraulic properties under drip irrigation. Geoderma 150, 158–165. https://doi.org/10.1016/j.geoderma.2009.01.022

Paige, G.B., Hillel, D., 1993. Comparison of three methods for assessing soil hydraulic properties. Soil Sci 155. https://doi.org/10.1097/00010694-199303000-00003

Philip, J.R., 1984. Travel Times From Buried and Surface Infiltration Point Sources. Water Resour Res 20, 990–994. https://doi.org/10.1029/WR020i007p00990

Philip, J.R., 1957. The theory of infiltration: 1. The infiltration equation and its solution. Soil Sci 83. https://doi.org/10.1097/00010694-195705000-00002

Prieksat, M.A., Kaspar, T.C., Ankeny, M.D., 1994. Positional and Temporal Changes in Ponded Infiltration in a Corn Field. Soil Science Society of America Journal 58. https://doi.org/10.2136/sssaj1994.03615995005800010026x

Radinja, M., Vidmar, I., Atanasova, N., Mikoš, M., Šraj, M., 2019. Determination of spatial and temporal variability of soil hydraulic conductivity for urban runoff modelling. Water (Switzerland) 11. https://doi.org/10.3390/w11050941

Reynolds, W.D., 2013. An assessment of borehole infiltration analyses for measuring field-saturated hydraulic conductivity in the vadose zone. Eng Geol 159. https://doi.org/10.1016/j.enggeo.2013.02.006

Reynolds, W.D., Bowman, B.T., Brunke, R.R., Drury, C.F., Tan, C.S., 2000. Comparison of Tension Infiltrometer, Pressure Infiltrometer, and Soil Core Estimates of Saturated Hydraulic Conductivity. Soil Science Society of America Journal 64, 478–484. https://doi.org/10.2136/sssaj2000.642478x

Reynolds, W.D., Drury, C.F., Yang, X.M., Tan, C.S., 2008. Optimal soil physical quality inferred through structural regression and parameter interactions. Geoderma 146. https://doi.org/10.1016/j.geoderma.2008.06.017

Reynolds, W.D., Elrick, D.E., 2002. Hydraulic Conductivity of Saturated Soils, Constant Head Method., in: Methods of Soil Analyses, Part 4, Physical Methods, Book Series 5. Soil Science Society of America, Madison, WI, pp. 694–700.

Reynolds, W.D., Elrick, D.E., 1987. A laboratory and numerical assessment of the guelph permeameter method. Soil Sci 144. https://doi.org/10.1097/00010694-198710000-00008

Reynolds, W.D., Elrick, D.E., 1985. In situ measurement of field-saturated hydraulic conductivity, sorptivity, and the α-parameter using the guelph permeameter. Soil Sci 140. https://doi.org/10.1097/00010694-198510000-00008

Reynolds, W.D., Topp, G.C., 2008. Soil water analyses: Principles and parameters, in: Carter, M.R., Gregorich, E.G. (Eds.), Soil Sampling and Methods of Analysis: Second Edition. CRC press, Boca Raton. https://doi.org/10.1201/9781420005271-81

Sakaguchi, A., Nishimura, T., Kato, M., 2005. The Effect of Entrapped Air on the Quasi-Saturated Soil Hydraulic Conductivity and Comparison with the Unsaturated Hydraulic Conductivity. Vadose Zone Journal 4. https://doi.org/10.2113/4.1.139

Somaratne, N.M., Smettem, K.R.J., 1993. Effect of cultivation and raindrop impact on the surface hydraulic properties of an Alfisol under wheat. Soil Tillage Res 26. https://doi.org/10.1016/0167-1987(93)90038-Q

Valiantzas, J.D., Pollalis, E.D., Soulis, K.X., Londra, P. A., 2011. Rapid Graphical Detection of Weakness Problems in Numerical Simulation Infiltration Models Using a Linearized Form Equation. Journal of Irrigation and Drainage Engineering, 137. https://doi.org/10.1061/(ASCE)IR.1943-4774.0000318.

van Genuchten, M.Th., 1980. A Closed-form Equation for Predicting the Hydraulic Conductivity of Unsaturated Soils. Soil Science Society of America Journal 44. https://doi.org/10.2136/sssaj1980.03615995004400050002x

Verbist, K.M.J., Cornelis, W.M., Torfs, S., Gabriels, D., 2013. Comparing Methods to Determine Hydraulic Conductivities on Stony Soils. Soil Science Society of America Journal 77. https://doi.org/10.2136/sssaj2012.0025

Warrick, A.W., 1998. Spatial variability, in: Enviromental Soil Physics Appendix 1. D. Hillel, California, pp. 665–675.

White, I., Sully, M.J., 1987. Macroscopic and microscopic capillary length and time scales from field infiltration. Water Resour Res 23. https://doi.org/10.1029/WR023i008p01514

Xu, X., Kiely, G., Lewis, C., 2009. Estimation and analysis of soil hydraulic properties through infiltration experiments: Comparison of BEST and DL fitting methods. Soil Use Manag 25. https://doi.org/10.1111/j.1475-2743.2009.00218.x

Xu, X., Lewis, C., Liu, W., Albertson, J.D., Kiely, G., 2012. Analysis of single-ring infiltrometer data for soil hydraulic properties estimation: Comparison of BEST and Wu methods. Agric Water Manag 107. https://doi.org/10.1016/j.agwat.2012.01.004

Yilmaz, D., Lassabatère, L., Angulo-Jaramillo, R., Deneele, D., Legret, M., 2010. Hydrodynamic Characterization of Basic Oxygen Furnace Slag through an Adapted BEST Method. Vadose Zone Journal 9. https://doi.org/10.2136/vzj2009.0039

Yilmaz, D., Lassabatère, L., Moret-Fernandez, D., Rahmati, M., Angulo-Jaramillo, R., Latorre, B., 2023. Soil-dependent β and γ shape parameters of the Haverkamp infiltration model for 3D infiltration flow. Hydrol Process 37. https://doi.org/10.1002/hyp.14928

Zhang, R., 1997. Determination of Soil Sorptivity and Hydraulic Conductivity from the Disk Infiltrometer. Soil Science Society of America Journal 61. https://doi.org/10.2136/sssaj1997.03615995006100040005x

2.3 Comparison of the single-ring pressure infiltrometer and SATURO methods for determination of field saturated soil hydraulic conductivity

D. Autovino[1], V. Bagarello[1], A. Basile[2], G. Caltabellotta[1], R. De Mascellis[2], M. Fusco[1], M. Iovino[1]

[1]Dipartimento di Scienze Agrarie, Alimentari e Forestali, Università di Palermo, dario.autovino@unipa.it
[2] Institute for Mediterranean Agriculture and Forestry Systems, National Research Council of Italy, Portici, Italy

Abstract

Both the classical pressure infiltrometer (PI) method and the recently introduced SATURO device can be used to determine field saturated soil hydraulic conductivity (K_{fs}) through a single-ring, steady-state experiment with two pressure heads. The introduction of this automated device raised questions about the validity criteria for infiltration data, its performance compared to the classical method, and the impact of a quick literature estimate of the α* parameter on K_{fs} calculations. For two sandy-loam soils and a clay soil, the SATURO criterion, denoted as criterion 1, differed from the classical, more stringent, criterion 2 in terms of valid measurements (success rates of 47-100% *vs* 13-87%, respectively) but not greatly in summary statistics (K_{fs}^{TPD} means equal to 65-527 mm h^{-1} in the former case and 70-300 mm h^{-1} in the latter one). The PI and SATURO yielded similar mean K_{fs}^{E} values (81-345 *vs* 78-192 mm h^{-1}, respectively), but SATURO tended to give relatively smaller individual values. Using the first approximation value of α^* instead of the experimental value led to differences in K_{fs} by 1.5 times at the most, depending on the site. The classical data validity criterion should be applied to exclude physically impossible results. In practical use, both methods with similar run durations and water volumes yield comparable K_{fs} values. The first approximation value of α^* could replace the experimental value in several cases. SATURO is a promising alternative to the PI for determining field saturated soil hydraulic conductivity via single-ring, steady-state infiltration. There is room for improving its performances and also for simplifying its application in the field.

Keywords: field saturated soil hydraulic conductivity; field measurement methods; steady-state infiltration tests; data validity criterion; experiment automation.

2.3.1 INTRODUCTION

Saturated soil hydraulic conductivity governs water movement through the soil, influencing various processes such as infiltration, runoff, drainage and erosion (Hillel, 2003). Accurate measurement of this property is essential for effective soil and water management in both agricultural and environmental contexts. Under natural conditions, air entrapment could yield field saturated soil hydraulic conductivity (K_{fs}) values lower than those corresponding to full saturation, that can only be achieved under laboratory conditions (Basile et al., 2003, 2006; Reynolds and Elrick, 2002).

Among the various field methods for determining K_{fs}, the steady, constant-head infiltration technique using a single ring is widely adopted, largely due to the physically based analysis of the process by Reynolds and Elrick (1990). This analysis considers the effects of soil capillarity, ponding depth, ring radius and ring insertion depth on the flow process. It provides the basis for calculating, in addition to K_{fs}, the matric flux potential, ϕ_m (Gardner, 1958), and the α^* parameter that represents the inverse of the macroscopic capillary length, λ_c (White and Sully, 1987). Practical reasons why single-ring, pressure infiltrometer (PI) experiments have received much interest in the literature (e.g., Vauclin et al., 1994; Ciollaro and Lamaddalena, 1998; Bagarello et al., 2000; Reynolds et al., 2000; Mertens et al., 2002; Gómez et al., 2005 among others) include: i) the higher reliability of steady-state infiltration data compared to the transient ones (Yilmaz et al., 2024); and ii) the availability of various approaches for conducting a PI experiment and analysing the data, which gives the methodology a certain flexibility. The most applied steady-state approaches are the One-Ponding-Depth (OPD) approach, that uses a single depth of ponding, H, on the infiltration surface and requires an a priori estimate of α^* for determining K_{fs}, and the Two-Ponding-Depth (TPD) approach, that uses two H levels to simultaneously estimate K_{fs}, ϕ_m and α^*. Three or more H levels can also be used to simultaneously estimate all mentioned parameters (Multiple-Ponding-Depth, MPD, approach).

The persistent interest in methods for determining K_{fs} using single-ring ponded infiltration experiments and steady-state data analysis procedures is evident from the recent development of SATURO (METER Group, Inc., USA). This device, constituting an automated version of the PI method, features specific peculiarities in its methodological approach. In particular, the run with SATURO includes an initial soak time, aimed to reach soil saturation, before beginning the so-called pressure cycles. SATURO automatically calculates K_{fs} by the TPD equation, in accordance with Reynolds and Elrick (1990).

The scientific community is starting to show some interest for SATURO. For example, Ravi et al. (2017) performed SATURO measurements to study ecohydrological processes associated with the so-called fairy circles in the Namib Desert. Zhang et al. (2019) used the device at a living filter wastewater tertiary treatment system. In a review paper on determination of K_{fs} in urban green infrastructures, Ebrahimian et al. (2020) included SATURO as one of the usable methods together with the single- and double-ring infiltrometers and the modified Philippe-Dunne method. Saha et al. (2024) used SATURO in a silty to silty-clay-loam soil to determine soil use and management effects on K_{fs}. More recently, Welker et al. (2025) applied SATURO in an investigation on K_{fs} in rain gardens and Garg et al. (2025) used the device to compare the effects of conventional and conservative management on the field saturated hydraulic conductivity of the surface layer in two silty-loam soils.

The availability of the new equipment leads to recognize that there is the need for further investigations on soil hydrodynamic characterization using steady-state, single-ring infiltration data.

An important question to consider is the validity of the TPD calculations. With SATURO, the experiment is deemed successful if K_{fs} is positive, which happens when the steady-state infiltration rate is higher for the larger pressure head than the smaller one. However, K_{fs} could be positive but ϕ_m could be negative and α* could assume unreliable values (Bagarello et al., 2013; Mertens et al., 2002; Reynolds and Elrick, 2002). Therefore, it seems that SATURO tends to consider K_{fs} values as valid even when they would be considered invalid according to other validity criteria. However, the extent to which these two validity criteria, positive K_{fs} values for SATURO versus positive K_{fs} and ϕ_m values along with reliable α* values (Reynolds and Elrick, 2002), differ in their impact on creating a K_{fs} dataset for an area of interest remains unclear.

The performances of SATURO still need to be compared with those by other methods (Ebrahimian et al., 2020). As pointed out by Reynolds et al. (2000), comparing techniques for determining K_{fs} is an imprecise and perhaps even dubious enterprise due to the lack of independent data upon which evaluation and judgments can be made. However, these comparisons are important, as they provide one of the few sources of information that practitioners can draw upon to select the most appropriate K_{fs} determination methods for their specific conditions. Comparisons between SATURO and other methods are starting to appear in the literature. For example, Zhang et al. (2019) compared SATURO with the double-ring infiltrometer and they concluded that the application procedure and settings of the new device should be optimized depending on the circumstances instead of using the default settings. The conclusion of a numerical study by Tecce et al. (2022) was that SATURO should yield estimates of K_{fs} differing by no more than nearly two times from the true value with a run of three hours or less. In the laboratory, Naik et al. (2024) compared SATURO with the mini-disk infiltrometer, a permeameter and a rainfall simulator for a loam and a sandy soil and they suggested that SATURO shows promise also for spatial variability investigations at the catchment scale. Using SATURO, Atalar et al. (2025) failed to capture significant differences between covers that were instead detected with other methods such as a rainfall simulator and a steady-state simplified method based on beerkan infiltration runs (Bagarello et al., 2017). These comparisons are overall encouraging but they are still too few to suggest conclusions of general validity.

When the TPD approach provides an invalid result, Reynolds and Elrick (2002) suggested to apply the OPD approach separately to each head and then averaging the two resulting estimates of the soil hydrodynamic parameter of interest. In other words, the failure of a TPD run does not impede estimation of K_{fs} at a given measurement site. The suggestion by Reynolds and Elrick (2002) is therefore useful not to lose the collected experimental information. Two alternative choices can be made to calculate K_{fs}. A possibility is using the valid TPD results to determine a site-specific estimate of α^* and hence using this value for applying the OPD approach to all infiltration runs. Another possible option is to consider a literature estimate of α^* (Reynolds and Elrick, 1990). This last choice is rather common in practical applications of the single-ring PI method and of other single-ring methods to determine K_{fs} (Bagarello and Sgroi, 2004; Verbist et al., 2009, 2010; Bagarello et al., 2014; Di Prima et al., 2018; Stewart et al., 2018). In particular, α^* = 12 m^{-1} appears to be a generally usable value since it represents the first choice for most soils (Elrick and Reynolds, 1992b) and the value most frequently applicable or most appropriate (Reynolds, 2008) for agricultural soils. The use of a literature value of α^* could therefore be expected to be accurate enough for practical applications. However, according to recent investigations, this suggestion does not seem to be always valid since using either the first approximation value of α^* or a soil-dependent estimate of this parameter could induce differences in K_{fs} predictions by up to 500%-600% (Di Prima et al., 2020). The conflicting information available in the literature suggests that further comparisons are needed between K_{fs} values obtained by a literature estimate of α^* and those obtained by its experimental determination.

The general objective of this investigation was to examine factors influencing field determination of saturated soil hydraulic conductivity by steady-state, constant-head, single-ring infiltration methods. With reference to three distinct field sites, the specific objectives were to: i) evaluate the effect of the assumed validity criterion of a Two-Ponding-Depth run on K_{fs} determination with the PI and SATURO methodological approaches; ii) establish a comparison between these two K_{fs} determination methods; and iii) compare the K_{fs} values obtained by a literature estimate of α^* with those calculated by its experimental determination.

2.3.2 THEORY

Both the classical PI and SATURO methods utilize the analytical expression for three-dimensional (3D) steady, ponded flow out of a ring into rigid, homogeneous, isotropic, and uniformly unsaturated soil (Reynolds and Elrick, 1990):

$$Q_s = \frac{r}{G}(K_{fs}H + \phi_m) + \pi r^2 K_{fs} \tag{1.0}$$

where Q_s (L^3T^{-1}) is the steady-state flow rate, r (L) is the ring radius, K_{fs} (L T^{-1}) is the field saturated soil hydraulic conductivity, H (L) is the ponded head of water on the infiltration surface, ϕ_m (L^2T^{-1}) is the matric flux potential and G is a dimensionless shape factor expressing the complex interactions between ring radius, depth of ring insertion, d (L), depth of ponding in the ring, soil capillarity and gravity. In practice, an estimate of G, denoted as G_e, can be obtained from the d/r ratio by the following relationship, which is strictly valid for $0.03 \leq d \leq 0.05$ m, $0.05 \leq r \leq 0.10$ m and $0.05 \leq H \leq 0.25$ m (Reynolds and Elrick, 1990):

$$G_e = 0.316\frac{d}{r} + 0.184 \quad (1.1)$$

According to Equation (1), steady-state flow rate out of the ring is the sum of three components, i.e., flow due to the hydrostatic pressure of the established depth of water on the infiltration surface (first term on the right of the equation), flow due to the capillarity of the unsaturated soil under and adjacent to the ring (second term) and flow due to gravity (third term).

With the single-ring pressure infiltrometer (PI) method, both K_{fs} and ϕ_m can be obtained by the Two-Ponding-Depth (TPD) approach (Reynolds and Elrick, 1990), also named Two-Head-Analysis (Reynolds and Elrick, 2002). The approach requires measuring the steady-state flow rates, Q_{s1} and Q_{s2}, corresponding to two ponding depths of water, H_1 and H_2 ($H_2 > H_1$), consecutively established on the infiltrating surface without occurrence of a drainage phase in the passage from H_1 to H_2. The following relationships yield K_{fs} and ϕ_m:

$$K_{fs} = \frac{G_e}{r}\left(\frac{Q_{s2} - Q_{s1}}{H_2 - H_1}\right) \quad (1.2)$$

$$\phi_m = \frac{G_e}{r}\left(\frac{H_2 Q_{s1} - H_1 Q_{s2}}{H_2 - H_1} - \pi r G_e \frac{Q_{s2} - Q_{s1}}{H_2 - H_1}\right) \quad (1.3)$$

Simultaneous calculation of K_{fs} and ϕ_m also yields an estimate of the α^* (L^{-1}) parameter (Reynolds and Elrick, 2002):

$$\alpha^* = \frac{K_{fs}}{\phi_m} \quad (1.4)$$

A limitation of the TPD approach is that unrealistic or negative, and therefore invalid, values for K_{fs}, ϕ_m, or α^* may be obtained when strong heterogeneity, an extreme vertical antecedent water content gradient, or insufficient equilibration time result in inappropriate Q_s values. When the TPD approach yields a negative result for either K_{fs} or ϕ_m, or an α^* value that falls substantially outside the realistic range of $1 \leq \alpha^* \leq 100$ m^{-1}, both K_{fs} and ϕ_m calculations have to be discarded (Reynolds and Elrick, 2002; Angulo-Jaramillo et al., 2016). In this case, the One-Ponding-Depth (OPD) approach (Reynolds and Elrick, 1990), also named Single-Head-Analysis, should be applied to each H value and the resulting K_{fs} and ϕ_m values averaged (Reynolds and Elrick, 2002). With the OPD approach, an estimate of K_{fs} is obtained from a single Q_s value by the following relationship:

$$K_{fs} = \frac{\alpha^* G_e Q_s}{r(\alpha^* H + 1) + G_e \alpha^* \pi r^2} \quad (1.5)$$

in which α^* can be estimated from a field evaluation of soil textural and structural characteristics or an a-priori knowledge of a field representative value of α^* (Elrick and Reynolds, 1992a, b).

2.3.3 MATERIALS AND METHODS

2.3.3.1 Field sites

This investigation was carried out in three distinct study areas: Acerra, Altofonte and Villabate (**Fig. 1**). The Acerra field is located in a flat region, approximately 20 km northeast of Naples, Italy (40°57'58" N, 14°25'47" E, 27 m above sea level). The area experiences a Mediterranean climate, characterized by a mean annual temperature of approximately 16.9 °C and an average annual precipitation of 876 mm. The primary land use in this area is cultivation of vegetable crops. The soil developed on volcanic material, exhibiting high chemical and physical fertility. According to the USDA soil classification system, the soil texture is sandy-loam, consisting of 11.9% clay, 35.8% silt and 52.3% sand.

The Altofonte site is situated in a hilly area, approximately 11 km southwest of Palermo, Italy (38°02'31" N, 13°16'18" E, 420 m above sea level). The site experiences a Mediterranean climate with a mean annual temperature of around 17 °C and an average annual precipitation of 843 mm. This field hosts a 50-year-old olive orchard, where the soil is not tilled and weed control is managed exclusively through mechanical means. According to the USDA soil classification system, the soil texture is classified as clay, with 47.6% clay, 39.0% silt and 13.4% sand.

The Villabate experimental site (38°04'53.1" N, 13°25'08.4" E, 35 m above sea level) is located near Palermo in the flat area historically referred to as the Conca d'Oro (Golden Basin). The region experiences a Mediterranean climate with a mean annual temperature of approximately 19 °C and an average annual precipitation of 803 mm. The field comprises a 30-year-old mandarin orchard with a 5 m × 5 m plant space. Like the Altofonte site, no-till farming management is employed and weed control is conducted mechanically. Based on the USDA soil classification, the soil texture is sandy-loam, consisting of 17.1% clay, 19.0% silt and 63.9% sand.

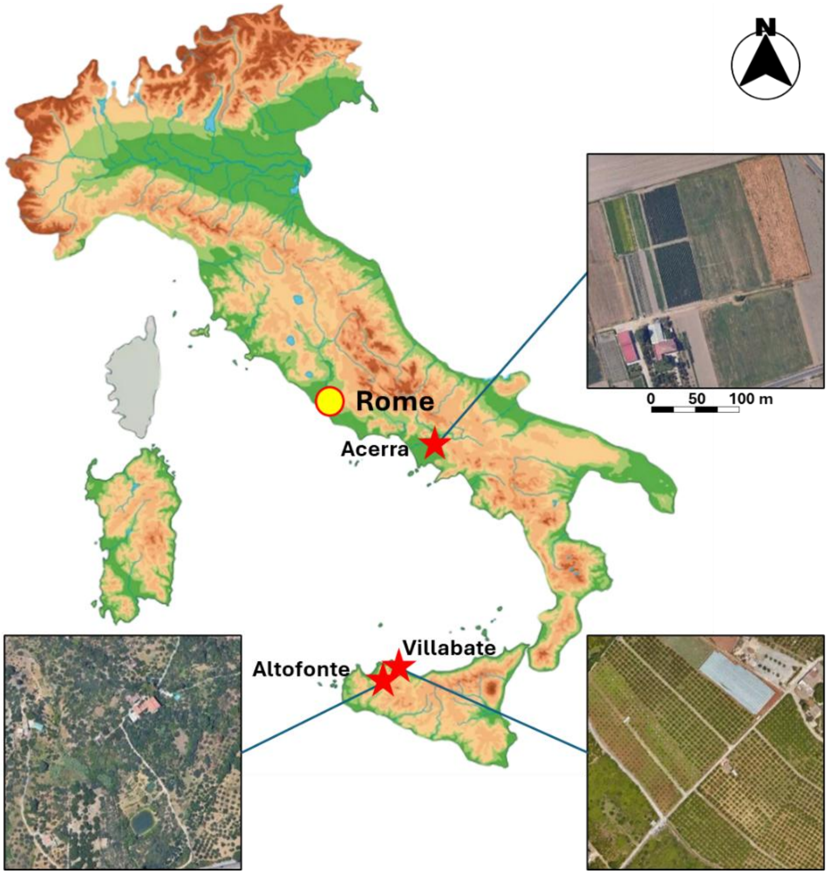

Fig. 1 Geographical location of the sampled field sites

2.3.3.2 Infiltration experiments

At each field site, infiltration runs were conducted over an area of approximately 350 m² using the PI and SATURO methods. At each site, sample locations for a method were selected randomly and the PI and SATURO measurements were randomly interspersed.

The PI, manufactured according to Ciollaro and Lamaddalena (1998), consisted of a stainless-steel ring with a radius $r = 7.5$ cm, inserted to a depth $d = 5$ cm into the initially unsaturated soil. A Mariotte bottle maintained a constant-head infiltration process by supplying water as needed during the test. The infiltration rate was determined by measuring the rate of water level decrease in the Mariotte bottle. Two constant water depths, $H_1 = 5$ cm followed by $H_2 = 10$ cm, were established in uninterrupted sequence on the soil surface confined by the ring. The test durations were site-specific, depending on the soil's hydraulic properties and initial soil moisture conditions, which determine the time required to reach steady-state flow conditions. At the Acerra site, H_1 was maintained for a minimum of 30 min and H_2 for 20 min. At the Altofonte site, the minimum durations were 60 min for H_1 and 30 min for H_2. At the Villabate site, shorter durations of 20 min for H_1 and 11 min for H_2 were used. In total, 45 two-level infiltration runs were performed with this apparatus, that is 15 runs at each field site.

The other device used in this study was SATURO, intended for fully automatic K_{fs} determination without requiring post-processing of the data. The device includes two insertion rings, each with r = 7.5 cm and options for insertion depths of 10 or 5 cm. For consistency with the PI experiments, the 5 cm depth ring was selected at all sites. The ring was inserted into the soil using a driving plate and a hammer. The infiltrometer head, comprising an airtight chamber, was connected to the ring via a quick-release mechanism. A control unit within the infiltrometer head pumps water to maintain a ponded water depth of approximately 5 cm on the soil surface and applies air pressure to establish the required pressure head. Infiltration rates were measured and logged at 1-min intervals throughout each test. The procedure began with an initial soaking phase, during which the infiltrometer applied water to saturate the soil while maintaining a pressure head of approximately 5 cm. The soaking phase lasted 25 min at all three study sites. After soaking, the infiltrometer performed a series of infiltration cycles alternating with two different pressure heads. Each cycle included a high pressure head (H_2 = 10 cm) applied for 15 min, followed by a low pressure head (H_1 = 5 cm) for another 15 min. These cycles ensured that steady-state infiltration rates were achieved.

The control unit takes the average infiltration rates at the two different pressure heads during the last pressure cycle to only calculate K_{fs} by the TPD equation, that is by Equation (3). Therefore, compared to theory and consolidated practical recommendations, the SATURO method is characterized by i) an inversion of the established pressure heads for determining K_{fs} (first the higher value and then the lower one) and ii) a lack of consideration for the possibility that the determination of K_{fs} is invalid because ϕ_m is negative or α^* falls outside the range of acceptable values. Instead, the method does not exclude that K_{fs} could be invalid when Q_{s2} is unrealistically smaller than Q_{s1}.

At the Altofonte and Villabate sites, three infiltration cycles were conducted while at the Acerra site only two cycles were performed due to the faster attainment of steady-state conditions. As a result, the total test durations were 115 min at Altofonte and Villabate and 85 min at Acerra. Upon completing each experiment, the SATURO device displayed the K_{fs} value calculated according to Equation (3) along with the associated standard error, calculated from the final pressure cycle data. The first two minutes of each pressure head setting were excluded from the calculation to allow the instrument to stabilize at the new pressure level. In total, 51 experiments were conducted with SATURO: 12 at Acerra, 24 at Altofonte and 15 at Villabate.

2.3.3.3 Field saturated soil hydraulic conductivity calculations

Different estimates of K_{fs} were considered in this investigation, depending on the experimental information used for the calculations and the choice made with reference to α^* (**Fig. 2**).

An estimate of K_{fs} was obtained by the TPD approach (K_{fs}^{TPD}). In this case, ϕ_m and α* were also calculated using Equations (4) and (5), respectively. For SATURO, the steady-state infiltration rates used by the device to yield K_{fs}^{TPD} were considered to also determine ϕ_m and hence α*.

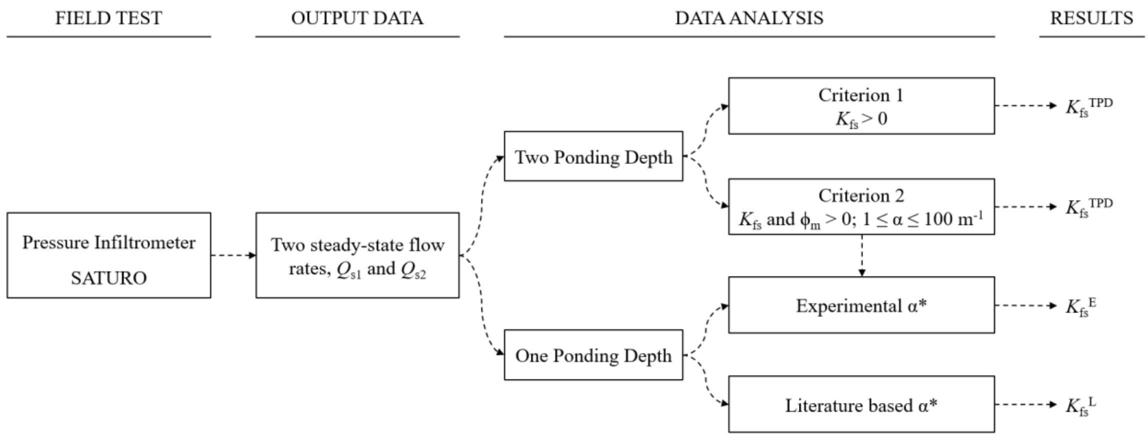

Fig. 2 Flowchart for estimating field saturated soil hydraulic conductivity with the PI and SATURO methods

The infiltration data were also analyzed by applying the OPD approach with each *H* value and then by averaging the two estimates of K_{fs}, according to Elrick and Reynolds (1992b) and Reynolds and Elrick (2002). Two different α* values were used at a given field site to apply Equation (6). A field-specific estimate of α* was calculated by averaging the α* values obtained from the valid TPD analysis of the PI and SATURO runs, only considering those within the range $1 \leq \alpha^* \leq 100$ m^{-1}. The two methods (PI and SATURO) were considered together since these runs were performed under comparable experimental conditions with reference to ring radius and established *H* values. The symbol K_{fs}^{E} (E stands for experimental) was used to denote the K_{fs} values obtained with the experimentally determined α* parameter. Another dataset was developed by the first approximation α* value ($\alpha^* = 12$ m^{-1}), valid for a wide range of soils (Elrick and Reynolds, 1992a,b). The symbol K_{fs}^{L} (L stands for literature) was used in this case.

2.3.4 Data analysis

The data analysis was performed according to the following steps:

i) initially, the PI and SATURO data obtained at the three field sites (Acerra, Altofonte, and Villabate) were analyzed by the TPD equations to establish a comparison between the two K_{fs} validity criteria, that is criterion 1 (Equation (3) yielding positive K_{fs}^{TPD} values) and the more stringent criterion 2 by Reynolds and Elrick (2002) (Equations (3) and (4) yielding positive values of K_{fs}^{TPD} and ϕ_m, respectively, and α* falling within the pre-established range of $1 \leq \alpha^* \leq 100$ m^{-1}). For a given site and an applied method, these two validity criteria were compared in terms of both success rates of the two-level infiltration runs and K_{fs}^{TPD} estimates;

ii) a comparison was then conducted between the K_{fs} values obtained using the PI and SATURO methods at each field site. The K_{fs}^{E} data were considered for this comparison to maximize the experimental information available for each developed dataset;

iii) finally, a comparison was established for each site between the estimates of K_{fs} obtained with the first approximation value of α^* (12 m^{-1} according to Elrick and Reynolds, 1992b; K_{fs}^{L}) and those obtained by the locally determined α^* value (K_{fs}^{E}). This comparison aimed to assess the extent to which simplifying estimation of α^* influences K_{fs} calculations.

The distribution of the data was checked with the Lilliefors (1967) test, considering both a normal and a log-normal distribution. An F-test and a two-tailed t-test were applied to compare the two datasets considering the ln-transformed data in the case of a log-normal distribution. All statistical tests were carried out at a significance level of $P = 0.05$.

2.3.5 RESULTS

2.3.5.1 Comparing criteria 1 and 2

With the PI, K_{fs}^{TPD} was always positive at Acerra and for the 87% and 47% of the runs at Altofonte and Villabate, respectively (**Table 1**). With SATURO, positive K_{fs}^{TPD} values were always obtained at Acerra and in the 71% and 93% of the cases at Altofonte and Villabate. With the validity criterion 2, the success rates of the PI runs were equal to 60%, 87% and 27% at Acerra, Altofonte and Villabate, respectively, and the corresponding percentages for SATURO were equal to 75%, 13% and 33%.

Table 1. Summary of the valid runs and the valid field saturated soil hydraulic conductivity values obtained by the two-level analysis, K_{fs}^{TPD}, for each site (Acerra, Altofonte, Villabate) and method (PI, classical single-ring pressure infiltrometer; SATURO)

Site	Method	Number of runs	Criterion 1				Criterion 2				Δ (%)
			Valid runs	Success rate (%)	K_{fs}^{TPD} Mean (mm h^{-1})	CV (%)	Valid runs	Success Rate (%)	K_{fs}^{TPD} Mean (mm h^{-1})	CV (%)	
Acerra	PI	15	15	100	64.7 a	52.2	9	60	70.1 a	62.5	-7.6
	SATURO	12	12	100	88.8 a	92.6	9	75	75.6 a	99.1	+17.5
Altofonte	PI	15	13	87	241.7	51.1	13	87	241.7	51.1	0
	SATURO	24	17	71	518.1 a	173.3	3	13	300.3 a	14.8	+72.6
Villabate	PI	15	7	47	125.9 a	84.9	4	27	197.0 a	75.5	-36.1
	SATURO	15	14	93	526.6 a	254.1	5	33	194.2 a	58.3	+171.1

Note: criterion 1 only implies positive K_{fs}^{TPD} values while criterion 2 requires positive K_{fs}^{TPD} and ϕ_m (matric flux potential) values and acceptable α^* values. Δ is the percentage difference between the means of K_{fs}^{TPD} obtained with the validity criteria 1 and 2. For given site and method, means of K_{fs}^{TPD} followed by the same letter were not significantly different according to an F test and a two-tailed t-test at P = 0.05. The means of K_{fs}^{TPD} obtained at Altofonte with the PI and the two applied criteria were not statistically compared since the two datasets were identical.

In general, applying the more stringent criterion 2, imposing constraints on K_{fs}, ϕ_m and α^*, resulted in decreased success rates compared to the less stringent criterion 1 which only imposes constraints on K_{fs}. In some instances, such as for SATURO runs at Altofonte and Villabate, this decrease was particularly notable. However, in a case, and specifically for the PI runs at Altofonte, no difference was observed between criteria 1 and 2.

With the validity criterion 2, the overall success rate of the runs was equal to 58% for the PI and 33% for SATURO. Therefore, the classical method (PI) was more appropriate than the automated one (SATURO) to obtain valid estimates of K_{fs}^{TPD} with the more stringent validity criterion. In both cases, however, the number of failures was rather high since one valid run was approximately obtained for every two or three runs performed. This result was not surprising since high failure rates have been reported in several studies using the PI method (Mertens et al., 2002; Bagarello et al., 2013, 2014). According to Reynolds and Elrick (2002), failure rates should not be excessively high, as the experiment is expected to show a reduced dependence on soil heterogeneity or antecedent water content gradients. Large failure rates imply that developing a representative dataset of valid K_{fs}^{TPD} calculations may require performing a rather large number of two-level infiltration runs in the field, with only a portion of the collected data being valid for inclusion.

Considering the Acerra and Villabate sites, there was a consistency between the PI and SATURO results since, with the criterion 2, the success rates for the two methods were similar at each of these two sites (60-75% at Acerra and 27-33% at Villabate) and higher at the former site than the latter one (**Table 1**). At Altofonte, the success rate differed appreciably between the two methods since it was equal to 87% for the PI and 13% for SATURO. These discrepancies suggested that the soil at Acerra was likely more homogeneous than at Altofonte and Villabate, since it had been tilled shortly before the infiltration runs, which may have contributed to greater homogeneity. Moreover, macropores at the soil surface were not noticed at Acerra while they were observed at both Altofonte and Villabate. Therefore, the success rates of the two tested methods were similar and relatively high in the soil that was homogenized by tillage. In more undisturbed conditions, the situation was more diversified because, in addition to a large number of successes (PI at Altofonte), it also happened that preferential flow zones and other local soil heterogeneities caused a more frequent failure of one (at Altofonte) or both (at Villabate) methods.

The distribution of K_{fs}^{TPD} was checked for 10 of the 12 developed datasets that is for three sites (Acerra, Altofonte, Villabate) × two methods (PI, SATURO) × two validity criteria (criteria 1 and 2). Two datasets were excluded from this check for the following reasons. At Altofonte with the PI, the same K_{fs}^{TPD} dataset was developed with the two validity criteria and, therefore, the distribution of the data was checked only once. At Altofonte with SATURO and the criterion 2, the sample size was too small ($N = 3$) according to Lilliefors (1967). The normal distribution hypothesis was not rejected in eight cases, but it was rejected in two cases. Instead, the log-normal hypothesis was never rejected. Therefore, the K_{fs}^{TPD} data were considered to be log-normally distributed and they were summarized by calculating the geometric mean and the associated *CV* according to Lee et al. (1985).

For a given site and method, a comparison was carried out between the two developed K_{fs}^{TPD} datasets (criteria 1 and 2). The corresponding mean values of K_{fs}^{TPD} were identical in one case (PI at Altofonte) and not significantly different in the other cases (**Table 1**). Therefore, the validity criterion did not influence significantly determination of a mean K_{fs}^{TPD} value. However, compared to criterion 1, criterion 2 determined in some cases an appreciable decrease of the relative variability of K_{fs} and also resulted in smaller mean values (SATURO at both Altofonte and Villabate).

Therefore, the two validity criteria can generally be expected to differ in terms of number of valid measurements but not appreciably with reference to the summary statistics of the data. However, the less stringent criterion may result in excessively high mean values and higher coefficient of variation values of K_{fs}^{TPD} compared to the more stringent criterion, at least occasionally.

Jointly considering the measurements performed with the PI and SATURO methods, the valid TPD calculations according to criterion 2 varied from a minimum of 9 at Villabate to a maximum of 18 at Acerra (**Table 1**). The normal distribution hypothesis of the α^* values experimentally obtained by Equation (5) was rejected at Altofonte whereas the log-normal distribution hypothesis was not rejected at any site. Therefore, a field-specific estimate of α^* was obtained by the geometric mean of the individual α^* values for that site (**Fig. 3**). The data were highly variable ($89\% \leq CV \leq 240\%$), especially at Villabate. However, the means ($5.2 \leq \alpha^* \leq 16$ m^{-1}) fell within the range of α^* values suggested by Reynolds and Elrick (1990) for estimating K_{fs} by the OPD approach ($1 \leq \alpha^* \leq 36$ m^{-1}). Therefore, these site-specific estimates of α^* were then considered for calculating K_{fs} with the OPD approach as an alternative to the literature value of this parameter.

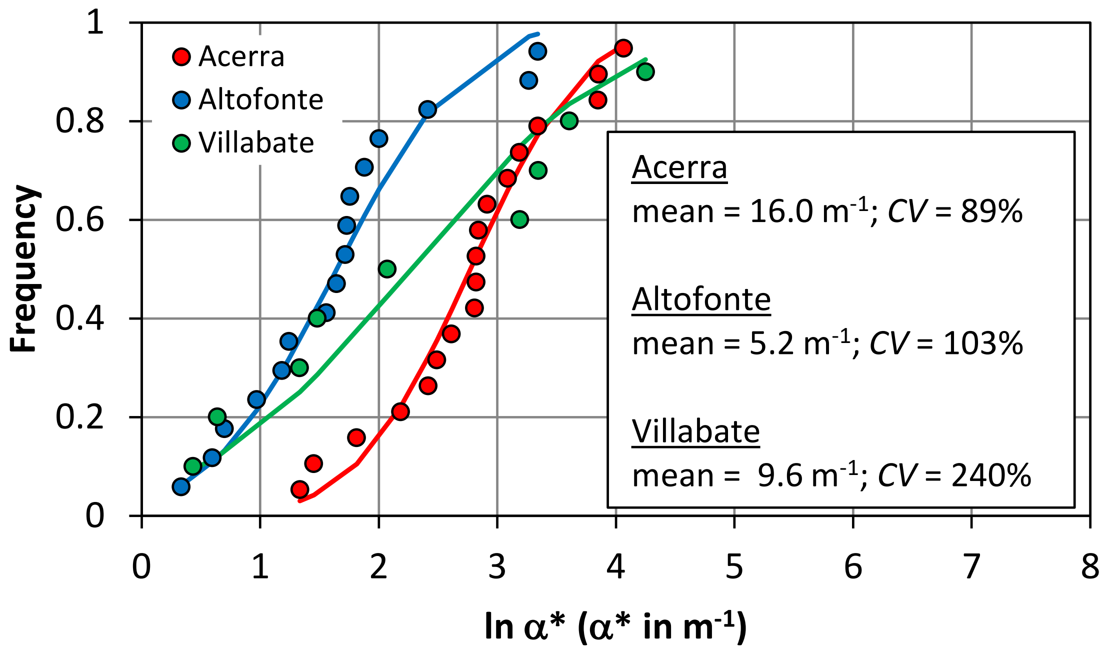

Fig. 3 Cumulative empirical frequency distribution of the α^* parameter values at the three sampled field sites (*CV* in the figure indicates the coefficient of variation)

2.3.5.2 Comparing the PI and SATURO

As with K_{fs}^{TPD}, the distribution of the K_{fs}^{E} data was checked for six datasets that is for three sites (Acerra, Altofonte, Villabate) × two methods (PI, SATURO). The normal distribution hypothesis was rejected in two cases, whereas the log-normal hypothesis was never rejected. Therefore, the data were considered to be log-normally distributed and were summarized using the geometric mean and the associated *CV* (**Table 2**).

Table 2. Summary statistics of the field saturated soil hydraulic conductivity, K_{fs}^{E}, values obtained at the three field sites (Acerra, Altofonte, Villabate) with the classical single-ring pressure infiltrometer (PI) method and with SATURO

Site	PI			SATURO			Δ (%)
	N	Mean (mm h^{-1})	*CV* (%)	*N*	Mean (mm h^{-1})	*CV* (%)	
Acerra	15	81.0 a A	100.7	12	77.9 a A	79.0	4.0
Altofonte	15	294.2 a B	27.0	24	174.7 b B	47.6	68.4
Villabate	15	345.0 a B	82.0	15	191.8 b B	58.3	79.9

Note: Δ = percentage difference between the means of K_{fs}^{E} obtained with the PI and SATURO. For given site, means of K_{fs}^{E} followed by the same lower-case letter were not significantly different according to an F test and a two-tailed t test at $P = 0.05$. Means followed by a different lower-case letter were significantly different. For given method, means of K_{fs}^{E} followed by the same upper-case letter were not significantly different according to an F test and a two-tailed t test at $P = 0.05$. Means followed by a different upper-case letter were significantly different.

At Acerra, the two mean values of K_{fs}^{E} were numerically similar (Δ = 4%) and not significantly different. Moreover, a considerable overlap of the two K_{fs}^{E} distributions was noticed in a rather wide range of frequency (F) values, that is for approximately $0.1 \leq F \leq 0.9$ (**Fig. 4**). However, the K_{fs}^{E} values obtained with the PI ranged from 22 to 472 mm h^{-1} (by 21.6 times) whereas those determined with SATURO ranged from 37 to 239 mm h^{-1} (by 6.5 times). Therefore, the K_{fs}^{E} dataset developed with the PI method included both smaller and larger values than the smallest and the largest estimates obtained with the SATURO method. As a results, while the two methods did not differ in terms of the estimated mean of K_{fs}^{E}, the SATURO method indicated lower variability in field saturated hydraulic conductivity compared to the PI method.

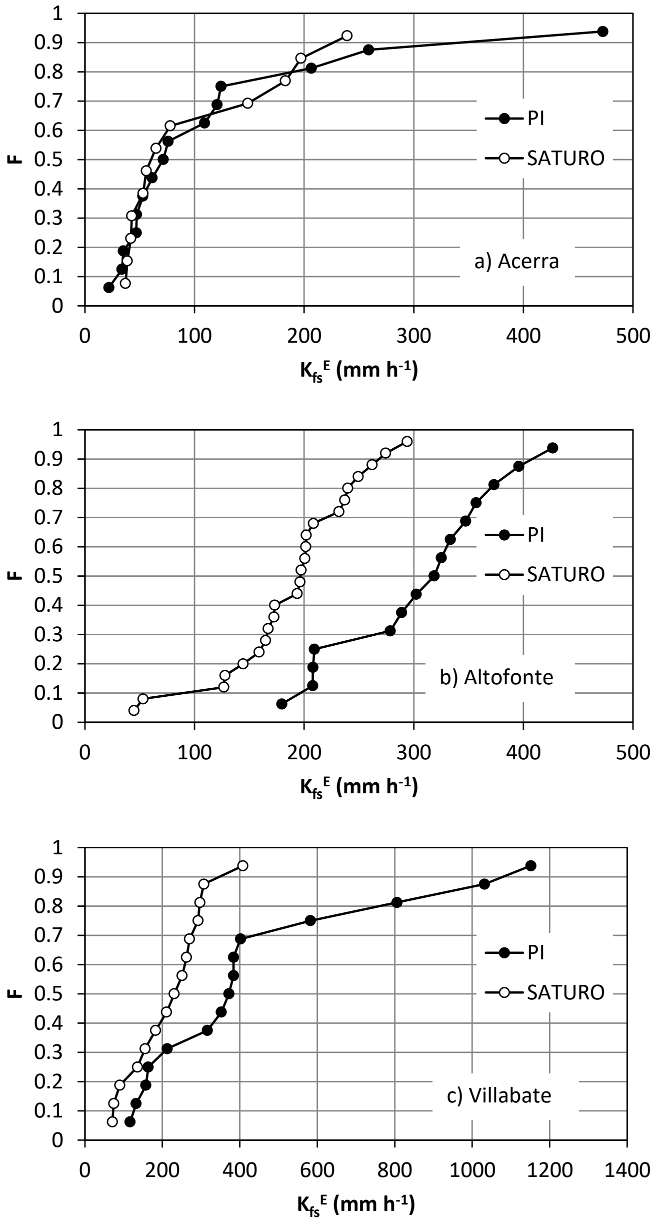

Fig. 4 Cumulative empirical frequency distribution of the field saturated soil hydraulic conductivity, K_{fs}^{E}, values obtained with the PI and the SATURO methods at the three sampled field sites

At Altofonte, the mean of K_{fs}^{E} obtained with the PI method was 68% higher than that obtained with the SATURO method, with the differences being statistically significant. In this case, there was not any overlap of the two K_{fs}^{E} distributions. The PI data ($180 \leq K_{fs}^{E} \leq 427$ mm h^{-1}; ratio between the two extreme values = 2.4) varied over a narrower range than the SATURO data ($45 \leq K_{fs}^{E} \leq 294$ mm h^{-1}; ratio = 6.6). Consequently, a smaller coefficient of variation was obtained with the PI as compared with SATURO. Both methods yielded individual K_{fs}^{E} values in the 180 to 300 mm h^{-1} range. However, only the PI method yielded $K_{fs}^{E} > 300$ mm h^{-1} ($N = 8$), while only the SATURO method yielded $K_{fs}^{E} < 180$ mm h^{-1} ($N = 10$). Therefore, the PI experiment suggested a more permeable and homogeneous soil than the SATURO one. Moreover, particularly high K_{fs}^{E} values were only obtained with the PI method whereas particularly low values were only obtained with the SATURO method.

Also at Villabate, the mean K_{fs}^{E} value obtained with the PI method was significantly higher than that obtained with the SATURO method, with the two means differing by 80%. Even in this case there was no overlap between the two K_{fs}^{E} distributions. The PI data ($117 \leq K_{fs}^{E} \leq 1151$ mm h^{-1}; ratio = 9.8) varied over a wider range than the SATURO data ($71 \leq K_{fs}^{E} \leq 408$ mm h^{-1}; ratio = 5.7). Consequently, a smaller coefficient of variation was obtained with the SATURO method as compared with the PI method. Both methods yielded individual K_{fs}^{E} values in the range of 120 to 410 mm h^{-1}. However, only the PI method yielded $K_{fs}^{E} > 410$ mm h^{-1} (N = 4), while only the SATURO method yielded $K_{fs}^{E} < 120$ mm h^{-1} (N = 3). Therefore, the PI experiment suggested a more permeable and heterogeneous soil than the SATURO one. Furthermore, as in the previous case, particularly high K_{fs}^{E} values were only obtained with the PI method, whereas particularly low values were only obtained with the SATURO method.

Both methods indicated that K_{fs}^{E} varied according to the sequence Villabate = Altofonte > Acerra, even if the PI method suggested a wider variation than the SATURO method since the ratio between the highest and the lowest mean of K_{fs}^{E} was equal to 4.3 with the PI method and to 2.5 with the SATURO method (**Table 2**).

In summary, means of K_{fs}^{E} were either statistically similar or differed by no more than 1.8 times. At two of the three sampled sites, several K_{fs}^{E} values obtained with the SATURO method were smaller than the lowest K_{fs}^{E} values obtained with the PI method. Additionally, at all sites, the highest K_{fs}^{E} values obtained with the SATURO method were lower than several values obtained with the PI method. Therefore, this investigation suggested a relative similarity between the two methods (Elrick and Reynolds, 1992b) but it also indicated a tendency of the SATURO method to overall yield lower K_{fs}^{E} values as compared to the PI method.

2.3.5.3 Using the first approximation value of α*

At Acerra, using the first approximation value of α* (12 m^{-1}) instead of the experimental value (16 m^{-1}) determined an underestimation of the saturated hydraulic conductivity by 8.3-8.5% (N = 27, i.e. 15 PI runs plus 12 SATURO runs, **Table 1**) (**Fig. 5**). At Altofonte, K_{fs}^{L} was higher than K_{fs}^{E} (α* = 5.2 m^{-1}) by 43.0-45.2% (N = 39). At Villabate, the estimate of K_{fs} obtained with the first approximation value of α* was greater than that obtained with the experimental α* value (9.6 m^{-1}) by 8.0-8.7% (N = 30). Therefore, the most appreciable effect of the choice of α* was detected at Altofonte, where two corresponding values differed by nearly 1.5 times. At the other two sites, two corresponding estimates of K_{fs} did not differ by more than 9%.

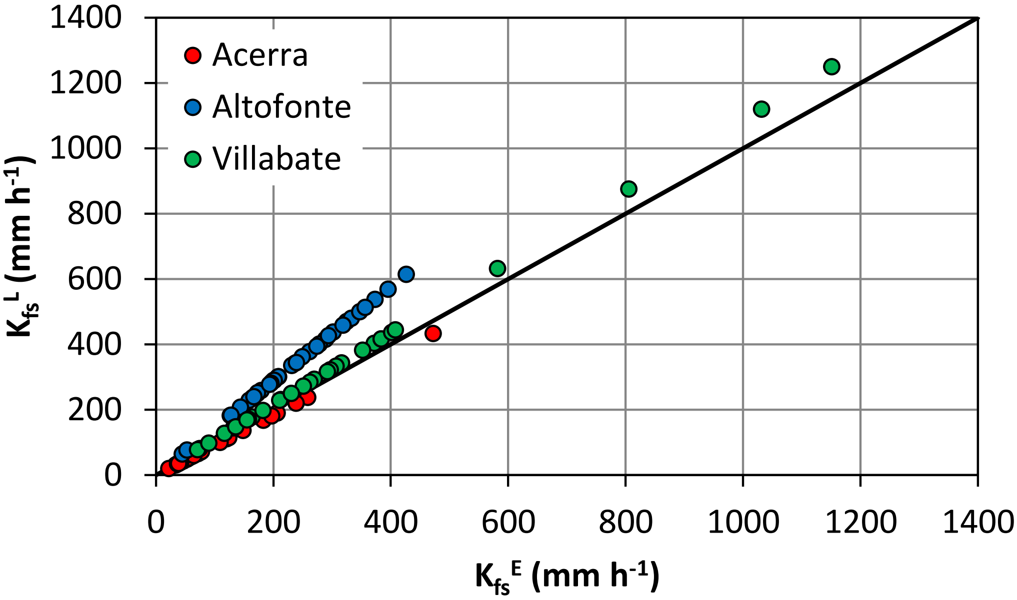

Fig. 5 Relationship between the field saturated soil hydraulic conductivity values obtained by the first approximation value of the α^* parameter, K_{fs}^{L}, and the corresponding values obtained by the experimental α^* parameter, K_{fs}^{E}

2.3.6 DISCUSSION

The detected differences between the two data validity criteria considered in this investigation (criteria 1 and 2; **Table 1**) implied establishing what is the best approach that should be considered in practice.

There is no doubt that the criterion 1 is preferable to the criterion 2, as it minimizes the risk of discarding data collected in the field. Moreover, the requirement that the run is valid if α^* falls within the 1 to 100 m^{-1} range could appear too restrictive. Values of α^* falling outside a wider range ($0.1 \leq \alpha^* \leq 1000$ m^{-1}) than the one suggested by Reynolds and Elrick (2002) can be found in literature (White and Sully 1992; Russo et al. 1997; Khaleel and Relyea 2001). Therefore, the restriction of considering only specific α^* values as valid may raise some doubts. However, apart from α^*, the key discriminating factor between the two criteria is the occurrence of negative ϕ_m values. A negative K_{fs}^{TPD} value implies the failure of the run, regardless of the criterion adopted. The matric flux potential is the integral of the soil hydraulic conductivity – pressure head relationship between an initial soil water pressure head and zero (Reynolds and Elrick, 1990). This integral cannot be negative and if this happens it indicates an anomaly in the Q_{s1} and Q_{s2} values used for its calculation. Of course, if these values are not usable to obtain a physically realistic value of ϕ_m, they are also unusable for calculating K_{fs}^{TPD}.

Considering that only the criterion 2 takes explicitly this last circumstance into account, it has to be suggested that this criterion should also be used to analyze the SATURO data. Criterion 1 is inadequate as it is not consistent with the TDP analysis or infiltration theory.

This investigation suggested that both the PI and SATURO methods yielded a similar information about relative differences between the three soils. The SATURO method showed a moderate tendency to yield generally lower K_{fs}^{E} values compared to the PI method. However, the reasons for this difference appeared to vary between the Acerra and Villabate sites on one hand and the Altofonte site on the other.

At the Acerra and Villabate sites, the runs conducted with the SATURO method were longer and required more water compared to those performed with the PI method. In particular, at Acerra, the mean duration, d_m, of the N = 15 PI runs was 63 min, with a mean applied water volume (V_m) of 5.0 L. In contrast, for SATURO (N = 12), the corresponding values were d_m = 93 min and V_m = 8.0 L. Similarly, at Villabate, the PI (N = 15) method resulted in d_m = 51 min and V_m = 16.2 L whereas the SATURO method (N = 15) required d_m = 115 min and V_m= 24.7 L.

A decrease in the measured K_{fs}^{E} value with longer runs and/or with more water used for the run can be expected to occur as a consequence of a better stabilization of the infiltration process (Elrick and Reynolds, 1992a; Reynolds et al., 2000), a progressive modification of the sampled soil volume close to the infiltration surface (Bagarello and David, 2020), and an increase in size of the sampled soil volume. Additionally, vertical gradients in antecedent soil water content and soil hydrodynamic properties may also contribute to this decrease (Wu et al., 1997; Vandervaere et al., 2000). Therefore, the differences between the two methods were consistent with differences in run duration and used water volumes. Moreover, with the PI method, the estimate of Q_{s1} was obtained approximately halfway through the run while that of Q_{s2} was obtained at the end of the run. Instead, with the SATURO method, both Q_{s1} and Q_{s2} were obtained at the end of the run. It can therefore be supposed that the Q_{s1} values obtained with the SATURO method were more reliable than those obtained with the PI method.

At the Altofonte field site, SATURO tended to yield lower K_{fs}^{E} values than the PI method. However, the run duration was relatively similar for the PI (N = 15, d_m = 133 min) and SATURO (N = 24, d_m = 115 min) runs. The volume of water used was larger for the PI (V_m = 55.4 L) compared to SATURO (V_m = 27.2 L). In this soil, there was a widespread presence of preferential flow zones which explains the use of large volumes of water for the PI runs. With this device, water was applied manually and maintaining a constant depth of water on the infiltration surface, especially in the early stages, was not particularly problematic since it only required a continuous presence of the operator. In contrast, with the automated device, many runs failed from the beginning since the water level remained below 4.3 cm for more than 10 min (METER Group, Inc., USA). Therefore, it was necessary a relocation of the ring to alternative sampling points in an attempt to find suitable conditions compatible with the execution of the run. In particular, immediate failure of the run occurred in 10 cases, against never at Acerra and three times at Villabate. Therefore, while with the PI the sampling was completely random and no measurement point was excluded, with SATURO it was unavoidable to exclude, due to the presence of preferential flow paths, the most permeable points from sampling. Consequently, SATURO overall yielded a smaller K_{fs}^{E} value than the PI for this soil. An implication of this interpretation is that the manual PI method is more versatile than the automated SATURO method.

The reason why SATURO appeared to yield smaller K_{fs} values as compared with the PI can also be discussed taking into account that, with the automated device, the highest measurable infiltration rate is equal to 1150 mm/h (METER Group, Inc., USA). By considering, for the used d and r values in this investigation, the maximum measurable flow rate, the site-specific α^* parameter (**Fig. 3**) and the applied ponded depths of water (5 and 10 cm), the maximum measurable K_{fs} values, calculated by equation (6), are equal to nearly 470, 300 and 400 mm h^{-1} at Acerra, Altofonte and Villabate, respectively. Comparing these values with those reported in **Fig. 4** shows that the maximum K_{fs} value measured with SATURO was well below the maximum measurable value at Acerra but it was essentially the same as the maximum measurable value at Altofonte and Villabate. It can therefore be supposed that the SATURO K_{fs} data were not high-end truncated at Acerra but they were very likely high-end truncated at Altofonte and Villabate. Consequently, the SATURO data largely matched the PI ones at Acerra but they were overall smaller at Altofonte and Villabate (**Fig. 4**). Hence, the SATURO K_{fs} results were likely a fairly good representation of both soil macropore and soil matrix permeability at the Acerra site, but appreciably biased towards soil matrix permeability at the Altofonte and Villabate sites. The reason was that the maximum SATURO pumping rate was apparently too slow for adequate measurement of infiltration through the soil structure domain of these agricultural soils.

In practical applications of the PI method, it cannot be excluded that an experimental value of α^* is unavailable, requiring an estimated value for determining K_{fs}. According to Reynolds (2013), two K_{fs} values that differ by less than 25% are practically equal, while differences by two to three times could still be considered relatively small, given the wide range of possible K_{fs} values and the extreme spatial variability of K_{fs} observed in the field (Elrick and Reynolds, 1992b). According to these K_{fs} similarity criteria, this investigation suggested that using the first approximation value of α^* instead of an experimental value of this parameter can be expected not to have any adverse effect on K_{fs}

calculation (Acerra and Villabate, **Fig. 5**) or it could have no more than a limited influence on these calculations (Altofonte).

Between the two alternatives, using an experimental value of α^* seems preferable in general since it assures a more site-specific characterization of the soil. However, this suggestion could also represent an excess of caution since, according to this investigation and in agreement with Elrick and Reynolds (1992b), the simpler choice of using a literature estimate of α^* can be expected not to largely distort estimation of K_{fs}.

Given that the SATURO K_{fs} data for the Altofonte clay soil likely excluded most of the preferential or macropore permeability (**Fig. 4**), it could be argued that the most appropriate literature α^* value for this soil was the one associated with matrix-dominated flow in clay soils, i.e. 4 m^{-1} rather than 12 m^{-1}, as proposed by Elrick and Reynolds (1992b). This would bring the K_{fs}^{L} and K_{fs}^{E} datasets for Altofonte much closer together, given that the experimental α^* value was equal to 5.2 m^{-1} at this site (**Fig. 3**). This argument also applies for the untilled Villabate soil (**Fig. 4**) but the α^* value for Villabate (9.6 m^{-1}) remained close to the default value of 12 m^{-1} since this soil was coarser than that at Altofonte. Finally, the experimental α^* values for the Acerra and Villabate sites averaged to a geometric mean of 12.4 m^{-1} and an arithmetic mean of 12.8 m^{-1} and both values were very close to the first approximation value for agricultural soils, i.e. $\alpha^* = 12$ m^{-1}, supporting this choice.

More investigations should be performed to definitely demonstrate that a literature estimate of α^* is a generally plausible alternative to the experimental determination of this parameter. Should this be the case, determination of K_{fs} by both manual (PI) and automated (SATURO) methodologies could appreciably be simplified. In particular, a single-level run, that is more rapid and less water demanding than a two-level run, could be enough to determine K_{fs} at a sampling point. It should not be complicated for the manufacturer to adapt SATURO so that the instrument i) establishes a single value of H for the entire duration of the run, ii) determines a steady-state flow rate using the last part of the run, and iii) finally yields an estimate of K_{fs} using a value of α^* chosen by the operator from a short list of possible values. An additional modification might be to allow establishing a wide range of ponded head which could easily be adapted in the early stages of the experiment to accommodate changing soil conditions both within and between field sites. With these adaptions of the SATURO experiment, possible uncertainties about the validity of the calculated K_{fs}^{TPD} values could no longer have any reason to exist. An experimental methodology that could also be evaluated is the one based on the MPD approach (Reynolds and Elrick, 1990). This approach is more complicated and slower than the TPD approach because it uses three or more ponded heads. An advantage, however, is that the MPD approach can be expected to generally be less sensitive to soil heterogeneity than the TPD approach because it uses regression fitting to nullify the effects of random data-point scattering.

Likely, the SATURO methodology could also be adapted to conduct an automated MPD analysis, perhaps without even increasing measurement time. This objective could be reached if the initial pre-soak phase is dropped and each successive ponded head is greater than the previous head (i.e. $H_3 > H_2 > H_1$), as has been recommended for years to avoid potential hysteresis-induced flow perturbations in the wetting zone (Angulo-Jaramillo et al., 2016).

2.3.7 CONCLUSIONS

The simplest data validity criterion 1, only requiring a positive K_{fs} value, can generally be expected to differ from the classical, more stringent criterion 2 by the number of valid measurements. The summary statistics of K_{fs} should not change appreciably between the two criteria even if, at least occasionally, the former criterion could yield excessively high and variable K_{fs} values as compared with the latter one. The classical data validity criterion 2 is preferable since it ensures that only physically reliable results are included in the dataset. Instead, criterion 1 is not consistent with the TDP analysis of the infiltration data. Additional studies should be carried out also with reference to criterion 2. In particular, a question to be considered is that, if both K_{fs} and ϕ_m are valid, then also α^* should be valid regardless of its numerical value.

According to this investigation, SATURO and the PI method generally yielded relatively similar mean K_{fs} values, even if SATURO tended to yield rather small individual values of K_{fs} more frequently than the PI method. This result was attributed to differences in run duration, water volume used, and the reliability of the estimated steady-state infiltration rates between the two methods as well as the extremely high heterogeneity of the soil, especially at one of the field sites. In a very heterogeneous soil with highly permeable points, the PI method should be preferred since, with SATURO, several runs can be expected to fail due to the inability of the device to sustain very high flow rates. In other words, the maximum SATURO pumping rate seems too small for adequate measurement of infiltration through the soil structure domain of several agricultural soils.

Using the first approximation value of the α^* parameter for calculating K_{fs} seems a plausible alternative to the use of the experimentally determined value of this parameter. This result requires additional support that it would be practically important trying to obtain. Establishing that using an independent estimate of α^* does not compromise calculation of K_{fs} implies that the experiment can be simplified, by limiting it to a run with a single pressure head, long enough to ensure flow stabilization. With the manual methodology, there is no difficulty in doing this type of test. The automatic methodology could also be appropriately adapted to allow a simplified application of SATURO in the field.

Although the single-ring, steady-state methodology for determining the soil hydrodynamic properties has been in routine use for at least 35 years, some further investigations, also of methodological nature, are therefore still necessary. Hopefully, the recent introduction of SATURO will give new impetus to these investigations. This device appears an interesting alternative to the classical PI method for determining soil hydrodynamic properties. There is room for improving its performances and also simplifying its application in the field.

REFERENCES

Angulo-Jaramillo, R., V. Bagarello, M. Iovino, and L. Lassabatère. 2016. Infiltration Measurements for Soil Hydraulic Characterization. Springer International Publishing, Switzerland, ISBN 978-3-319-31786-1, 978-3-319-31788-5 (eBook), doi: 10.1007/978-3-319-31788-5, 386 pp.

Atalar, F., P.A.M. Leite, and B.P. Wilcox. 2025. A comparison of three methodologies for determining soil infiltration capacity in thicketized Oak woodlands and adjacent grasslands. Water, 17(4), 17 pp., doi: 10.3390/w17040518.

Bagarello, V., G. Baiamonte, M. Castellini, S. Di Prima, and M. Iovino. 2014. A comparison between the single ring pressure infiltrometer and simplified falling head techniques. Hydrological Processes, 28(18), 4843-4853, doi: 10.1002/hyp.9980.

Bagarello, V., M. Iovino, and J. Lai. 2013. Field and numerical tests of the two-ponding depth procedure for analysis of single-ring pressure infiltrometer data. Pedosphere, 23(6), 779-789, doi: 10.1016/S1002-0160(13)60069-7.

Bagarello, V., M. Iovino, and G. Tusa. 2000. Factors affecting measurement of the near-saturated soil hydraulic conductivity. Soil Science Society of America Journal, 64(4), 1203-1210, doi: 10.2136/sssaj2000.6441203x.

Bagarello, V., S. Di Prima, and M. Iovino. 2017. Estimating saturated soil hydraulic conductivity by the near steady-state phase of a Beerkan infiltration test. Geoderma, 303, 70-77, doi: 10.1016/j.geoderma.2017.04.030.

Bagarello, V., and A. Sgroi. 2004. Using the single-ring infiltrometer method to detect temporal changes in surface soil field-saturated hydraulic conductivity. Soil & Tillage Research, 76(1), 13-24, doi: 10.1016/j.still.2003.08.008.

Basile, A., G. Ciollaro, and A. Coppola. 2003. Hysteresis in soil water characteristics as a key to interpreting comparisons of laboratory and field measured hydraulic properties. Water Resources Research, 39(12), 12 pp., doi: 10.1029/2003WR002432.

Basile, A., A. Coppola, R. De Mascellis, and L. Randazzo. 2006. Scaling approach to deduce field unsaturated hydraulic properties and behavior from laboratory measurements on small cores. Vadose Zone Journal, 5(3), 1005-1016, doi: 10.2136/vzj2005.0128.

Ciollaro, G., and N. Lamaddalena. 1998. Effect of tillage on the hydraulic properties of a vertic soil. Journal of Agricultural and Engineering Research, 71(2), 147-155, doi: 10.1006/jaer.1998.0312.

Di Prima, S., L. Lassabatere, J. Rodrigo-Comino, R. Marrosu, M. Pulido, R. Angulo-Jaramillo, X. Úbeda, S. Keesstra, A. Cerdà and M. Pirastru. 2018. Comparing transient and steady-state analysis of single-ring infiltrometer data for an abandoned field affected by fire in Eastern Spain. Water, 10(4), 18 pp., doi: 10.3390/w10040514.

Di Prima, S., R.D. Stewart, M. Castellini, V. Bagarello, M.R. Abou Najm, M. Pirastru, F. Giadrossich, M. Iovino, R. Angulo-Jaramillo, and L. Lassabatere. 2020. Estimating the macroscopic capillary length from Beerkan infiltration experiments and its impact on saturated soil hydraulic conductivity predictions. Journal of Hydrology, 589, 11 pp., doi: 10.1016/j.jhydrol.2020.125159.

Ebrahimian, A., K. Sample-Lord, B. Wadzuk, and R. Traver. 2020. Temporal and spatial variation of infiltration in urban green infrastructure. Hydrological Processes, 34(4), 1016-1034, doi: 10.1002/hyp.13641.

Elrick, D.E., and W.D. Reynolds. 1992a. Infiltration from constant-head well permeameters and infiltrometers. Advances in Measurement of Soil Physical Properties: Bringing Theory into Practice. John Wiley & Sons, Ltd. pp. 1–24.

Elrick, D.E., and W.D. Reynolds. 1992b. Methods for analyzing constant-head well permeameter data. Soil Science Society of America Journal, 56(1), 320-323, doi: 10.2136/sssaj1992.03615995005600010052x.

Gardner, W.R. 1958. Some steady-state solutions of the unsaturated moisture flow equation with application to evaporation from a water table. Soil Science, 85(4), 228-232, doi: 10.1097/00010694-195804000-00006.

Garg, A., S. Kwakye, A. Cates, H. Peterson, K. LaBine, G. Olson, and V. Sharma. 2025. Field-saturated and near-saturated soil hydraulic conductivity as influenced by conventional and soil health management systems. Soil & Tillage Research, 248, 9 pp., doi: 10.1016/j.still.2025.106467.

Gómez, J.A., K. Vanderlinden, and M.A. Nearing. 2005. Spatial variability of surface roughness and hydraulic conductivity after disk tillage: Implications for runoff variability. Journal of Hydrology, 311(1–4), 143-156, doi: 10.1016/j.jhydrol.2005.01.014.

Hillel, D. 2003. Introduction to Environmental Soil Physics. Academic Press, doi: https://doi.org/10.1016/B978-0-12-348655-4.X5000-X, 498 pp.

Khaleel, R., and J.F. Relyea. 2001. Variability of Gardner's α for coarse-textured sediments. Water Resources Research, 37(6), 1567-1575, doi: 10.1029/2000WR900398.

Lee, D.M., W.D. Reynolds, D.W. Elrick, and B.E. Clothier. 1985. A comparison of three field methods for measuring saturated hydraulic conductivity. Canadian Journal of Soil Science, 65(3), 563-573, doi: 10.4141/cjss85-060.

Lilliefors, H.W. 1967. On the Kolmogorov-Smirnov test for normality with mean and variance unknown. Journal of the American Statistical Association, 62(318), 399-402, doi: 10.1080/01621459.1967.10482916.

Mertens, J., D. Jacques, J. Vanderborght, and J. Feyen. 2002. Characterisation of the field-saturated hydraulic conductivity on a hillslope: In situ single ring pressure infiltrometer measurements. Journal of Hydrology, 263(1–4), 217-229, doi: 10.1016/S0022-1694(02)00052-5.

Naik, A.P., T. Norbu, and S. Pekkat. 2024. Comparison of flux-based and head-based methods for determination of near-surface saturated hydraulic conductivity. Hydrological Sciences Journal, 69(3), 275-293, doi: 10.1080/02626667.2024.2305745.

Ravi, S., L. Wang, K.F. Kaseke, I.V. Buynevich, and E. Marais. 2017. Ecohydrological interactions within "fairy circles" in the Namib Desert: Revisiting the self-organization hypothesis. Journal of Geophysical Research: Biogeosciences, 122(2), 405-414, doi: 10.1002/2016JG003604.

Reynolds, W.D. 2008. Chapter 77. Saturated hydraulic properties: Ring infiltrometer. In M. R.Carter & E. G. Gregorich (Eds.), Soil sampling and methods of analysis, 2nd ed., Boca Raton, Canadian Society of Soil Science, ISBN-13: 978-0-8493-3586-0 (alk. paper), pp. 1043-1056.

Reynolds, W.D. 2013. An assessment of borehole infiltration analyses for measuring field-saturated hydraulic conductivity in the vadose zone. Engineering Geology, 159, 119-130, doi: 10.1016/j.enggeo.2013.02.006.

Reynolds, W.D., B.T. Bowman, R.R. Brunke, C.F. Drury, and C.S. Tan. 2000. Comparison of tension infiltrometer, pressure infiltrometer, and soil core estimates of saturated hydraulic conductivity. Soil Science Society of America Journal, 64(2), 478-484, doi: 10.2136/sssaj2000.642478x.

Reynolds, W.D., and D.E. Elrick. 1990. Ponded infiltration from a single ring: I. Analysis of steady flow. Soil Science Society of America Journal, 54(5), 1233-1241, doi: 10.2136/sssaj1990.03615995005400050006x.

Reynolds, W.D., and D.E. Elrick. 2002. Pressure infiltrometer. In: Dane, J.H. and Topp, G.C., editors, Methods of Soil Analysis, Part 4, Physical Methods, Number 5. Book Series, Inc., Madison, WI, USA. pp. 826–836.

Russo, D., I. Russo, and A. Laufer. 1997. On the spatial variability of parameters of the unsaturated hydraulic conductivity. Water Resources Research, 33(5), 947-956, doi: 10.1029/96WR03947.

Saha, A.K., J.T. McMaine, T. Trooien, P. Sexton, and C. Graham. 2024. Impact of no-till, crop rotation, cover crop, and drainage on soil physical and hydraulic properties. Soil Science Society of America Journal, 88(2), 239-257, doi: 10.1002/saj2.20614.

Stewart, R.D., and M.R. Abou Najm. 2018. A comprehensive model for single ring infiltration. I: Initial water content and soil hydraulic properties. Soil Science Society of America Journal, 82(3), 548-557, doi: 10.2136/sssaj2017.09.0313.

Tecca, N.P., J. Nieber, and J. Gulliver. 2022. Bias of stormwater infiltration measurement methods evaluated using numerical experiments. Vadose Zone Journal, 21(5), 16 pp., doi: 10.1002/vzj2.20210.

Vandervaere, J.-P., M. Vauclin, and D.E. Elrick. 2000. Transient flow from tension infiltrometers. I. The two-parameter equation. Soil Science Society of America Journal, 64(4), 1263-1272, doi: 10.2136/sssaj2000.6441263x.

Vauclin, M., D.E. Elrick, J.L. Thony, G. Vachaud, P. Revol, and P. Rouelle. 1994. Hydraulic conductivity measurements of the spatial variability of a loamy soil. Soil Technology, 7(3), 181-195, doi: 10.1016/0933-3630(94)90020-5.

Verbist, K., J. Baetens, W.M. Cornelis, D. Gabriels, C. Torres, and G. Soto. 2009. Hydraulic conductivity as influenced by stoniness in degraded drylands of Chile. Soil Science Society of America Journal, 73(2), 471-484, doi: 10.2136/sssaj2008.0066.

Verbist, K., S. Torfs, W.M. Cornelis, R. Oyarzún, G. Soto, and D. Gabriels. 2010. Comparison of single- and double-ring infiltrometer methods on stony soils. Vadose Zone Journal, 9(2), 462-475, doi: 10.2136/vzj2009.0058.

Welker, A., J. Press, K. Sample-Lord, and V. Smith. 2025. Estimation of rain garden field hydraulic conductivity based on spot infiltration tests. Water, 17(3), 17 pp., doi: 10.3390/w17030418.

White, I., and M.J. Sully. 1987. Macroscopic and microscopic capillary length and time scales from field infiltration. Water Resources Research, 23(8), 1514-1522, doi: 10.1029/WR023i008p01514.

White, I., and M.J. Sully. 1992. On the variability and use of the hydraulic conductivity alpha parameter in stochastic treatments of unsaturated flow. Water Resources Research, 28(1), 209-213, https://doi.org/10.1029/91WR02198.

Wu, L., L. Pan, M.J. Roberson, and P.J. Shouse. 1997. Numerical evaluation of ring-infiltrometers under various soil conditions. Soil Science, 162(11), 771-777, doi: 10.1097/00010694-199711000-00001.

Yilmaz, D., M. Sağlam, S. İç, R.D. Stewart, and L. Lassabatere. 2024. K_s estimates using macroscopic capillary length estimated from soil hydraulic shape coefficients and Haverkamp infiltration model. Soil & Tillage Research, 244, 13 pp., doi: 10.1016/j.still.2024.106235.

Zhang, S.Y., I. Hopkins, L. Guo, and H. Lin. 2019. Dynamics of infiltration rate and field-saturated soil hydraulic conductivity in a wastewater-irrigated cropland. Water, 11(8), 21 pp., doi: 10.3390/w11081632.

CHAPTER 3: Monitoring of the Soil-Plant-Atmosphere (SPAc) System

Background

The SPAc represents a dynamic and interconnected system through which water moves along energy potential gradients, linking soil water storage, plant transport mechanisms, and atmospheric demand. First conceptualized by John Philip (1966), the SPAc framework has become a cornerstone in ecohydrology and precision water management in agricultural systems, offering a unifying perspective on the processes that govern water transfer from the soil to the atmosphere (Sperry et al., 2003; Ranatunga, 2012; De Swaef et al., 2022).

Within this continuum, water movement is not merely a physical process but results from the interaction of multiple biophysical mechanisms controlled by plant physiology, soil hydraulic properties, and atmospheric forcing variables such as radiation, temperature, and vapor pressure deficit (Manzoni et al., 2012; Mencuccini et al. 2019; Ma et al., 2022). Understanding these linkages is crucial because changes in one compartment can propagate throughout the system, affecting plant water status, transpiration dynamics and, ultimately, crop productivity.

In the context of increasing climatic variability and mounting pressure on freshwater resources, monitoring individual components of the SPAc continuum has proven to be an inadequate approach for developing sustainable and resilient irrigation strategies (Rallo et al., 2018; Zhang et al., 2021; Schweiger et al., 2023). An integrated monitoring approach enables the simultaneous quantification of energy exchanges and water dynamics across soil, plant, and atmospheric compartments, thereby revealing the feedbacks and functional relationships that govern soil water redistribution, crop physiological responses, and environmental drivers of plant growth (Raij-Hoffman et al., 2024; Vanella et al., 2025; Conesa et al., 2023).

Recent advances in sensor technology and data analytics now enable high-resolution, continuous, and non-destructive quantification of key variables such as soil moisture, plant water potential, and evapotranspiration. The integration of these multi-source data streams supports the validation of process-based models and the development of predictive tools for adaptive irrigation management (Zhang et al., 2019; Cecilia et al., 2022; Saggi and Jain, 2022). Ultimately, the mechanistic understanding derived from continuous SPAc monitoring offers the quantitative basis required to implement deficit irrigation strategies tailored to crop-specific physiological thresholds. By linking real-time information on soil water availability, plant water potential, and atmospheric demand, this approach enables dynamic irrigation scheduling that maximizes water use efficiency, minimizes losses, and strengthens the resilience of cropping systems to climatic variability (El-Naggar et al., 2020; Jamroen et al., 2020; Zhang et al., 2021; Bwambale et al., 2022; Lee et al., 2023).

To investigate the interactions within the SPAc under real operating conditions, an integrated monitoring platform was established at the Villabate experimental site (Sicily, Italy), enabling the continuous assessment of soil, plant, and atmospheric variables under contrasting irrigation strategies.

Chapter 3 is organized as follows. Chapter **3.1**, based on the paper *"The open-Lab vision of Prof. Provenzano at the Villabate site: integration of novel technologies for sensor-driven irrigation management"* published in *QUADERNI DI IDRONOMIA MONTANA* (Alagna et al., 2024) introduces the "open-Lab" vision of Professor Provenzano at the Villabate experimental site (Sicily, Italy), detailing the creation of a field laboratory where novel technologies for sensor-driven irrigation management are integrated and tested under real operating conditions. Chapter **3.2** describes the integrated monitoring framework implemented at the Villabate site and the theoretical principles and operational characteristics of the main sensor systems adopted to monitor the three components of the SPAc. Particular attention is devoted to the continuous acquisition of atmospheric variables (ETo), soil water status (Drill & Drop probes), plant water status (Scholander pressure chamber and FloraPulse microtensiometers), and plant transpiration dynamics through sap flow sensors. Chapter **3.3** presents the results of the SPAc monitoring campaign conducted during the 2022–2024 irrigation seasons, which corresponded with the PhD period. The chapter analyses the interactions between climatic variability, irrigation management, soil water availability, plant water status, and transpiration dynamics under Full Irrigation (FI), Deficit Irrigation (DI), and farmer-managed irrigation (TI). Particular emphasis is placed on the coupled behaviour of soil water content, stem water potential, and sap flow as indicators of the physiological response of mandarin trees to contrasting irrigation regimes. Finally, Chapter **3.4**, based on the paper "*Assessing microtensiometers for monitoring stem water potential in mandarin (Citrus reticulata Blanco) orchard under different irrigation regimes"* published in *Agricultural Water Management* (Vaccaro et al., 2025), assesses the reliability of innovative FloraPulse microtensiometers for continuous monitoring of stem water potential in mandarin orchards by comparing their performance with that of the conventional Scholander pressure chamber under different irrigation strategies.

REFERENCES

Autovino, D., Rallo, G., & Provenzano, G., 2018. Predicting soil and plant water status dynamic in olive orchards under different irrigation systems with Hydrus-2D: Model performance and scenario analysis. *Agricultural water management*, *203*, 225-235.

Bwambale, E., Abagale, F. K., & Anornu, G. K., 2022. Smart irrigation monitoring and control strategies for improving water use efficiency in precision agriculture: A review. *Agricultural Water Management*, *260*, 107324.

Cecilia, B., Francesca, A., Dalila, P., Carlo, S., Antonella, G., Francesco, F., ... & Mauro, C., 2022. On-line monitoring of plant water status: Validation of a novel sensor based on photon attenuation of radiation through the leaf. *Science of The Total Environment*, *817*, 152881.

Conesa, M. R., Conejero, W., Vera, J., & Ruiz-Sánchez, M. C. 2023. Assessment of trunk microtensiometer as a novel biosensor to continuously monitor plant water status in nectarine trees. *Frontiers in Plant Science, 14,* 1123045.

De Swaef, T., Pieters, O., Appeltans, S., Borra-Serrano, I., Coudron, W., Couvreur, V., ... & Wyffels, F., 2022. On the pivotal role of water potential to model plant physiological processes. *in silico Plants*, *4*(1), diab038.

El-Naggar, A. G., Hedley, C. B., Horne, D., Roudier, P., & Clothier, B. E., 2020. Soil sensing technology improves application of irrigation water. *Agricultural Water Management*, *228*, 105901.

Jamroen, C., Komkum, P., Fongkerd, C., & Krongpha, W., 2020. An intelligent irrigation scheduling system using low-cost wireless sensor network toward sustainable and precision agriculture. *Ieee Access*, *8*, 172756-172769.

Lee, T., Jang, W. S., Chun, B., Ahmad, M. J., Jung, Y., Kim, J., & Shin, Y., 2023. Development of irrigation schedule and management model for sustaining optimal crop production under agricultural drought. *Paddy and Water Environment*, *21*(1), 31-45.

Ma, Y., Liu, H., Yu, Y., Guo, L., Zhao, W., & Yetemen, O., 2022. Revisiting soil water potential: Towards a better understanding of soil and plant interactions. *Water*, *14*(22), 3721.

Manzoni, S., Vico, G., Porporato, A., & Katul, G., 2013. Biological constraints on water transport in the soil–plant–atmosphere system. *Advances in Water Resources*, *51*, 292-304.

Mencuccini, M., Manzoni, S., & Christoffersen, B., 2019. Modelling water fluxes in plants: from tissues to biosphere. *New Phytologist*, *222*(3), 1207-1222.

Philip, J. R. 1966. Plant water relations: Some physical aspects. *Annual Review of Plant Physiology, 17,* 245-268.

Raij-Hoffman, I., Vanella, D., Ramírez-Cuesta, J. M., Peddinti, S. R., & Kisekka, I. 2024. Detecting soil water redistribution in subsurface drip irrigated processing tomatoes using electrical resistivity tomography, proximal sensing and hydrological modelling. *Science of the Total Environment, 912,* 169620.

Ranatunga, K., 2012. Soil-tree-atmosphere water relations. *Atmospheric Model Applications. Cranberra: Bureau of Metorology*, 157-194.

Saggi, M. K., & Jain, S., 2022. A survey towards decision support system on smart irrigation scheduling using machine learning approaches: Ks saggi, s. jain. *Archives of computational methods in engineering*, *29*(6), 4455-4478.

Schweiger, A. H., Zimmermann, T., Poll, C., Marhan, S., Leyrer, V., & Berauer, B. J., 2023. The need to decipher plant drought stress along the soil–plant–atmosphere continuum. *Oikos*, *2023*(9), e10136.

Sperry, J. S., Stiller, V., & Hacke, U. G. 2003. Xylem hydraulics and the soil–plant–atmosphere continuum: opportunities and unresolved issues. *Agronomy Journal, 95(6),* 1362-1370.

Vanella, D., Guarrera, S., Ferlito, F., Longo-Minnolo, G., Milani, M., Pappalardo, G., ... & Consoli, S. 2025. Effects of organic mulching and regulated deficit irrigation on crop water status, soil and yield features in an orange orchard under Mediterranean climate. *Science of The Total Environment, 958,* 177528.

Zhang, J., Guan, K., Peng, B., Pan, M., Zhou, W., Grant, R. F., ... & Wu, G., 2021. Assessing different plant-centric water stress metrics for irrigation efficacy using soil-plant-atmosphere-continuum simulation. *Water Resources Research*, *57*(9), e2021WR030211.

Zhang, X., Zhang, F., Zhang, Y., & Ai, X., 2019. Water saving irrigation decision-making method based on big data fusion. *International Journal of Performability Engineering*, *15*(11), 2916.

3.1 The open-Lab vision of Prof. Provenzano at the Villabate site: integration of novel technologies for sensor-driven irrigation management

V. Alagna[1], D. Autovino[1], V. Bagarello[1], G. Baiamonte[1], G. Ciraolo[2], D. De Caro[2], L. Franco[3], M. Fusco[1], M. Iovino[1], M. Ippolito[2], A. Motisi[1], G. Vaccaro[1]

[1] Dipartimento di Scienze Agrarie, Alimentari e Forestali, Università di Palermo, mariachiara.fusco@unipa.it

[2] Dipartimento di Ingegneria, Università di Palermo, Viale delle scienze, 8 - 90128 Palermo PA - Italy

[3] Irritec S.p.A., Via Gambitta Conforto, 98071 Capo D'Orlando, ME, Italy

Sommario

Il sistema continuo suolo-pianta-atmosfera, SPAc, è caratterizzato da continui scambi di flussi di massa ed energia il cui monitoraggio è importante ai fini di una efficiente gestione idrica in agricoltura.

Il Professore Provenzano, nel corso dei suoi trent'anni di attività accademica, si è occupato di tematiche relative alla gestione dell'irrigazione, focalizzando il tema del risparmio idrico a diverse scale spaziali. Dal 2017, ha concentrato i propri sforzi nella realizzazione di un laboratorio a cielo aperto nell'agro di Villabate (Palermo, Italia). Secondo la Sua visione, il concetto di open-Lab prevedeva l'integrazione di nuove tecnologie per la gestione dell'irrigazione tramite sensori, dando la possibilità all'utenza (industria dell'irrigazione, gruppi di ricerca, agricoltori, studenti, ecc.) di testare le proprie tecnologie, e di condividere conoscenze ed esperienze pratiche nel campo dell'irrigazione di precisione. Considerata la complessità degli agrumeti, l'open-Lab di Villabate pone attenzione sulla sensoristica di ultima generazione per il monitoraggio del sistema SPAc, utilizzando anche tecnologie ICT, e sui modelli agro-idrologici e di bilancio energetico per la gestione esperta dell'irrigazione.

Il sito sperimentale comprende tre parcelle gestite con diverse strategie irrigue, una delle quali dotata di un sistema irriguo a spruzzo e le altre due di un sistema di subirrigazione.

Le informazioni acquisite negli ultimi sei anni dal complesso dei sensori presenti presso l'open-Lab rappresentano un robusto set di dati utilizzabile per migliorare la gestione dell'irrigazione in sistemi di colture sparse come gli agrumeti. In particolare, l'implementazione di queste tecniche di monitoraggio in un sistema di supporto alle decisioni può consentire di sviluppare indirizzi gestionali finalizzati al risparmio idrico in un'ottica di adattamento al cambiamento climatico.

Abstract

The soil-plant-atmosphere continuum, SPAc, is characterized by continuous fluxes of mass and energy, which need to be monitored for an efficient water management in agriculture.

Professor Provenzano, during his thirty years of academic activities, has dealt with issues related to irrigation management and has focused on water saving at different spatial scales. Since 2017, he has concentrated his efforts on the creation of an irrigation open-Lab at Villabate (Palermo, Italy). According to his vision, the concept of open-Lab envisaged the integration of novel technologies for

sensor-driven irrigation management and gave the possibility to anyone (irrigation industry, research groups, farmers, students, etc.) to test their technologies, to join know-how and practical experiences in the field of precision irrigation. Considering the complexity of the citrus orchard system, the Villabate open-Lab focalizes attention on the last-generation sensors for the soil-plant water status monitoring, also using ICT technologies, and on agro-hydrological and energy balance models for expert irrigation management, according to the well-known water-saving strategies (sustainable and/or regulated deficit irrigation), thus involving different water distribution systems.

The experimental site consists of three plots managed with different irrigation strategies, one equipped with a sprinkler irrigation system and the other two with a subsurface drip irrigation system.

The information acquired by the sensors system in the last six years at the open-Lab represents a robust dataset useful to improve irrigation management in sparse crop systems like the citrus orchards. Specifically, the implementation of these technologies in a Decision Support System can be utilized for developing improved management practices aimed at water saving in the frame of contrasting the climate change impacts.

3.1.1 Introduzione

Nel prossimo futuro la produzione agricola dovrà aumentare per soddisfare la domanda alimentare di una popolazione in continua crescita. Si stima che, per garantire la sicurezza alimentare della popolazione globale, il Mondo debba produrre circa il 60% di cibo in più entro il 2050, e che per farlo debba preservare e valorizzare le risorse naturali di base (FAO, 2021).

Considerando che tra i vari settori produttivi dell'uomo, l'agricoltura assorbe la maggior parte di queste risorse e, considerata la necessità di adattamento ai cambiamenti climatici, salvaguardando la resilienza degli agrosistemi, sarà necessario ripensare allo sviluppo agricolo attraverso l'applicazione di strategie e metodi per il miglioramento della sostenibilità delle produzioni, soprattutto quel-le in irriguo, per adeguarsi alle continue evoluzioni del sistema (Provenzano et al., 2014).

Molte aree a vocazione arboricola-frutticola richiedono notevoli volumi idrici destinati all'irrigazione per garantire il successo della coltivazione, e la redditualità aziendale. In tal senso, l'innovazione tecnologica ha introdotto numerose novità in materia di irrigazione, permettendo di risparmiare notevolmente la risorsa idrica. Il progresso delle conoscenze nel campo dell'irrigazione di precisione ha contribuito a migliorare l'uniformità della distribuzione dell'acqua, e allo stesso tempo a ridurre i volumi idrici somministrati e l'energia necessaria per gli adacquamenti, promuovendo l'applicazione di metodi di irrigazione più efficienti, come quello dell'irrigazione localizzata a bassa pressione.

Nell’ambito di tale metodo irriguo, la subirrigazione (SDI) permette di applicare acqua e sostanze nutritive direttamente nel volume di suolo occupato dall’apparato radicale delle piante e, quindi, di limitare le perdite per evapora-zione superficiale e percolazione profonda, pur garantendo un’elevata produttività (Rallo et al., 2011). Questa tecnica permette di raggiungere elevati valori di efficienza d’utilizzo dell’acqua, spesso superiori al 90%, se associata ad un monitoraggio delle componenti del sistema continuo Suolo-Pianta-Atmosfera, SPAc, e ad una corretta stima delle esigenze della coltura. Tuttavia, vi è incertezza nel prendere decisioni in materia di irrigazione in assenza di dati di campo che includano anche la variabilità temporale e spaziale del sistema SPAc. Di conseguenza, l'uso di indicatori che misurano direttamente lo stato idrico del suolo e delle piante, rappresenta un passo significativo verso l'irrigazione di precisione per evitare sia condizioni di stress idrico indesiderate, che possono penalizzare la qualità e la resa della produzione, sia un eccesso dei volumi irrigui che può causare lo spreco di acqua e fertilizzanti, aumentando così i costi e influendo negativamente sulla sostenibilità ambientale dell’irrigazione.

Al fine di ottimizzare l’efficienza d’uso dell’acqua è necessario, quindi, da una parte, progettare sistemi di irrigazione finalizzati ad ottenere elevati valori di uniformità di distribuzione in campo e, dall’altra, che durante la gestione si utilizzino strategie irrigue che prevedano l’applicazione di volumi idrici strettamente necessari a soddisfare le esigenze di consumo della coltura.

Inoltre, i volumi d’adacquamento possono essere ulteriormente ridotti, applicando condizioni di deficit idrico (DI) controllato durante specifiche fasi del ciclo fenologico delle colture senza influenzarne il risultato produttivo e, talvolta, migliorandone la qualità (Kennedy et al., 2002; Castellarin et al., 2007). La gestione del DI è effettivamente applicabile soltanto se supportata da un sistema di monitoraggio in campo che consenta di conoscere, in tempo reale, lo stato idrico della coltura (Capra et al., 2008).

Le moderne tecnologie dell'informazione e della comunicazione (ICT), integrate con la sensoristica per il monitoraggio dello stato idrico nel sistema SPAc, permettono di creare un ambiente intelligente in grado di fornire informazioni in tempo reale agli agricoltori tramite applicazioni accessibili su dispositivi mobili o computer, nonché di utilizzare avanzate strategie di gestione irrigua, come l'applicazione del DI controllato per le piante (Provenzano et al., 2018).

3.1.2. Open-Lab di Villabate

Tra le colture tipiche del Mediterraneo, gli agrumi rappresentano la seconda coltura frutticola più coltivata nell'Unione Europea (Rallo et al.,2017). Considerando l’elevato fabbisogno idrico degli agrumi e l’ampia superficie coinvolta, vi è un crescente interesse nel migliorare la sostenibilità colturale, ottimizzando l’uso dell’acqua, e al contempo, preservando la produttività e massimizzando i benefici economici (Provenzano et al., 2013, Rodriguez-Sinobas et al., 2016). Risulta quindi importante digitalizzare la pratica irrigua per il comparto agrumicolo in maniera tale da utilizzare efficientemente la risorsa idrica.

In ambito accademico, la “terza missione” è basata sul trasferimento tecnologico e sulla divulgazione scientifica delle attività svolte nell’ambito della ricerca, al fine di promuovere la corretta informazione dei cittadini su tematiche di impatto sociale, ambientale ed economico, utili a favorire la consapevolezza del progresso delle conoscenze e delle società. Per adempiere agli scopi della terza missione, il Professore Provenzano ideò la realizzazione di un laboratorio irriguo a cielo aperto costituito da un campo sperimentale in cui si potesse realizzare l’integrazione delle più avanzate tecnologie per la gestione esperta dell’irrigazione mediante l’utilizzo di sensori. Al contempo, l’open-lab avrebbe dovuto offrire la possibilità a diversi attori, come le industrie del settore dell’irrigazione, i consorzi di bonifica, gli agricoltori e gli studenti, di testare le proprie tecnologie e condividere conoscenze ed esperienze pratiche sulla gestione dell'irrigazione di precisione.

In quest’ottica, su un agrumeto commerciale impiantato a mandarino Tardivo di Ciaculli, ubicato nel territorio di Villabate, è stata effettuata la riconversione di un impianto irriguo tradizionale a spruzzo sottochioma con un più moderno impianto in subirrigazione automatizzato. Inoltre, il campo sperimentale è stato attrezzato con un sistema di sensori di ultima generazione per il monitoraggio in tempo reale del sistema SPAc, finalizzato alla determinazione dei parametri di programmazione dell’irrigazione, anche in condizioni di DI controllato, con rilievi automatici e continui dello stato idrico della pianta e dei flussi traspirativi. L’attività di ricerca che si svolge presso l’agrumeto di Villabate è pertanto indirizzata verso alcuni obiettivi principali come: 1) valutare le performance di un sistema di subirrigazione; 2) valutare gli effetti di strategie di deficit idrico controllato sul mandarineto; 3) confrontare diverse tipologie di sensori per il monitoraggio del SPAc. Tali attività di ricerca, tuttavia, sono in continua evoluzione, e di pari passo con le più aggiornate innovazioni nel campo della sensoristica e della modellazione agroidrologica.

3.1.3. Storia del campo sperimentale

Il mandarineto sperimentale di Villabate (**Fig. 1**) è costituito da tre parcelle di 0,4 ha ciascuna. In due di queste, nel 2017, in collaborazione con la Irritec ® S.p.A., è stato installato un impianto in subirrigazione dotato di ali gocciolanti con gocciolatori trattati con differenti sostanze allelopatiche per contrastare l’intrusione radicale, tipica degli impianti SDI. In particolare, vi sono quattro settori, ognuno con una replica, dotati di gocciolatori contenenti i seguenti principi attivi: rame (Cu), Trifluralin (R1) e Preventol ® (R2) e le loro performance vengono confrontate con quelle di analoghi gocciolatori non additivati (controllo, C).

Nelle due parcelle in cui è stato installato il sistema SDI vengono applicate due strategie irrigue. Nello specifico, in una parcella si applica la piena restituzione del fabbisogno idrico della coltura (Full Irrigation, FI); mentre nell'altra è prevista l'applicazione di condizioni di deficit idrico controllato (Deficit Irrigation, DI) nella seconda fase del ciclo fenologico della coltura, ossia nel periodo che va da inizio luglio a metà agosto.

Infine, nella terza parcella, l'irrigazione viene gestita dall'agricoltore secondo la sua esperienza (Traditional Irrigation, TI) e l'acqua viene somministrata con un sistema irriguo tradizionale del tipo "a baffo" tipico della zona.

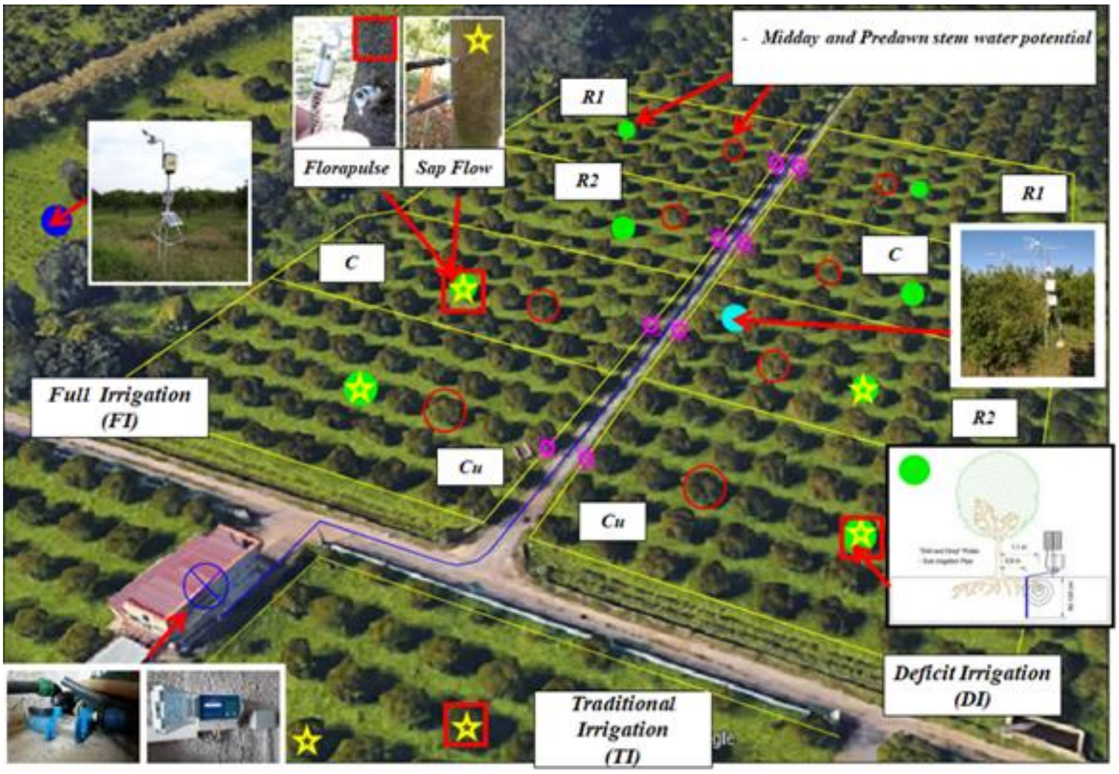

Fig. 1. Layout attuale dell'agrumeto di Villabate. Vengono indicate le tre parcelle di cui è composto il campo sperimentale (FI, DI e TI) ed evidenziati gli otto settori irrigui di cui si compongono le due parcelle in SDI con i diversi modelli di gocciolatori (Cu, C, R1 ed R2). È altresì indicata la posizione della stazione climatica (punto in blu) e la torre per la misura dei flussi evapotraspirativi secondo la tecnica Eddy Covariance (punto in azzurro), nonché i sensori Drill & Drop per il monitoraggio del contenuto idrico del suolo (punti in verde), i Sap-Flow per il monitoraggio dei flussi linfatici (stella gialla) e le sonde FloraPulse per il monitoraggio dei potenziali idrici delle piante (quadrato rosso).

Sempre nel 2017, in collaborazione con la Agrinet/Tuctronics (Walla Walla, WA, USA), sono state installate le sonde capacitive del tipo "drill & dropTM" per il monitoraggio in continuo del contenuto idrico del suolo. Le sonde permettono la misura contemporanea dell'umidità e della temperatura del suolo ogni 10 cm di profondità. Il sistema di acquisizione dei dati misurati dalle sonde "drill & dropTM" permette l'ottenimento dei dati da remoto e in tempo reale su pc o su smartphone, con l'impiego di una specifica applicazione (Agrinet, Tuctronics).

Dal 2018 ad oggi, il monitoraggio dello stato idrico della pianta è stato eseguito mediante la camera pressiometrica di Scholander, seguendo i protocolli di misura indicati da Turner e Jarvis (1982). Queste misure, negli anni, sono state affiancate dalla misura in continuo del potenziale xilematico attraverso l'utilizzo di psicrometri PSY1 della ICT International (Armidale, NSW, Australia). Il sensore utilizza due termocoppie collegate in serie all'interno di una camera in ottone cromato. La camera funge da isolante termico e permette la misura del differenziale di temperatura del tessuto vegetale e dell'aria della camera stessa. Applicando una corrente di raffreddamento e misurando la depressione psicrometrica generata all'interno della camera, è possibile ottenere misure del potenziale idrico della pianta a scala oraria ed in continuo.

Recentemente, i potenziali idrici misurati con la camera pressiometrica sono stati confrontati con quelli ottenuti tramite i microtensiometri FloraPulse che consentono la misura del potenziale idrico della pianta attraverso un sensore di pressione micro-elettromeccanico che può eseguire misurazioni in situ con scansione temporale di 20 minuti.

Per completare le acquisizioni sulle condizioni dello stato idrico delle piante, sono stati installati otto sensori per la stima del flusso linfatico (Sap-flow). Il metodo di misura si basa su una evoluzione del Transient Thermal Dissipation, proposto da Do and Rocheteau (2002), che utilizza lo stesso tipo di sensori del metodo Costant Thermal Dissipation (Granier, 1985). Quest'ultimo fa uso di sensori costituiti da una coppia di aghi, inseriti nell'alburno (legno tenero), ciascuno contenente una termocoppia e avvolti con un rivestimento resistivo. La differenza di temperatura che si genera tra il sensore superiore (costantemente riscaldato) e quello inferiore (che registra la temperatura del legno) fornisce un indice dell'attività traspirativa della pianta, espresso come variazione della densità di flusso linfatico, Ju (ml/cm^2 min). Successivamente, nel 2022, sono testati i sensori commerciali Treetoscope, che sono in grado di monitorare i flussi traspirativi delle piante. A differenza dei Sap-flow, quest'ultimi sono dotati di un singolo ago più robusto e seguono un differente modello di dissipazione del calore per misurare il movimento dell'acqua all'interno dell'alburno degli alberi.

La caratterizzazione agro-climatica dell'area di studio è stata condotta utilizzando i dati raccolti a partire dal giugno 2017 dalla stazione climatica WatchDog 2000 (Spectrum Technologies, Inc.), installata nei pressi dell'agrumeto. La stazione acquisisce, con cadenza semioraria, le grandezze fondamentali per la stima della richiesta evapotraspirativa dell'atmosfera, quali: la direzione e la velocità del vento a 2 m di altezza, la radiazione solare incidente, l'altezza di precipitazione, la temperatura media e l'umidità relativa dell'aria. A partire dal 2019, grazie alla collaborazione con il Dipartimento di Ingegneria, il monitoraggio delle variabili micro-metereologiche viene eseguito anche con una torre Eddy Covariance (EC) equipaggiata con: un anemometro sonico, un misuratore di concentrazione di H_2O e CO_2 in atmosfera, un radiometro netto e una piastra di flusso (CNR4, Campbell Scientific Inc., CSAT3-D, Campbell Scientific Inc., Li-7500, Li-cor bioscience Inc., HFP01SC, Hukseflux Inc.) per l'applicazione del bilancio energetico di superficie. La torre EC permette una stima dei flussi energetici e quindi una stima indiretta dell'evapotraspirazione effettiva.

Infine, alle misure acquisite a terra tramite la sensoristica, si sono recentemente raccolti dati telerilevati, termici e multispettrali, tra cui indici di vegetazione, ricavati da acquisizioni satellitari (Landsat-8, Sentinel-2 e PlanetScope) che da drone, Parrot Anafi thermal, equipaggiato con camera termica FLIR LEPTON 3.5 e camera RGB SONY CMOS 1/2.4".

3.1.4. Considerazioni conclusive

Il Professore Provenzano, nel corso dei suoi trent'anni di attività accademica, si è occupato di tematiche relative alla gestione dell'irrigazione, focalizzando il tema del risparmio idrico a diverse scale spaziali: dalla pianta al distretto irriguo.

Prima della sua tragica e prematura scomparsa, a partire dal 2017, ha concentrato i propri sforzi nella realizzazione di un laboratorio a cielo aperto nell'agro di Villabate, con l'obiettivo di promuovere il trasferimento tecnologico e la divulgazione dell'irrigazione di precisione, al fine di ottenere agroecosistemi più resilienti e sostenibili.

Considerata la complessità degli agrumeti, nell'open-Lab di Villabate viene focalizzata l'attenzione su dispositivi, modelli agro-idrologici e modelli di bilancio energetico di ultima generazione per il monitoraggio del sistema SPAc e per la gestione esperta dell'irrigazione, secondo le ben note strategie di risparmio idrico (sostenibili e/o deficit idrico controllato) che coinvolgono anche diversi sistemi di distribuzione irrigua.

Nel corso degli anni, quindi, grazie alle collaborazioni nazionali e internazionali e ai progetti di ricerca di cui Egli stesso era responsabile scientifico, sono stati implementati e testati diversi sensori che hanno permesso di ottenere un ricco database utilizzabile per la calibrazione dei parametri ecofisiologici che figurano nei modelli di simulazione agro-idrologica.

L'uso congiunto di tecniche irrigue ad alta efficienza, quali la subirrigazione, associate al monitoraggio ambientale delle componenti del SPAc permetteranno di ottenere mappe dettagliate dei consumi colturali e della produttività in funzione degli input colturali. Questo consentirà di mettere a punto un sistema efficace di supporto alle decisioni che possa assistere l'agricoltore nella scelta dei parametri di gestione irrigua tecnicamente ed economicamente più convenienti.

Il compito che i colleghi, i collaboratori e gli allievi del Professore Provenzano si onoreranno di proseguire sarà quello di mantenere attivo l'open-lab attraverso l'esecuzione di ulteriori campagne di misura, che arricchiranno il già rilevante database, e l'implementazione di nuova sensoristica, come lo SWATMO-kcb per la misura dell'evapotraspirazione di riferimento per la quale è già stata avviata una collaborazione con l'Università di Pisa.

BIBLIOGRAFIA

Capra, A., Consoli, S., & Scicolone, B. 2008. Water management strategies under deficit irrigation. *Journal of Agricultural Engineering, 39(4),* 27-34.

Castellarin, S. D., Matthews, M. A., Di Gaspero, G., & Gambetta, G. A. 2007. Water deficits accelerate ripening and induce changes in gene expression regulating flavonoid biosynthesis in grape berries. *Planta, 227(1),* 101-112.

Do, F., & Rocheteau, A. 2002. Influence of natural temperature gradients on measurements of xylem sap flow with thermal dissipation probes. 1. Field observations and possible remedies. *Tree physiology, 22(9),* 641-648.

Food and Agriculture Organization (FAO). 2021. The State of the World's Land and Water Resources for Food and Agriculture—Systems at Breaking Point. *Relatório Síntese 2021.*

Granier, A. 1985. Une nouvelle méthode pour la mesure du flux de sève brute dans le tronc des arbres. *In Annales des Sciences forestières* (Vol. 42, No. 2, pp. 193-200). EDP Sciences.

Kennedy, J. A., Matthews, M. A., & Waterhouse, A. L. 2002. Effect of maturity and vine water status on grape skin and wine flavonoids. *American Journal of Enology and Viticulture, 53(4),* 268-274.

Provenzano, G., & Sinobas, L. R. 2014. Special issue on trends and challenges of sustainable irrigated agriculture. *Journal of Irrigation and Drainage Engineering, 140(9),* A2014001.

Provenzano, G., Franco, L., Camboni, F., & Tuker, J. 2018. Implementing a cyber-physical system to monitor soil water status and environmental variables for irrigation scheduling. In *EGU General Assembly Conference Abstracts* (p. 12636).

Provenzano, G., Tarquis, A. M., & Rodriguez-Sinobas, L. 2013. Soil and irrigation sustainability practices. *Agricultural Water Management, 120*, 1-4.

Rallo, G., Agnese, C., Minacapilli, M., & Provenzano, G. 2012. Comparison of SWAP and FAO agro-hydrological models to schedule irrigation of wine grapes. *Journal of irrigation and drainage engineering, 138(7),* 581-591.

Rallo, G., González-Altozano, P., Manzano-Juarez, J., & Provenzano, G. 2017. Using field measurements and FAO-56 model to assess the eco-physiological response of citrus orchards under regulated deficit irrigation. *Agricultural water management, 180,* 136-147.

Rodríguez Sinobas, L., Provenzano, G., & Roldán Cañas, J. 2016. Water management strategies in irrigated areas. *Agricultural Water Management, 170,* 1-4.

Turner, N. C. 1988. Measurement of plant water status by the pressure chamber technique. *Irrigation science, 9(4),* 289-308.

3.2 Monitoring system and sensor network

The experimental field described in **Chapter 3.1** was equipped with an integrated monitoring system aimed at continuously characterizing the SPAc under different irrigation management strategies. The monitoring setup included sensors and instruments dedicated to the assessment of soil water status, plant water status, sap flow dynamics, and agro-meteorological variables. Measurements were acquired continuously during the irrigation seasons in order to evaluate the temporal response of the soil–plant system to atmospheric demand and irrigation scheduling.

The monitoring configuration evolved during the experimental period according to both research objectives and field constraints. In particular, additional sensors for soil water status monitoring were installed in the farmer-managed treatment during the 2024 season to extend the comparative analysis among irrigation strategies.

The following sections describe the instrumentation adopted, sensor installation procedures, monitored variables, and data acquisition protocols used throughout the study.

3.2.1 ETo Monitoring

Reference Evapotranspiration (ETo) represents the core agro-meteorological variable for quantifying atmospheric water demand and constitutes the basis for all irrigation scheduling models. It is defined as the amount of water that evaporates and transpires from a standardized reference surface, an extensive, uniformly grassed area, actively growing and not limited by water availability conditions (Allen et al., 1998). Expressed in daily millimetres, ETo provides the fundamental input for estimating crop water consumption (ETc) through the application of crop-specific coefficients (K_c) that account for species, canopy structure, and phenological stage.

ETo monitoring primarily relies on indirect methods based on physic-mathematical models that processing meteorological variable acquired by standard weather station WD 2000 (**Fig. 1**), installed nearby the experimental field.

Fig. 1 WatchDog 2000 series weather station

The FAO-56 Penman-Monteith equation (Allen et al., 1998), globally recognized as the most robust and transferable formulation, integrates net radiation, relative humidity, air temperature, and wind speed through the equation:

$$ETo = \frac{0.408(R_n - G) + \gamma \frac{900}{T+273} u_2(e_s - e_a)}{\Delta + \gamma(1 + 0.34u_2)} \quad (1.0)$$

where R_n is net radiation, G is soil heat flux, T is air temperature, u_2 is wind speed at 2 m height, e_s is saturation vapour pressure, e_a is actual vapour pressure, Δ is slope of vapour pressure curve, and γ is psychrometric constant.

In situations with limited meteorological data, simplified empirical approaches, such as the Hargreaves-Samani equation (Hargreaves & Samani, 1985) provide a practical alternative, although with reduced accuracy in contexts characterized by strong winds, high humidity, or variable cloud cover as uses only maximum and minimum For this reason, empirical formulations are recommended primarily for preliminary assessments or remote regions with minimal monitoring infrastructure (Pereira et al., 2015; 2021).

Direct methods for ETo measurement, while conceptually straightforward trough weighing lysimeters capable of detecting mass variations of the reference crop, remains restricted to experimental stations due to high installation costs, strict maintenance requirements, and challenges in reproducing standardized reference conditions at field scale (Pütz et al., 2018; López-Urrea et al., 2021; Kumari et al., 2022). Consequently, lysimeters are mainly used for validating theoretical models or refining K_c values.

The widespread deployment of automated weather stations equipped with high-precision sensors and real-time computing systems now enables continuous and reliable daily ETo estimation. These systems allow its integration into soil water status balance models, in which irrigation is triggered when cumulative water deficit exceeds predefined thresholds. This approach ensures efficient water use, aligning irrigation supply with both actual atmospheric demand and crop physiological needs, and represents a cornerstone of modern precision irrigation strategies.

3.2.2 Soil Water Status Monitoring

Soil water content represents the primary reservoir from which the plant draws, and its accurate assessment is a prerequisite for rational irrigation management within the SPAc (Bwambale et al., 2022). Monitoring soil water status is essential not only for optimizing water use efficiency but also for maintaining crop productivity and environmental sustainability. Measurement techniques are divided into direct methods, which quantify water through physical extraction and weighing procedures, and indirect methods, which infer water content from relationships between the soil physical properties of the and sensor signals. The gravimetric method (Topp and Ferré, 2002) represents the simplest and most widely used direct approach, involving sample collection, wet-weight measurement, oven-drying at 105°C until constant weight, and reweighing to calculate gravimetric water content (U [g/g]) and subsequently volumetric water content (θ) through the relation:

$$\theta = U \times \left(\frac{\rho_b}{\rho_w}\right) \tag{1.1}$$

where ρ_b and ρ_w are the bulk density of soil and water, respectively. While this method provides high accuracy and serves as a reference for calibrating other sensors, its destructive nature makes it unsuitable for continuous monitoring.

In contrast, indirect techniques enable continuous, non-destructive assessment of soil moisture dynamics, providing the temporal resolution necessary for adaptive irrigation strategies such as deficit irrigation (Bwambale et al., 2022; Zhang et al., 2024). Among these, Neutron Scattering (NS) provides highly precise measurements of soil water status by, detecting the thermalization of fast neutrons emitted from a radioactive source as they collide with hydrogen atoms in soil water. Despite its accuracy, technique is constrained by several factors that limit its application including health risks due to radiation, high cost, and insensitivity near the soil surface to shallow depth ($\leq$ 0.3 m) (Evett and Steiner, 1995; Visvalingam & Tandy, 1972; Jarvis and Leeds-Harrison, 1987; Quan et al., 2021; Zhan et al., 2022; Rasheed et al., 2022).

More practical for routine and field-scale applications are dielectric methods such as Frequency Domain Reflectometry (FDR) and Time Domain Reflectometry (TDR) (Robinson et al., 2008). These techniques estimate volumetric water content (θ_v) by measuring the soil's dielectric permittivity, which increases significantly with water content due to the high dielectric value of water ($\varepsilon \approx 80$) compared with that of air ($\varepsilon \approx 1$) and the solid phase ($\varepsilon \approx 3$–7). FDR and TDR sensors offer an excellent compromise between accuracy, cost, and operational simplicity, making them suitable for distributed sensor networks and real-time monitoring. Their performance, however, depends on proper installation, site-specific calibration and careful consideration of factors such as salinity and soil texture, which may influence the dielectric response (Topp, et al., 1984; Topp et al., 2003; Abdulraheem et al., 2024).

Complementary to water content measurements, tensiometers provide a direct measure of the tension with which water is held in the soil (matric potential, ψ_m), a key parameter for defining irrigation thresholds based on the soil water retention curve, as it indicates the effort required by the root system to extract water. To overcome the spatial limitations of point measurements, advanced geophysical techniques like Electrical Resistivity Tomography (ERT) allow for 2D or 3D visualization of soil moisture distribution across larger volumes, effectively capturing soil profile heterogeneity, wetting patterns and root-zone dynamics essential for assessing irrigation uniformity (Zhou et al., 2001; Michot et al., 2003; de Jong et al., 2020).

Looking ahead, monitoring strategies in perennial systems such as a citrus orchard are expected to evolve toward the synergistic integration of advanced sensing technologies. Wireless sensor networks and IoT platforms already allow real-time, multi-depth acquisition of hydrological parameters along the soil profile, optimizing water application at different depth, where the citrus root system is most active. The integration of these datasets with artificial intelligence algorithms allows the development of predictive systems capable of aligning irrigation scheduling to the physiological needs of the plant and the hydro-physical properties of the soil. By transforming point data into spatial and temporal variability maps, these technologies support site-specific irrigation decisions, maximizing water use efficiency and the productive quality of citrus orchards, while ensuring environmental and economic sustainability.

Within this technological landscape, the present study adopts Drill & Drop sensors, integrated with cloud platform, as the core instrument for continuous soil water status monitoring in the experimental mandarin orchard located at Villabate.

Drill & Drop sensors

The Drill & Drop probes (Sentek Pty, Ltd) represent a significant advancement in soil moisture monitoring technology, integrating multi-level capacitance sensors (FDR) along a single vertical rod to obtain high-resolution measurements across the root zone profile. Their ability to capture vertical soil water dynamics with minimal disturbance, coupled with their compatibility with automated data logging systems, makes them particularly suitable for evaluating the effects of Full and Deficit irrigation strategies within the SPAc monitoring framework.

The operating principle of Drill & Drop probes (**Fig. 2**) is based on the relationship between the apparent dielectric constant of the soil (ε) and its volumetric water content (θ), formalized by the calibration equation:

$$\theta = \frac{(SF-c)^{\frac{1}{b}}}{a} \quad (1.2)$$

where SF represents the scaled frequency normalized between air and water, while the parameters a, b, c, n are coefficients optimized for different soil types.

Fig. 2 Drill & Drop sensors

The simplified installation, requiring only standard drilling without the need for wells or access tubes, preserves the structural integrity of the soil profile while reducing the risk of air pocket formation. Despite the need of specific calibration for clay or organic soils and a high initial cost, their accuracy reaches ±0.03 m^3/m^3 after calibration, with automatic compensation for temperature and salinity effects.

3.2.3 Plant Water Status Monitoring

The assessment of plant water status represents a central component of SPAc monitoring, as it provides direct physiologically grounded measure of how crops respond to fluctuations in soil moisture and atmospheric evaporative demand. In contrast to soil-based measurements, which characterize water availability, plant-based indicators quantify the actual hydraulic functioning of the crop, capturing stress onset, diurnal dynamics, and cultivar-specific regulation mechanisms (Matese et al., 2018; Parkash and Singh, 2020; Losciale et al., 2023). For this reason, plant water status is considered the most reliable criterion for implementing precision irrigation strategies, including regulated and sustained deficit irrigation (Intrigliolo and Castel, 2004; Fernández et al., 2017; Blanco-Cipollone et al., 2017; Temnani et al., 2023).

The methods for monitoring the plant water status can be grouped into three main categories: i) osmotic/biochemical, ii) gravimetric/tissue hydration, and iii) thermodynamic/hydraulic approaches, each with specific principles, applications, and limitations.

i. Osmotic (or biochemical) methods exploit the ability of plant cells to release or absorb water when immersed in solutions with different osmotic potential (e.g., tissue immersion in reference solutions). Although useful for physiological studies on cell resistance and recovery from water loss, these approaches are destructive and poorly suited for field monitoring (Turner, 1981; Awad-Allah, 2020; Juenger and Verslues, 2023).

ii. Gravimetric methods and water content measurement techniques, which directly quantify the water content of plant tissue. These include calculating the absolute water content, expressed as the ratio between fresh weight and dry weight, and the relative water content (RWC), which measures the amount of water present compared to the maximum content at full turgor, providing a functional index of water status (Arndt et al., 2015; Noun et al., 2022; Ievinsh, 2023). The variation in leaf thickness, measured with magnetic or optical sensors, is also used as a non-destructive proxy. Although simple and widespread, their sensitivity to diurnal and seasonal variations in biomass and the often destructive of most measurements limit their applicability in operational irrigation management.

iii. Thermodynamic methods, based on the measurement of water potential (ψ), i.e., the energy state of water in the tissues offer the most robust and widely adopted metrics for field irrigation scheduling (Turner, 1981; Koide et al., 1989; Rodriguez-Dominguez et al., 2022). The reference technique uses a Scholander pressure chamber to measure the water potential of leaves or branches and the midday stem water potential is recognised as indicator for defining irrigation thresholds (Scholander et al., 1965; Jones, 2007; Fernández, 2017; Blanco and Kalcsits, 2021). Complementary tools include psychrometers and micro-tensiometers, such as the innovative FloraPulse probes, which enable continuous and automatable measurements of the xylem water potential directly in the trunk, overcoming the temporal limitations of traditional methods and providing high-frequency data suitable for automated irrigation decision support (Pagay, 2021; Pagay 2022; Lakso et al., 2022; Dainese et al., 2022; Conesa et al., 2023).

For a direct measurement of water consumption, Sap flow sensors offering an integrated assessment of whole plant transpiration by measuring the velocity and quantity of water transported in the xylem (Marshall, 1985; Davis et al., 2012; Forster, 2019; Capurro et al., 2024). These approaches are precise and informative but may require specific calibration. In addition to quantifying whole-plant water use, sap flow measurements provide an essential benchmark for validating SPAc transfer models and irrigation decision-support tools, as they directly quantify transpiration (Fuchs et al., 2017; Zhang et al., 2024; Zhao et al, 2025).

In recent years, advances in proximal sensing, biosensors, thermal and multispectral imaging, and satellite-based indices (e.g. NDVI, NDWI, CWSI) have further expanded the capacity to monitor plant water status across larger spatial scales overcoming the spatial and temporal limits of point measurements (Veysi et al., 2017; Marusig et al., 2020; Mohammad et al., 2025). The integration of these approaches with soil moisture measurements and atmospheric data within the SPAc framework provides a comprehensive description of SPAc interactions and facilitates the development of predictive, sensor-based irrigation strategies.

In the present thesis, plant water status in the mandarin orchard was monitored using a combination of Pressure Chamber, FloraPulse microtensiometers, and Sap Flow sensors, enabling both discrete and continuous evaluation of plant hydraulic responses under Full and Deficit irrigation treatments.

Scholander pressure chamber

The Scholander pressure chamber (Scholander et al., 1965), or "pressure bomb," is the reference instrument for the direct measurement of leaf or xylem water potential (Ψ_x). Its functioning is based on a mechanical principle of pressure balance between an externally applied gas pressure that counteracts the tension of the water column in the xylem, allowing the internal water potential of the plant tissue (symplast) to be inferred from the pressure required to force sap back to the cut surface.

The device (**Fig. 3**) consists of a robust metal container with thick walls, connected to a precision pressure gauge and a cylinder of inert gas (nitrogen), complete with an airtight sealing system for plant samples. During measurement, a plant sample (leaf or small shoot) is secured inside the chamber with the cut surface visible externally. By gradually applying nitrogen pressure, the cells surrounding the xylem vessels are compressed until the equilibrium pressure (P) is reached, at which sap reappears on the cut surface, corresponding to the xylem matric potential (Ψ_{mx}), according to the relation Ψ_x = -P.

Fig. 3 Scholander pressure chamber

The pressure chamber is considered the gold standard for accuracy and calibration in agronomy, particularly predawn (Ψ_{pd}) and midday (Ψ_{md}) measurements are used to assess water stress and define irrigation thresholds. Specifically, the Ψ_{pd} is representative of the soil water potential, Ψ_s, assuming that during the night the plant transpiration is close to zero (Rallo and Provenzano, 2013), while the Ψ_{md} measured on a non-transpiring stem provides an estimate of the plant water status that is strongly influenced by soil water status (Begg' And and Turner, 1970). Despite the pressure chamber is considered an affordable method for direct determinations of plant water status, it does have certain limitations. Measurements are destructive, discontinuous in time, provides only point measurements, and influenced by factors such as incomplete nocturnal rehydration soil–root hydraulic discontinuities, or nighttime transpiration under high vapor pressure deficits. These issues may reduce the reliability of Ψ_{pd} as an estimator of soil potential under extreme aridity or humidity conditions (Turner, 1981; Blanco & Kalcsits, 2021; Rodriguez-Dominguez et al., 2022).

FloraPulse sensors

FloraPulse sensors (**Fig. 4**) represent the technological evolution towards continuous and automated monitoring of xylem (stem) water potential (Ψ_{stem}), overcoming the limitations of destructiveness and discontinuity inherent in the Scholander pressure chamber (Blanco & Kalcsits, 2021; Lakso et al., 2022). The sensor functions as a microchip-based microtensiometer embedded in the woody tissue, where it equilibrates hydraulically with the surrounding xylem and directly measures water potential through a microfabricated diaphragm coupled to a piezoresistive pressure transducer (Pagay et al., 2014). When properly installed, the sensor provides accurate, stable, and high-frequency measurements of plant water status, enabling a truly continuous representation of plant hydraulic dynamics.

Fig. 4 FloraPulse sensor

The sensors are available in two versions: an SDI-12 digital probe and an analog probe, both equipped with a removable 5-pin connector for easy installation and maintenance. The digital version requires a 3.6-16V power supply and communicates via SDI-12 protocol, allowing direct integration into automated datalogging systems, while the analogue sensor uses a differential signal between positive and negative sense pins. Technical specifications include a water potential measurement range from 0.1 to 50 bar (±10% accuracy) and an operational temperature range of 0°C -70°C, with a standard cable length of 3 meters (extendable up to 50 m, though longer lengths may compromise data accuracy).

Installation is preferably done during morning hours when stem temperatures and transpiration rates are moderate. A narrow, precise hole is drilled in a flat and clean area of the trunk, to ensure intimate hydraulic contact between the sensor and the xylem; prolonged interruptions during installation must be avoided to prevent tissue desiccation or sensor malfunction. Once inserted and sealed, the sensor is connected to a datalogger to monitor parameters such as voltage, temperature, and current in real time, enabling continuous data collection and analysis via dedicated software.

The operating principle of FloraPulse microtensiometers is based on classical tensiometry, which relies on the thermodynamic equilibrium established between a small volume of pure water contained within the sensor and the surrounding xylem water. The sensing element consists of a microfabricated cavity filled with water and connected to the plant tissue through a nanoporous membrane with pore diameters of approximately 2 nm. Because the membrane is permeable to water but prevents air entry, the water inside the sensor equilibrates with the water potential of the surrounding xylem (Pagay et al., 2014).

At equilibrium, the chemical potential of water inside the sensor equals that of the external xylem water (Pagay et al., 2014, eq. 1):

$$\mu_{\mathrm{w,liq}}(T, P_{\mathrm{liq}}) = \mu_{\mathrm{w,xylem}}(T, P_{\mathrm{xylem}}) \tag{1.3}$$

Where: $\mu_{w,liq}$ is the chemical potential of water inside the sensor [J mol^{-1}]; $\mu_{w,xylem}$ is the chemical potential of xylem water [J mol^{-1}]; T is the absolute temperature K; P_{liq} is the pressure of the water contained within the sensor cavity [MPa]; and P_{xilem} is the pressure of water within the xylem conduits [MPa].

When transpiration increases, water within the xylem is subjected to increasingly negative pressures (tension). To maintain thermodynamic equilibrium, water evaporates from the sensor through the nanoporous membrane, causing a reduction in the pressure of the internal liquid. This pressure change induces a deformation of a silicon diaphragm integrated into the sensor. The diaphragm deformation is detected by a piezoresistive pressure transducer and converted into an electrical signal proportional to the internal water pressure.

Under thermodynamic equilibrium, the pressure of the water contained within the sensor cavity becomes directly related to the water potential of the surrounding xylem tissue. Consequently, the pressure difference between the internal liquid and the atmosphere provides a direct estimate of stem water potential according to:

$$\Psi_w = P_{liq} - P_{atm} \tag{1.4}$$

Where: Ψ_w is the water potential *[MPa]*; P_{liq} is the pressure of the water contained within the sensor cavity [MPa]; and P_{atm} is the atmospheric pressure [MPa].

In practical applications, P_{liq} is lower than atmospheric pressure; therefore, Ψ_w assumes negative values that reflect the tension under which water is held within the xylem.

Thus, the sensor provides a direct measurement of xylem water potential rather than an indirect estimation derived from empirical relationships. Within the range typically encountered in agricultural systems, the measured pressure difference can be considered numerically equivalent to stem water potential when expressed in MPa.

A key innovation of the microtensiometer design is the use of a nanoporous membrane, which greatly extends the operational range compared with conventional tensiometers. The maximum pressure difference that can be sustained before air enters the sensor is governed by the Young–Laplace equation:

$$\Delta P_{\text{max}} = \frac{2\sigma\cos\theta}{r_{\text{pore}}} \quad (1.5)$$

Where: $\Delta P_{max}$is the maximum pressure difference sustainable by the nanoporous membrane before air invasion occurs [MPa]; $\sigma$is the surface tension of water [N m^{-1}]; θ is the contact angle between water and the pore wall [°]; and $r_{pore}$is the pore radius $[m]$.

This relationship shows that smaller pore diameters allow the membrane to sustain larger negative pressures, thereby extending the operational range of the microtensiometer. Because the membrane pores are only a few nanometres in diameter, the sensor can maintain water under very high tension without cavitation, allowing stable measurements at water potentials below −10 MPa without cavitation of the internal water reservoir (Pagay et al., 2014). This extended measurement range makes microtensiometers particularly suitable for continuous monitoring of plant water status under both well-watered and water-limited conditions.

Once installed within the woody stem tissue, the sensor continuously tracks variations in stem water potential at high temporal resolution, providing detailed information on plant hydraulic responses to changes in soil water status and atmospheric evaporative demand. Compared with conventional pressure chamber measurements, microtensiometers enable automated, non-destructive and continuous monitoring of plant water status, making them particularly valuable for precision irrigation applications.

The strength of this technology lies in its ability to provide extremely high temporal resolution data without damaging the plant, enabling precision irrigation based on the plant's actual physiological state. However, its promising performance, large-scale adoption remains limited due to high costs, the need for accurate initial calibration, and the specialized expertise required for installation and data interpretation (Blanco & Kalcsits, 2021; Lakso et al., 2022). Furthermore, these sensors are relatively recent and have not yet been validated for all crop species, a gap that motivated the work carried out in this PhD thesis on citrus (Chapter **3.4**). Consequently, FloraPulse microtensiometers represent a valuable tool for investigating plant hydraulic behaviour, validating SPAc models, and supporting sensor-based precision irrigation strategies.

Sap Flow sensors

Sap flow sensors (**Fig. 5**) provide a direct measurement of water movement through the xylem, allowing the quantification of plant transpiration and water use. Unlike water potential measurements, which describe the hydraulic status of the plant at a given moment, sap flow measurements characterize the dynamic flux of water through the SPAc.

Fig. 5 Sap Flow sensors

The measurement method is based on the transient thermal dissipation (TTD) method following Isarangkool Na Ayutthaya et al. (2010). This approach, originally developed by Do and Rocheteau (2002a, 2002b), relies on the temporal variation of the temperature difference between two probes radially inserted into the xylem, one heated and the other unheated, with the heated probe operating under a cyclic heating-cooling regime. Compared with the classical constant heating method (Granier, 1985, 1987), the TTD method reduces sensitivity to natural thermal gradients, lowers energy consumption, and minimises thermal disturbance to plant tissues. The method relies on the difference in temperature, ΔT, between the heated and reference probes during successive heating and cooling phases. The resulting temperature signal is related to the convective cooling produced by sap movement or sup flux density, J_s [cm/min], within the xylem.

The transient temperature signal, ΔT_a was defined as:

$$\Delta T_a = \Delta T_{on} - \Delta T_{off} \quad (1.6)$$

where ΔT_{on} is the temperature difference at the end of the heating phase (10 min), and ΔT_{off} is the temperature difference after the cooling phase (20 minutes), resulting in a 30 min measurement interval for J_s.

The alternate flow index, K_a, was calculated as:

$$K_a = \frac{\Delta T_{0a} - \Delta T_{ua}}{\Delta T_{ua}} \tag{1.7}$$

where ΔT_{0a} is the maximum alternate temperature difference obtained under zero-flow conditions, and ΔT_{ua} is the measured signal under actual flow conditions. Using the multi-species linear calibration proposed by Isarangkool Na Ayutthaya et al. (2010), J_s was computed as:

$$J_s = 12.95K_a \tag{1.8}$$

At the whole-tree scale, transpiration flow, F_{tree} (L h^{-1}), is defined as:

$$F_{tree} = 10^{-3} J_s A_{sw} f_r \tag{1.9}$$

where $F_{tree}$is whole-tree transpiration flow (L h^{-1}), A_{sw} (cm^3) is the sap wood area, and f_r is a dimensionless radial correction factor ($f_r = 0.874$) accounting for the decline in flow towards the inner xylem (Isarangkool Na Ayutthaya et al., 2010).

Hourly J_s was calculated by averaging measurements from the two sap flow sensors installed on opposite sides of each tree.

A reduction in sap flow may result either from limited soil water status or from stomatal regulation aimed at preventing excessive declines in plant water potential. Consequently, sap flow measurements provide information on the actual physiological response of the plant to water stress, complementing water potential observations that describe the hydraulic status of the plant. Within the SPAc, sap flow therefore represents the functional link between water availability in the soil, plant hydraulic regulation, and atmospheric evaporative demand.

A custom low-power acquisition system based on an ESP8266 (Espressif Systems) microcontroller is used to record sap flow measurements. The system is powered by a solar-recharged lithium battery and enabled wireless data transmission via LoRa communication (RFM95W, HopeRF). Thermocouple signals were processed at the end of each heating–cooling cycle, and both raw and processed data were stored and transmitted for subsequent analysis.

Unlike the Scholander chamber (which provides discrete measurements of plant water stress) and FloraPulse probes (which continuously monitor plant water potential), sap flow sensors capture the plant's dynamic physiological response to environmental conditions. Within the SPAc framework, sap flow represents the functional response of the plant to the combined effects of soil water status and atmospheric demand. Consequently, sap flow measurements provide information not only on transpiration rates but also on the efficiency with which the plant is able to transport water from the soil to the atmosphere. Therefore, they are essential for water balance studies, evapotranspiration estimation at the single-plant level, and irrigation optimization based on actual consumption.

Because sap flow techniques measure transpiration directly, they are also valuable for validating biophysical models of plant water use and for refining ET estimates derived from indirect methods (e.g., Ψ-based stress coefficients, stomatal models, or remote sensing). A major limitation concerns calibration, which must account for species-specific wood anatomy, probe geometry, and especially the thickness of the active sapwood (Bush et al., 2010; Fuchs et al., 2017; Hu et al., 2022). Since sap flow estimates must be scaled by the cross-sectional area of functional xylem, accurate determination of sapwood depth is essential; however, its measurement is often invasive, time-consuming, or uncertain (particularly in species with gradual heartwood–sapwood transitions) introducing potential bias in transpiration estimates. In the present study, sap flow measurements were continuously acquired throughout the monitoring period; however, the conversion of sap flux density into whole-tree transpiration was not performed because the active sapwood area was not determined. Consequently, sap flow data were analysed as relative indicators of plant hydraulic activity and physiological response to the different irrigation treatments. However, when combined with continuous measurements of stem water potential, sap flow sensors enable a comprehensive interpretation of plant hydraulic behaviour by linking water transport, hydraulic status, and plant responses to environmental stress.

3.3 Results of Villabate SPAc monitoring

3.3.1 Climatic characterization

The climatic characterization was carried out using a standard weather station (WatchDog, WD 2000) installed near the experimental field. The agro-climatic variables required for the application of agrometeorological and agro-hydrological models were continuously acquired and analysed continuously in real time throughout the 2022–2024 monitoring period. The recorded sub-hourly dataset includes daily measurements of minimum and maximum air temperature [Tmin and Tmax, °C]; minimum and maximum relative humidity [RHmin and RHmax, %]; solar radiation [Rs, MJ/m²/d]; mean daily wind speed at 2 m above the soil [Ws, km/h]; daily rainfall and its cumulative values [Rain and Rain_cum, mm]; and the reference crop evapotranspiration, [ETo, mm] computed according to the FAO-56 Penman–Monteith formulation described in Section 3.2.1. These variables constitute the atmospheric boundary conditions of the SPAc and define the evaporative demand imposed on the three experimental plots, which were managed under subsurface drip irrigation with Full and Deficit treatments and under farmer-managed sprinkler irrigation (see section 3.1).

Figure 6 shows the evolution of the principal climatic parameters, aggregated at daily time scale, over the three growing seasons. Across the observation period, marked interannual variability was observed in temperature regime, radiation load, and rainfall distribution.

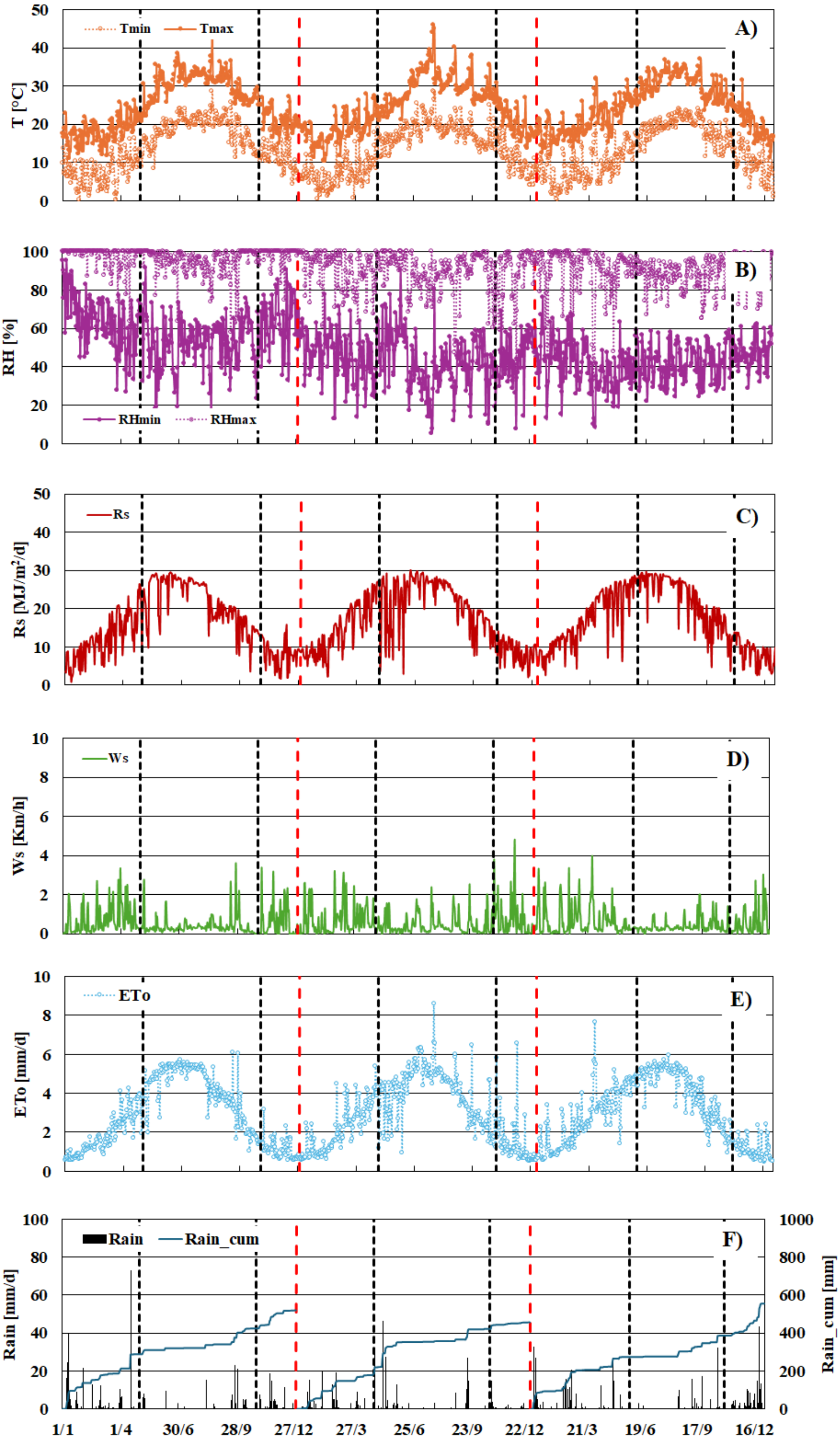

Fig. 6 Daily dynamics of a) maximum and minimum air temperatures (T_{max} and T_{min}), b) minimum and maximum relative air humidity (RH_{max} and RH_{min}), c) solar radiation (Rs), d) wind speed (Ws), e) crop reference evapotranspiration (ETo) and f) daily rainfall and its cumulative values (Rain and Rain_cum) for the 2022-2024 observation period. Black dashed lines denote the irrigation season, while red dashed lines indicate the end of the year.

During the irrigation season (June–September), the 2022 campaign exhibited marked intra-seasonal variability. Maximum air temperature frequently exceeded 35 °C, reaching a peak of 44.2 °C during mid-summer. Solar radiation showed substantial day-to-day fluctuations, particularly in July and August, while relative humidity minima varied considerably throughout the peak evaporative period. Although rainfall events occurred during the irrigation months, their cumulative contribution equal to 86.11 mm remained limited and was unevenly distributed, resulting in a seasonal ETo of 564.05 mm and the pluviometric deficit equal to 478 mm.

The 2023 irrigation season was characterized by more persistent high-temperature conditions. Maximum temperatures reached 45.4 °C, and extended dry intervals were observed between rainfall events. Relative humidity minima remained consistently low during July and August, while solar radiation was high and sustained during the central irrigation period, and lower and more variable at the beginning of the season. The combination of these atmospheric drivers led to a cumulative evaporative demand ETo of 560.50 mm over the June–September interval. While the cumulative rainfall was 88.12 mm over the same time interval, resulting in a pluviometric deficit of 472 mm.

In contrast, the 2024 irrigation season showed comparatively moderated maximum temperatures, with a peak of 37.0 °C. The early irrigation phase was characterized by slightly milder thermal conditions relative to the previous years. However, elevated solar radiation during July and August maintained significant evaporative demand despite lower absolute temperature extremes. The distribution of rainfall within the irrigation period was irregular, reaching 27.18 mm. This was the lowest amount recorded compared to other years. Meanwhile, the cumulative ETo was 552.09 mm, which was the lowest seasonal atmospheric demand of the three monitored years, but there was also the largest rainfall deficit, at 525 mm.

Overall, when restricted to the June–September irrigation period, interannual differences were primarily associated with maximum temperature extremes, persistence of high radiation during peak summer months, and cumulative rainfall and ETo. In particular, the precipitation for the three years of observation was 518 mm (in 2022), 455 mm (in 2023) and 554 mm (in 2024) respectively, and was concentrated in the periods from January and May, and from September and December. There were differences in terms of both rainy days and the daily amount, as specified below. These differences defined distinct atmospheric demand scenarios in which the Full, Deficit, and farmer-managed irrigation treatments were evaluated within the SPAc monitoring framework.

3.3.2 Irrigation scheduling and seasonal water application

Irrigation scheduling and water application differed among treatments and seasons, reflecting both experimental design and external constraints (**Figs. 7** and **8**). The experimental design included three irrigation treatments: Full Irrigation (FI) and Deficit Irrigation (DI), both managed through subsurface drip irrigation (SDI), and a farmer-managed treatment (TI) irrigated using a sprinkler system. A summary of irrigation management strategies, irrigation systems, and monitoring configuration adopted during the three monitored seasons is reported in **Table 1**.

Table 1. Summary of irrigation systems, irrigation management strategies, deficit application, and soil water content (SWC) monitoring configuration adopted in the FI, DI, and TI treatments during the 2022–2024 irrigation seasons.

Year	Treatment	Irrigation system	Irrigation management	Deficit application	SWC monitoring
2022 & 2023	FI	SDI	Full irrigation	No	Yes
	DI	SDI	Deficit irrigation	Yes	Yes
	TI	Sprinkler	Farmer-managed	No	No
2024	FI	Sprinkler	Farmer-managed	No	Yes
	DI	Sprinkler	Farmer-managed	No*	Yes
	TI	Sprinkler	Farmer-managed	No	Yes

Note: *Although the DI plot retained its original experimental designation in 2024, deficit irrigation was not applied due to water restrictions and the suspension of SDI water delivery.

While **Fig. 7** provides a quantitative synthesis of cumulative water inputs and atmospheric demand, **Fig. 8** illustrates the temporal distribution of irrigation and rainfall events. Irrigation events were generally concentrated within the period of highest reference evapotranspiration (ETo), which peaked during summer months. Rainfall events were sporadic during the irrigation season and contributed only marginally to crop water supply, reinforcing the dominant role of irrigation in determining plant water status.

The cumulative reference evapotranspiration (ETo) was comparable across years, reaching 1043 mm in 2022, 1076 mm in 2023, and 1092 mm in 2024. On average, approximately 50% of the atmospheric water demand was supplied by rainfall, with the remaining portion provided through irrigation, although relevant interannual differences were observed.

Rainfall distribution played a key role in determining seasonal water availability. In 2023, despite a higher number of rainy days (117), only 37 events exceeded 2.5 mm d^{-1}, compared to 45 out of 100 days in 2022 and 47 out of 98 days in 2024. This resulted in a lower effective contribution of rainfall to crop water supply in 2023, making it the driest year in terms of agronomic water availability. Consequently, water reserves in the dam were severely depleted, leading the irrigation authority to suspend water delivery for agricultural purposes in 2024, prioritizing civil use. As a result, the FI and DI plots retained their original experimental designation; however, both treatments were managed under the same farmer-operated sprinkler irrigation regime following the suspension of SDI water supply, consequently the irrigation patterns were more similar to those observed in the TI treatment. In fact, this shift resulted in less frequent but larger irrigation events compared to the previous seasons, as also evident from the temporal patterns shown in **Fig. 8**.

In 2022 and 2023, the Full Irrigation (FI) treatment was managed to fully satisfy crop evapotranspiration demand through subsurface drip irrigation (SDI), with frequent and regular irrigation events throughout the season. The Deficit Irrigation (DI) treatment followed the same scheduling except during the deficit period (from July 1st to August 15th), when irrigation frequency was reduced by approximately one event per week, resulting in a clear divergence in cumulative water application (**Fig. 7**).

The Farmer-managed treatment (TI), based on sprinkler irrigation, showed a different pattern characterized by lower frequency and higher volumes per event, leading to a more uneven temporal distribution of water inputs. The higher application efficiency of SDI led to significant water savings compared to the farmer-managed sprinkler system, with TI generally applying more water than SDI in 2022 and 2023, as reflected in cumulative volumes. In particular, FI reduced water use by 13.2% in 2022 and 35.1% in 2023, while DI achieved even greater savings of 33.2% and 60.0%, respectively. In contrast, in 2024, water savings were minimal (4.4% for both FI and DI), as all treatments were irrigated using the same sprinkler system due to water restrictions, leading to a convergence of irrigation practices.

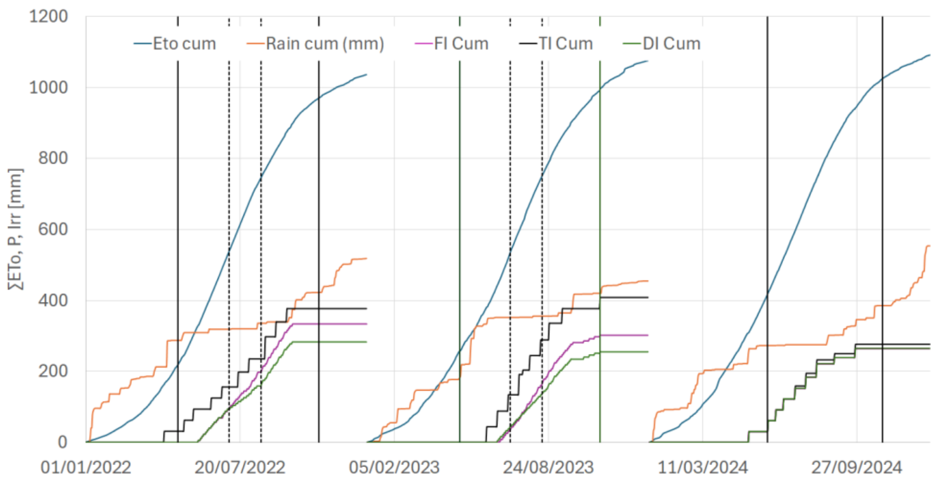

Fig. 7 Cumulative rainfall (Rain cum), cumulative crop reference evapotranspiration (ETo cum), and cumulative irrigation volumes for the Full Irrigation (FI), Deficit Irrigation (DI), and Traditional Irrigation (TI) treatments during the 2022–2024 period. The vertical black lines indicate the beginning and the end of the irrigation season, while the dashed lines indicate the beginning and the end of the deficit application period.

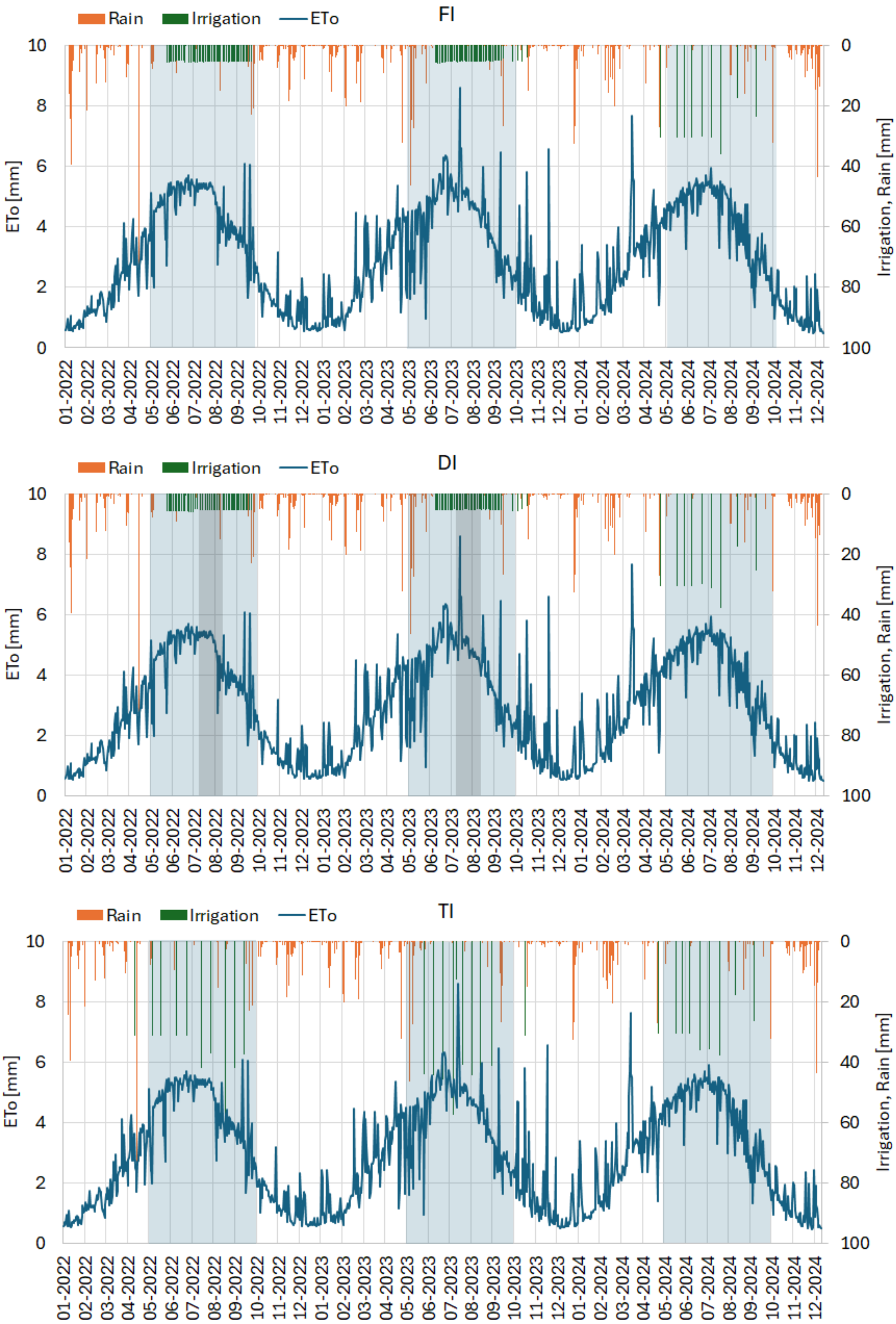

Fig. 8 Temporal dynamic of crop reference evapotranspiration (ETo), rainfall (Rain), and amount of irrigation (Irrigation), from 2022 to 2024, for the Full Irrigation (FI), Deficit Irrigation (DI), and Traditional Irrigation (TI) treatments. The light box indicates the irrigation season, while the dark box identifies the period of deficit application.

3.3.3 Soil water status dynamics

Soil water content (SWC) dynamics were analyzed over the period from July 14th to September 30th for all monitored seasons (**Figs. 9** and **10**), in order to ensure consistency with the time window of plant water status measurements. In all figures, blue dots represent the average SWC over the 0–0.60 m soil profile, while the shaded area indicates the associated standard deviation. Irrigation and rainfall events are shown as orange and green bars, respectively.

In 2022 and 2023 (**Fig. 9**), SWC was monitored only in the FI and DI treatments under subsurface drip irrigation (SDI), while no measurements were available for the farmer-managed treatment (TI). In 2024, SWC monitoring was extended to the TI plot (Fig. 9); however, due to water restrictions, all treatments were irrigated using a sprinkler system, resulting in more comparable irrigation patterns.

Under FI, SWC remained relatively stable in both 2022 and 2023, with values consistently ranging between approximately 30 and 32%, reflecting the high frequency and regularity of irrigation events typical of SDI systems. In contrast, DI exhibited a progressive decline in SWC during the deficit period. In 2022, SWC decreased from values close to 30% down to approximately 25%, followed by a rapid recovery after rainfall and the resumption of full irrigation, stabilizing again around 30%. In 2023, SWC remained lower throughout the deficit period, with values close to 25%, and showed only a limited recovery, thereafter, not exceeding 28–29% by the end of the monitoring period. This behaviour is consistent with the reduced effective contribution of rainfall observed in 2023 and the overall drier conditions.

The temporal patterns of SWC closely followed irrigation inputs (**Fig. 9**), with SDI treatments characterized by small and frequent increases in soil moisture, whereas rainfall events produced only short-lived responses.

In 2024 (**Fig. 10**), SWC dynamics differed markedly from previous seasons due to the shift in irrigation management. All treatments were irrigated using a sprinkler system and managed by the farmer, resulting in less frequent but higher-volume irrigation events (approximately on a biweekly basis). This led to more pronounced oscillations in soil moisture in both FI and DI, generally ranging between 20 and 30%, with sharp increases following irrigation events and subsequent gradual declines. In contrast, the TI treatment maintained consistently higher SWC values, ranging approximately between 30 and 38%, with peaks following irrigation. These differences likely reflect site-specific soil conditions and water retention capacity.

The variability of SWC, as indicated by the standard deviation, was generally comparable among treatments, although slightly lower variability was observed in the TI plot in 2024, suggesting more homogeneous soil moisture conditions.

Overall, SDI ensured stable soil moisture conditions through frequent and low-volume applications, while sprinkler irrigation led to more pronounced wetting–drying cycles. The adoption of deficit irrigation amplified soil moisture depletion, particularly under high evaporative demand, with effects that were more evident in drier seasons.

These differences in SWC, driven by irrigation scheduling and seasonal conditions, directly influenced plant water status. In particular, the more stable soil moisture conditions observed under FI, compared to the progressive soil drying under DI and the larger wetting–drying cycles under farmer-managed irrigation in 2024, likely resulted in distinct plant water stress responses, as discussed in the following section.

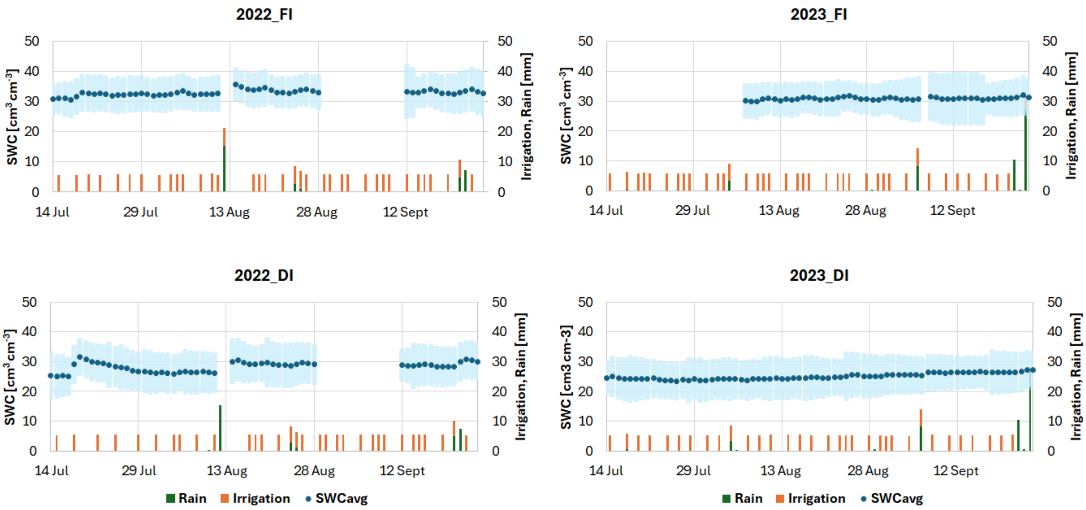

Fig. 9 Average soil water content (0-0.6 m) for the FI and DI treatments under subsurface drip irrigation during the 2022 and 2023 seasons. Water inputs (irrigation and rainfall) and standard deviation (light blue area) are shown.

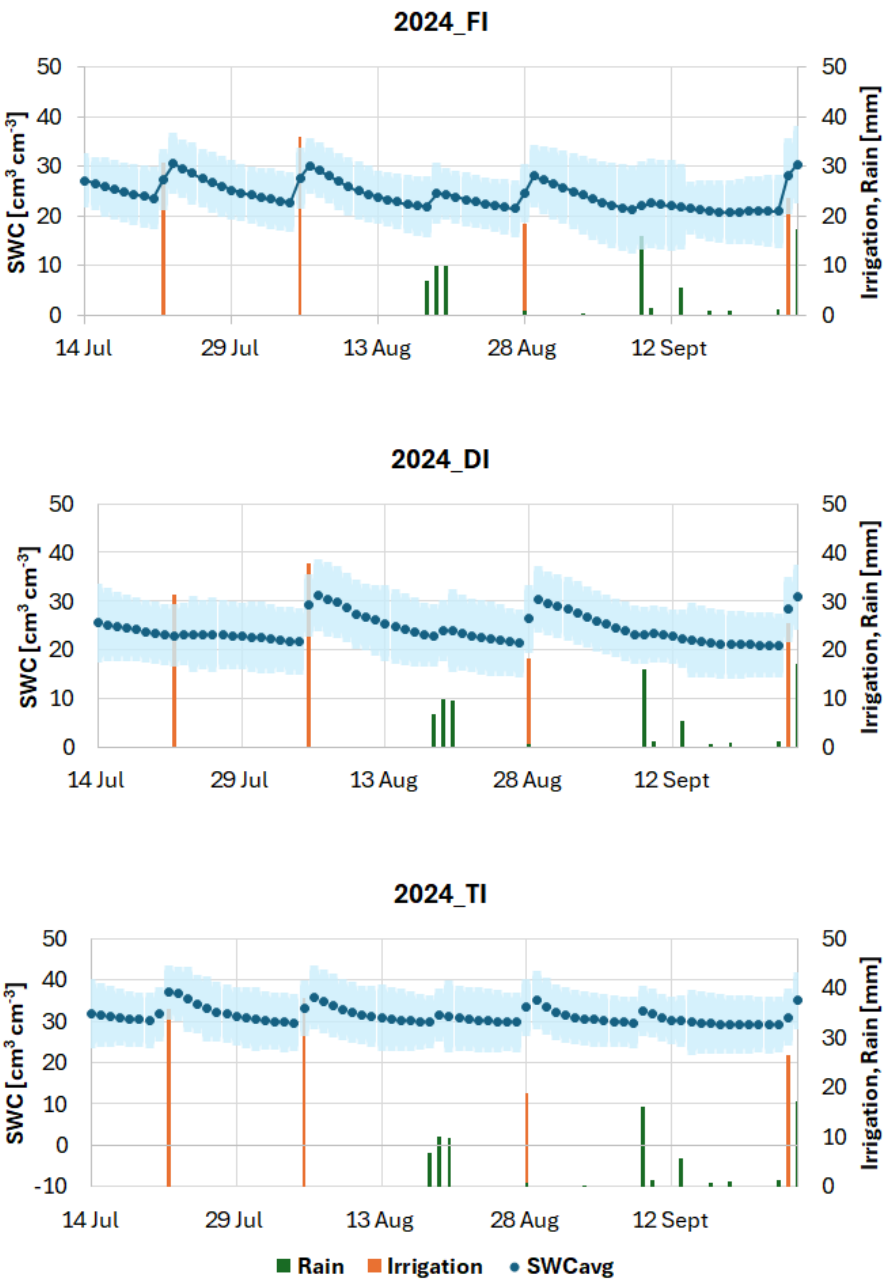

Fig. 10 Soil water content dynamics (0-60 cm) for FI, DI, and TI treatments under traditional micro-sprinkler irrigation during the 2024 season. Irrigation events, rainfall standard deviation (light blue area) are shown.

3.3.4 Plant water status dynamics

Figure 11 shows the temporal dynamics of stem water potential (Ψ) measured continuously by the FloraPulse sensors (Ψ_{mt}) and periodically with the pressure chamber (Ψ_{pc}) in the TI, FI and DI plots during the monitoring period (14 July – 22 September) across the 2022, 2023 and 2024 irrigation seasons. Irrigation, based on the adopted irrigation management strategy, and rainfall events are also shown.

Both measurement methods (FloraPulse sensors and pressure chamber) captured clear differences in Ψ dynamics among TI, FI, and DI treatments. Across all treatments and years, Ψ_{mt} exhibited a marked diurnal pattern, with minimum values occurring around midday, followed by a gradual recovery during the afternoon and nighttime. The amplitude and baseline of these oscillations were strongly influenced by soil water status (**Figs. 9–10**) and atmospheric demand, particularly during periods of high evaporative demand and heat-wave events observed during the monitored seasons. In general, Ψ_{mt} values were consistently less negative than Ψ_{pc} values, with differences between the two methods being more pronounced during the afternoon and under drier soil conditions, particularly before irrigation events.

In 2022, relatively stable climatic conditions and adequate irrigation supply resulted in limited plant water stress, especially under FI. In this treatment, Ψ_{mt} generally ranged between −0.5 and −1.3 MPa, consistent with the stable SWC values (~30–32%) observed over the same period. In DI, reduced irrigation frequency led to a gradual decline in plant water status during the deficit phase, with Ψ_{mt} reaching values close to −1.5 MPa, in agreement with the observed decrease in SWC (**Fig. 9**). The heat wave occurring around 18 August further highlighted differences among treatments: in FI Ψ_{mt} was equal to −1.7 and decreased to approximately −1.9 and −2.0 MPa in DI and TI, respectively. Following rainfall events and the resumption of full irrigation, a rapid recovery of both SWC and Ψ was observed.

In 2023, plant water status reflected the combined effect of reduced effective rainfall and higher evaporative demand. Despite a higher number of rainfall events, their low intensity resulted in limited soil water recharge, leading to persistently lower SWC values (~25–28%) in DI. Under these conditions, Ψ_{mt} reached more negative values than in 2022, with minima approaching −1.3 MPa in DI, while FI maintained less negative values, albeit with slightly greater variability compared to the previous year. During the extreme heat-wave event (air temperatures exceeding 45 °C; **Fig. 6**), Ψ_{mt} values were approximately −1.5 MPa in TI and reached up to −2.0 MPa in FI, suggesting that plant water status was influenced not only by instantaneous soil water status but also by antecedent conditions.

In 2024, plant water status was strongly influenced by the shift in irrigation management imposed by water restrictions, as the adoption of farmer-managed irrigation, characterized by less frequent, higher-volume applications, resulted in continuous oscillations between saturation and water deficit conditions in the soil (**Fig. 10**), directly reflected in Ψ dynamics. In both FI and DI, Ψ_{mt} showed large oscillations, typically ranging between −0.5 and −2.5 MPa, with rapid declines during drying phases and sharp recoveries following irrigation events. Differences between FI and DI remained detectable despite similar SWC trends, possibly reflecting differences in plant response or plant–sensor coupling.

At the beginning of the monitoring period, the TI plot showed less negative Ψ_{mt} values compared to FI and DI. This behaviour may be related to differences in root system development and adaptation to irrigation regimes, as plants under long-term sprinkler management could have developed a more extensive root system, enabling access to a larger soil volume.

The plant water status closely tracked both soil moisture dynamics and irrigation scheduling across years. Stable SWC conditions under SDI (FI) supported relatively favourable plant water status, whereas deficit irrigation induced controlled water stress, which was more pronounced under drier climatic conditions (2023). In contrast, the irregular irrigation regime adopted in 2024 led to increased variability in both soil and plant water status.

The comparison between Ψ_{mt} and Ψ_{pc} showed good agreement in terms of temporal trends and treatment differences, with Ψ_{pc} values generally falling within the range of daily minimum Ψ_{mt}, confirming the reliability of continuous measurements for capturing plant water stress dynamics.

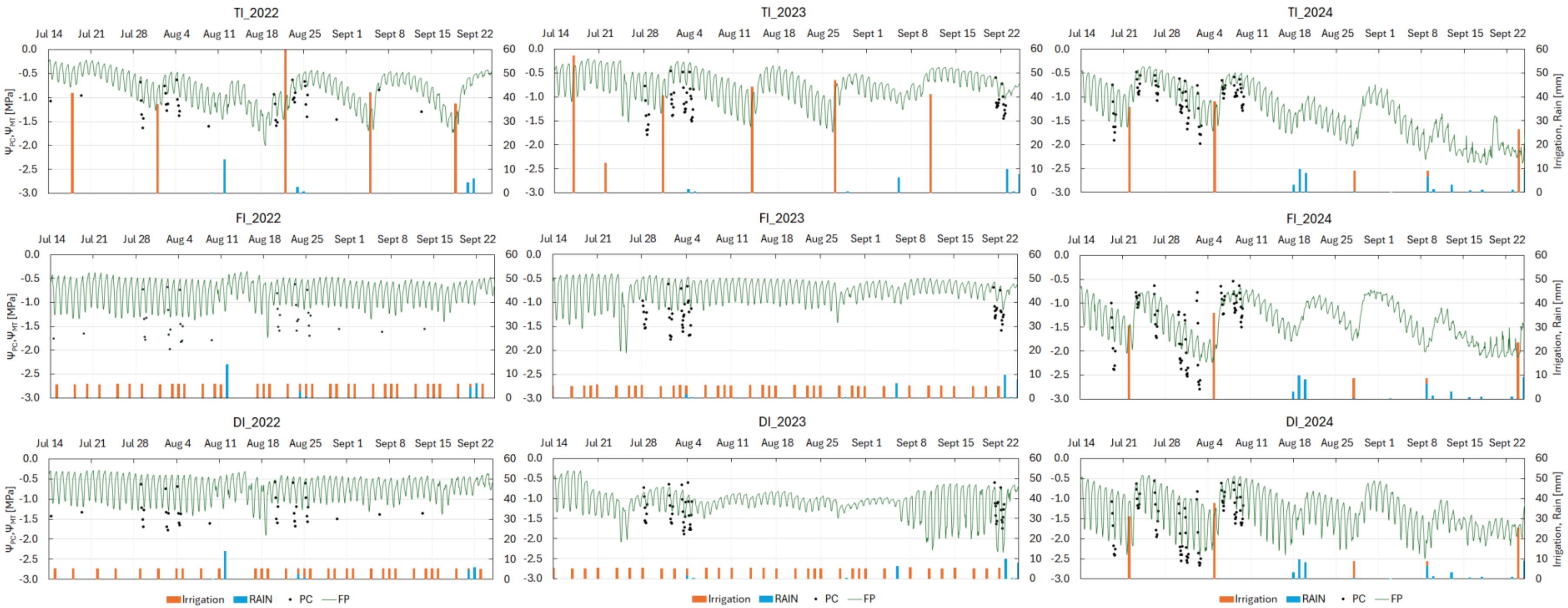

Fig. 11 Temporal dynamics of Ψmt, Ψpc, irrigation, and rainfall during the 2022, 2023 and 2024 monitoring periods

3.3.5 Sap flow dynamics and its relationship with soil water content

The assessment of the plants' physiological response to different irrigation regimes was complemented by monitoring sap flow. **Figure 12** shows the temporal dynamics of sap flux density (J_s , cm min^{-1}) measured in the FI, DI, and TI treatments during the monitoring period (14 July–30 September) across the 2022, 2023, and 2024 irrigation seasons, together with reference evapotranspiration (ETo, mm h^{-1}), used as an indicator of atmospheric water demand. Across all treatments and years, J_s exhibited a clear diurnal pattern closely coupled with atmospheric demand, increasing during the morning, peaking around midday, and gradually declining during the afternoon and nighttime. Sap flow dynamics closely followed the hourly variations in ETo, both during clear-sky days, characterized by smooth and continuous patterns, and during cloudy days, when rapid fluctuations in ETo were reflected by corresponding variations in J_s. Each panel reports the three irrigation treatments, allowing direct comparison among irrigation management strategies.

Analysis of the daily sap flow patterns highlights that, despite the application of deficit irrigation (DI treatment), plants were generally able to satisfy atmospheric demand during the early morning and evening hours, when transpiration requirements were lower. During the first part of the day, sap flow was likely sustained by the partial recovery of plant water status occurring overnight. However, in the central hours of the day, reduced soil water status under DI limited the plant's ability to maintain sap flow rates comparable to those observed under FI and TI conditions.

In 2022, under relatively stable climatic conditions and adequate soil water status, J_s closely tracked ETo in all treatments, indicating a weak limitation of transpiration. Peak J_s values were generally higher in FI and TI (approximately 0.6–0.7 cm min^{-1}) compared to DI (around 0.4–0.5 cm min^{-1}), reflecting the reduced water availability under deficit irrigation. The DI treatment showed a progressive reduction in peak *u* during the deficit period, consistent with the decline in SWC (**Fig. 9**). Following rainfall events and the resumption of full irrigation, J_s increased, confirming the strong coupling between soil water status and plant transpiration.

In 2023, sap flow dynamics reflected the combined effect of high atmospheric demand and reduced effective rainfall. Despite lower SWC values compared to 2022, particularly in DI, J_s values remained comparable to or slightly higher than those observed in the previous season. In DI, peak J_s values generally remained above 0.4 cm min^{-1} throughout the monitoring period, indicating that transpiration was maintained despite reduced soil water status and more negative Ψ values. FI and TI showed patterns broadly comparable to 2022, although TI exhibited a progressive reduction in peak U towards the end of the season. These results suggest that plants were able to sustain transpiration under drier conditions, likely through increased water potential gradients between soil and atmosphere.

In 2024, sap flow dynamics were strongly influenced by the shift from SDI to farmer-managed sprinkler irrigation. Compared to previous years, FI generally exhibited lower J_s values, likely reflecting the transition from frequent low-volume irrigation to less frequent and higher-volume applications. In contrast, DI maintained J_s values comparable to those observed in previous seasons, despite pronounced wetting–drying cycles in soil moisture. This behaviour may indicate a greater physiological adaptation of DI plants to fluctuating water availability, as plants previously exposed to deficit conditions appeared less affected by the transition in irrigation management.

Unlike previous seasons, differences among treatments were often more pronounced during specific periods, particularly between late July and early August. During these phases, TI generally exhibited higher J_s values than FI and DI, consistent with the higher SWC observed in this treatment (**Fig. 10).** The greater water availability in TI likely supported higher transpiration rates during the days following irrigation events.

A characteristic response associated with sprinkler irrigation management was observed in TI throughout all monitored seasons and in FI and DI during 2024. In these cases, maximum J_s values were typically reached 2–3 days after irrigation rather than immediately after water application. This delayed response suggests a progressive recharge and redistribution of water within the soil profile, followed by a gradual recovery of plant transpiration.

Overall, sap flow density dynamically responded to the interaction between atmospheric demand, soil water status, and irrigation management. While SDI promoted relatively stable transpiration patterns through frequent water supply, sprinkler irrigation induced more pronounced temporal fluctuations in J_s associated with alternating wetting and drying cycles. The maintenance of relatively high J_s values under DI, particularly in 2023 and 2024, suggests that plants subjected to controlled water deficit were able to sustain transpiration even under reduced soil water status, highlighting the complex physiological adjustment of the soil–plant continuum to irrigation regime.

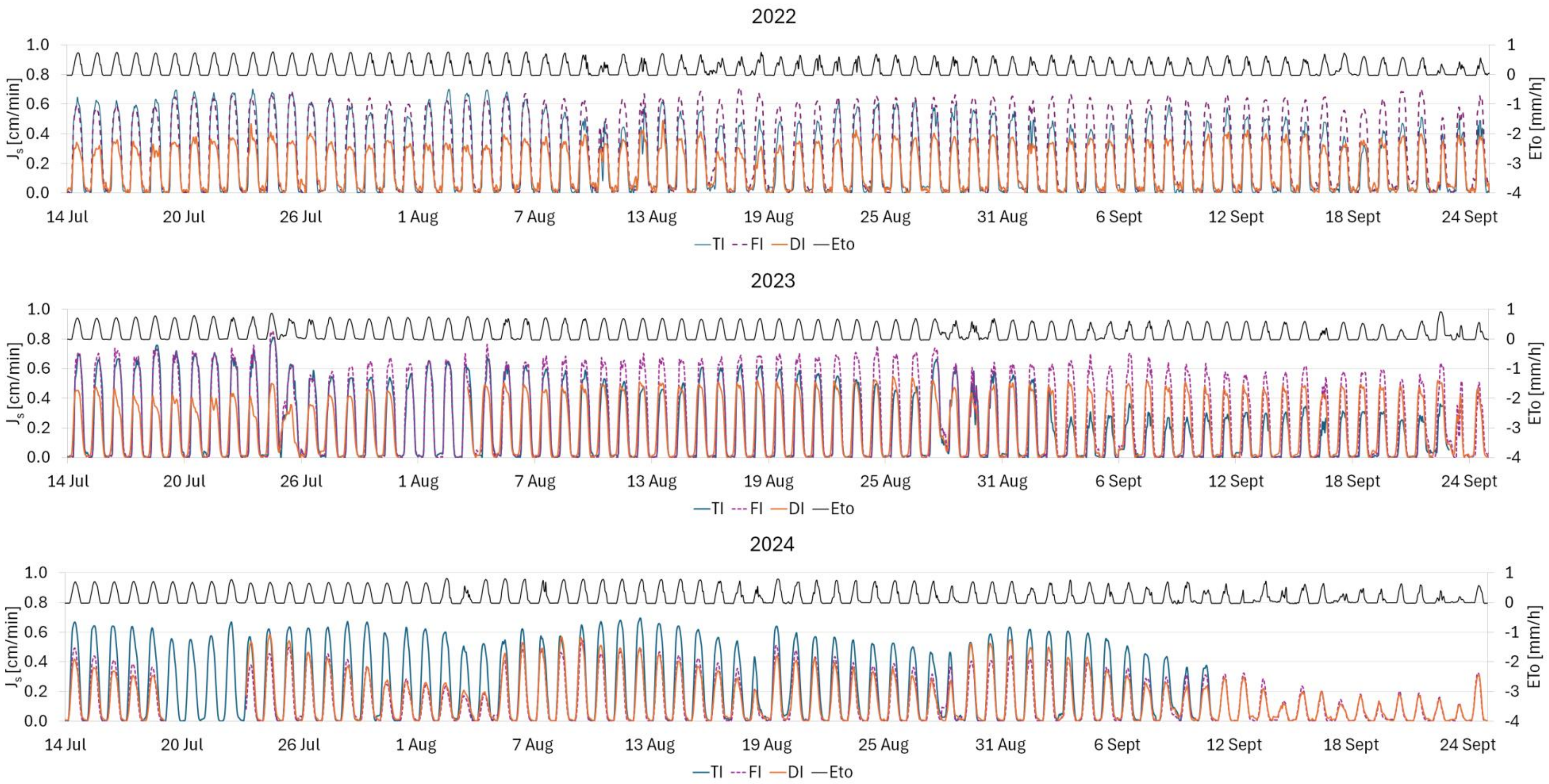

Fig. 12 Temporal dynamics of sap flux density (J_s) measured in the FI, DI, and TI treatments, and reference evapotranspiration (ETo) during the 2022, 2023, and 2024 monitoring period.

Figure 13 shows the relationship between hourly sap flux density (J_s) and reference evapotranspiration (ETo) for the FI, DI, and TI treatments during the 2022, 2023, and 2024 irrigation seasons. Across all years, J_s increased with increasing atmospheric demand, confirming the strong dependence of plant transpiration on evaporative conditions. However, the response differed among treatments and seasons, reflecting the influence of irrigation management and soil water status on plant hydraulic behaviour.

A rapid increase in J_s was observed for ETo values up to approximately 0.2 mm h^{-1}, indicating that under low-to-moderate atmospheric demand, transpiration was primarily driven by evaporative conditions. For higher ETo values, the increase in J_s became progressively less pronounced, suggesting the emergence of physiological and hydraulic constraints limiting plant transpiration. These constraints are likely associated with plant water availability, hydraulic conductivity within the soil–plant continuum, and stomatal regulation under increasing atmospheric demand.

This behaviour is particularly evident when comparing the FI and DI treatments in 2022 and 2023. Under non-limiting water conditions (FI), plants maintained higher J_s values across the entire ETo range compared to DI. In contrast, differences between treatments were less pronounced at ETo values below approximately 0.2 mm h^{-1}, corresponding to periods of lower transpiration demand, such as early morning and late afternoon. Under these conditions, even plants subjected to water deficit were generally able to satisfy atmospheric demand, as previously discussed. Furthermore, the dispersion of J_s values increased with increasing ETo, indicating a progressively stronger influence of soil water status and plant physiological status under high evaporative demand.

In 2022, the FI treatment exhibited the highest J_s values for a given ETo, with a relatively well-defined positive relationship and peak J_s values frequently exceeding 0.6 cm min^{-1} under high atmospheric demand. TI showed a similar trend, although with greater dispersion at intermediate ETo values. In contrast, DI consistently exhibited lower U values across the entire ETo range, with a tendency toward saturation under high evaporative demand, suggesting a progressive limitation of transpiration due to reduced soil water status.

In 2023, the relationships became more scattered, particularly in TI and DI, reflecting the greater climatic variability and lower effective rainfall characterizing this season. Despite lower SWC values observed in DI, J_s remained responsive to increasing ETo, although maximum values generally remained below those observed in FI. The FI treatment maintained the highest transpiration rates under elevated atmospheric demand, whereas TI showed lower J_s values during part of the season, consistent with the progressive decline in plant water status observed during late summer.

In 2024, differences among treatments were markedly reduced compared to previous years. The shift from SDI to farmer-managed sprinkler irrigation resulted in a convergence of the relationships between J_s and ETo, with all treatments showing broader dispersion and overlapping distributions. Nevertheless, TI frequently exhibited higher J_s values at moderate-to-high ETo levels, likely associated with the greater soil water status observed in this treatment (**Fig. 10**). Compared to previous seasons, the relationships also showed a stronger hysteretic-like dispersion, indicating that transpiration responses were increasingly influenced by transient soil moisture conditions and irrigation timing rather than atmospheric demand alone.

The relationship between J_s and ETo highlights the strong coupling between plant transpiration and atmospheric demand under well-watered conditions, while under water-limited conditions the response became increasingly constrained and variable. In particular, DI showed evidence of partial transpiration limitation at high ETo, whereas FI generally maintained higher sap flow rates across the full range of atmospheric demand.

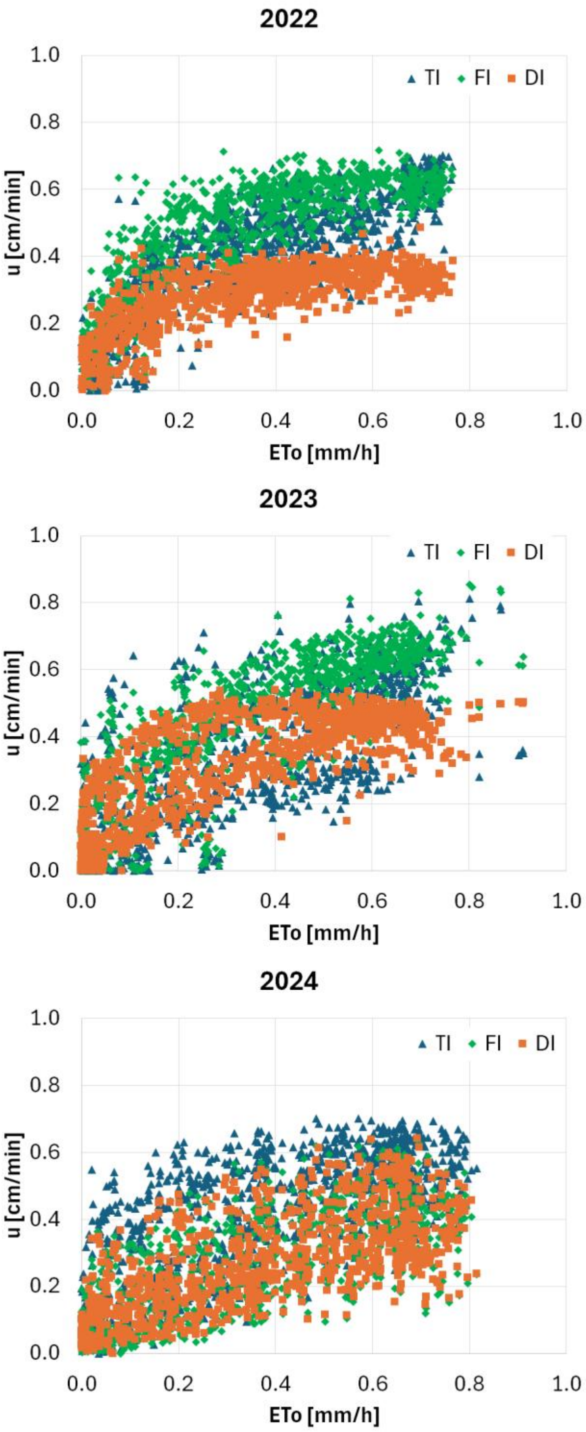

Fig. 13 Relationship between sap flux density (J_s) and hourly reference evapotranspiration (ETo) for the FI, DI, and TI treatments across the 2022, 2023, and 2024 irrigation seasons.

Figure 14 shows the relationship between daily sap flux density (J_s) and daily reference evapotranspiration (ETo) under different soil water content (SWC) conditions for the FI and DI treatments during the 2022 and 2023 irrigation seasons. Daily SWC values recorded during the monitoring period were divided into two classes corresponding to lower and higher soil moisture conditions, identified using the intervals between minimum-to-mean and mean-to-maximum SWC values, respectively.

Across all treatments and years, J_s generally increased with increasing ETo, confirming the dominant role of atmospheric demand in regulating plant transpiration. However, the response to increasing evaporative demand differed according to irrigation treatment and soil water status.

In FI_2022, differences between SWC classes were relatively limited, and J_s values remained consistently high across the entire ETo range, reflecting the stable soil moisture conditions maintained under SDI management. Similarly, plant water status remained relatively stable throughout the season, with Ψ values generally less negative than those observed under DI conditions. Under these non-limiting soil water conditions, transpiration appeared to be primarily driven by atmospheric demand rather than by soil moisture availability.

In DI_2022, the separation between SWC classes was less evident, as similar J_s values were observed under both soil moisture conditions across most of the ETo range. This suggests that, within the observed SWC interval (~25–32%), transpiration remained only partially constrained by soil water status. Despite the lower SWC and more negative Ψ values observed during the deficit period, plants were still able to maintain relatively stable sap flow rates, indicating an effective physiological adjustment to moderate water deficit conditions.

In 2023, the relationships between J_s and ETo showed greater dispersion compared to the previous season, reflecting the combined effects of higher atmospheric demand, reduced effective rainfall, and increased variability in plant water status. In FI_2023, J_s maintained a strong positive relationship with ETo under both SWC classes, although higher SWC conditions were generally associated with slightly greater J_s values. However, the overlap between moisture classes indicates that atmospheric demand remained the primary driver of transpiration under well-watered conditions.

In DI_2023, no clear enhancement of J_s was observed under higher SWC conditions. In some cases, slightly lower J_s values were associated with the higher SWC class, particularly at elevated ETo values. This behaviour suggests that factors other than soil moisture alone contributed to the regulation of transpiration. In addition to the progressive acclimation of plants to deficit conditions, temporary reductions in transpiring leaf area caused by pruning operations performed during the season may have contributed to the observed variability in J_s. Furthermore, the more negative Ψ values recorded during 2023 indicate that plants operated under stronger hydraulic tension, while still maintaining relatively sustained sap flow rates.

Figure 14 highlights that under SDI management, transpiration was strongly controlled by atmospheric demand, whereas the influence of soil water status became more evident only under prolonged or more severe deficit conditions. The increasing dispersion of J_s values at high ETo suggests that transpiration progressively shifted from being primarily atmosphere-driven to increasingly influenced by plant hydraulic regulation and soil water status.

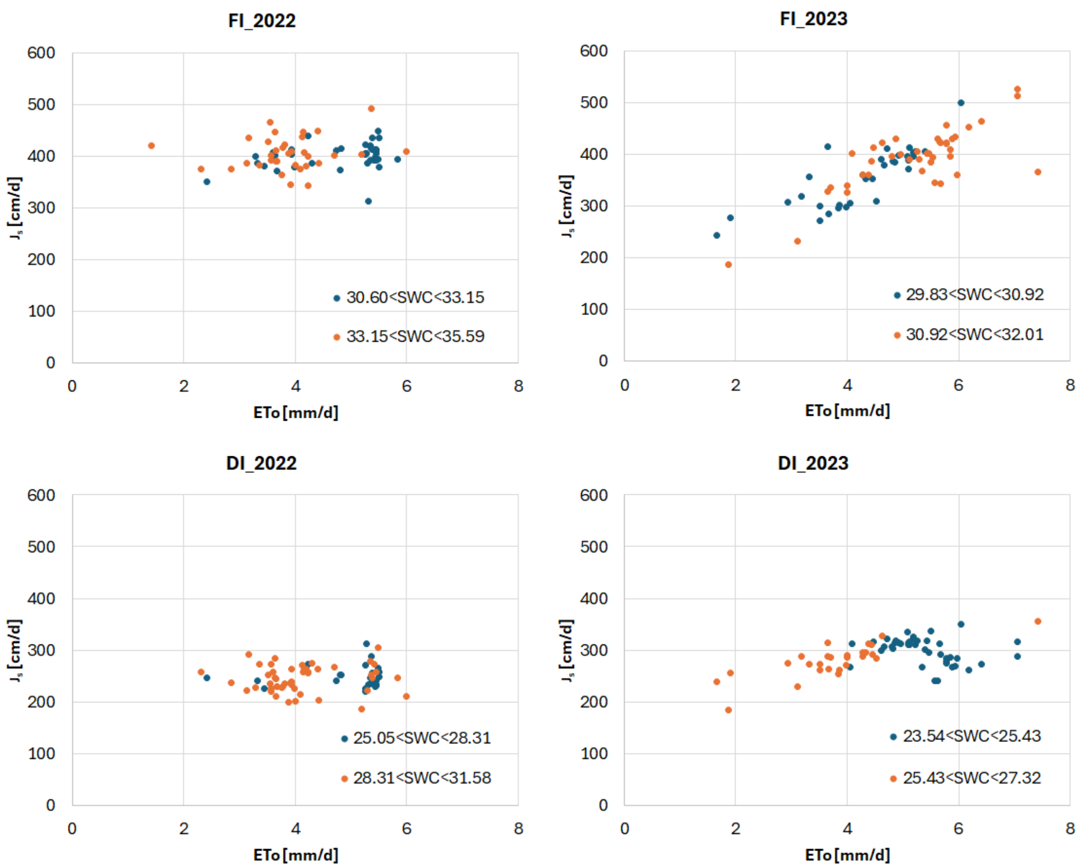

Fig. 14 Relationship between daily sap flux density (J_s) and daily reference evapotranspiration, (Eto) under different soil moisture conditions for the for the FI and DI treatments managed with SDI system during the 2022 and 2023 irrigation seasons.

Figure 15 shows the relationship between daily sap flux density (J_s) and daily reference evapotranspiration (ETo) under different soil water content (SWC) conditions for the FI, DI, and TI treatments during the 2024 irrigation season. The TI treatment was included only in 2024 because SWC measurements were not available for this plot during the 2022 and 2023 seasons. Although the FI and DI plots retained their original experimental designation, deficit irrigation was not applied in 2024 due to water restrictions and the transition to farmer-managed sprinkler irrigation. Consequently, all treatments were subjected to the same irrigation management strategy.

Unlike the previous seasons characterized by high irrigation frequency via SDI system, the farmer irrigation management via sprinkler system adopted in 2024 involved less frequent and higher-volume irrigation applications, resulting in marked alternations between wet and dry soil phases and greater temporal variability in plant water status. These dynamics were directly reflected in the relationships between J_s and ETo, which showed substantially greater dispersion compared to 2022 and 2023.

In both FI_2024 and DI_2024, lower SWC conditions were generally associated with lower J_s values, particularly under elevated ETo, indicating a stronger limitation imposed by soil water depletion compared to previous years. However, despite the similar irrigation management and SWC dynamics observed in FI and DI during 2024, the DI plot maintained transpiration rates broadly comparable to those recorded in previous seasons. Although deficit irrigation was no longer applied, this behaviour may reflect a residual acclimation effect associated with the historical exposure of these plants to deficit irrigation during the previous monitoring seasons.

The TI_2024 treatment generally exhibited higher J_s values compared to FI and DI, particularly under moderate-to-high ETo conditions. This response is consistent with the higher SWC values observed in TI during the monitoring period and with the less negative Ψ values measured following irrigation events. The greater soil water status likely reduced hydraulic limitation and supported higher transpiration rates.

A characteristic feature associated with sprinkler irrigation management was the marked increase in the dispersion of J_s values at elevated ETo. This variability reflects the strong influence of irrigation timing and transient soil moisture conditions on transpiration dynamics. In contrast to SDI systems, where soil moisture remained relatively stable, sprinkler irrigation generated alternating wetting and drying phases that directly affected plant water status and sap flow response.

Overall, **Figure 15** highlights how the transition from SDI to sprinkler irrigation altered the coupling between atmospheric demand and plant transpiration. Under these conditions, transpiration responses became increasingly influenced by short-term fluctuations in soil water status, plant hydraulic status, and irrigation timing, resulting in a more heterogeneous physiological response among treatments.

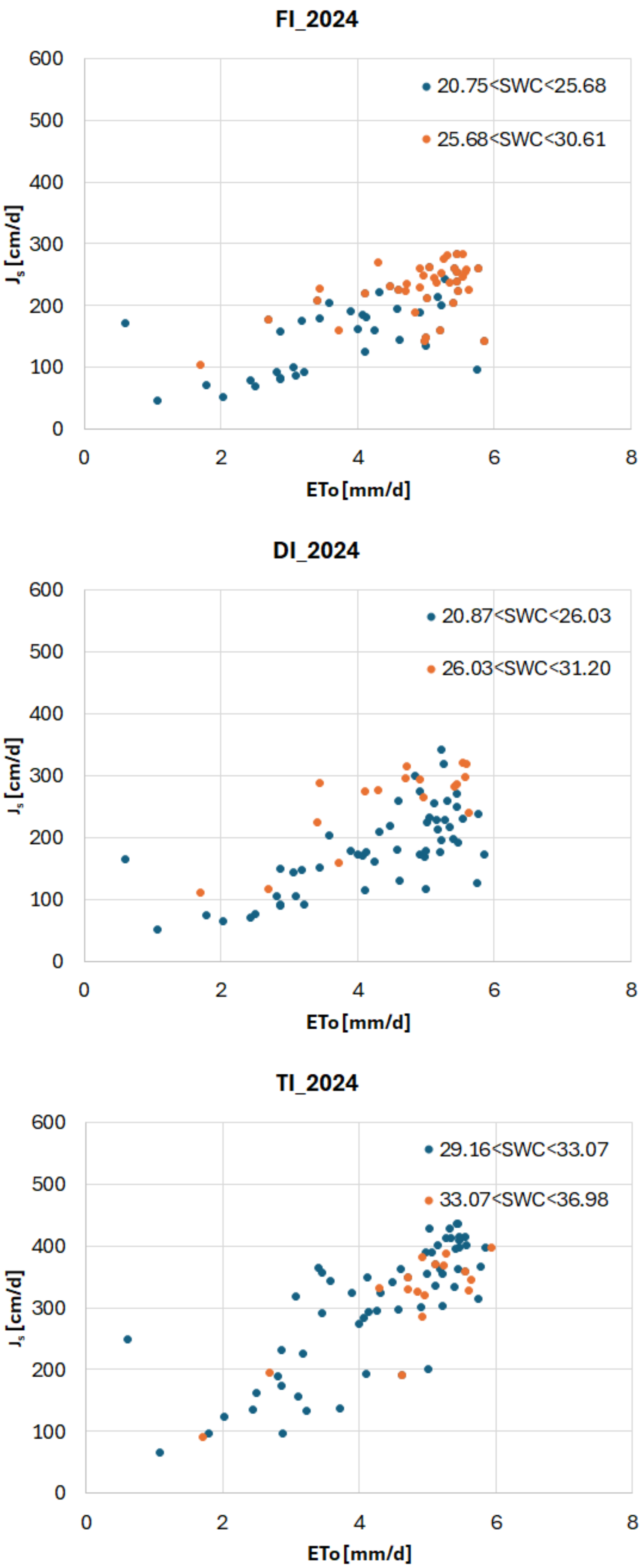

Fig. 15 Relationship between daily sap flux density (J_s) and daily reference evapotranspiration, (ETo) under different soil moisture conditions for the FI, DI and TI treatments during the 2024 monitoring period under farmer- managed sprinkler irrigation.

3.3.6 Conclusions

The monitoring of the SPAc during the 2022–2024 irrigation seasons highlighted the strong interaction between climatic forcing, irrigation management, soil water status, and plant physiological response.

The three monitored seasons were characterized by markedly different climatic conditions, particularly in terms of rainfall distribution, evaporative demand, and occurrence of extreme heat events. Among them, 2023 represented the most critical season from an agronomic perspective due to the limited effectiveness of rainfall events in replenishing soil water reserves, despite the relatively high number of rainy days. The severe depletion of water resources that followed ultimately affected irrigation management during 2024, when the suspension of SDI water delivery forced the adoption of farmer-managed sprinkler irrigation in all experimental plots.

Under SDI management, FI maintained relatively stable soil moisture conditions through frequent and low-volume irrigation events, resulting in less negative stem water potential values and more stable transpiration dynamics. In contrast, DI induced a progressive reduction in soil water status and more negative Ψ values, particularly during the driest periods. Nevertheless, plants subjected to deficit irrigation maintained relatively sustained sap flow rates, indicating an effective physiological adjustment of the soil–plant continuum to moderate water deficit conditions.

The transition to sprinkler irrigation in 2024 substantially modified soil and plant water dynamics. The lower irrigation frequency and larger irrigation volumes generated pronounced wetting–drying cycles, resulting in greater temporal variability in SWC, Ψ, and sap flow. Under these conditions, transpiration responses became increasingly influenced by short-term fluctuations in soil moisture and irrigation timing. A delayed increase in sap flow, typically occurring 2–3 days after irrigation events, was consistently observed under sprinkler management, suggesting progressive redistribution of water within the soil profile and gradual recovery of plant hydraulic functioning.

The combined analysis of soil water content, stem water potential, and sap flow highlighted the complementary role of continuous monitoring techniques in characterizing the functioning of the SPAc. Soil moisture measurements described water availability within the root zone, stem water potential reflected the hydraulic status of the plant, whereas sap flow represented the dynamic physiological response to the combined effects of soil water status and atmospheric evaporative demand. Their integrated interpretation provided a more comprehensive understanding of crop water use and stress adaptation than any individual indicator considered separately.

The results demonstrate that irrigation strategy strongly influences the hydraulic functioning of the soil–plant continuum. SDI improved irrigation efficiency and promoted more stable soil and plant water conditions, whereas deficit irrigation allowed significant water savings while maintaining plant transpiration within physiologically sustainable limits. These findings confirm the potential of continuous monitoring approaches for supporting precision irrigation strategies under increasingly variable climatic conditions and for improving water use efficiency while maintaining plant functioning under Mediterranean semi-arid conditions. Furthermore, the monitoring platform established during this study provides a valuable experimental framework for the calibration and validation of SPAc models and for the development of sensor-based irrigation management strategies.

REFERENCES

Abdulraheem, M. I., Chen, H., Li, L., Moshood, A. Y., Zhang, W., Xiong, Y., ... & Hu, J. 2024. Recent advances in dielectric properties-based soil water content measurements. *Remote Sensing*, *16*(8), 1328.

Arndt, S. K., Irawan, A., & Sanders, G. J., 2015. Apoplastic water fraction and rehydration techniques introduce significant errors in measurements of relative water content and osmotic potential in plant leaves. *Physiologia plantarum*, *155*(4), 355-368.

Awad-Allah, E. F., 2020. Indispensable measuring techniques for water relations of plants and soils: A review. *Open J. Soil Sci*, *10*(12), 616-630.

Blanco, V., & Kalcsits, L. 2021. Microtensiometers accurately measure stem water potential in woody perennials. *Plants*, *10*(12), 2780.

Blanco-Cipollone, F., Lourenço, S., Silvestre, J., Conceição, N., Moñino, M. J., Vivas, A., & Ferreira, M. I., 2017. Plant water status indicators for irrigation scheduling associated with iso-and anisohydric behavior: Vine and plum trees. *Horticulturae*, *3*(3), 47.

Bush, S. E., Hultine, K. R., Sperry, J. S., & Ehleringer, J. R., 2010. Calibration of thermal dissipation sap flow probes for ring-and diffuse-porous trees. *Tree physiology*, *30*(12), 1545-1554.

Bwambale, E., Abagale, F. K., & Anornu, G. K., 2022. Smart irrigation monitoring and control strategies for improving water use efficiency in precision agriculture: A review. *Agricultural Water Management*, *260*, 107324.

Capurro, M. C., Ham, J. M., Kluitenberg, G. J., Comas, L., & Andales, A. A., 2024. A novel sap flow system to measure maize transpiration using a heat pulse method. *Agricultural Water Management*, *301*, 108963.

Conesa, M. R., Conejero, W., Vera, J., & Ruiz-Sánchez, M. C., 2023. Assessment of trunk microtensiometer as a novel biosensor to continuously monitor plant water status in nectarine trees. *Frontiers in Plant Science*, *14*, 1123045.

Dainese, R., de Cfl Lopes, B., Tedeschi, G., Lamarque, L. J., Delzon, S., Fourcaud, T., & Tarantino, A., 2022. Cross-validation of the high-capacity tensiometer and thermocouple psychrometer for continuous monitoring of xylem water potential in saplings. *Journal of Experimental Botany*, *73*(1), 400-412.

Davis, T. W., Kuo, C. M., Liang, X., & Yu, P. S., 2012. Sap flow sensors: construction, quality control and comparison. *Sensors*, *12*(1), 954-971.

de Jong, S. M., Heijenk, R. A., Nijland, W., & van Der Meijde, M. 2020. Monitoring soil moisture dynamics using electrical resistivity tomography under homogeneous field conditions. *Sensors*, *20*(18), 5313.

Do, F., Rocheteau, A., 2002a. Influence of natural temperature gradients on measurements of xylem sap flow with thermal dissipation probes. 1. Field observations and possible remedies. Tree Physiol. 22, 641–648. https://doi.org/10.1093/treephys/22.9.641

Do, F., Rocheteau, A., 2002b. Influence of natural temperature gradients on measurements of xylem sap flow with thermal dissipation probes. 2. Advantages and calibration of a noncontinuous heating system. Tree Physiol. 22, 649–654. https://doi.org/10.1093/treephys/22.9.649

Evett, S. R., & Steiner, J. L. 1995. Precision of neutron scattering and capacitance type soil water content gauges from field calibration. *Soil Science Society of America Journal*, *59*(4), 961-968.

Fernández, J. E., 2017. Plant-based methods for irrigation scheduling of woody crops. *Horticulturae*, *3*(2), 35.

Forster, M. A., 2019. The dual method approach (DMA) resolves measurement range limitations of heat pulse velocity sap flow sensors. *Forests*, *10*(1), 46.

Fuchs, S., Leuschner, C., Link, R., Coners, H., & Schuldt, B., 2017. Calibration and comparison of thermal dissipation, heat ratio and heat field deformation sap flow probes for diffuse-porous trees. *Agricultural and Forest Meteorology*, *244*, 151-161.

Granier, A., 1985. Une nouvelle méthode pour la mesure du flux de sève brute dans le tronc des arbres, in: Annales Des Sciences Forestières. EDP Sciences, pp. 193–200.

Granier, A., 1987. Evaluation of transpiration in a Douglas-fir stand by means of sap flow measurements. Tree Physiol. 3, 309–320.

Hargreaves, G. H., & Samani, Z. A., 1985. Reference crop evapotranspiration from temperature. *Applied engineering in agriculture*, *1*(2), 96-99.

Hu, M., Ma, C., Zhang, J., Ma, Y., Li, C., & Xiong, W., 2022. Calibration of thermal dissipation probes for xylem sap flow in the wood of a diffuse-porous and a conifer species under cyclic heating. *Forests*, *13*(11), 1964.

Ievinsh, G., 2023. Water content of plant tissues: So simple that almost forgotten? *Plants*, *12*(6), 1238.

Intrigliolo, D. S., & Castel, J. R., 2004. Continuous measurement of plant and soil water status for irrigation scheduling in plum. *Irrigation science*, *23*(2), 93-102.

Isarangkool Na Ayutthaya, S., Do, F.C., Pannengpetch, K., Junjittakarn, J., Maeght, J.-L., Rocheteau, A., Cochard, H., 2010. Transient thermal dissipation method of xylem sap flow measurement: multi-species calibration and field evaluation. Tree Physiol. 30, 139–148. https://doi.org/10.1093/treephys/tpp092

Jarvis, N. J., & Leeds-Harrison, P. B., 1987. Some problems associated with the use of the neutron probe in swelling/shrinkling clay soils. *Journal of Soil Science*, *38*(1), 149-156.

Jones, H. G., 2007. Monitoring plant and soil water status: established and novel methods revisited and their relevance to studies of drought tolerance. *Journal of experimental botany*, *58*(2), 119-130.

Juenger, T. E., & Verslues, P. E., 2023. Time for a drought experiment: do you know your plants' water status? *The Plant Cell*, *35*(1), 10-23.

Koide, R. T., Robichaux, R. H., Morse, S. R., & Smith, C. M., 1989. Plant water status, hydraulic resistance and capacitance. In *Plant physiological ecology: field methods and instrumentation* (pp. 161-183). Dordrecht: Springer Netherlands.

Kumari, A., Upadhyaya, A., Jeet, P., Al-Ansari, N., Rajput, J., Sundaram, P. K., ... & Kuriqi, A., 2022. Estimation of actual evapotranspiration and crop coefficient of transplanted puddled rice using a modified non-weighing paddy lysimeter. *Agronomy*, *12*(11), 2850.

Lakso, A. N., Santiago, M., & Stroock, A. D., 2022. Monitoring stem water potential with an embedded microtensiometer to inform irrigation scheduling in fruit crops. *Horticulturae*, *8*(12), 1207.

López-Urrea, R., Pardo, J. J., Simón, L., Martínez-Romero, Á., Montoya, F., Tarjuelo, J. M., & Domínguez, A., 2021. Assessing a removable mini-lysimeter for monitoring crop evapotranspiration using a well-established large weighing lysimeter: a case study for barley and potato. *Agronomy*, *11*(10), 2067.

Losciale, P., Gaeta, L., Corsi, M., Galeone, C., Tarricone, L., Leogrande, R., & Stellacci, A. M., 2023. Physiological responses of apricot and peach cultivars under progressive water shortage: Different crop signals for anisohydric and isohydric behaviours. *Agricultural Water Management*, *286*, 108384.

Marshall, D. C., 1958. Measurement of sap flow in conifers by heat transport. *Plant physiology*, *33*(6), 385.

Marusig, D., Petruzzellis, F., Tomasella, M., Napolitano, R., Altobelli, A., & Nardini, A., 2020. Correlation of field-measured and remotely sensed plant water status as a tool to monitor the risk of drought-induced forest decline. *Forests*, *11*(1), 77.

Matese, A., Baraldi, R., Berton, A., Cesaraccio, C., Di Gennaro, S. F., Duce, P., ... & Zaldei, A., 2018. Estimation of water stress in grapevines using proximal and remote sensing methods. *Remote Sensing*, *10*(1), 114.

Michot, D., Benderitter, Y., Dorigny, A., Nicoullaud, B., King, D., & Tabbagh, A. 2003. Spatial and temporal monitoring of soil water content with an irrigated corn crop cover using surface electrical resistivity tomography. *Water Resources Research*, *39*(5).

Mohammad, A. H., Ghanem, M., De La Hera-rica, P. A., Al Rowwad, A. A., & Shatanawi, K., 2025. Satellite-based drought indicators for supporting sustainable water management. *Global Journal of Environmental Science and Management*, *11*(4), 1493-1508.

Noun, G., Lo Cascio, M., Spano, D., Marras, S., & Sirca, C., 2022. Plant-based methodologies and approaches for estimating plant water status of Mediterranean tree species: a semi-systematic review. *Agronomy*, *12*(9), 2127.

Pagay, V., 2021. Dynamic aspects of plant water potential revealed by a microtensiometer. *BioRxiv*, 2021-06.

Pagay, V., 2022. Evaluating a novel microtensiometer for continuous trunk water potential measurements in field-grown irrigated grapevines. *Irrigation Science*, *40*(1), 45-54.

Parkash, V., & Singh, S., 2020. A review on potential plant-based water stress indicators for vegetable crops. *Sustainability*, *12*(10), 3945.

Pütz, T., Fank, J., & Flury, M., 2018. Lysimeters in vadose zone research. *Vadose Zone Journal*, *17*(1), 1-4.

Quan, Q., Gao, S., Shang, Y., & Wang, B., 2021. Assessment of the sustainability of Gymnocypris eckloni habitat under river damming in the source region of the Yellow River. *Science of the Total Environment*, *778*, 146312.

Rasheed, M. W., Tang, J., Sarwar, A., Shah, S., Saddique, N., Khan, M. U., ... & Sultan, M., 2022. Soil moisture measuring techniques and factors affecting the moisture dynamics: A comprehensive review. *Sustainability*, *14*(18), 11538.

Robinson, D. A., Campbell, C. S., Hopmans, J. W., Hornbuckle, B. K., Jones, S. B., Knight, R., ... & Wendroth, O., 2008. Soil moisture measurement for ecological and hydrological watershed-scale observatories: A review. *Vadose zone journal*, *7*(1), 358-389.

Rodriguez-Dominguez, C. M., Forner, A., Martorell, S., Choat, B., Lopez, R., Peters, J. M., ... & Sack, L. 2022. Leaf water potential measurements using the pressure chamber: synthetic testing of assumptions towards best practices for precision and accuracy. *Plant, Cell & Environment*, *45*(7), 2037-2061.

Scholander, P. F., Bradstreet, E. D., Hemmingsen, E. A., & Hammel, H. T., 1965. Sap Pressure in Vascular Plants: Negative hydrostatic pressure can be measured in plants. *Science*, *148*(3668), 339-346.

Temnani A., Berríos, P., Zapata-García, S., Espinosa, P. J., & Pérez-Pastor, A., 2023. Threshold values of plant water status for scheduling deficit irrigation in early apricot trees. *Agronomy*, *13*(9), 2344.

Topp, G. C. 2003. State of the art of measuring soil water content. *Hydrological Processes*, *17*(14), 2993-2996.

Topp, G. C., & Ferré, P. A., 2002. Thermogravimetric determinations using convective oven-drying. *Methods of soil analysis. part*, *4*, 422-424.

Topp, G. C., Zebchuk, W. D., Davis, J. L., & Bailey, W. G. 1984. The measurement of soil water content using a portable TDR hand probe. Canadian Journal of Soil Science, 64(3), 313-321.

Turner, N. C., 1981. Techniques and experimental approaches for the measurement of plant water status. *Plant and soil*, *58*(1), 339-366.

Veysi, S., Naseri, A. A., Hamzeh, S., & Bartholomeus, H., 2017. A satellite based crop water stress index for irrigation scheduling in sugarcane fields. *Agricultural water management*, *189*, 70-86.

Visvalingam, M., & Tandy, J. D. 1972. The neutron method for measuring soil moisture content—a review. *Journal of Soil Science*, *23*(4), 499-511.

Zhan, C., Dai, Z., Samper, J., Yin, S., Ershadnia, R., Zhang, X., ... & Soltanian, M. R., 2022. An integrated inversion framework for heterogeneous aquifer structure identification with single-sample generative adversarial network. *Journal of Hydrology*, *610*, 127844.

Zhang, R., Chai, Y., Liang, X., Liu, X., Wang, X., & Hu, Z., 2024. A new plant-wearable sap flow sensor reveals the dynamic water distribution during watermelon fruit development. *Horticulturae*, *10*(6), 649.

Zhang, X., Feng, G., & Sun, X., 2024. Advanced technologies of soil moisture monitoring in precision agriculture: A Review. *Journal of Agriculture and Food Research*, *18*, 101473.

Zhao, Y., Wang, Y., Zeng, X., & Morishima, K., 2025. Heat Transfer-Based Monitoring System for Sap Flow in Plants. In *2025 IEEE International Conference on Mechatronics and Automation (ICMA)* (pp. 469-474). IEEE.

Zhou, Q. Y., Shimada, J., & Sato, A. 2001. Three-dimensional spatial and temporal monitoring of soil water content using electrical resistivity tomography. *Water Resources Research*, *37*(2), 273-285.

3.4 Assessing microtensiometers for monitoring stem water potential in mandarin (*Citrus reticulata* Blanco) orchard under different irrigation regimes

G. Vaccaro[1], M. Fusco[1], V. Alagna[1], L. Franco[2], A. Motisi[1], M. Iovino[1]

[1]Dipartimento di Scienze Agrarie, Alimentari e Forestali, Università di Palermo, mariachiara.fusco@unipa.it
[2] Irritec S.p.A., Via Gambitta Conforto, 98071 Capo D'Orlando, ME, Italy

Abstract

Stem water potential (Ψ_{stem}) is the standard indicator of crop water status, commonly estimated using the Scholander pressure chamber (PC). However, it does not allow continuous monitoring, limiting real-time decision-making. The recently developed microtensiometer (MT) offers continuous Ψ_{stem} monitoring, overcoming the PC limitations. This study assesses the MT's reliability in monitoring Ψ_{stem} dynamics in a mandarin orchard in Sicily, Italy, under two irrigation regimes: i) a frequent irrigation regime via subsurface drip irrigation (SDI) system, employed to ensure well-watered conditions, and ii) an ordinary irrigation management typical of the area, provided by a micro-sprinkler (SPR) system. Over two seasons, Ψ_{stem} measurements obtained with the MT (Ψ_{mt}) were compared with those from the PC (Ψ_{pc}). Shading trials were also conducted to evaluate the sensor's ability to detect the plant reactions to external perturbations. A step-change in solar radiation imposed by artificial shading revealed different signal dynamics of MT sensors compared to pressure chamber Ψ_{pc} measurements, characterised by a 4-fold increase in signal time constant. This led to a consequential impact on Ψ_{stem} estimation, resulting in both a substantial time lag and attenuation, consistent with first-order sensor dynamics. Across both seasons and irrigation regimes, daily Ψ_{mt} overestimated Ψ_{stem} compared to Ψ_{pc}, along with a clear time lag coherent with the first-order response shown by the sensor-tree-complex. Under the SDI irrigation regime, Ψ_{mt} was significantly correlated with vapour pressure deficit, indicating a strong plant-atmosphere coupling under stable soil moisture conditions. Normalised cross-correlation analysis between reference evapotranspiration and Ψ_{mt} showed variable time lags, specifically in the SPR plot, subjected to alternating soil moisture conditions. These findings suggest that MTs are a promising tool for real-time monitoring of mandarin water status. However, the first-order dynamics of the sensor-tree-complex response signal preclude the use of Ψ_{mt} as a direct replacement for pressure-chamber Ψ_{stem} measurements. Consequently, suitable compensation protocols accounting for a large time constant should be developed to apply Ψ_{mt} readings to currently published crop-specific Ψ_{stem} thresholds for irrigation scheduling protocols.

Keywords: Stem potential, Microtensiometer, Scholander pressure chamber, Irrigation regimes, Subsurface drip irrigation, Micro-sprinkler irrigation

3.4.1 Introduction

Efficient water management is crucial for irrigated agriculture, particularly in light of climate change and increasing water scarcity in arid and semi-arid areas (Galindo et al., 2018). The expected intensification of drought events under climate change scenarios is expected to increase crop stress due to rising thermal gradients and reduced precipitation, negatively affecting agricultural productivity (Ciais et al., 2005). For citrus crops in a Mediterranean semi-arid environment, yield success relies heavily on adequate irrigation (Rallo et al., 2017). Therefore, to optimise the productivity of citrus orchards, it is essential to manage the available water resources sustainably and, at the same time, also consider their potential cultivation under water shortage conditions.

One of the most water-efficient and precise methods of surface irrigation systems is drip irrigation, which can minimise water losses due to evaporation, surface runoff, and deep percolation (Ravikumar, 2023; Singh and Su, 2022). Unlike drip irrigation systems, subsurface drip irrigation (SDI) systems are characterised by buried emitters, effectively reducing water loss due to evaporation (Cahn and Hutmacher, 2024; Camp, 1998; Provenzano, 2007). Lamm et al. (2021) summarised recent research progress of SDI systems (from 2010 to 2020). They highlighted SDI's advantages, including high water use efficiency, uniform water application and the ability to apply water and nutrients directly and efficiently within the crop root zone compared to other systems, such as sprinkler irrigation.

Optimising water use efficiency requires selecting and designing appropriate irrigation systems and implementing management practices that supply water in volumes precisely aligned with crop water requirements. A fundamental aspect of fine-tuning irrigation scheduling is understanding the plant water status. Several studies have specifically highlighted the importance of stem water potential (Ψ_{stem}), which is widely recognised as the key indicator of a plant's water status and a valuable index for making irrigation decisions (Choné, 2001; Jones, 2004; Ortuño et al., 2006). Stem water potential assessments are typically conducted at pre-dawn or midday. In citrus trees, which exhibit low resistance to water stress, irrigation scheduling is often guided by plant water stress thresholds, with midday Ψ_{stem} values commonly ranging between -1.3 and -1.5 MPa (Ballester et al., 2011; García-Tejero et al., 2010; González-Altozano and Castel, 1999).

Traditionally, Ψ_{stem} is estimated with the Scholander pressure chamber (Scholander et al., 1965). Although this is a reliable measurement, it is destructive, time-consuming, and does not provide real-time continuous data on the plant water status. Additionally, Levin (2019) investigated several factors affecting the pressure chamber (PC) method, including the impact of re-cutting the petiole before placing the leaf in the chamber, the period between sample excision and pressurisation, the sample equilibration duration, and the operator's influence. The operator's effect consistently outweighed the other effects, thus demonstrating that proper training of technicians is crucial for achieving reliable and accurate estimations of Ψ_{stem} by the PC technique (Ψ_{pc}).

Physiologically, certain species, such as mandarin trees, are less drought-tolerant than other crops, primarily due to their low hydraulic conductance (Romero-Trigueros et al., 2021). Water stress can lead to cavitation-induced embolism in the xylem (Hacke and Sperry, 2001; Poggi et al., 2007), reducing xylem flow and weakening the hydraulic connection between the trunks and stems. While this phenomenon is reversible, it plays a crucial role in regulating transpiration in plants under water stress (Clearwater and Goldstein, 2005). For such crops, Ψ_{pc} may be prone to inaccuracies, failing to reflect the actual water status.

The practical limitations of the PC technique impede its application for determining optimal irrigation timing and management. However, in the context of precision irrigation or plant stress diagnostics, continuous monitoring of plant water status is of utmost importance; thus, research efforts have increasingly focused on enhancing existing devices and developing new technologies for easily and accurately monitoring plant water status.

Over the years, various plant-based monitoring technologies, including sap flow probes, leaf pressure probes and psychrometers for measuring plant water potential, have been developed to enhance irrigation management.

Sap flow measurement is a widely used method for directly quantifying plant water use and transpiration by assessing water transport within the vascular system. Unlike indirect methods, which rely on environmental parameters, this technique provides accurate, plant-based physiological data, enabling precise irrigation scheduling tailored to actual plant water requirements and significantly reducing water waste (Capurro et al., 2024; Mancha et al., 2021; Venturin et al., 2020). However, sap flow methods have inherent limitations. They are primarily applicable to woody species, and their measurement accuracy can be compromised by natural temperature gradients, radial variations in sap flow, and the selection of data-processing methods, all of which introduce uncertainty (Rabbel et al., 2016). Furthermore, upscaling from individual tree measurements to whole stands requires careful sampling strategies and precise quantification of sapwood area, as variability among trees can be substantial (Lundblad et al., 2001).

The ZIM-probe method measures leaf turgor pressure using a highly sensitive pressure sensor, which is clamped to a leaf and evaluates the pressure transfer function across a patch of intact leaf tissue, showing an inverse correlation with turgor pressure (Zimmermann et al., 2008). The ZIM-probe has been recognised as a user-friendly and easily installable technique, offering significant potential for field application by growers (Fernández, 2014). However, limitations include the need for accurately species-specific calibration to interpret turgor pressure, as well as potential variability due to microclimate effects and leaf anatomical differences across different canopy positions (Bader et al., 2014; Martínez-Gimeno et al., 2017).

Recognising the importance of Ψ_{stem} as a key indicator of crop water status, various sensors have been developed to facilitate its continuous measurement. Among these, the thermocouple psychrometer emerges as an effective device for assessing Ψ_{stem} by employing psychrometric principles to determine the water potential in stem tissue through vapour pressure measurements. This sensor provides real-time data and has been proven to monitor water potential reliably (Dainese et al., 2022). However, despite its reliability, the thermocouple psychrometer has several drawbacks, including the necessity for calibration with standard solutions, a challenging installation procedure, and relatively high costs (Quick et al., 2016). The relative humidity of the air surrounding the sensing junction is crucial, as it significantly influences the temperature difference between the wet sensing junction and the dry reference junction (Rawlins, 1966). Moreover, its accuracy can decline under relative humidity nearing vapour saturation, corresponding to water potential values approaching zero (Bulut and Leong, 2008).

More recently, Pagay et al. (2014) developed the so-called microtensiometer (MT), a device capable of measuring water potentials of external matrices below -10 MPa, using a microelectromechanical pressure sensor. The MTs, which are inserted directly into the plant tissue, represent an innovative technology for continuous real-time monitoring of stem water potential (Ψ_{mt}). Several studies have assessed the performance of MTs under field conditions for different crops, including kiwifruit (Di Biase et al., 2025), cotton (Christenson et al., 2024), pear (Blanco and Kalcsits, 2023), nectarine (Conesa et al., 2023), and grapevines (Pagay, 2022).

Despite their successful use in other crops, the application of MTs to mandarin species remains unexplored. Citrus orchards are one of the best-adapted tree species to Mediterranean environments. Traditionally, in Sicily, mandarin orchards have been irrigated using under-canopy micro-sprinkler (SPR) irrigation systems with low-frequency scheduling. However, due to the region's semi-arid climate and frequent water scarcity, there is a growing shift toward adopting more efficient irrigation technologies, such as the SDI system, to enhance water use efficiency.

The main objective of this study was to fill the existing knowledge gap regarding the potential benefits of using MTs to monitor Ψ_{stem} of mandarin trees under Mediterranean climate conditions, within the framework of precision irrigation. For this purpose, MT performance was tested under two irrigation regimes: a frequent irrigation regime to ensure a well-watered condition maintained through an SDI system, and an ordinary irrigation management typical of the growing area, provided by a SPR system. Specific objectives also aimed at analysing (i) the accuracy of Ψ_{mt} in comparison with the established Ψ_{pc}, (ii) the MT's ability to detect plant reaction to external perturbations induced by shading trials, and (iii) the sensitivity of Ψ_{mt} values to varying climatic conditions.

3.4.2. Materials and Methods

3.4.2.1. Experimental site

The experiment was conducted during the 2022 and 2023 irrigation seasons in a 30-year-old mandarin orchard (*Citrus reticulata* Blanco cv. Tardivo di Ciaculli grafted onto *Citrange* "Carrizo"), spaced 5 × 5 m and located near Palermo, Italy (38°4′53.4″ N, 13°25′8.2″ E). The climate is classified as Csa under the Köppen-Geiger system, indicating a warm temperate humid climate with hot, dry summers. The mean annual temperature reaches approximately 17 °C, while average annual rainfall amounts to 655 mm, primarily concentrated during the autumn and winter seasons.

The mandarin orchard is divided into two plots, with one representative tree selected in each plot to monitor stem water potential under different irrigation regimes. One plot has been equipped with a subsurface drip irrigation system (SDI plot) since 2018 to improve water use efficiency (**Fig. 1**, red polygon). To check that the tree was under well-watered conditions for the duration of the irrigation season, a 0.60 m long "Drill & Drop" probe (Sentek Pty Ltd., Stepney, Australia) was positioned 0.3 m from a single emitter and approximately 0.8 m from the tree trunk (**Fig. 1**). The probe measured both volumetric soil water content (SWC) and temperature from the surface to a depth of 0.60 m at 0.10 m intervals with data recorded every 20 minutes. The second plot (**Fig. 1**, green polygon) uses a traditional under-canopy micro-sprinkler irrigation system (SPR plot) commonly employed in Sicily for citrus orchards. In both plots, the soil (typic Rhodoxeralf) remained untilled, with weed control carried out mechanically during harvest or in summer.

The SDI plot features a relatively uniform soil texture that, according to the USDA (United States Department of Agriculture) classification, is classified as sandy clay loam or sandy loam, with a moderate gravel content in the top layer. The hydrological soil characteristics, for the 0-0.60 m depth profile, were determined using pressure plate extractors (Dane et al., 2002) for pressure head values of -1 m and -150 m. The average volumetric SWC at field capacity (θ_{fc}) and at wilting point (θ_{wp}) were 0.254 and 0.143 cm^3 cm^{-3}, respectively, resulting in an available water fraction of 0.111 cm^3 cm^{-3}. Soil organic matter was determined using the loss-on-ignition method (Bengtsson and Enell, 1986; Dean, 1974), yielding an average of 2.44%. The SPR plot exhibited a more heterogeneous soil texture, ranging from clay to sandy clay loam (USDA). In the 0 - 0.60 m soil profile, the θ_{fc} and θ_{wp} were 0.317 and 0.195 cm^3 cm^{-3}, respectively, resulting in an available water fraction of 0.122 cm^3 cm^{-3}. The average soil organic matter content in this plot was higher than that of the SDI plot, reaching 3.38%.

The SDI irrigation system features two drip lines per row, buried at a depth of 0.30 m and positioned approximately 1.1 m on both sides of the tree trunk. The drip lines are equipped with self-compensating drippers discharging 2.1 L h^{-1} at a pressure of 100 kPa (Multibar C model, Irritec®) spaced 0.5 m apart. The SPR irrigation system is characterised by two micro-sprinklers per tree, delivering a flow rate of 200 L h^{-1} at a pressure of 150 kPa, wetting an area almost corresponding to the projection of the mandarin tree canopy.

The SDI plot was managed with a high-frequency irrigation regime aimed at preventing crop water stress. At this aim, the SWC along the root zone was monitored with the Drill & Drop sensor, ensuring that the values remained consistently close to θ_{fc}. In contrast, the SPR plot was managed by the farmer following a nearly uniform, lower-frequency irrigation schedule. Irrigation events typically occurred according to a biweekly plan, unless there were no rainfall events, and water application volumes were determined by his practical experience.

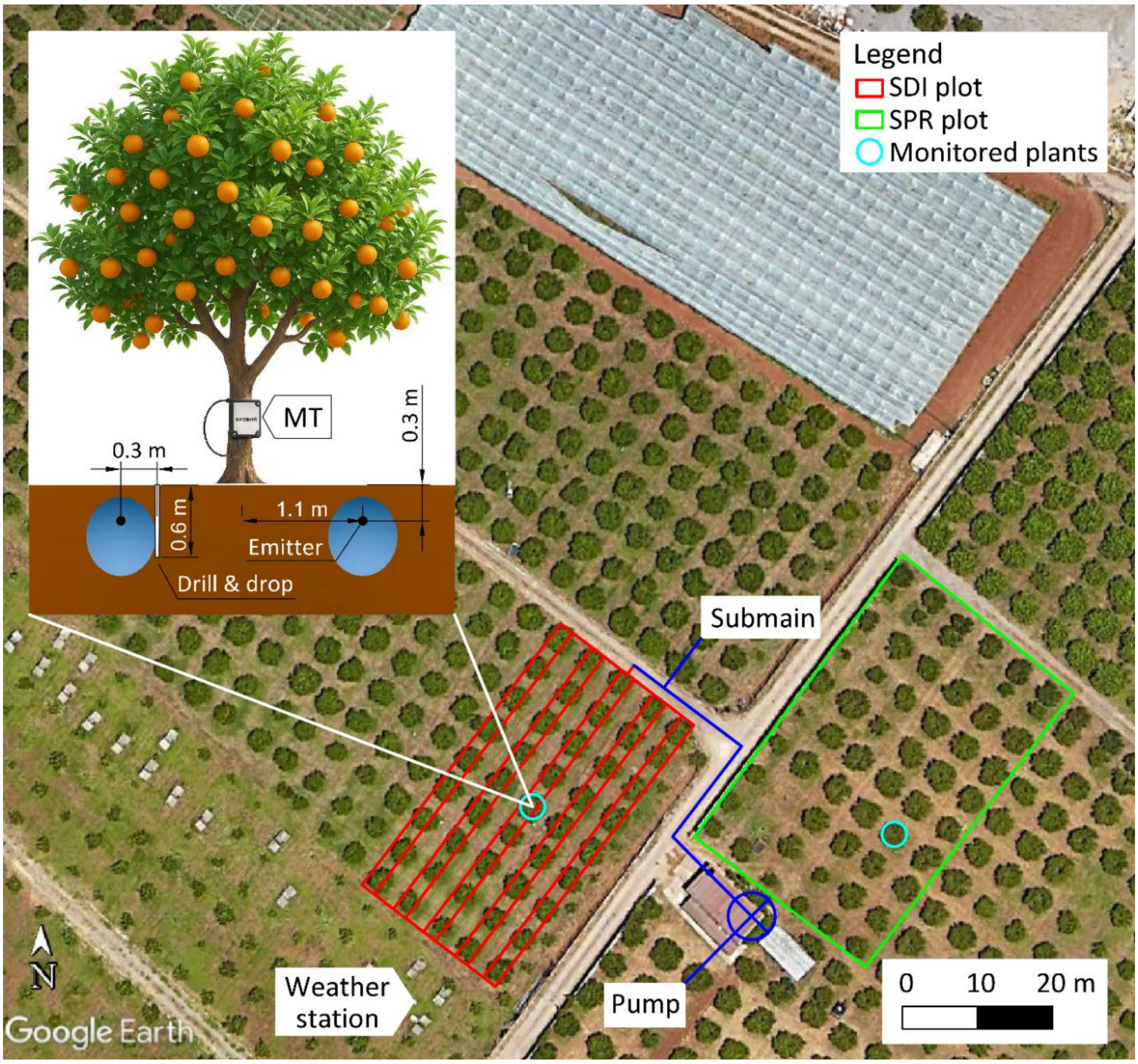

Fig. 1 Experimental layout of the SDI and SPR plots. For the SDI plot, the positions of the emitters and the soil water content probe are also displayed.

3.4.2.2. Climate and micrometeorological data

Air temperature, T (°C), relative humidity, RH (%), thus vapour pressure deficit, VPD (kPa), precipitation, P (mm), solar radiation, SR (MJ m^{-2} h^{-1}), wind speed, u (m s^{-1}) were recorded, with a time-step of 30 min, by a WatchDog 2000 series weather station (Spectrum Technologies, Inc., Aurora, IL, USA) installed inside the field (**Fig 1**). The hourly average values of meteorological variables were used to estimate the hourly grass reference evapotranspiration, ETo (mm h^{-1}), using the FAO-56 Penman-Monteith equation (Allen et al., 1998).

3.4.2.3. Stem water potential estimations

Continuous monitoring of stem water potential (Ψ_{mt}) was conducted using four commercial microtensiometers (FloraPulse, Davis, CA, USA), with two sensors installed in the trunk of a representative tree in each plot. These microtensiometers (MT) were connected to the FloraPulse data logger, which automatically records Ψ_{mt} every 20 minutes and uploads the data to the FloraPulse cloud. Sensor calibration is not required before field installation, as each MT is individually factory-calibrated (https://www.florapulse.com/resources). The MT installation, following the manufacturer's recommendation, involved several key steps to ensure precise attachment and optimal functioning. The tree trunk phloem tissue was exposed by carefully removing the bark from a selected flat section. A stainless-steel sleeve was inserted into the trunk with a hammer to position it securely. A drill was used to penetrate the sleeve and drill into the xylem tissue, removing the tissue within. This cavity was filled with a kaolin-based mating compound to create a stable interface between the sensor and the tree's xylem. The hydrated MT was then placed into the compound. To seal the installation, a stainless-steel cap was added to close the sleeve, and the sleeve's exterior was covered with silicone to ensure an airtight and waterproof seal. Finally, thermal insulation was applied by wrapping the sensor to minimise external temperature fluctuations. The sensors equilibrated with the mandarin trunk through the mating compound within two days of installation. The collected data were then aggregated at an hourly scale, and the average values recorded from the two MT were used for analysis.

Estimation of stem water potential by Scholander pressure chamber (Ψ_{pc}) was conducted on the same mandarin trees monitored with MT, following the protocols suggested by Turner (1988). During the two irrigation seasons, Ψ_{pc} were carried out throughout the day on two healthy stems, each wrapped in an aluminium foil approximately one hour before the test, and the average value was considered. Specifically, Ψ_{pc} tests were scheduled considering the farmer's irrigation management carried out in the SPR plot, aiming to capture potential water stress three days before irrigation and to assess plant water status recovery the following day. This low-frequency irrigation management was expected to induce marked fluctuations in soil moisture and, consequently, in tree water status. In the SDI plot, Ψ_{pc} tests were performed simultaneously with those in the SPR plot, regardless of whether they occurred before or after irrigation application, since this irrigation regime involved more frequent water application. At each measurement day, Ψ_{pc} tests were performed every three hours, from 6:00 am to 06:00 pm, in the 2022 irrigation season, and every two hours, from 6:00 am to 8:00 pm, in the 2023 irrigation season.

To evaluate the short-term responsiveness of Ψ_{mt} to external perturbations, two shading experiments were conducted at the peak and end of summer to assess the sensor behaviour under different *SR* conditions. An 80% black shading net was applied from noon on 3 August 2023 until the same time the following day. During the shading trial, Ψ_{pc} measurements were also performed at two-hour intervals from dawn to dusk. The same trial was replicated on 21-22 September.

3.4. 2.4. Statistical analyses

Correlation analysis was performed using data collected simultaneously from MTs and the PC over the two experimental years to validate Ψ_{mt} against Ψ_{pc} for both irrigation regimes.

Scatter group analysis was performed to assess the correlation between Ψ_{mt} and VPD across different phases of tree diurnal water dynamics, and 90% confidence ellipses were determined for each group for the two monitored mandarin trees under different irrigation regimes.

Time-lagged normalised cross-correlation was performed in MATLAB programming software (v.9.14.0, R2023a, The MathWorks, Inc., Natick, MA, USA) using 1-minute interpolated continuous data between ETo and Ψ_{mt}. Normalised cross-correlation assesses the correlations between two temporally shifted time series datasets (Chatfield and Xing 2019), repeatedly computing the Pearson Product Moment Correlation (cross-correlation) Coefficient (XCC) after each shift. In this study, the resulting 'offset' values, each representing a 1-minute interval, are identified at the highest absolute normalised XCC within the series and indicate the time shift between the two specific time series. The time shift and XCC were computed on a daily basis across both seasons for the SDI and SPR irrigation regimes.

3.4.3. Results

3.4.3.1. Climate conditions, irrigation amounts, and soil water content dynamics

Maximum vapour pressure deficit (VPD$_{max}$), daily crop reference evapotranspiration (ETo), daily maximum air temperature (T_{max}), precipitation (P) and irrigation amounts (I) delivered in the SDI and SPR plots for the two monitored irrigation seasons (2022 - 2023) are shown in **Fig. 2**. The study period was characterised by consistently high temperatures, with T_{max} values regularly exceed 30 °C in both seasons. Extreme T_{max} peaks reached 44.2 °C in August 2022 and 45.4 °C in July 2023. However, in 2022, the variability of T_{max} increased markedly toward the end of the season, whereas in 2023, greater T_{max} variability was observed primarily during the early part of the season.

Daily ETo values were generally greater than 5.4 mm d^{-1} until early August, after which they gradually declined. Late-season peaks reached 6.0 mm d^{-1} on 17 September 2022 and 7.4 mm d^{-1} on 22 September 2023, both associated with concurrent high temperatures, low *RH*, and increased wind speed (*u* data not shown). For the observation periods, total ETo was 340.38 and 367.87 mm in 2022 and 2023, respectively.

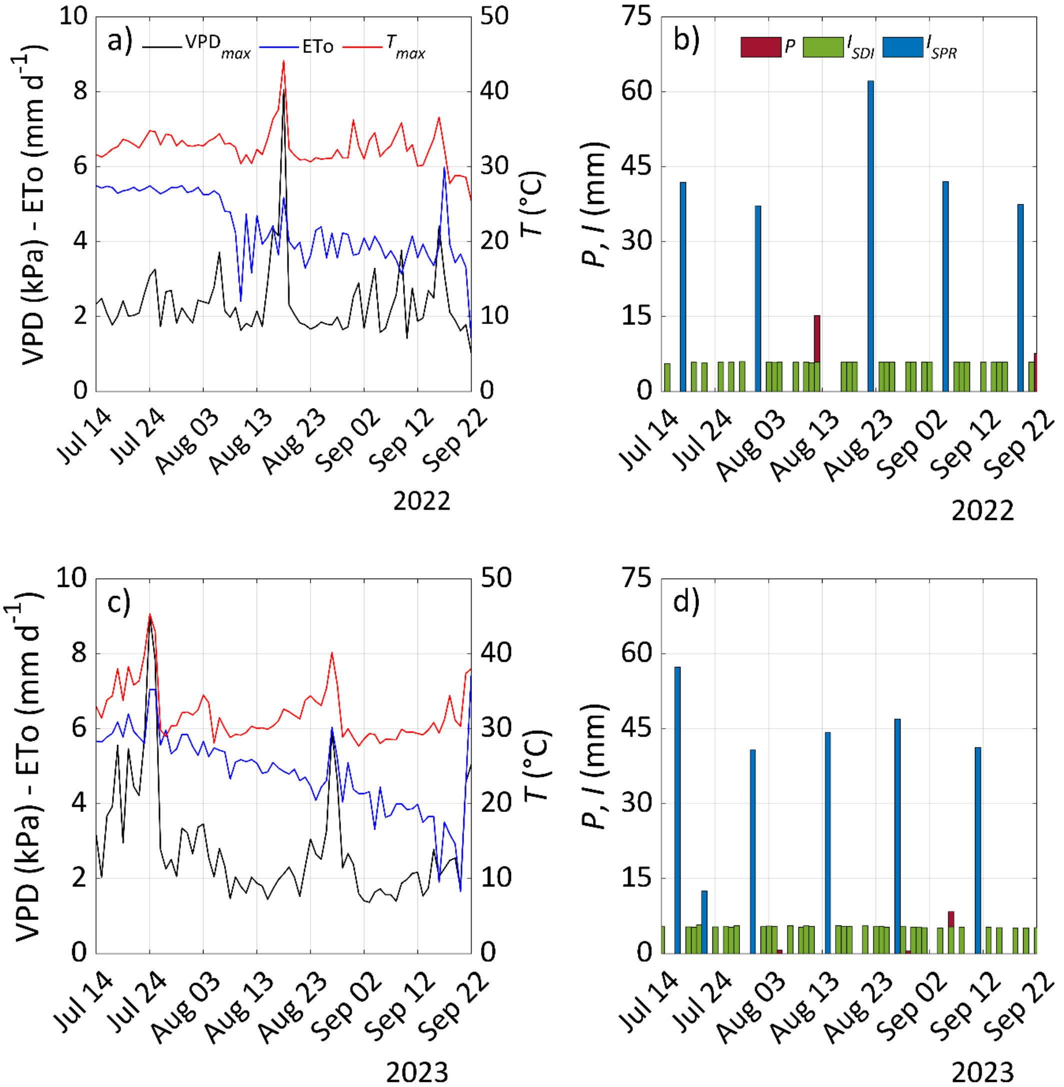

Fig. 2 Time evolution of maximum vapour pressure deficit (VPD$_{max}$), daily reference evapotranspiration (ETo) and maximum daily temperature (T_{max}) during **a**) the 2022 and **c**) the 2023 irrigation seasons. Precipitation and irrigation amount under the SDI (I_{SDI}) and SPR (I_{SPR}) irrigation regimes for **b**) the 2022 and **d**) the 2023 irrigation seasons.

VPD$_{max}$ exhibited pronounced diurnal fluctuations in both seasons. Notably, the 2023 season experienced a higher frequency of days in July with VPD$_{max}$ values exceeding 4 kPa and peaking up to 9 kPa, indicating a stronger atmospheric water demand compared to 2022, which showed a single extreme event on 18 August. Extreme VPD events likely intensified crop transpiration rates, thereby exposing plants to water stress conditions, particularly in the presence of limited soil moisture availability.

Rainfall during the monitoring periods consisted of three events in 2022 (15.2 mm on 12 August, 2.8 mm on 24 August, and 4.4 mm on 21 September) and two in 2023 (2.8 mm on 4 August and 8.4 mm on 6 September).

Figure 2b and **d** illustrate the SPR irrigation events (blue bars) during the Ψ_{mt} monitoring period. Across the full irrigation season (June -October), the farmer applied nine irrigation events in both 2022 and 2023, corresponding to total irrigation volumes of 296.43 mm and 351.66 mm, respectively. In contrast, 59 and 54 irrigation applications were employed in the SDI plot, delivering seasonal irrigation volumes of 323.21 mm and 292.94 mm, in 2022 and 2023, respectively.

Soil water content dynamics for the SDI plot are shown in **Fig. 3a** and **b** for the 2022 and 2023 seasons, respectively. Across the 0 - 0.60 m soil profile, SWC values ranged from 0.160 to 0.376 cm^3 cm^{-3}. As shown, the frequent irrigation management adopted in this plot successfully maintained well-watered conditions, with average SWC consistently close to the red horizontal line representing the θ_{fc} threshold.

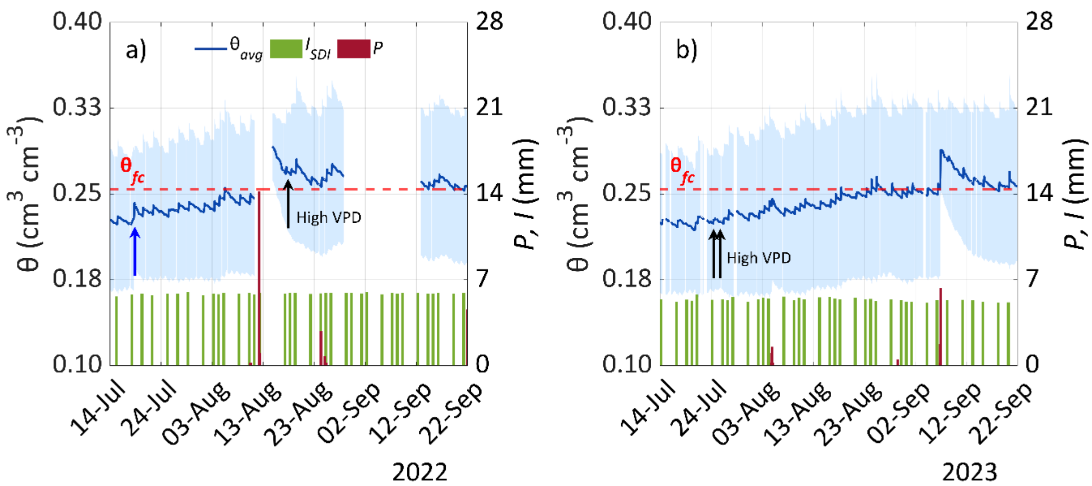

Fig. 3 Daily dynamics of the average soil water content (θ_{avg}) and its standard deviation (blue shaded area) along the 0 - 0.6 m soil profile within the SDI plot during **a**) the 2022 and **b**) the 2023 irrigation seasons. Irrigation events (I_{SDI}) and precipitation (P) are also shown. The red dashed horizontal line indicates the soil water content at field capacity (θ_{fc}). The blue arrow indicates a supplementary irrigation event applied by the farmer.

It is noteworthy that the SWC values marked by the black arrows in **Fig. 3a** and **3b** exhibited no appreciable variation in response to the VPD peaks recorded on 18 August 2022 (**Fig. 2a**) and 24-25

July 2023 (**Fig. 2c**), respectively. In **Fig. 3a**, the blue arrow indicates an increase in SWC resulting from a small irrigation event applied by the farmer using the existing micro-sprinkler system, aimed at moistening the soil surface to facilitate mechanical weed control.

3.4.3.2. Stem water potential monitored with microtensiometer

Temporal patterns of Ψ_{mt} under frequent irrigation (via SDI) and ordinary irrigation (via SPR) regimes during the 2022 and 2023 growing seasons are shown in **Fig. 4**.

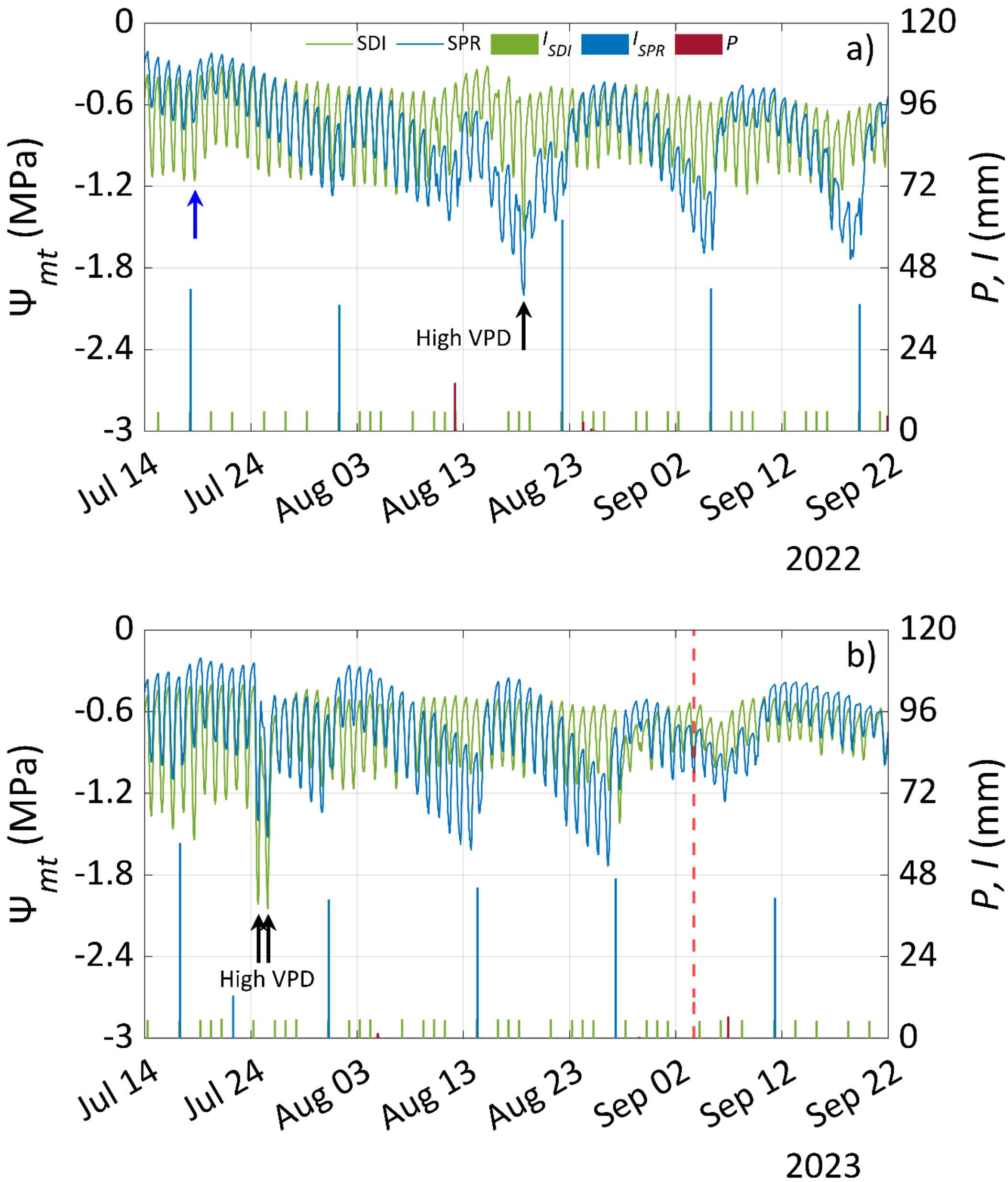

Fig.4 Time series of Ψ_{mt} for a) the 2022 and b) the 2023 growing seasons, under both SDI and SPR irrigation regimes. Precipitation and the corresponding irrigation events of the SDI (I_{SDI}) and SPR (I_{SPR}) irrigation regimes are also shown. The blue arrow indicates a supplementary irrigation event applied by the farmer.

Continuous MT monitoring revealed the difference in Ψ_{mt} dynamics between the two regimes, evident both on an hourly basis and on longer time intervals (i.e., on a day-to-day time scale). Specifically, diurnal changes in Ψ_{mt} showed the expected hourly pattern, with minimum values occurring during midday hours, corresponding to the increase in air temperature, *SR* and VPD from dawn to midday, followed by a gradual rebound of Ψ_{mt} in the afternoon and nighttime. Dependence of Ψ_{mt} on ETo, VPD and *SR* was particularly evident during the heat-wave events that occurred in both seasons. During such events, with air temperature, VPD and ETo values as high as 45°C, 8-9 kPa and 9 mm day^{-1}, respectively (**Fig. 2**), the lowest Ψ_{mt} values were observed (**Fig. 4**) for both irrigation regimes.

In the SDI plot, day-to-day changes of the Ψ_{mt} remained relatively stable compared to those recorded in the mandarin tree under the SPR regime, reflecting the stabilising effect of the high-frequency irrigation schedule, which maintained a consistent SWC across the seasons (**Fig. 3**). As reported in **Table 1**, lower coefficients of variation (*CV*) were observed in pre-dawn (Ψ_{pd}) and midday (Ψ_{md}) Ψ_{mt} compared to the SPR plot.

Table 1. Summary statistics of stem water potential at predawn, Ψ_{pd} (MPa), and midday, Ψ_{md} (MPa), for SDI and SPR systems across both 2022 and 2023 irrigation seasons.

Statistics	2022				2023			
	SDI		SPR		SDI		SPR	
	Ψ_{pd}	Ψ_{md}	Ψ_{pd}	Ψ_{md}	Ψ_{pd}	Ψ_{md}	Ψ_{pd}	Ψ_{md}
Min	-0.71	-1.53	-1.31	-2.00	-0.87	-2.05	-0.98	-1.74
Max	-0.31	-0.71	-0.21	-0.52	-0.40	-0.69	-0.20	-0.68
Mean	-0.48	-1.08	-0.61	-1.06	-0.53	-1.07	-0.52	-1.05
δ	0.09	0.14	0.26	0.36	0.08	0.23	0.19	0.27
CV (%)	18.22	13.00	41.81	33.50	15.88	21.65	36.73	25.61

However, Ψ_{pd} values, despite non-limiting soil water status, can be influenced by environmental factors. For instance, on 25 July 2023, during the heat-wave event, a high-VPD occurred (**Fig. 2c**), and the mandarin tree exhibited more negative Ψ_{pd} values (**Fig. 4b**, black arrows) compared to the preceding day, indicating an incomplete overnight recovery from atmospheric stress. The most substantial recovery occurred within the first 24 hours, with increases of 40.68 % from the Ψ_{pd} value recorded during the peak stress. Full recovery to pre-event levels was achieved four days later. On the same date, Ψ_{md} reached its most negative value, equal to -2.05 MPa (**Fig. 4b**, black arrows), indicating that Ψ_{md} is also highly responsive to environmental drivers. The atypical increase in Ψ_{mt} recorded between in early 2022 season (**Fig. 4a**, blue arrow), which can be ascribed to the small irrigation event previously described, highlighs the MT sensitivity to short-term changes in plant water status.

Due to the low-frequency irrigation scheduling, the day-to-day changes of hourly Ψ_{mt} values in the SPR plot were more pronounced. Indeed, *CV* values (**Table 1**) of Ψ_{pd} and Ψ_{md} were higher compared to the SDI plot, especially in the 2022 season. Notably, in the SPR plot, a major pruning carried out on September 3rd, 2023 (indicated by the dashed red line in **Fig. 4b**), reduced the crop transpiration (Ye et al., 2021), dampening plant water potential fluctuations.

Regarding the Ψ_{pd}, the most negative values are usually recorded on the day of the water application, as the farmer generally begins irrigating after pre-dawn. Following each irrigation event, the tree exhibited a progressive recovery of its stem water potential over the subsequent days followed by a almost linear decrease. The observed linear decline in Ψ_{mt} following the progressive soil drying, along with the onset of crop water stress, is consistent with the near-anisohydric behaviour attributed to mandarins. Unlike other citrus species, mandarins tend to lower their water potential in response to decreasing soil moisture availability within the irrigation cycle (Romero-Trigueros et al., 2021). The extent and rate of this recovery depended primarily on the initial Ψ_{pd} values before the irrigation event, which can also be influenced by external factors such as VPD. **Table 2** shows all pre-irrigation Ψ_{pd} values for SPR plot, together with the corresponding daily percentage recovery relative to the pre-irrigation condition.

Table 2. Daily percentage recovery of predawn stem water potential, $\%\Delta\Psi_{pd}$ (t), relative to the Ψ_{pd} pre-irrigation condition for both irrigation seasons in the SPR plot.

Year	Date	Ψ_{pd} pre-irrig. (MPa)	$\%\Delta\Psi_{pd}$ (t)						
			t = 1	t = 2	t = 3	t = 4	t = 5	t = 6	t = 7
2022	18 Jul	-0.35	24.54	10.90	-2.14	-6.79	-10.36	-7.94	-12.46
	1 Aug	-0.74	**28.42**	8.50	-1.17	-4.80	-7.84	-12.29	-7.01
	22 Aug	-0.98	**35.00**	12.11	5.71	2.08	-0.68	-2.81	-4.38
	5 Sep	-1.24	**43.11**	15.49	4.37	-2.54	0.71	-0.23	-5.31
	19 Sep	-1.32	**43.72**	11.91	5.26	4.23	2.37	-0.32	-1.27
2023	17 Jul	-0.34	26.84	13.64	-7.44	-5.10	-9.39	6.52	2.83
	22 Jul	-0.28	8.01	3.48	-166.94	82.81	-7.63	7.50	-3.14
	31 Jul	-0.62	43.23	14.82	-1.54	-2.17	-12.59	-7.66	-7.90
	14 Aug	-0.90	**40.75**	16.95	3.36	-1.53	-6.90	-5.46	-8.83
	27 Aug	-0.73	**18.59**	9.59	2.37	-4.35	-6.52	-15.68	-0.15
	11 Sep	-0.41	4.31	-0.33	-1.90	-5.88	-9.88	-0.64	-5.93

In all water applications, Ψ_{pd} showed a marked recovery on the first day after the irrigation event, followed by a reduced rate of recovery over the subsequent days. In the most stressed periods, maximum recovery increases up to 40 % of the initial value (**Table 2**, bold values) with the highest recovery rate after one day (43.1%) when the most negative initial Ψ_{pd} values (e.g., -1.32 MPa) occurred. Additionally, the effect of irrigation ends within the first 24 - 48 hours, after which the recovery tends to stabilise or decline. Notably, the sharp decrease of -166.94 % is attributable to the VPD peak event that occurred in 2023 (**Fig. 2c**), which likely counteracted the benefits of irrigation. Following this extreme event, Ψ_{pd} did not return to its pre-event level until the subsequent water application (**Fig. 4b**), suggesting a plant's hydraulic dysfunction. The most negative Ψ_{pd} (-1.31 MPa) and Ψ_{md} (-2.00 MPa) values (**Fig. 4a**, black arrow) recorded in the SPR plot were again attributed to the high VPD and ETo levels observed during a heat-wave event, in this case registered on 18 August 2022 (**Fig. 2a**), when the farmer withheld irrigation due to a preceding rainfall event.

3.4.3.3. Microtensiometer vs pressure chamber

An example of the daily patterns of stem water potential estimated using the pressure chamber (Ψ_{pc}) and the microtensiometer (Ψ_{mt}) along with vapour pressure deficit (VPD), over two days of the 2023 season for both irrigation regimes is illustrated in **Fig. 5**.

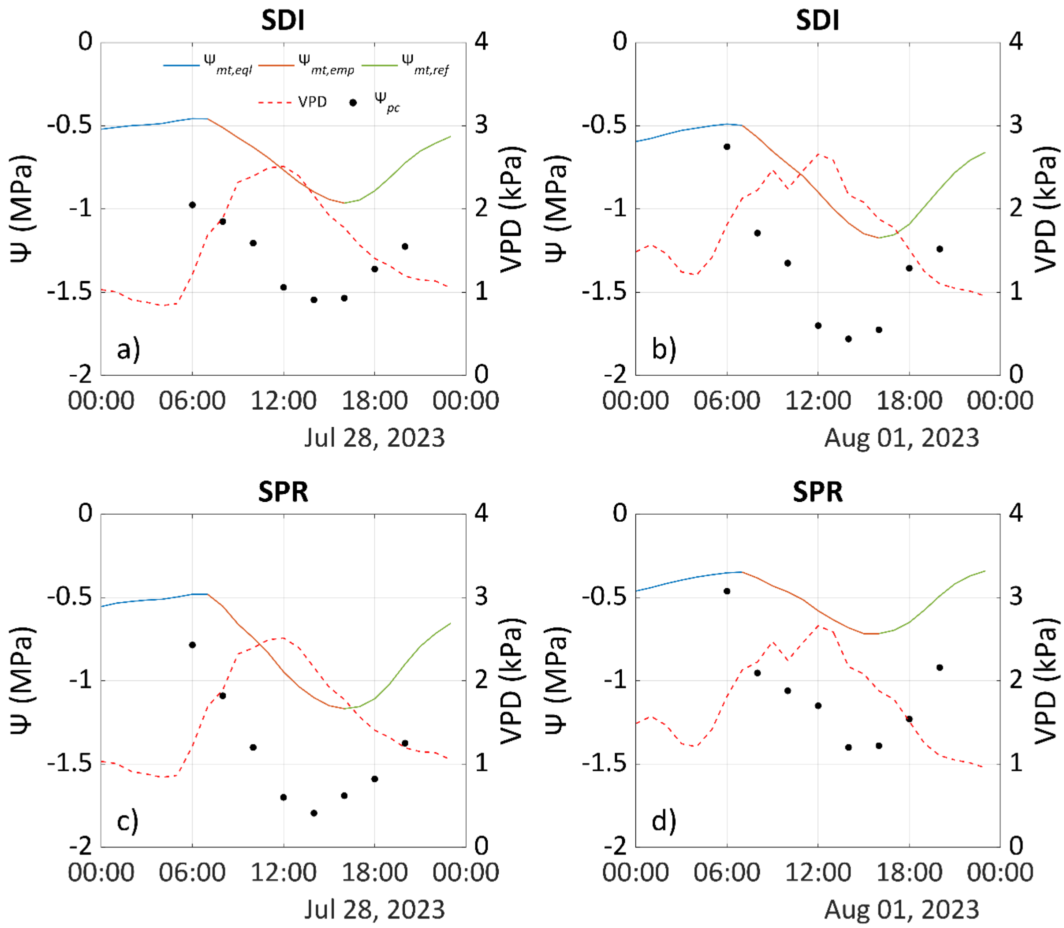

Fig. 5 Daily dynamics of Ψ_{pc} and Ψ_{mt} at the equilibrium ($\Psi_{mt,eql}$), emptying ($\Psi_{mt,emp}$) and refilling ($\Psi_{mt,ref}$) phases under SDI and SPR irrigation regimes. Vapour pressure deficit (VPD) data are also plotted.

The data refer to Ψ_{pc} tests conducted three days before (**Fig. 5c**) and one day after (**Fig. 5d**) the irrigation event in the SPR plot; the simultaneous tests performed in the frequently irrigated SDI plot are representative of post-irrigation (**Fig. 5a**) and pre-irrigation (**Fig. 5b**). Both MT and PC methods effectively distinguished the impacts of the two different irrigation regimes on tree water status, showing significant differences in stem water potential under similar VPD conditions. In general, Ψ_{mt} values were consistently less negative than Ψ_{pc} values, with the differences between the two methods being greater in the afternoon and more pronounced before irrigation (**Fig. 5b** and **c** for SDI and SPR irrigation regimes, respectively). For both irrigation regimes, the most negative values of the Ψ_{pc} were usually recorded at 14:00. Conversely, the minimum value of the Ψ_{mt} generally occurred approximately two hours later, emphasising a certain time lag between the two methods. Additionally, the higher VPD were recorded at midday on both sampling days, further indicating a time lag of two and four hours between the atmospheric water demand and Ψ_{pc} and Ψ_{mt}, respectively.Daily pattern of Ψ_{mt} provides to identify the well-known three distinct time slots of plant water dynamics (**Fig. 5**): (i) the equilibrium phase (00:00 - 07:00, blue line), (ii) the emptying phase (08:00 - 16:00, orange line), and (iii) the refilling phase (17:00 - 23:00, green line). These time slots and/or phases were used to assess the scatter group analysis between Ψ_{mt} and VPD, which is discussed in the next Section.

Figure 6 illustrates the two shading experiments conducted under similar conditions of solar radiation (*SR*) to assess the ability of Ψ_{mt} and Ψ_{pc} to evaluate the plant reaction to covering and uncovering with a black shade net. The MTs responded readily to the shading experiment, especially during the peak of summer (**Fig. 6a** and **b**), in contrast to the attenuated response observed at the end of summer (**Fig. 6c** and **d**).

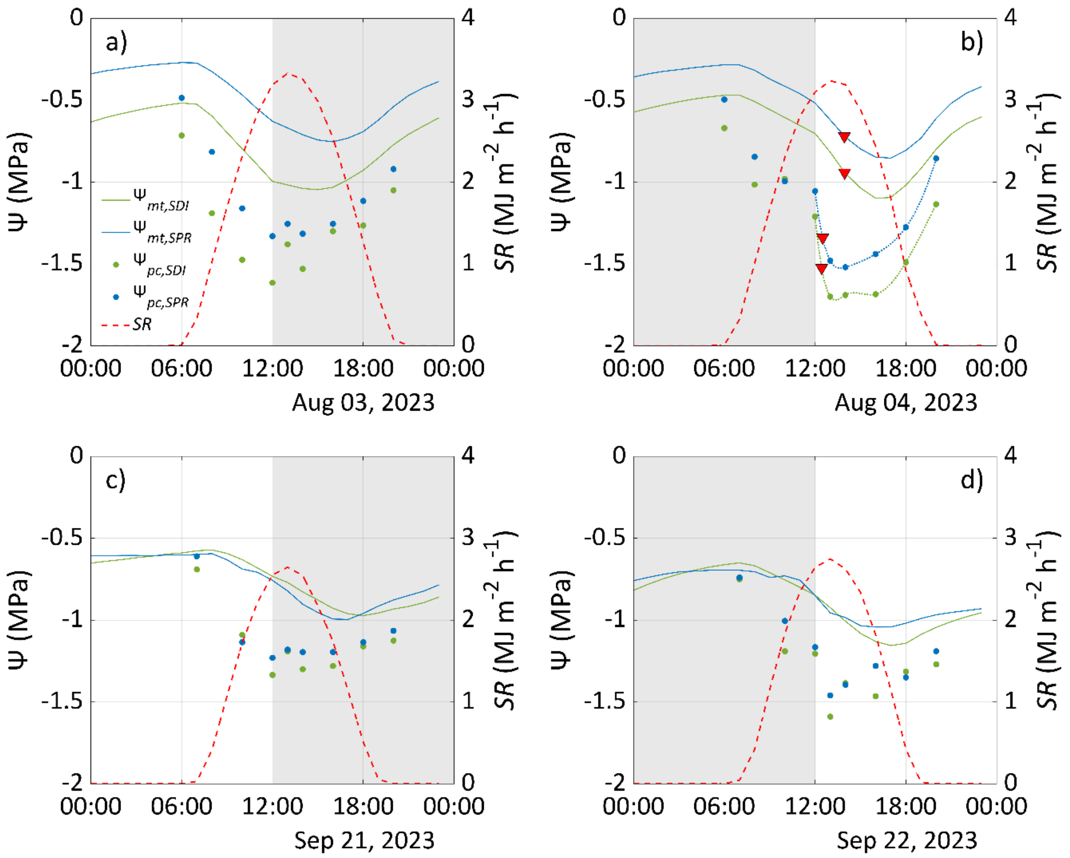

Fig. 6 Daily evolution of Ψ_{mt} and Ψ_{pc} under the SDI ($\Psi_{mt,SDI}$ and $\Psi_{pc,SDI}$, respectively) and the SPR ($\Psi_{mt,SPR}$ and $\Psi_{pc,SPR}$, respectively) irrigation regimes, along with solar radiation (*SR*) levels during the shading tests. The grey areas correspond to the trees' shading period. For both irrigation regimes, red triangles represent the Ψ_{stem} values of both PC and MT methods at their respective time constants (τ), defined as the time following a disturbance when 63 % of the total change has been recorded.

This dynamic was evident from the change in the slope of the Ψ_{mt} vs time relationship, which decreased after covering and increased after uncovering. The application of the shade net resulted in consistently less negative Ψ_{mt} values during the covered intervals, as a consequence of the physiological response to reduced transpiration demand due to decreased incident *SR*. Upon removal of the shade, Ψ_{mt} immediately declined, as a consequence of an increase in transpiration rate and a swift shift in plant water status, suggesting a prompt responsiveness of the MT to the microclimate change. Similar trends were observed for Ψ_{pc} in both shading experiments. Compared to Ψ_{mt}, Ψ_{pc} remained responsive to changes in microclimatic conditions even in late summer. It is worth noting that, following the disturbance events, Ψ_{pc} values remained consistently more negative than Ψ_{mt}. This divergence is related to the dynamics of both Ψ_{mt} and Ψ_{pc} at the time of disturbance: at the moment of covering, Ψ_{stem} was in the decreasing stage within the diurnal cycle and shading halted the decreasing trend of Ψ_{stem}. This effect was observed using both techniques (MT or PC), but with a different dynamic. The Ψ_{pc} stabilised almost immediately, while the Ψ_{mt} displayed a more gradual response, slowing down but continuing to decrease for up to four hours before stabilising (**Fig. 6a** and **6c**). Interestingly, these contrasting dynamics were evident not only during the transition from full sunlight to shade but also upon shade to full sunlight. Ψ_{pc} decreased almost immediately after exposure to sunlight (**Fig. 6b** and **d**), reaching a minimum within two hours; in contrast, Ψ_{mt} showed a slower response, reaching the minimum 4-5 hours later. To further characterise the dynamic response of the sensor-tree complex, an approximate estimation of the time constant (τ), defined as the time required to reach 63% of the change following a disturbance in a first-order system (Nobel, 2009; Phillips et al., 2004), was calculated for both Ψ_{mt} and Ψ_{pc}. The calculation was limited to the uncovering phase of the experiment performed at the peak of summer (3-4 August session, **Fig. 6b)**, when the dynamics of the changes were sufficiently large. For Ψ_{pc}, 63% of the change occurred 29 and 32 minutes after disturbance (sunlight exposure), respectively, in SDI and SPR; in contrast, Ψ_{mt} reached 63% of the total change after 122 and 125 minutes (**Fig. 6b**, filled triangles).Linear regression analysis was performed between Ψ_{mt} and Ψ_{pc} for the SDI and SPR irrigation regimes, pooling the data collected in the two irrigation seasons. The relationship between Ψ_{mt} and Ψ_{pc} exhibited similar slopes and coefficient of determination, with R^2 of 0.62 ($p < 0.0001$) in the SDI plot (**Fig. 7a**) and R^2 of 0.63. ($p < 0.0001$) in the SPR plot (**Fig. 7b**), showing a significant relationship between the Ψ_{stem} estimated by the two methods. However, the relationship between Ψ_{mt} and Ψ_{pc} deviated from the identity line, especially for the SDI plot, with more negative values for Ψ_{pc} compared to Ψ_{mt} (**Fig. 7a**).

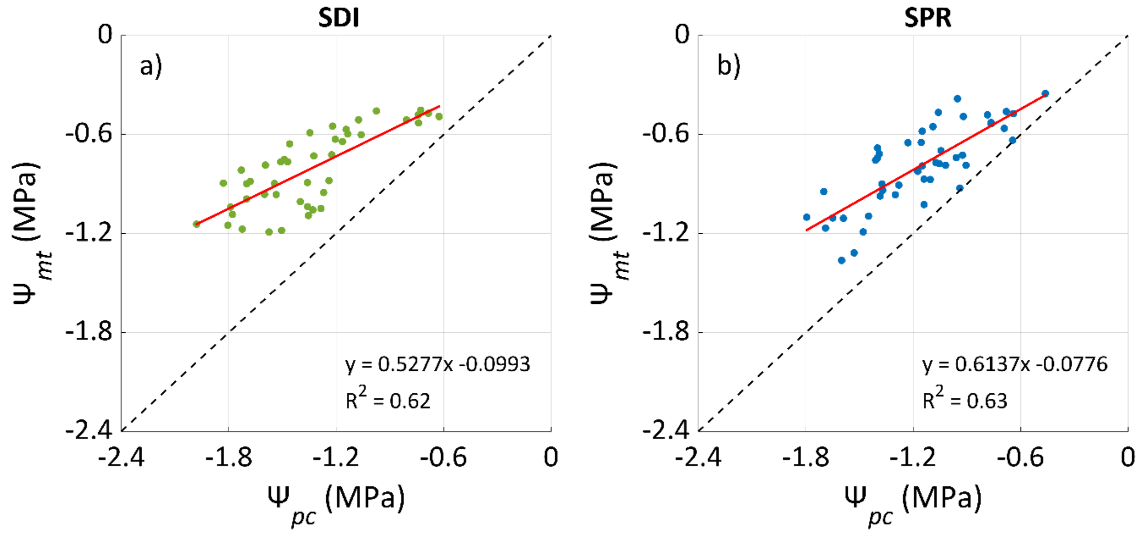

Fig. 7 Linear relationship between stem water potential estimated with the microtensiometers, Ψ_{mt}, and the pressure chamber, Ψ_{pc}, under the **a**) SDI and **b**) SPR irrigation regimes.

3.4.3.4. Correlation between Ψ_{mt} and vapour pressure deficit

Figure 8 shows the relationship between Ψ_{mt} and VPD under SDI and SPR irrigation regimes using scatter plots of hourly data collected in both years during the monitoring period.

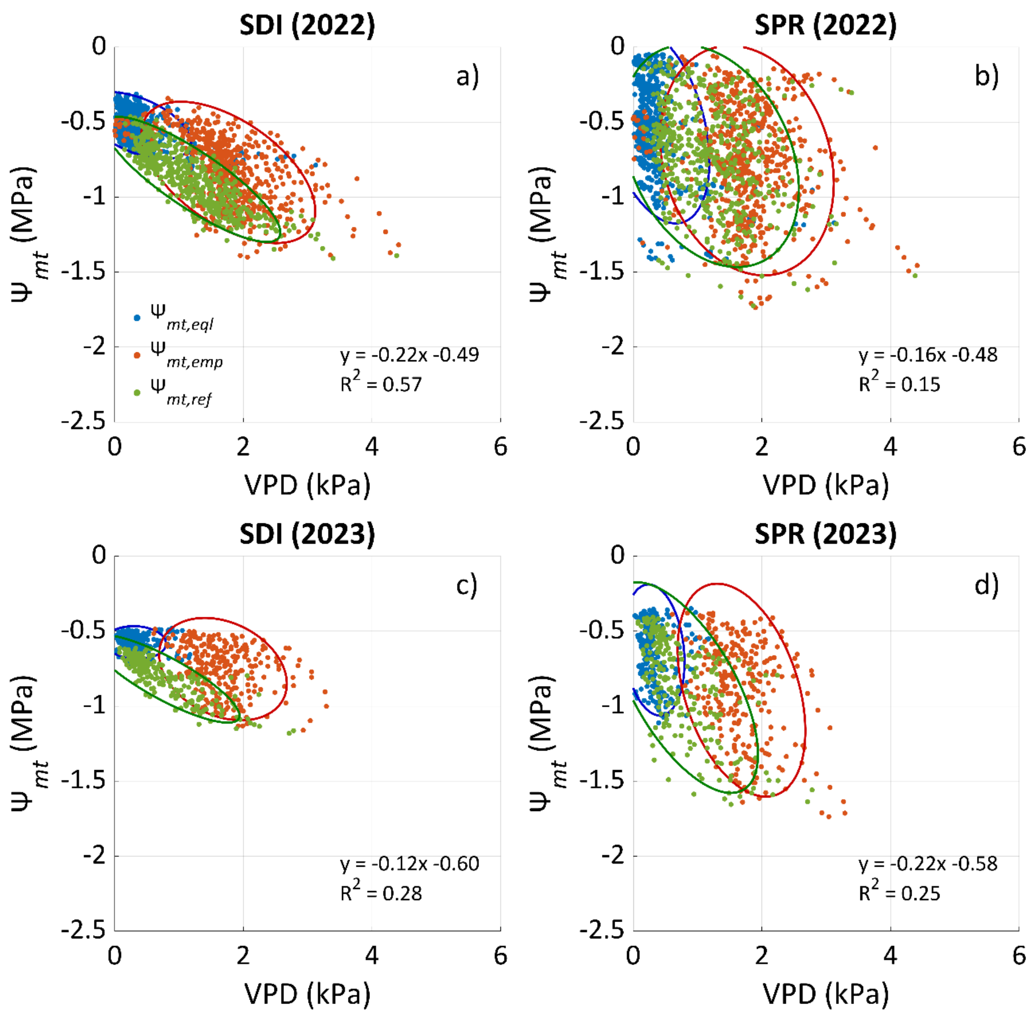

Fig. 8 Scatter group plot between Ψ_{mt} and VPD in the three distinct dynamic hydraulic phases of the tree (00:00 - 07:00 equilibrium, $\Psi_{mt,eql}$, 08:00 - 16:00 emptying, $\Psi_{mt,emp}$, and 17:00 - 23:00 refilling, $\Psi_{mt,ref}$) for the 2022 and 2023 irrigation seasons under (**a**, **c**) the SDI and (**b**, **d**) the SPR irrigation regimes. The ellipse function draws a 90% confidence level for each phase group.

The scatterplots generally align with the expected negative relationship between Ψ_{mt} and VPD. However, the two irrigation regimes exhibited different levels of dispersion, with the frequently irrigated SDI (**Fig. 8a** and **c**) showing lower variability than the ordinary irrigated SPR plot (Fig. **8b** and **d**). In the SDI plot, where SWC remained consistently stable over time (Fig. **3a** and **b**), Ψ_{mt} showed a strong sensitivity to VPD. This relationship was particularly evident in the 2022 season, in which VPD variability was comparatively lower ($R^2 = 0.57$, $p < 0.0001$; **Fig. 8a**). Conversely, in the SPR irrigation regime, Ψ_{mt} displayed weaker correlations with VPD, indicating a stronger influence of SWC on Ψ_{mt} dynamics.

Further analysis of the scatterplots shows that, even at the same VPD level, Ψ_{mt} values vary depending on the time of day. Specifically, higher water potential values were recorded in the early morning, while the lowest values were observed during midday and early afternoon. To capture these diurnal dynamics, data were divided into the three distinct time slots mentioned before. For each time slot, a 90% confidence ellipse was calculated to better visualise the distribution of data. These phases reflect the tree's water dynamics throughout the day: an equilibrium phase in which stem and soil water potentials are balanced under minimal transpiration (Yang et al., 2013; Zhang et al., 2023); an emptying phase in which increasing VPD drives water loss from plant reserves; and a refilling phase in which decreasing VPD allows plants to replenish water stores (Phillips et al., 2004; Vogel et al., 2017). The analysis showed significant variation between the time slots and the irrigation regimes across both seasons. In the SDI irrigation regime and for both seasons (**Fig. 8a** and **c**), Ψ_{mt} vs VPD values recorded in the equilibrium phase exhibit a small size of the ellipse, especially in the 2023 irrigation season (**Fig. 8c**), indicating more concentrated data around the mean (-0.54 MPa for the 2022 season and -0.58 MPa for the 2023 season). For the emptying phase, the ellipse is larger than in the equilibrium phase, suggesting greater variability in the data. For the refilling phase, a more elongated ellipse is shown, indicating a stronger correlation between Ψ_{mt} and VPD ($R^2 = 0.70$ for both irrigation seasons).

In the SPR irrigation regime and for both seasons (**Fig. 8b** and **d**), the sizes of the ellipses of the three distinct time slots are larger than in the SDI plot, suggesting less predictability in the data, with a weaker correlation between Ψ_{mt} and VPD, due to circular shapes of the ellipses, especially in the 2022 irrigation season (**Fig. 8b**). Moreover, the data are more diffusely and irregularly distributed, reflecting greater variability within the group.

3.4.3.5. Sensitivity of Ψ_{mt} to reference evapotranspiration

Time-lagged normalised cross-correlation analysis was used to examine the interpolated 1-minute time series (Phillips et al., 1997, 2004) datasets of ETo and Ψ_{mt} for SDI and SPR irrigation regimes across the 2022 and 2023 growing seasons. **Figure 9** illustrates the highest values of normalised cross-correlation coefficient (XCC, **Fig. 9a** and **b**), and the daily values of the time shifts (**Fig. 9c** and **d**) for both seasons. Additionally, the maximum water pressure deficit (VPD_{max}) values exceeding 6 kPa (black dashed lines), the precipitation (red dashed lines), and, only for the SPR plot, the irrigation events (blue dashed lines) are also dipsyed **(Fig. 9c** and **d**).

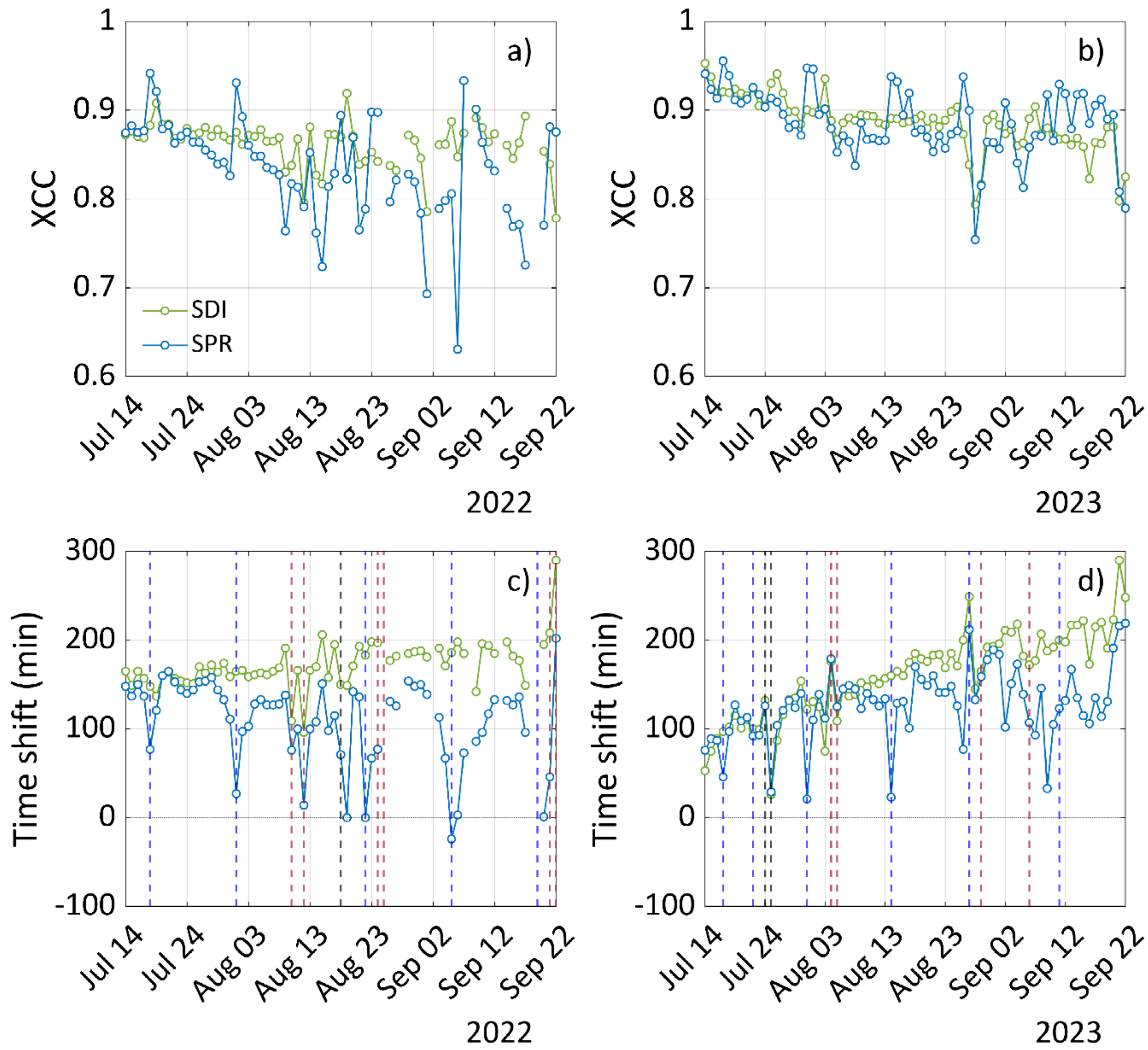

Fig. 9 Daily dynamics of (**a**, **b**) maximum normalised cross-correlation coefficient (XCC) and (**c**, **d**) corresponding time shift between Ψ_{mt} and daily reference evapotranspiration (ETo) under the SDI and SPR irrigation regimes across both seasons. Black dashed lines denote days with VPD_{max} > 6 kPa; red dashed lines indicate precipitation events; and blue dashed lines show farmer irrigation events in the SPR plot.

For both seasons, the highest XCC values declined over time in both irrigation regimes, with fluctuations on days of high VPD_{max} or rainfall. In the SPR plot, XCC also responded to farmer-applied irrigation events, and on these days, time shifts varied markedly.

To characterise the dynamic response of the sensor-tree complex over a longer period than the two-day shading trials, daily values of Ψ_{mt} time constant (Fig. 10) were estimated from the inversion of the relation between τ and the phase delay (φ), calculated from the normalised cross-correlation analysis performed against ETo, for the response of a first-order system to a sinusoidal input with angular frequency ω, according to the following equation:

$$\tau = \frac{-tan(\varphi)}{\omega} \quad (1.0)$$

with ω equal to $2\pi f$ and f representing the frequency of the 24-hour diel cycle, with the simplifying assumption that ETo follows a sinusoidal pattern (Monteith and Unsworth, 2008). The analysis was limited to cloudless days of the 2022 season (**Fig. 9c**). Data are shown for a period covering and extending over a full cycle of SPR irrigations (**Fig. 10**).

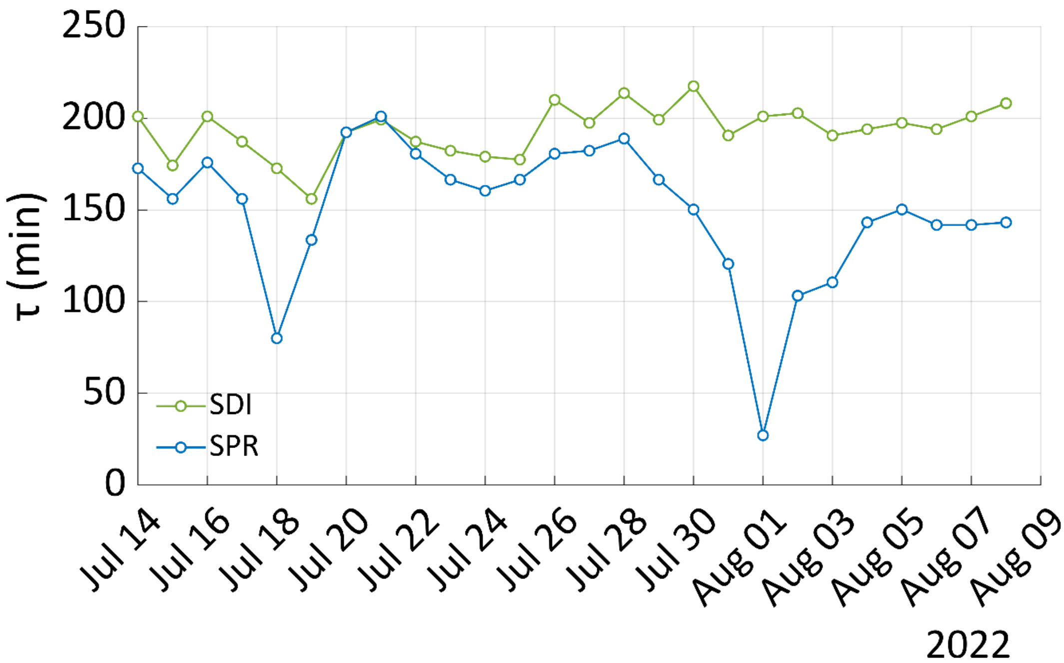

Fig. 10 Daily changes of time constant (τ) for Ψ_{mt} observations under the SDI and SPR irrigation regimes over one SPR irrigation cycle in the 2022 season. Values reported were estimated, in cloudless days, from phase lags obtained by cross-correlation between ETo and Ψ_{mt}.

Over the observation period, Ψ_{mt} time constant showed a different dynamic between SDI and SPR irrigation regimes. In SDI, τ resulted fairly stable, with minor fluctuations during the observation period, whereas in SPR, daily τ changes exhibited a distinctive pattern within the irrigation cycle, decreasing progressively in the days following irrigation, then increasing sharply after the subsequent irrigation event (**Fig. 10**).

3.4.4. Discussion

Although this study was not specifically designed to assess water use efficiency, the differing irrigation frequencies and volumes applied generated distinct soil moisture dynamics, providing valuable conditions for evaluating plant water status using microtensiometers and assessing their performance in a mandarin orchard. Frequent water applications through SDI maintained relatively stable SWC over time, as evidenced by soil moisture sensor data (**Fig. 3**), while the farmer's 14-day irrigation schedule caused pronounced fluctuations in Ψ_{mt} and, consequently, in soil water content. These contrasting irrigation regimes offered an effective framework to evaluate the sensor's sensitivity in detecting variations in stem water potential under dynamic soil moisture and atmospheric conditions, representative of Mediterranean climates.

Vapour pressure deficit is an environmental variable which, under steady-state SWC conditions, regulates plant water relations and, in turn, stem water potential by affecting leaf transpiration and water transport (Mayr, 2021). In the monitored period, VPD_{max} frequently exceeded 3 kPa and peaked up to 9 kPa, especially in the 2023 season (**Fig. 2c**). On such extreme days, even when the soil water content was not a limiting factor, a prolonged but moderate increase in VPD and air temperature led to hydraulic dysfunctions, including limited stomatal closure, elevated transpiration, and more negative plant water potentials (Schönbeck et al., 2022). These phenomena were observed in the mandarin tree within the SDI plot (**Fig. 4b**, black arrows), in which well-water conditions were ensured by high irrigation frequency, maintaining SWC nearly at the field capacity (**Fig. 3a** and **b**). Exposure to high VPD conditions led to a noticeable decline in Ψ_{pd} values on the following morning compared to pre-event values, suggesting that plants were unable to fully recover overnight from the stress imposed by these extreme atmospheric demands. These results align with those obtained in cotton by Christenson et al. (2024), in which the plants were subjected to continued, high evaporative demand conditions. In our study, the most significant recovery (40.68%) occurred within the first 24 hours, yet full restoration of pre-event levels required up to four days. The observed recovery dynamics align with previous studies on mandarin trees' hydraulic responses under fluctuating atmospheric demands (Dzikiti et al., 2010). Notably, the absence of full recovery in the SPR-irrigated tree (**Table 2** and **Fig. 4b**, black arrows) further indicates that less frequent irrigation exacerbates these delays, likely due to insufficient soil water availability.

Under constant SWC conditions, a relatively stable VPD (**Fig. 2a**) satisfactorily drives Ψ_{mt}, especially during the 2022 season (**Fig. 8a**, $R^2 = 0.57$). These results align with those in well-watered kiwi fruits (Di Biase et al., 2025), pear (Blanco and Kalcsits, 2023), apple (Gonzalez Nieto et al., 2023) and grapevine (Pagay, 2022). Focusing on the refilling phase (**Fig. 8a** and **c**, green ellipse), the correlation between Ψ_{mt} and VPD strengthens considerably, reaching an R^2 of 0.70 in both irrigation seasons. Moreover, it is interesting to note that the separation between morning and afternoon data is preserved, reflecting an underlying hysteresis daily cycle that can be recognised even by pooling all the seasonal data gathered throughout each year of observation, with data dispersed within a well-defined envelope over an approximately elliptical boundary (**Fig. 8a** and **c**). Even if specific data on the hourly-based relationship between Ψ_{mt} and VPD are not available for mandarin, a similar dispersion for the Crop Water Stress Index (CWSI), which is indirectly linked to water potential, can be inferred for this citrus crop (Appiah et al., 2022, figure 8). In tree species with significant capacitance effects, such separation can be expected by observing these relations within a short-term diurnal cycle, often showing a hysteresis-like pattern because of the lag between potential transpiration demand and root water uptake (Phillips et al., 1997, 2004; Zhuang et al., 2014).

In contrast, the SPR irrigation regime exhibited weaker correlations between Ψ_{mt} and VPD across the three plant water dynamic phases (**Fig. 8b** and **d**), with a larger scatter and overlap of observations of both the emptying (red dots) and refilling (green dots), suggesting no steady-state condition of SWC was achieved. This variability was particularly evident during the equilibrium phase (**Fig. 8b** and **d**, blue ellipse), where Ψ_{mt} values spanned from well-watered to water-stressed soil moisture conditions. Given that Ψ_{pd} reflects equilibrium between the stem and soil water potential under minimal transpiration (Yang et al., 2013; Zhang et al., 2023), these fluctuations suggest that Ψ_{mt} under the SPR irrigation regime was predominantly influenced by soil water potential rather than atmospheric demand (VPD). During the most water-stressed periods, the SPR irrigated mandarin trees displayed marked physiological responses to the farmer's irrigation events, with Ψ_{pd} recovering up to 40% of the pre-irrigation value (**Table 2**) within 24 hours post watering, highlighting the tree's capacity to respond rapidly when relieved from severe water deficit. Most of the recovery occurred within the first 24-48 hours, after which the tree's water status improvements plateaued or declined, indicating a limited plant's recovery window. Overall, the ability of trees to rapidly restore physiological processes after irrigation highlights the importance of timely water management in mitigating the impacts of drought and supporting tree health and productivity (Cermak et al., 1993; Jamshidi et al., 2021).

To evaluate the microtensiometers' ability to quantify stem water potentials relative to known and traditional approaches, a comparison was performed with those estimated using a pressure chamber. Diurnal observation of Ψ_{mt} and Ψ_{pc} follows similar daily trends, with slight differences between the MT and PC methods in both irrigation regimes. The Ψ_{pc} consistently recorded more negative values than the Ψ_{mt} ones, particularly during early afternoon when transpiration demand peaked (**Fig. 5**). However, this discrepancy tends to reduce at higher values of stem water potential (Di Biase et al., 2025; Pagay, 2022; Zucchini et al., 2023), indicating better alignment between the two methods. Our findings showed an average 0.66 MPa offset in the afternoon between Ψ_{pc} and Ψ_{mt}. The lowest Ψ_{mt} values were usually recorded between 16:00 and 17:00, while the lowest Ψ_{pc} values were recorded at 14:00, showing a time-lag regardless of the irrigation regime adopted. Similar lags between Ψ_{mt} and Ψ_{pc} can also be observed in Pagay (2022) for grapevine.

The observed time shift in the Ψ_{mt} response compared to Ψ_{pc} denotes a slower dynamic behaviour, indicating a marked time constant of the microtensiometer, which could be linked to its intrinsic characteristic or the result of the whole complex sensor installation (the sensor itself, the mating paste and wood characteristics), as observed by Lakso et al. (2022). The slow sensor response not only determines a lag in the timing of minimum values but can also be the cause of overestimation of Ψ_{mt} relative to Ψ_{pc}, as a consequence of the smoothing effect exerted by the sensor (or the sensor-tree complex) time constant on the expected true signal of the tree water potential (Ψ_{stem}), acting as a "first-order filter" (similar to a resistance-capacitance network, under the assumption that the Ohm's law analogy holds).

On the contrary, the Ψ_{stem} time-course can be more closely approximated by Ψ_{pc}. While it is arguable that neither Ψ_{mt} or Ψ_{pc} can be assumed as the "true" Ψ_{stem}, since manual readings of water potential (leaf or stem) by pressure chamber is well known to be biased by a significant "operator effect" (Turner, 1985; Levin, 2019), these factors primarily affect only the absolute value of Ψ_{pc} rather than the temporal dynamics. In this sense, differently from Ψ_{mt}, a zero-time lag can be assumed between Ψ_{pc} and the actual Ψ_{stem}.

Sensor time constant (τ) was reported by Lakso et al. (2022) as less than 15 minutes for the sensor itself; however, the Authors recognise that the τ value of the complex "sensor - mating paste - plant tissue" is difficult to determine, and it may vary on a species- or even plant-basis. Additionally, they highlighted that such an effect could sum up to stem capacitance effects and wood characteristics, to be specifically addressed. A non-zero sensor time constant implies a time lag in Ψ_{mt} vs. Ψ_{pc} readings, particularly during the most dynamic parts of the day when rapid changes in Ψ_{stem} following transpiration demand peaks occur. However, Lakso et al. (2022) reported a good correlation with maximal (pre-dawn) and minimal (afternoon) values (i.e., the values occurring in the less dynamic parts of the day), which are the most relevant values for irrigation management.

In the present study, Ψ_{mt} and Ψ_{pc} in mandarin trees were significantly correlated under both irrigation regimes ($R^2 = 0.62$, $p < 0.0001$, for SDI tree and $R^2 = 0.63$, $p < 0.0001$, for SPR). However, the slopes of the linear regression lines (**Fig. 7**) deviated from the identity line, indicating a dissimilarity between the two methods. Similar deviations have been reported in other woody crops, such as grapevines (Pagay, 2022), olive orchards (Zucchini et al., 2023) and orange orchards (Vanella et al., 2025). In contrast, near-unity slopes have been observed in smaller or well-watered annual crops, such as nectarines (Conesa et al., 2023) and cotton (Christenson et al., 2024). For cotton, in particular, the stronger agreement could be related to its smaller canopy size, compared to the mandarin tree, which allows microtensiometers to better reflect the whole plant water potential (Blanco and Kalcsits, 2021; Pagay, 2022).

The slopes of the linear regression lines (**Fig. 7**) observed in our study suggest that Ψ_{mt} changed at a more attenuated extent compared to the Ψ_{pc}, resulting in a systematic overestimation of Ψ_{stem} compared to Ψ_{pc} readings. From a practical point of view, this aspect does not necessarily preclude the use of Ψ_{mt} for irrigation management in mandarin orchards. However, appropriate adjustments are required to account for the low (less-than-one) slope values of the regression lines, as observed under both SDI and SPR irrigation regimes. Similar conclusions were expressed by other Authors (e.g., Pagay, 2022; Conesa et al., 2023) who suggested that, in cases where absolute Ψ_{stem} values are required, the need for crop-specific thresholds is necessary for integrating Ψ_{mt} into irrigation scheduling protocols.

The varying degrees of scattering observed in tree-based measurements, such as Ψ_{mt} vs VPD or ETo, may be linked to the differing levels of dynamic coupling between tree-level processes and changes in atmospheric variables influenced by the irrigation regime. The time lags between tree water potential, estimated by microtensiometer, and atmospheric variables like ETo or VPD create hysteresis-like patterns that may add up to other better-known sources of hysteresis (Wan et al., 2023; Zhang, 2014; Tuzet et al., 2003; Phillips, 1997). This raises the need for a careful assessment of these effects to evaluate the reliability of microtensiometer data as an indicator of water status in mandarin trees. In this sense, it is necessary to consider the importance of the timing of readings. Lags in diurnal changes in Ψ_{mt} compared to VPD (**Fig. 5**) or other atmospheric demand variables, such as ETo (**Fig. 9**), need to be properly addressed, considering both the diurnal and seasonal effects. Hourly Ψ_{mt} values can be used to identify the daily time lag, using the cross-correlation coefficient (**Fig. 9**). Over the season, a decrease in the maximum cross-correlation coefficient could be observed for both irrigation regimes. Such a decrease paralleled the seasonal reduction of ETo (**Fig. 2**), but other effects could be involved (Kaner et al., 2020; Phillips et al., 2004; Vogel et al., 2017) since time constant effects can be modulated by changes in physiological aspects other than capacitance (Zhuang et al., 2014).

The substantial time shift and signal attenuation observed across both years make the direct use of raw MT signals as a proxy for Ψ_{stem} challenging. The minimum Ψ_{mt} occurred up to two hours after the observed Ψ_{pc} minimum, while signal attenuation led to systematic overestimation of Ψ_{stem} due to the first-order response characteristics of the sensor-tree complex. Indications of the presence of such features in the dynamic response of MT sensors and about the difference in the technical behaviour of sensors when characterized in laboratory (with a 15-minutes time shift) in comparison to their response when installed on the tree were reported by Lakso et al. (2022), stating the need to consider the output signal as the result of the interaction of the xylem with the sensor and the interfacing compound. Other subsequent studies (Di Biase et al., 2025; Zucchini et al., 2023; Pagay, 2022) reported the presence of such effects and their impact on the correlations between Ψ_{mt} and Ψ_{pc} on different species. In the present study on mandarin citrus, such effects had a large impact on the possibility of a direct comparison of Ψ_{mt} vs. Ψ_{pc}.

At a more general level, directly comparing Ψ_{mt} and Ψ_{pc} in the presence of large time constants would be problematic, particularly on an hourly basis. The predictable differences between signals due to the substantial time shifts observed (up to two hours in this study) would make comparisons with currently published irrigation thresholds of limited practical value. Moreover, a comparison with measurements taken in a specific moment of the day, such as the commonly used "midday" or "pre-dawn" Ψ_{stem}, would discard the valuable time information provided by MTs. Under these ideas, an appropriate characterisation of the dynamic behaviour of the sensor-tree interaction as a composite system could provide a useful insight of trees' condition. In this context, the time constant should not be viewed merely as a hindrance to sensor adoption, but rather as an informative indicator of tree physiological status. Both the time shift and time constant demonstrated sensitivity to different irrigation regimes in the present study, as shown in **Figure 10**. Developing suitable models of the sensor-tree complex's dynamic response to environmental variables would significantly improve the quality of information obtainable from MTs by fully utilising the temporal information provided by the sensors.

Overall, these findings underscore that microtensiometers provide valuable high-resolution monitoring of tree water status, yet their integration into irrigation scheduling protocols requires a sophisticated understanding of the temporal coupling between plant water potential and evaporative demand. This consideration becomes even more critical when attempting to predict stem water potential indirectly from its relationship with environmental drivers such as VPD or ETo, particularly in scenarios where the use of microtensiometers is limited by technical constraints or economic inaccessibility, particularly for small-scale growers.

3.4.1 Limitations and future research

Continuous MT readings captured stem water potential dynamics with high temporal resolution, demonstrating their potential to rapidly detect physiological responses that could be missed by discrete pressure chamber data. These findings support the use of in situ microtensiometers as reliable tools for real-time irrigation scheduling and stress monitoring under fluctuating environmental conditions. However, several practical limitations were also observed.

In both irrigation seasons, unrealistic Ψ_{mt} values were observed in late September, likely due to water infiltration into the sensor insulation that degraded after 2-3 months of operation. **Figure 11a** illustrates the MT failure that occurred in 2023 following consecutive rainfall events. Additionally, in 2023, a second monitored mandarin tree under the SDI plot experienced sensor malfunction following the two consecutive days of elevated VPD (**Fig. 11b**, black arrows). The Ψ_{mt} readings deviated from expected patterns, suggesting poor xylem contact or internal disconnection. Notably, reinstallation of the sensor was unsuccessful in restoring signal continuity (**Fig. 11b**, red arrow).

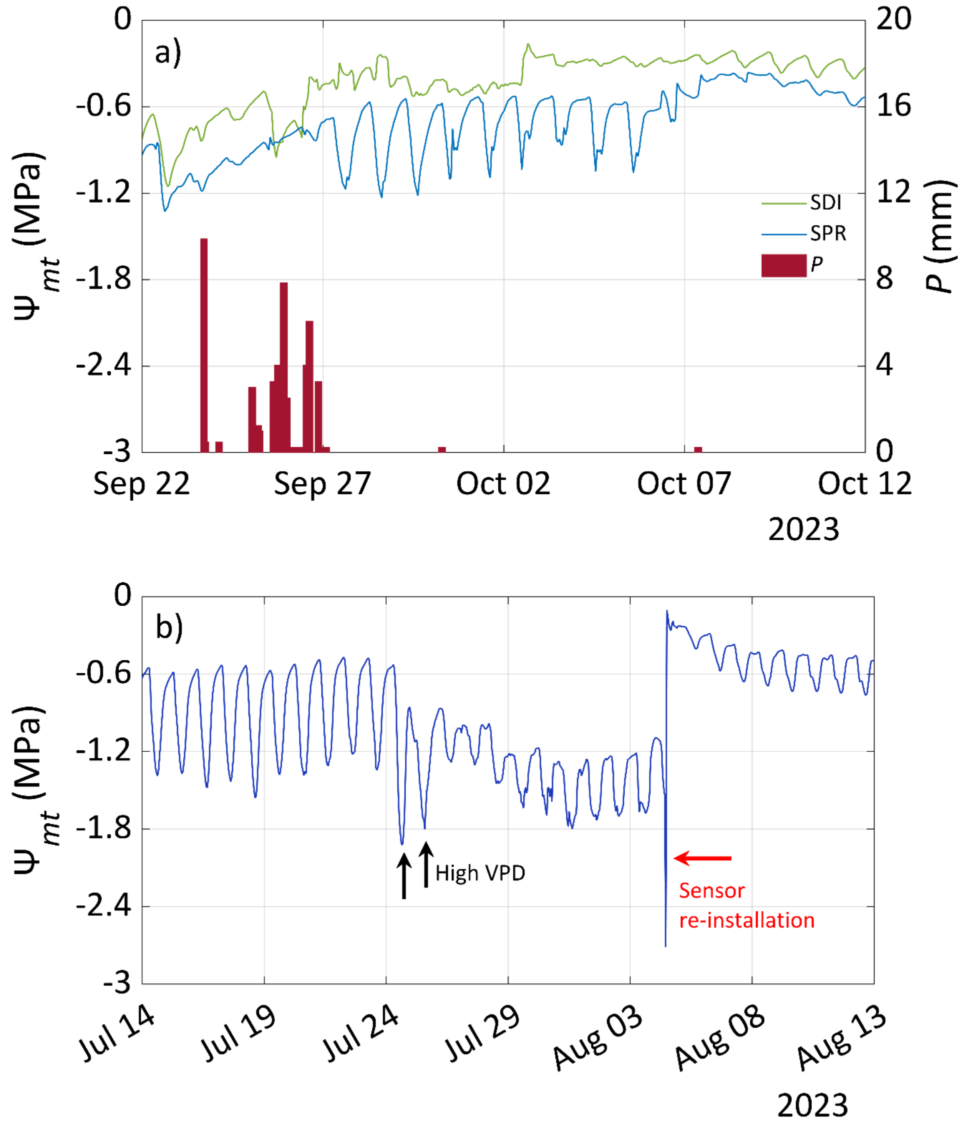

Fig. 11 Observed limitations of MT: **a**) sensor failure following a sequence of precipitation events in late September 2023, and **b**) sensor failure following high VPD events (black arrows) for another monitored tree of the SDI plot (red arrow indicates sensor re-installation).

Our findings indicate that predawn Ψ_{mt}, as the most stable indicator unaffected by diurnal or plant-driven fluctuations (i.e., the sensor-tree-complex response), can be used for real-time irrigation management of mandarin orchards in Mediterranean climates under well-watered conditions, with a threshold of -0.51 ± 0.09 MPa. To define physiologically meaningful thresholds of Ψ_{pd} and Ψ_{md} for irrigation scheduling and support the implementation of water-saving strategies such as regulated deficit irrigation, further research is warranted. In particular, a comprehensive assessment incorporating stem water potential, soil water content, and transpiration rate, will be essential to characterise the water status across a range of stress levels (from moderate to severe) and to evaluate the hydraulic responses of mandarin trees under different SWC conditions, such as those observed in the SPR plot, where greater variation in Ψ_{pd} and Ψ_{md} occurs (**Table 1**).

3.4.5. Conclusions

This study demonstrates the potential of microtensiometers as a reliable tool for continuously monitoring stem water potential (Ψ_{stem}) in *C. reticulata* under Mediterranean climate conditions and different irrigation regimes. The high temporal resolution of microtensiometers' readings (Ψ_{mt}) allows the detection of diurnal variations in plant water status, reflecting the combined effect of atmospheric demand, soil water content, and irrigation management. Frequent irrigation via subsurface drip irrigation ensured a more stable Ψ_{mt} and a tighter coupling between plant and atmospheric conditions. Whereas the ordinary low-frequency irrigation scheduling via micro-sprinkler resulted in greater variability and stronger dependence on soil water availability. The comparison between Ψ_{mt} and conventional pressure chamber readings (Ψ_{pc}) revealed a significant correlation, although differences in magnitude and timing were observed. Following an external disturbance induced by shading of the tree, Ψ_{pc} and Ψ_{mt} responded similarly in trend but differed substantially in dynamics, with Ψ_{pc} reacting promptly to microclimate changes, while Ψ_{mt} exhibited a delayed and smoothed response. This delay, quantified through the markedly higher time constant of Ψ_{mt} compared to Ψ_{pc}, reflects the slower response of the microtensiometer sensor-tree complex as a whole, leading to overestimation of Ψ_{stem} when compared to pressure chamber estimations. These findings suggest that the first-order dynamics of the sensor-tree-complex response signal hinder the direct use of Ψ_{mt} as a direct replacement of pressure-chamber Ψ_{stem} measurements. Consequently, compensation protocols accounting for a large time constant should be developed to apply Ψ_{mt} readings to currently published crop-specific Ψ_{stem} thresholds for irrigation scheduling protocols, generally obtained by pressure chamber, that could suitably take into account the full dynamics of the signal. In this respect, the sensitivity shown by Ψ_{mt} time constant to different irrigation regimes and the changes occurring within each irrigation cycle seems to be a promising feature of MTs that could allow for making full use of the timing information provided by the sensor, continuous by nature, in contrast to the point measurements as "midday" and "pre-dawn" water potentials.

REFERENCES

Allen, R.G., Pereira, L.S., Raes, D., Smith, M., 1998. Crop evapotranspiration. FAO Irrig Drain Pap 56. 65–88

Appiah, S.A., Li, J., Lan, Y., Darko, R.O., Alordzinu, K.E., Al Aasmi, A., Asenso, E., Issaka, F., Afful, E.A., Wang, H., Qiao, S., 2022. Real-Time Assessment of Mandarin Crop Water Stress Index. Sensors 22, 4018. https://doi.org/10.3390/s22114018

Bader, M.K. -F., Ehrenberger, W., Bitter, R., Stevens, J., Miller, B.P., Chopard, J., Rüger, S., Hardy, G.E.S.J., Poot, P., Dixon, K.W., Zimmermann, U., Veneklaas, E.J., 2014. Spatio-temporal water dynamics in mature *Banksia menziesii* trees during drought. Physiol. Plant. 152, 301–315. https://doi.org/10.1111/ppl.12170

Ballester, C., Castel, J., Intrigliolo, D.S., Castel, J.R., 2011. Response of Clementina de Nules citrus trees to summer deficit irrigation. Yield components and fruit composition. Agric. Water Manag. 98, 1027–1032. https://doi.org/10.1016/j.agwat.2011.01.011

Bengtsson, L., Enell, M., 1986. Chemical analysis. Handbook of Holocene palaeoecology and palaeohydrology: 423-451.

Blanco, V., Kalcsits, L., 2023. Long-term validation of continuous measurements of trunk water potential and trunk diameter indicate different diurnal patterns for pear under water limitations. Agric. Water Manag. 281, 108257. https://doi.org/10.1016/j.agwat.2023.108257

Bulut, R., Leong, E., 2008. Indirect measurement of suction. Geotechnical and Geological Engineering 26: 21–32.

Cahn, M., Hutmacher, R., 2024. Subsurface drip irrigation. Microirrigation for Crop Production. Elsevier Science, pp 257–301

Camp, C.R., 1998. Subsurface drip irrigation: a review. Trans. ASAE 41, 1353–1367. https://doi.org/10.13031/2013.17309

Capurro, M.C., Ham, J.M., Kluitenberg, G.J., Comas, L., Andales, A.A., 2024. A novel sap flow system to measure maize transpiration using a heat pulse method. Agric. Water Manag. 301, 108963. https://doi.org/10.1016/j.agwat.2024.108963

Cermak, J., Matyssek, R., Kucera, J., 1993. Rapid response of large, drought-stressed beech trees to irrigation. Tree Physiol. 12, 281–290. https://doi.org/10.1093/treephys/12.3.281

Chatfield, C., Xing, H., 2019. The analysis of time series: an introduction with R. Chapman & Hall/CRC texts in statistical science series, Seventh edition. edn. CRC Press, Taylor & Francis Group, Boca Raton

Choné, X., 2001. Stem Water Potential is a Sensitive Indicator of Grapevine Water Status. Ann. Bot. 87, 477–483. https://doi.org/10.1006/anbo.2000.1361

Christenson, C.G., Gohardoust, M.R., Calleja, S., Thorp, K.R., Tuller, M., Pauli, D., 2024. Monitoring cotton water status with microtensiometers. Irrig. Sci. 42, 995–1011. https://doi.org/10.1007/s00271-024-00930-w

Ciais, Ph., Reichstein, M., Viovy, N., Granier, A., Ogée, J., Allard, V., Aubinet, M., Buchmann, N., Bernhofer, Chr., Carrara, A., Chevallier, F., De Noblet, N., Friend, A.D., Friedlingstein, P., Grünwald, T., Heinesch, B., Keronen, P., Knohl, A., Krinner, G., Loustau, D., Manca, G., Matteucci, G., Miglietta, F., Ourcival, J.M., Papale, D., Pilegaard, K., Rambal, S., Seufert, G., Soussana, J.F., Sanz, M.J., Schulze, E.D., Vesala, T., Valentini, R., 2005. Europe-wide reduction in primary productivity caused by the heat and drought in 2003. Nature 437, 529–533. https://doi.org/10.1038/nature03972

Clearwater, M.J., Goldstein, G., 2005. Embolism Repair and Long Distance Water Transport, in: Vascular Transport in Plants. Elsevier, pp. 375–399. https://doi.org/10.1016/B978-012088457-5/50020-4

Conesa, M.R., Conejero, W., Vera, J., Ruiz-Sánchez, M.C., 2023. Assessment of trunk microtensiometer as a novel biosensor to continuously monitor plant water status in nectarine trees. Front. Plant Sci. 14, 1123045. https://doi.org/10.3389/fpls.2023.1123045

Dainese, R., De Cfl Lopes, B., Tedeschi, G., Lamarque, L.J., Delzon, S., Fourcaud, T., Tarantino, A., 2022. Cross-validation of the high-capacity tensiometer and thermocouple psychrometer for continuous monitoring of xylem water potential in saplings. J. Exp. Bot. 73, 400–412. https://doi.org/10.1093/jxb/erab412

Dane, J H., Hopmans, J.W., Topp, G.C., 2002. Pressure plate extractor. Methods of soil analysis: Physical methods. 3rd ed. Madison: Soil Science Society of America, 688-90.

Dean, W.E., 1974. Determination of carbonate and organic matter in calcareous sediments and sedimentary rocks by loss on ignition; comparison with other methods. J. Sediment. Res. 44(1), 242-248.

Di Biase, R., Calabritto, M., Mininni, A.N., Montanaro, G., Dichio, B., 2025. Microtensiometer-based trunk water potential as a plant water status indicator in kiwifruit under different soil water availability. Irrig. Sci. https://doi.org/10.1007/s00271-025-01020-1

Dzikiti, S., Verreynne, J.S., Stuckens, J., Strever, A., Verstraeten, W.W., Swennen, R., Coppin, P., 2010. Determining the water status of Satsuma mandarin trees [Citrus Unshiu Marcovitch] using spectral indices and by combining hyperspectral and physiological data. Agric. For. Meteorol. 150, 369–379. https://doi.org/10.1016/j.agrformet.2009.12.005

Fernández, J.E., 2014. Plant-based sensing to monitor water stress: Applicability to commercial orchards. Agric. Water Manag.

Galindo, A., Collado-González, J., Griñán, I., Corell, M., Centeno, A., Martín-Palomo, M.J., Girón, I.F., Rodríguez, P., Cruz, Z.N., Memmi, H., Carbonell-Barrachina, A.A., Hernández, F., Torrecillas, A., Moriana, A., Pérez-López, D., 2018. Deficit irrigation and emerging fruit crops as a strategy to save water in Mediterranean semiarid agrosystems. Agric. Water Manag. 202, 311–324. https://doi.org/10.1016/j.agwat.2017.08.015

García-Tejero, I., Romero-Vicente, R., Jiménez-Bocanegra, J.A., Martínez-García, G., Durán-Zuazo, V.H., Muriel-Fernández, J.L., 2010. Response of citrus trees to deficit irrigation during different phenological periods in relation to yield, fruit quality, and water productivity. Agric. Water Manag. 97, 689–699. https://doi.org/10.1016/j.agwat.2009.12.012

Gonzalez-Altozano, P., Castel, J.R., 1999. Regulated deficit irrigation in ‘Clementina de Nules’ citrus trees. I. Yield and fruit quality effects. J Hortic Sci Biotechnol 74(6):706–713

Gonzalez Nieto, L., Huber, A., Gao, R., Biasuz, E.C., Cheng, L., Stroock, A.D., Lakso, A.N., Robinson, T.L., 2023. Trunk Water Potential Measured with Microtensiometers for Managing Water Stress in “Gala” Apple Trees. Plants 12, 1912. https://doi.org/10.3390/plants12091912

Hacke, U.G., Sperry, J.S., 2001. Functional and ecological xylem anatomy. Perspectives in plant ecology, evolution and systematics, 4(2), 97-115.

Jamshidi, S., Zand-Parsa, S., Niyogi, D., 2021. Physiological responses of orange trees subject to regulated deficit irrigation and partial root drying. Irrig. Sci. 39, 441–455. https://doi.org/10.1007/s00271-020-00709-9

Jones, H.G., 2004. Irrigation scheduling: advantages and pitfalls of plant-based methods. J. Exp. Bot. 55, 2427–2436. https://doi.org/10.1093/jxb/erh213

Kaner, A., Preisler, Y., Grünzweig, J.M., Mau, Y., 2020. Internal water storage buffering maintains plant function under drought as described by a general hydraulic model. https://doi.org/10.1101/2020.02.11.943563

Lakso, A.N., Santiago, M., Stroock, A.D., 2022. Monitoring Stem Water Potential with an Embedded Microtensiometer to Inform Irrigation Scheduling in Fruit Crops. Horticulturae 8, 1207. https://doi.org/10.3390/horticulturae8121207

Lamm, F.R., Colaizzi, P.D., Sorensen, R.B., Bordovsky, J.P., Dougherty, M., Balkcom, K., Zaccaria, D., Bali, K.M., Rudnick, D.R., Peters, R.T., 2021. A 2020 Vision of Subsurface Drip Irrigation in the U.S. Trans. ASABE 64, 1319–1343. https://doi.org/10.13031/trans.14555

Levin, A.D., 2019. Re-evaluating pressure chamber methods of water status determination in field-grown grapevine (Vitis spp.). Agric. Water Manag. 221, 422–429. https://doi.org/10.1016/j.agwat.2019.03.026

Lundblad, M., Lagergren, F., Lindroth, A., 2001. Evaluation of heat balance and heat dissipation methods for sapflow measurements in pine and spruce. Ann. For. Sci. 58, 625–638. https://doi.org/10.1051/forest:2001150

Mancha, L., Uriarte, D., Prieto, M., 2021. Characterization of the Transpiration of a Vineyard under Different Irrigation Strategies Using Sap Flow Sensors. Water 13, 2867. https://doi.org/10.3390/w13202867

Martínez-Gimeno, M.A., Castiella, M., Rüger, S., Intrigliolo, D.S., Ballester, C., 2017. Evaluating the usefulness of continuous leaf turgor pressure measurements for the assessment of Persimmon tree water status. Irrig. Sci. 35, 159–167. https://doi.org/10.1007/s00271-016-0527-3

Monteith, J.L., Unsworth, M.H., 2008. Principles of Environmental Physics. Plants, Animals, and the Atmosphere. Academic Press.

Mayr, S., 2021. Relevance of time and spatial scales in plant hydraulics. Tree Physiol. 41, 1781–1784. https://doi.org/10.1093/treephys/tpab093

Nobel, P.S., 2009. Physicochemical and Environmental Plant Physiology. Fourth edition. Chapter 9 - Plants and Fluxes, Pages 438-505. Academic Press.

Ortuño, M.F., García-Orellana, Y., Conejero, W., Ruiz-Sánchez, M.C., Alarcón, J.J., Torrecillas, A., 2006. Stem and leaf water potentials, gas exchange, sap flow, and trunk diameter fluctuations for detecting water stress in lemon trees. Trees 20, 1–8. https://doi.org/10.1007/s00468-005-0004-8

Pagay, V., 2022. Evaluating a novel microtensiometer for continuous trunk water potential measurements in field-grown irrigated grapevines. Irrig. Sci. 40, 45–54. https://doi.org/10.1007/s00271-021-00758-8

Pagay, V., Santiago, M., Sessoms, D.A., Huber, E.J., Vincent, O., Pharkya, A., Corso, T.N., Lakso, A.N., Stroock, A.D., 2014. A microtensiometer capable of measuring water potentials below -10 MPa. Lab Chip 14, 2806–2817. https://doi.org/10.1039/C4LC00342J

Phillips, N., Nagchaudhuri, A., Oren, R., Katul, G., 1997. Time constant for water transport in loblolly pine trees estimated from time series of evaporative demand and stem sapflow. Trees 11, 412. https://doi.org/10.1007/s004680050102

Phillips, N.G., Oren, R., Licata, J., Linder, S., 2004. Time series diagnosis of tree hydraulic characteristics. Tree Physiol. 24, 879–890. https://doi.org/10.1093/treephys/24.8.879

Poggi, I., Polidori, J.J., Gandoin, J.M., Paolacci, V., Battini, M., Albertini, M., Améglio, T., Cochard, H., 2007. Stomatal regulation and xylem cavitation in Clementine (*Citrus clementina* Hort) under drought conditions. The Journal of Horticultural Science and Biotechnology, 82(6), 845–848. https://doi.org/10.1080/14620316.2007.11512316

Provenzano, G., 2007. Using HYDRUS-2D Simulation Model to Evaluate Wetted Soil Volume in Subsurface Drip Irrigation Systems. J. Irrig. Drain. Eng. 133, 342–349. https://doi.org/10.1061/(ASCE)0733-9437(2007)133:4(342)

Quick, D.D., Espino, S., Morua, M.G., Schenk, H.J. 2016. Effects of thermal gradients in sapwood on stem psychrometry. In International Symposium on Sensing Plant Water Status-Methods and Applications in Horticultural Science 1197 (pp. 23-30)

Rabbel, I., Diekkrüger, B., Voigt, H., Neuwirth, B., 2016. Comparing ΔTmax Determination Approaches for Granier-Based Sapflow Estimations. Sensors 16, 2042. https://doi.org/10.3390/s16122042

Rallo, G., González-Altozano, P., Manzano-Juárez, J., Provenzano, G., 2017. Using field measurements and FAO-56 model to assess the eco-physiological response of citrus orchards under regulated deficit irrigation. Agric. Water Manag. 180, 136–147. https://doi.org/10.1016/j.agwat.2016.11.011

Ravikumar, V., 2023. Sprinkler and drip irrigation: theory and practice. Springer Nature, Cham

Rawlins, S.L., 1966. Theory for thermocouple psychrometers used to measure water potential in soil and plant samples. Agricultural Meteorology, 3(5-6), 293-310

Romero-Trigueros, C., Gambín, J.M.B., Nortes Tortosa, P.A., Cabañero, J.J.A., Nicolás Nicolás, E., 2021. Isohydricity of Two Different Citrus Species under Deficit Irrigation and Reclaimed Water Conditions. Plants 10, 2121. https://doi.org/10.3390/plants10102121

Scholander, P.F., Bradstreet, E.D., Hemmingsen, E.A., Hammel, H.T., 1965. Sap Pressure in Vascular Plants: Negative hydrostatic pressure can be measured in plants. Science 148, 339–346. https://doi.org/10.1126/science.148.3668.339

Schönbeck, L.C., Schuler, P., Lehmann, M.M., Mas, E., Mekarni, L., Pivovaroff, A.L., Turberg, P., Grossiord, C., 2022. Increasing temperature and vapour pressure deficit lead to hydraulic damages in the absence of soil drought. Plant Cell Environ. 45, 3275–3289. https://doi.org/10.1111/pce.14425

Singh, V.P., Su, Q., 2022. Irrigation engineering. Principles, processes, procedures, design, and management. Cambridge University Press, Cambridge

Turner, N.C., 1988. Measurement of plant water status by the pressure chamber technique. Irrig. Sci. 9, 289–308. https://doi.org/10.1007/BF00296704

Tuzet, A., Perrier, A., Leuning, R., 2003. A coupled model of stomatal conductance, photosynthesis and transpiration. Plant Cell Environ. 26, 1097–1116. https://doi.org/10.1046/j.1365-3040.2003.01035.x

Vanella, D., Guarrera, S., Ferlito, F., Longo-Minnolo, G., Milani, M., Pappalardo, G., Nicolosi, E., Giuffrida, A.G., Torrisi, B., Las Casas, G., Consoli, S., 2025. Effects of organic mulching and regulated deficit irrigation on crop water status, soil and yield features in an orange orchard under Mediterranean climate. Sci. Total Environ. 958, 177528. https://doi.org/10.1016/j.scitotenv.2024.177528

Venturin, A.Z., Guimarães, C.M., Sousa, E.F.D., Machado Filho, J.A., Rodrigues, W.P., Serrazine, Í.D.A., Bressan-Smith, R., Marciano, C.R., Campostrini, E., 2020. Using a crop water stress index based on a sap flow method to estimate water status in conilon coffee plants. Agric. Water Manag. 241, 106343. https://doi.org/10.1016/j.agwat.2020.106343

Vogel, T., Votrubova, J., Dohnal, M., Dusek, J., 2017. A Simple Representation of Plant Water Storage Effects in Coupled Soil Water Flow and Transpiration Stream Modeling. Vadose Zone J. 16, 1–10. https://doi.org/10.2136/vzj2016.12.0128

Wan, L., Zhang, Q., Cheng, L., Liu, Y., Qin, S., Xu, J., Wang, Y., 2023. What determines the time lags of sap flux with solar radiation and vapor pressure deficit? Agric. For. Meteorol. 333, 109414. https://doi.org/10.1016/j.agrformet.2023.109414

Yang, Y., Guan, H., Hutson, J.L., Wang, H., Ewenz, C., Shang, S., Simmons, C.T., 2013. Examination and parameterization of the root water uptake model from stem water potential and sap flow measurements. Hydrol. Process. 27, 2857–2863. https://doi.org/10.1002/hyp.9406

Ye, M., Zhao, X., Biswas, A., Huo, G., Yang, B., Zou, Y., Siddique, K.H.M., Gao, X., 2021. Measurements and modeling of hydrological responses to summer pruning in dryland apple orchards. J. Hydrol. 594, 125651. https://doi.org/10.1016/j.jhydrol.2020.125651

Zhang, X., Yang, H., Shukla, M.K., Du, T., 2023. Proposing a crop-water-salt production function based on plant response to stem water potential. Agric. Water Manag. 278, 108162. https://doi.org/10.1016/j.agwat.2023.108162

Zhuang, J., Yu, G.-R., Nakayama, K., 2014. A Series RCL Circuit Theory for Analyzing Non-Steady-State Water Uptake of Maize Plants. Sci. Rep. 4, 6720. https://doi.org/10.1038/srep06720

Zimmermann, D., Reuss, R., Westhoff, M., Geßner, P., Bauer, W., Bamberg, E., Bentrup, F.-W., Zimmermann, U., 2008. A novel, non-invasive, online-monitoring, versatile and easy plant-based probe for measuring leaf water status. J. Exp. Bot. 59, 3157–3167. https://doi.org/10.1093/jxb/ern171

Zucchini, M., Guzmán-Delgado, P., Santos, E., Synstelien, T., Marino, G., 2023. Preliminary observations on the use of microtensiometers to continuously measure water potential in a mature olive orchard, in: 2023 IEEE International Workshop on Metrology for Agriculture and Forestry (MetroAgriFor). Presented at the 2023 IEEE International Workshop on Metrology for Agriculture and Forestry (MetroAgriFor), IEEE, Pisa, Italy, pp. 268–272. https://doi.org/10.1109/MetroAgriFor58484.2023.10424405.

CHAPTER 4: Agro-hydrological Models

Background

The experimental activities described in the previous chapters provided the empirical basis for understanding and modelling water dynamics in the SPAc of the Villabate mandarin orchard. In particular, the soil hydraulic characterization presented in **Chapter 2** and the continuous monitoring of atmospheric demand, soil water content, plant water status, and sap flow described in Chapter 3 generated a detailed dataset suitable for supporting the application of agro-hydrological models under Mediterranean semi-arid conditions. In these environments, the growing threat of water scarcity, exacerbated by climate change, poses a significant challenge to agriculture, particularly to perennial crops with high water requirements, such as citrus fruits.

In this context, Agro-hydrological models represent a valuable tools for interpreting soil water dynamics, estimating crop water requirements, and supporting irrigation management (Rallo and Provenzano, 2016; Autovino et al., 2018; Pereira et al., 2020). However, their application to citrus orchards irrigated with localized systems presents specific challenges. Conventional approaches based on the FAO-56 soil water balance model, generally conceptualize the root zone as a single uniformly wetted reservoir, of fixed capacity, with spatially averaged soil water content. Although this approach is widely used and operationally robust, it may be inadequate for systems characterized by strong spatial heterogeneity in soil moisture distribution, such as drip and subsurface drip irrigation.

In subsurface drip irrigation systems (SDI) water is applied below the soil surface to a limited soil volume and directly within the root zone, generating a localized wetting pattern around each emitter while large portions of the soil volume may remain comparatively dry. Under these conditions, the assumption of a uniformly wetted root zone becomes critical. Soil evaporation is also reduced because the surface layer often remains dry. Meanwhile, root water uptake is concentrated in the wetted volume where roots tend to proliferate preferentially. This adds another layer of complexity that conventional models, which assume uniformly distributed roots, fail to capture (Friend, 2001; Knauer et al., 2018). These features are particularly relevant at the Villabate experimental site, where the mandarin orchard is characterized by discontinuous canopy cover, layered soil hydraulic properties, and localized irrigation through buried drip lines.

To address these limitations, AquaCitrus (Boubakri et al., 2023), was considered in this thesis. AquaCitrus is an R-based agro-hydrological model specifically developed for citrus orchards and designed to represent the main components of the soil water balance under localized irrigation. Compared with conventional bucket-type approaches, the model introduces a conceptual distinction between wet and dry soil fractions, allows a differentiated representation of root water uptake, and separately simulates evaporation and transpiration processes. These characteristics make the model potentially suitable for describing the heterogeneous soil moisture patterns typically generated by localized irrigation systems.

The modelling activity presented in this chapter was carried out within the framework of a research stay at the Polytechnic University of Valencia. The original objective was to apply AquaCitrus to the Villabate experimental site by using historical datasets (2018-2021) for model calibration and the monitoring data collected during the PhD period (2022-2024) for independent validation. The model was also intended to be applied to the different irrigation treatments present in the orchard, namely Full Irrigation (FI), Deficit Irrigation (DI), and farmer-managed irrigation (TI).

However, the application of AquaCitrus to the Villabate case study required additional adaptations to represent the specific hydrological behaviour of subsurface drip irrigation. In particular, the modelling framework had to account for irrigation water applied directly at the depth of the buried drip lines, the reduced contribution of surface evaporation, and the localized development of the wetted soil volume. During the research stay, the Villabate input datasets were prepared and discussed with the host research group, the SDI-specific model adaptations were analysed, and the simulation outputs were subsequently evaluated. It should be noted that the code modifications were not directly implemented by the present author.

For these reasons, the results presented in this chapter must be considered preliminary. The analysis was limited to the FI treatment and to a single irrigation season (2018), and an independent validation using data not involved in model development has not yet been completed. Nevertheless, this preliminary application provides a first assessment of the suitability of AquaCitrus for simulating soil water dynamics in a Mediterranean citrus orchard irrigated with SDI and offers a basis for future model calibration, validation, and extension to other irrigation treatments.

This chapter is organized as follows. Chapter **4.1** describes the FAO-56 soil water balance model, with particular attention to its main assumptions and limitations when applied to localized irrigation system. Chapter **4.2** presents the AquaCitrus model, focusing on its wet/dry soil compartment structure, root water uptake representation, and adaptations required for the Villabate SDI system. Chapter **4.3** describes the parameterization of the FAO-56 and AquaCitrus models for the Villabate case study. Chapter **4.4** reports the statistical indicators used to evaluate model performance. Chapter **4.5** presents the preliminary results of applying the model to the Villabate experimental orchard, comparing observed and simulated soil water. Finally, Chapter **4.6** discusses the main conclusions and future research perspectives.

4.1 FAO56 Agro-Hydrological Model

The FAO-56 approach represents one of the most widely adopted operational methods for estimating crop evapotranspiration and managing irrigation scheduling. Its strength lies in its simplicity, limited input requirements, and broad applicability across different crops and environments. For these reasons, it was used in this study as a conventional benchmark against which the preliminary performance of AquaCitrus was compared.

The FAO56 model conceptualizes the root zone as a single soil water reservoir, whose storage capacity depends on rooting depth and soil hydraulic properties. As schematized in **Figure 1**, the model represents the SPAc through three main components: the atmospheric compartment, which imposes the evaporative demand through reference evapotranspiration (ETo); the plant compartment, which regulates transpiration through crop coefficients and water stress functions; and the soil compartment, which stores water available for root uptake.

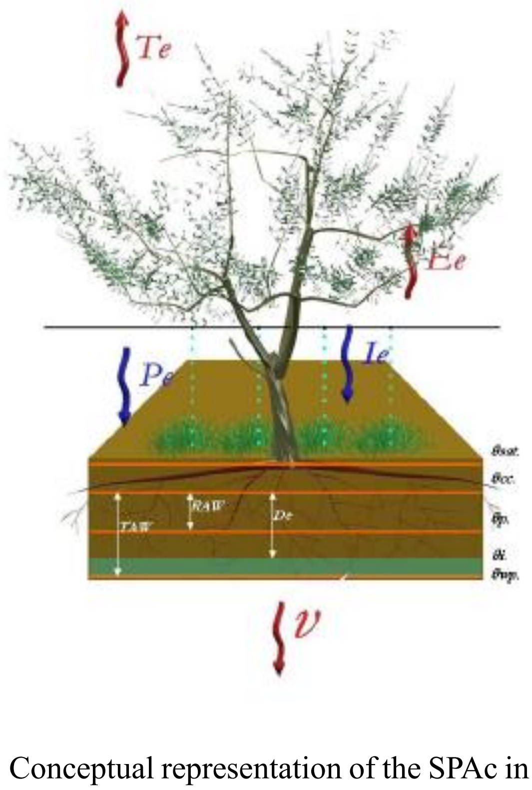

Fig. 1 Conceptual representation of the SPAc in the FAO-56 soil water balance model. The root zone is represented as a single soil water reservoir, where water inputs, outputs, and crop water stress are computed from root zone depletion

The daily soil water balance is expressed in terms of root zone depletion, Dr, which represents the amount of water required to restore the soil profile to field capacity. The depletion at the end of day *i* can be calculated as:

$$D_i = D_{i-1} - (P_i - RO_i) - I_i - CR_i + ET_{a,i} + DP_i \quad (1.0)$$

where: D_i and D_{i-1} (mm) are the water depletions in the root zone at the end of day i and $i-1$ respectively, P_i (mm) is the net precipitation, RO_i (mm) is the surface runoff, I_i (mm) is the depth of irrigation applied, CR_i (mm) is the capillary rise from a groundwater table, $ET_{a,i}$ (mm) is the actual crop evapotranspiration, DP_i (mm) is the deep percolation of water moving out of the root zone.

For the Villabate case study, capillary rise can be considered negligible because the water table is located at great depth (below 5–6 m), and no significant upward flux occurs. The main input terms are therefore precipitation, irrigation, while the main output terms are actual evapotranspiration and, under some conditions, deep percolation. Deep percolation may be particularly relevant under subsurface drip irrigation when water applied below the soil surface exceeds the storage capacity of the wetted root zone. At the Villabate site, this risk was specifically considered in the definition of the irrigation management strategy. Preliminary observations of soil water content dynamics measured with Drill & Drop probes showed that irrigation durations longer than approximately three hours produced increases in soil moisture also below the main root zone, indicating a higher risk of deep percolation. For this reason, a fixed irrigation duration of three hours was adopted for subsequent irrigation events.

The maximum amount of water available to the crop within the root zone is defined as Total Available Water (TAW) (mm):

$$TAW = 1000(\theta_{fc} - \theta_{wp})z_r \quad (1.1)$$

Where θ_{fc} and θ_{wp} are the soil water contents at field capacity and permanent wilting point, respectively, and Z_r is the rooting depth. The fraction of TAW that can be depleted before the onset of water stress is referred to as readily available water, RAW:

$$RAW = p\,TAW \quad (1.2)$$

where p is the depletion fraction. When root zone depletion remains below RAW, the crop is assumed to transpire under non-limiting water conditions. When depletion exceeds RAW, transpiration is reduced through the water stress coefficient K_s.

In the dual crop coefficient approach, crop evapotranspiration is partitioned into transpiration and soil evaporation components. Potential transpiration is represented by the basal crop coefficient, K_{cb}, whereas soil evaporation is described by the evaporation coefficient, K_e. Actual crop evapotranspiration, ET_a, is therefore expressed as:

$$ET_a = (K_s\,K_{cb} + K_e)ETo \quad (1.3)$$

where ETo is reference evapotranspiration and K_s accounts for the reduction in transpiration induced by soil water depletion. The coefficient K_s is equal to 1 under non-stressed conditions and decreases when root zone depletion exceeds RAW:

$$K_s = \frac{TAW - D_i}{TAW - RAW} \quad (1.4)$$

For D_i > RAW while K_s= 1 for $D_i \leq$ RAW.

The evaporation component is represented through the evaporation coefficient, K_e, which depends on the amount of water available in the surface evaporation layer and on the exposed and wetted soil fraction. This formulation is effective for many surface-irrigated or uniformly wetted systems, but it becomes more uncertain under localized irrigation. In subsurface drip irrigation, water is applied below the soil surface, and the upper 0 soil layer may remain dry for most of the irrigation season. Consequently, the FAO-56 evaporation routine may overestimate soil evaporation if the reduction in surface wetting is not properly accounted for.

A further limitation of the FAO-56 approach in the Villabate case study concerns the spatial representation of soil water content. The model returns a single vertically averaged soil water content or depletion value for the entire root zone. This assumption is poorly suited to subsurface drip irrigation systems, where soil moisture is highly heterogeneous and concentrated around the buried emitters. Under such conditions, the average root zone water content may not adequately represent the coexistence of wetter soil volumes near the drip lines and drier soil volumes outside the wetted bulb.

These limitations are particularly relevant in mature citrus orchards, where the canopy is discontinuous, soil evaporation is spatially variable, and roots may be preferentially concentrated in the wetted volume generated by localized irrigation. Therefore, although FAO-56 provides a robust and operationally simple reference framework, its bucket-type representation may be insufficient to describe the vertical and lateral heterogeneity of soil water dynamics under SDI. This provides the rationale for comparing its performance with AquaCitrus, which explicitly distinguishes wet and dry soil fractions and simulates soil water content at different depths.

4.2 AquaCitrus

AquaCitrus is an R-based agro-hydrological model developed to simulate the daily soil water balance of citrus orchards under arid and semi-arid conditions (Boubakri et al., 2023). The model was designed to address some of the limitations of conventional approaches when applied to perennial tree crops irrigated with localized systems (Foster et al., 2017; Steduto et al., 2012). In particular, citrus orchards are characterized by discontinuous canopy cover, spatially variable soil evaporation, non-uniform root distribution, and heterogeneous wetting patterns generated by drip or subsurface drip irrigation.

The model is inspired by the AquaCrop framework but focuses on the water balance component rather than on crop growth and yield simulation. Since it is intended for mature citrus orchards, AquaCitrus assumes that canopy cover and root development remain relatively stable during the irrigation season. The model operates at a daily time step and represents soil water dynamics along the vertical profile through a set of soil compartments characterized by specific thickness, texture, hydraulic properties, and initial soil water content.

The conceptual structure of AquaCitrus is shown in **Figure 2**. The model represents the SPAc by linking atmospheric forcing, canopy processes, soil water balance, and plant water use. Atmospheric variables provide the evaporative demand through reference evapotranspiration, while rainfall is first intercepted by the citrus canopy and only net precipitation reaches the soil surface. Within the plant component, transpiration is regulated by crop characteristics and soil water stress conditions.

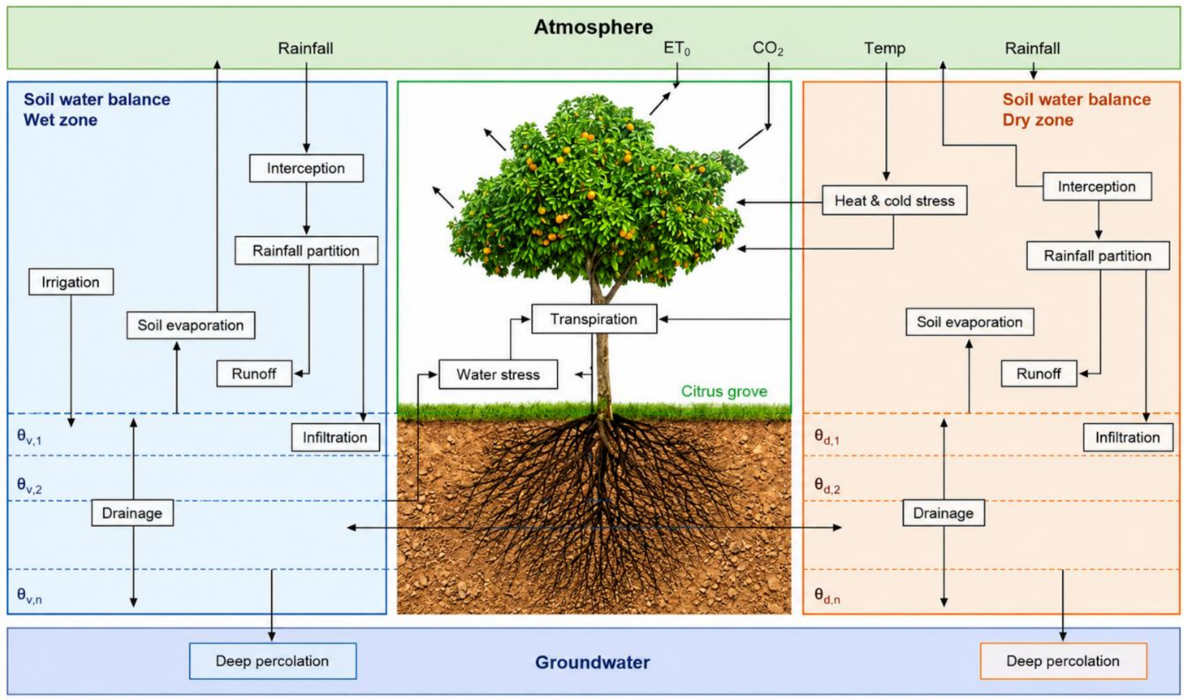

Fig. 2 Conceptual structure of the AquaCitrus model. The model simulates the main water fluxes within the SPAc and distinguishes between wet and dry soil fractions to represent the heterogeneous soil moisture distribution induced by localized irrigation. Adapted from Boubakri et al. (2023).

As shown in **Figure 2**, a key element of the model structure is the separation of the soil domain into wet and dry fractions. The wet fraction represents the portion of soil directly affected by localized irrigation, whereas the dry fraction represents the remaining soil volume, which receives water mainly from rainfall. For each fraction, AquaCitrus computes the main components of the soil water balance, including infiltration, runoff, soil evaporation, transpiration, drainage, and deep percolation. The two balances are then integrated to estimate the overall water dynamics of the root zone.

This conceptual partitioning is particularly relevant for citrus orchards irrigated with localized systems, where soil moisture is not uniformly distributed within the root zone. In these systems, relatively wet soil volumes develop close to the emitters, while other portions of the soil may remain comparatively dry for long periods. Therefore, the wet/dry structure provides a more suitable framework than a single-reservoir approach for representing the heterogeneous soil water conditions observed under drip and subsurface drip irrigation.

The general soil water balance equation adopted by the model is as follows:

$$P_{net}(t) + Irr(t) + CR(t) - DP(t) - E(t) - Tr(t) = \Delta S \qquad (1.5)$$

Where: P_{net} is net precipitation (mm), *Irr(t)* is irrigation amount (mm), *CR* is capillary rise (mm), *DP* is deep percolation (mm), *RO* is surface runoff (mm), *E* is soil evaporation (mm), *Tr* is cropping transpiration (mm) and ΔS is change in soil water storage (mm). In the first version of AquaCitrus, capillary rise is not considered, as the model was developed for conditions in which the groundwater table does not directly affect the root zone.

A distinctive feature of AquaCitrus is the representation of partial soil wetting under localized irrigation. Instead of treating the root zone as a single uniformly wetted reservoir, the model distinguishes between a wet fraction and a dry fraction of the soil. The wet fraction represents the portion of the soil affected by irrigation, while the dry fraction represents the remaining soil volume, which receives water mainly from rainfall. Separate water balances are computed for the two fractions and subsequently integrated at the root-zone scale. This structure allows the model to represent the coexistence of relatively wet soil volumes close to the emitters and drier soil volumes outside the wetted area.

For the entire root zone, the integrated water balance of the two fractions is expressed as:

$$P_{net,wet}(t) + P_{net,dry}(t) + Irr(t) - DP_{wet}(t) - DP_{dry}(t) - RO_{wet}(t) - RO_{dry}(t) - E_{wet}(t) - E_{dry}(t) - Tr_{wet}(t) - Tr_{dry}(t) = F_{wet} \times \Delta S_{wet} + (1 - F_{wet})\Delta S_{dry} \quad (1.6)$$

The wetted soil fraction, F_{wet}, can be determined applying the following equation:

$$F_{wet} = \frac{A_{wet/p}}{A_f} \quad (1.7)$$

Where $A_{wet/p}$ is the wetted area per plant (m^2) and A_f is the planting frame area (m^2). In the original AquaCitrus formulation, the wetted area depends on irrigation system characteristics, emitter discharge, number of emitters per plant, soil texture, and the geometry of the wetted bulb. This parameter is particularly important because it controls the relative contribution of the irrigated and non-irrigated soil fractions to the overall soil water balance.

AquaCitrus also includes specific routines for the main components of the SPAc water balance. Rainfall interception by the citrus canopy is estimated before net precipitation reaches the soil. Soil evaporation and crop transpiration are calculated separately, allowing the distinction between non-beneficial water losses from the soil surface and plant water use through transpiration. Soil evaporation is represented using a two-stage approach, whereas crop transpiration is estimated through a basal crop coefficient approach and reduced under water stress conditions through a stress coefficient.

Another relevant feature of AquaCitrus is the representation of root water uptake. The model uses two parameters to describe root distribution. The parameter γ describes the vertical distribution of roots among soil compartments, whereas λ represents the proportion of active roots concentrated within the wet fraction. This is particularly relevant for localized irrigation systems, where roots tend to proliferate preferentially in the wetted volume. Through these parameters, the model can represent both the vertical stratification of the root system and the preferential uptake of water from the irrigated fraction.

For the Villabate case study, the original AquaCitrus code required specific modifications to represent subsurface drip irrigation. In the experimental orchard, irrigation water is supplied through buried drip lines installed at approximately 0.30 m depth. Therefore, the modified model version allowed irrigation water to be applied directly to deeper soil layers corresponding to the depth of the drip lines, rather than to the soil surface. This modification made it possible to bypass the direct contribution of irrigation water to surface evaporation, which is expected to be limited under SDI conditions.

A second modification concerned the calculation of the wetted fraction, F_{wet}, which was adjusted to account for the buried wetting pattern generated by subsurface emitters. Unlike surface drip irrigation, where the wetted area can develop from the soil surface downward, SDI produces a wetted volume centred around the buried drip line. This required an adaptation of the model setup to better represent the geometry of the wetted soil volume under the specific hydraulic conditions of the Villabate orchard.

A third modification involved the evaporation routine. In the original formulation, the exposed and wetted soil fraction, f_{ew}, can be estimated as a fraction of F_{wet}. For the Villabate SDI system, this value was reduced from the default proportion of one third of F_{wet} to a value calibrated on field observations collected by Drill & Drop probes, which provided continuous soil moisture profiles. Specifically, the calibration focused on matching the simulated and measured water content at the 10 cm depth layer during the drying phases following irrigation, optimizing the multiplier until the best fit was achieved. This modification should not be interpreted as a complete suppression of soil evaporation, since rainfall can still wet the soil surface, but rather as a reduction of the evaporation component directly associated with irrigation water.

The main outputs of AquaCitrus include soil water content at different depths, evaporation, transpiration, infiltration, runoff, drainage, deep percolation, and changes in soil water storage. In this thesis, the analysis focused primarily on simulated soil water content in the wet fraction, which was compared with measurements acquired by Drill & Drop probes installed within the wetted soil volume. Therefore, the application presented here should be interpreted as a preliminary assessment of the ability of the modified AquaCitrus framework to reproduce soil water dynamics under SDI conditions, rather than as a complete calibration and independent validation of the model for operational irrigation scheduling.

4.3. Parameterization and input data of FAO56 and AquaCitrus models

The FAO-56 and AquaCitrus models were parameterized using the available information for the Villabate experimental orchard. Although both models were applied to simulate soil water content dynamics, they differ substantially in their conceptual structure and input data requirements. FAO-56 requires a limited number of aggregated soil, crop, meteorological, and irrigation parameters, whereas AquaCitrus requires a more detailed description of the soil profile, irrigation system, crop characteristics, root distribution, and initial soil water conditions.

The simulations presented in this chapter refer to the 2018 irrigation season and to the Full Irrigation (FI) treatment. This season represents the first application of the modelling framework to the historical dataset originally intended for model calibration.

For both models, the meteorological input data consisted of daily variables recorded by the WatchDog 2000 weather station installed at the experimental site. These data were used to estimate reference evapotranspiration (ETo) according to the FAO Penman–Monteith method. Irrigation inputs were derived from the volumes supplied to the FI sector during each irrigation event. These volumes were converted into irrigation depths by considering the number of trees in the irrigated sector and the canopy projection area of each tree, used as a practical approximation of the horizontal extension of the mandarin root system.

The FI plot was irrigated through a subsurface drip irrigation system, with irrigation events scheduled every two days and a fixed duration of three hours. This management strategy was consistently applied throughout the irrigation season to maintain soil water content within the wetted root zone while minimizing deep percolation losses.

The soil physical characterization used to support model parameterization is reported in **Table 1**. The table describes the textural variability of the Villabate soil profile at the investigated depths and provides the basis for interpreting the vertical heterogeneity of soil water dynamics.

Table 1 Soil texture characterization of the Villabate FI plot at the investigated depths

Texture Class	**Depth** cm	**Sand** %	**Clay** %	**Silt** %
Sandy Clay Loam	0-20	54.89	22.87	22.24
Sandy Clay Loam	20-40	50.63	26.4	22.97
Clay Loam	40-60	39.39	28.52	32.09
Loam	60-80	40.26	17.79	41.95

The AquaCitrus required layer-specific hydraulic properties, including soil water content at saturation, field capacity, permanent wilting point, and saturated hydraulic conductivity. The model soil profile extended to 0.80 m and was divided into six computational layers, as reported in **Table**

2. This vertical discretization allowed AquaCitrus to simulate soil water content dynamics at different depths and to account for the heterogeneity of the soil profile.

Table 2 Layer-specific hydraulic parameters adopted as AquaCitrus soil input for the Villabate FI plot

Layer N°	**Layer Thickness**	**Θ_{SAT} ($m^3\ m^{-3}$)**	**Θ_{FC} ($m^3\ m^{-3}$)**	**Θ_{WP} ($m^3\ m^{-3}$)**	**K_{SAT} ($mm\ d^{-1}$)**
1	0.1	0.34 [a]	0.22 [a]	0.08 [a]	527.52 [a]
2	0.1	0.32 [b]	0.25 [b]	0.17 [b]	250.4 [b]
3	0.2	0.26 [a]	0.23 [a]	0.16 [a]	111.12 [a]
4	0.1	0.45 [a]	0.42 [a]	0.35 [a]	78.54 [a]
5	0.1	0.57 [b]	0.54 [b]	0.48	34.33 [b]
6	0.2	0.61 [a]	0.58 [a]	0.52 [a]	8.88 [a]

NOTE: [a] estimated through pedotransfer functions, [b] interpolated to match the AquaCitrus discretization

The texture data reported in **Table 1** and the hydraulic parameters reported in **Table 2** do not necessarily refer to the same vertical discretization. Therefore, the hydraulic parameters should be interpreted as the layer-specific values adopted in the AquaCitrus input file, rather than as a direct one-to-one transformation of the texture data reported in the previous table.

In addition to layer-specific hydraulic properties, AquaCitrus required further crop, irrigation, and root-distribution parameters to represent the Villabate FI plot. These parameters included crop height, canopy cover, rooting depth, dripline depth, irrigation efficiency, the wetted soil fraction, the exposed wetted fraction. The values adopted in the AquaCitrus input file are summarized in **Table 3**.

Table 3 Crop, irrigation and root-distribution parameters used as AquaCitrus input for the Villabate FI plot

Parameter	Symbol	Unit	Value
Crop height	h	m	2.5
Canopy cover	CC	%	49
Rooting depth	Z_r	m	0.8
Dripline depth	—	m	0.3
Irrigation efficiency	IE	%	90
Wetted soil fraction	F_{wet}	–	0.4
Exposed wetted fraction	few	–	0.13
Initial soil water content	θ_{ini}	$m^3\ m^{-3}$	0.12

For the FAO-56 model, the soil profile was represented as a single root-zone reservoir. Consequently, soil hydraulic properties were introduced as aggregated values rather than layer-specific parameters. Field capacity and permanent wilting point were calculated as weighted averages of the corresponding values used in AquaCitrus for the upper 0.60 m of soil, corresponding to the root-zone depth adopted in the FAO-56 simulation (**Table 4**). The maximum rooting depth was set to 0.60 m, whereas crop height was set to 2.5 m.

Since irrigation water was supplied through buried drip lines and did not directly wet the exposed soil surface, the fraction of soil surface wetted by irrigation, f_w, was set to 0.01. This assumption was introduced to represent the negligible surface wetting under SDI conditions and to limit the evaporation component directly associated with irrigation.

Table 4 Aggregated soil and crop parameters used for the FAO-56 model

FAO-56 parameters		**Values**
Field capacity, θ_{fc} [cm3/cm3]		0,315
wilting point, θ_{wp} [cm3/cm3]		0,233
Water available to plant [mm/m]		65
Total available soil water in the root zone, TAW, [mm/m]		49
total evaporable water, TEW [mm]		8,17
readily evaporable water, REW [mm]		4,08
evapotranspiration depletion factor, p [% TAW]		50
Exposed and wetted soil fraction, few		0,6
Fraction of soil surface wetted by irrigation, fw		0.01
	$K_{cb\ ini}$	0,75
basal crop coefficient	$K_{cb\ mid}$	0,75
	$K_{cb\ end}$	0,75
Maximum crop height, h_{crop} [m]		2,5
Maximum rooting depth Z_{msx}[m]		0.6

Overall, the different parameterization requirements reflect the different modelling approaches. FAO-56 provides a simplified and operational representation of the root zone based on average soil water depletion, whereas AquaCitrus requires a more detailed input dataset but allows a more explicit representation of vertical soil heterogeneity, root distribution, and localized wetting patterns under subsurface drip irrigation.

4.4 Statistical indicators for model performance evaluation

The accuracy of the simulations was evaluated by comparing the estimated soil water content (SWC) with data measured using Drill & Drop probes, employing statistical indicators such as Root Mean Square Error (RMSE), mean Bias, percent bias (PBias), Nash-Sutcliffe Efficiency index (NSE), and the coefficient of determination (R^2).

The Root Mean Square Error (RMSE) was adopted as the primary metric; it measures the average magnitude of the prediction errors and approaches zero when perfect agreement exists between simulated and observed values:

$$RMSE = \sqrt{\frac{\sum_{i=1}^{n}(y_i - x_i)^2}{n}} \tag{1.8}$$

Where y_i is the simulated value, x_i is the corresponding observed value, and n is the total number of observations. The RMSE approaches zero when perfect agreement exists between simulated and observed values.

The mean Bias error and Percent Bias (PBIAS) were used to evaluate the model's systematic tendency to overestimate or underestimate observed values. Bias provides an absolute measure of the average directional difference, while PBIAS expresses this tendency as a percentage. For Bias and PBIAS, positive values indicate overestimation (simulated > observed), negative values indicate underestimation (simulated < observed), and the optimal value is zero. The indicators are calculated as follows:

$$Bias = \frac{\sum_{i=1}^{n}(y_i - x_i)}{n} \tag{1.9}$$

$$PBIAS = 100 \times \frac{\sum_{i=1}^{n}(y_i - x_i)}{\sum_{i=1}^{n} x_i} \tag{2.0}$$

Where y_i is the simulated value, x_i is the observed value, and n is the total number of observations.

The Nash-Sutcliffe Efficiency (NSE) was also computed to assess the predictive skill of the model by comparing the residual variance with the residual variance of the observed data. The target value is 1, indicating perfect agreement between simulated and observed values. Values close to 1 indicate good model performance, values close to 0 indicate that the model predictions are comparable to using the mean of the observed data as a predictor, while negative values indicate that the observed mean performs better than the model simulations (Nash and Sutcliffe, 1970). The NSE is expressed as:

$$NSE = 1 - \frac{\sum_{i=1}^{n}(y_i - x_i)^2}{\sum_{i=1}^{n}(x_i - \bar{x})^2} \tag{2.1}$$

Where y_i is the simulated value of the i-th sample, x_i is the corresponding observed value, $\bar{x}$ is the mean of the observed data, and n is the total number of observations.

Finally, the coefficient of determination (R^2) is used to quantify the proportion of the variance in the observed data that is explained by the simulated values. R^2 ranges from 0 to 1, with a target value of 1 indicating perfect linear correlation between simulated and observed values (i.e., all data points lie exactly on the regression line). Values close to 1 indicate that the model captures most of the variability in the observed data, while values close to 0 indicate little or no linear relationship. R^2 is calculated as follows:

$$R^2 = \left(\frac{\sum_{i=1}^{n}(x_i - \bar{x})(y_i - \bar{y})}{\sqrt{\sum_{i=1}^{n}(x_i - \bar{x})^2} \times \sqrt{\sum_{i=1}^{n}(y_i - \bar{y})^2}} \right)^2 \tag{2.2}$$

Where x_i is the observed value, $\bar{x}$ is the mean of the observed data, y_i is the simulated value, $\bar{y}$ is the mean of the simulated data, and n is the total number of observations.

4.5 Preliminary evaluation of AquaCitrus model for simulating soil water dynamics under subsurface drip irrigation

The preliminary evaluation of AquaCitrus was carried out for the Full Irrigation (FI) treatment during the 2018 irrigation season. This season was used as a first test case within the historical dataset initially available for model calibration. Since the application of AquaCitrus to the Villabate site required specific adaptations to represent subsurface drip irrigation (SDI), the analysis was limited to the FI treatment and focused on assessing the ability of the modified model to reproduce soil water content dynamics within the wetted soil volume. The FI plot was irrigated through a SDI system consisting of two buried drip lines per tree row, installed at a depth of 0.30 m. Drippers were spaced 0.50 m apart and delivered a nominal discharge of 2 L h^{-1}. Irrigation events were generally applied every second day, with a duration of approximately three hours. Soil water content was monitored using Drill & Drop probes installed approximately 0.30 m from the drip line and facing the emitters. Therefore, the measured soil water content can be considered representative of the wetted soil volume generated by the SDI system.

Figure 3 illustrates the temporal dynamics of observed and simulated soil water content (SWC) at different depths within the soil profile. Since AquaCitrus explicitly distinguishes between wet and dry soil compartments, the comparison was performed using the simulated SWC of the wet fraction, which is consistent with the location of the Drill & Drop probes within the wetted zone.

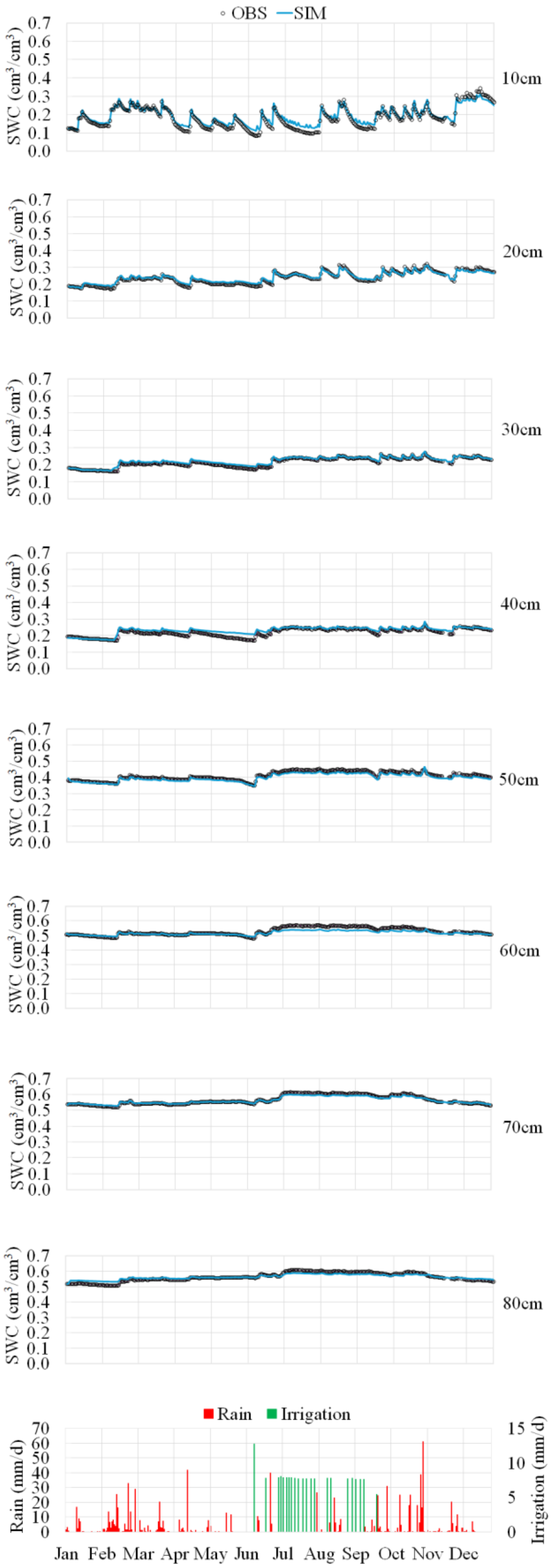

Fig. 3 Temporal dynamics of observed (OBS) and simulated (SIM) soil water content at different depths. Rainfall and irrigation events are reported in the lower panel.

The comparison between measured and simulated SWC indicates that the model was generally able to reproduce the seasonal evolution of soil moisture throughout the profile. Nevertheless, model performance varied with depth, reflecting the different hydrological processes governing soil water dynamics within the wetted bulb.

The shallowest layers (0.1–0.2 m) exhibited the highest temporal variability, mainly due to their strong sensitivity to rainfall events and atmospheric demand. Both observed and simulated data showed rapid fluctuations following precipitation events, although the model tended to slightly overestimate SWC during some periods.

At depths of 0.3 and 0.4 m, corresponding to the soil layers most directly influenced by the buried drip lines, the observed SWC showed clear responses to irrigation events during the summer season. These layers represent the portion of the profile where soil water dynamics are characterized by steep moisture gradients and pronounced spatial heterogeneity. AquaCitrus was able to reproduce the general temporal pattern of wetting and drying cycles, although discrepancies between observed and simulated values were more evident than at other depths. This behaviour is consistent with the greater complexity of representing water redistribution processes in the vicinity of the emitters, where small differences in the simulated geometry of the wetted bulb can produce substantial variations in local soil moisture.

In the deeper layers (0.5–0.8 m), SWC exhibited a smoother temporal evolution, with a gradual increase during the irrigation season, likely associated with downward water movement and redistribution within the profile. Under these conditions, AquaCitrus showed a closer agreement with the observations, suggesting that the model adequately captured the overall water storage dynamics below the main irrigation zone.

The accuracy of the simulations was evaluated by comparing the estimated SWC with data measured using Drill & Drop probes, employing the statistical indicators (RMSE, mean Bias, PBias, NSE, R^2) described in chapter 4.4.

As shown in **Table 5**, the statistical indicators confirmed the generally satisfactory agreement between observed and simulated SWC values. RMSE values ranged from 0.007 to 0.019 $cm^3\ cm^{-3}$, while R^2 values varied between 0.812 and 0.998, indicating a strong correspondence between simulated and measured temporal patterns across all depths.

Table 5 Statistical comparison between observed and simulated SWC data at different depths

Depth (m)	RMSE (cm^3/cm^3)	Bias (cm^3/cm^3)	PBias (%)	NSE (-)	R^2 (-)
0.1	0.019	0.011	6.192	0.895	0.967
0.2	0.009	0.004	1.644	0.941	0.981
0.3	0.010	0.008	3.864	0.865	0.963
0.4	0.016	0.012	5.635	0.550	0.812
0.5	0.012	-0.011	-2.625	0.800	0.982
0.6	0.015	-0.009	-1.657	0.640	0.967
0.7	0.007	0.000	-0.064	0.943	0.998
0.8	0.013	0.000	-0.006	0.772	0.979

The model tended to overestimate SWC in the upper part of the profile (0.1–0.4 m), as indicated by the positive Bias and PBias values, whereas a slight underestimation was observed at depths of 0.5–0.6 m. These systematic deviations were nevertheless limited in magnitude and remained within acceptable ranges for a preliminary application.

The best overall performance was achieved at a depth of 0.7 m, where the model produced an NSE value of 0.943 and an R^2 value of 0.998. Conversely, the lowest performance was observed at 0.4 m, where NSE decreased to 0.550. This result is not unexpected, considering that the 0.3–0.4 m layers are located close to the buried drip line and therefore correspond to the zone characterized by the strongest moisture gradients and the highest spatial variability. In contrast, deeper layers are typically characterized by smoother SWC dynamics and a more homogeneous distribution of moisture, conditions that are generally easier to reproduce using one-dimensional water balance approaches.

To provide a broader comparison with conventional modelling approaches, **Figure 4** reports the temporal evolution of the average SWC within the upper 0.60 m of soil as observed by the Drill & Drop probes and simulated by both AquaCitrus and the FAO-56 model.

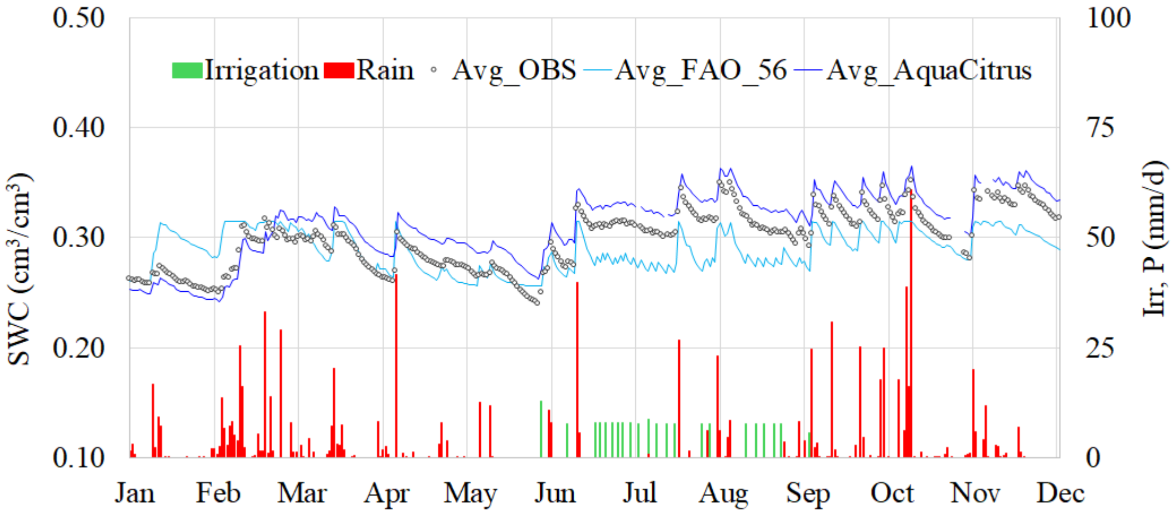

Fig. 4 Temporal dynamics of mean SWC observed by Drill & Drop probes (AVG_OBS) and simulated by FAO-56 (AVG_FAO_56) and AquaCitrus (AVG_AquaCitrus) models during the 2018 season. Rainfall and irrigation events are also shown.

Both models were able to reproduce the seasonal trend of SWC; however, AquaCitrus showed a closer agreement with the observations, particularly during the summer period when SWC dynamics were primarily controlled by SDI. The FAO-56 model tended to underestimate the observed SWC during prolonged irrigation periods, whereas AquaCitrus more effectively captured the overall seasonal evolution of soil moisture.

This improved performance is likely associated with the conceptual structure of AquaCitrus, which explicitly accounts for the spatial heterogeneity of soil moisture generated by localized irrigation systems through the separation of wet and dry soil fractions. Nevertheless, given that the present analysis was limited to a single season and a single irrigation treatment, these results should be interpreted with caution.

4.5 Conclusion and future research perspectives

This chapter presented a preliminary modelling assessment of SWC dynamics in the Villabate mandarin orchard, with particular attention to the application of AquaCitrus under subsurface drip irrigation (SDI). The analysis was framed by a comparison with the FAO-56 soil water balance approach, which was used as a conventional benchmark.

The FAO-56 model provides a simple and operational representation of the root zone, based on aggregated soil hydraulic parameters and average root-zone depletion. This approach is useful for irrigation scheduling and for estimating crop water requirements, but it has important limitations when applied to localized irrigation systems. In particular, the assumption of a uniformly wetted root zone is poorly suited to SDI, where water is applied below the soil surface and soil moisture is concentrated around the buried drip lines.

AquaCitrus offers a more suitable conceptual structure for this type of system because it explicitly distinguishes wet and dry soil fractions and simulates SWC at different depths. For the Villabate case study, the model required specific adaptations to represent the buried wetting pattern generated by SDI, including the application of irrigation water directly to deeper soil layers, the adjustment of the wetted fraction, and the reduction of the exposed wetted fraction involved in soil evaporation.

The preliminary results obtained for the FI treatment during the 2018 irrigation season showed that the modified AquaCitrus framework was able to reproduce the main temporal patterns of SWC within the wetted soil volume. The agreement between observed and simulated values was generally satisfactory across the monitored depths, suggesting that the model structure is appropriate for representing the heterogeneous soil water status induced by SDI. By contrast, FAO-56 provided a more simplified description of soil water status, reflecting its single-reservoir representation of the root zone.

However, the results presented in this chapter must be interpreted with caution. The analysis was limited to one irrigation treatment and one irrigation season, and the full calibration and independent validation strategy originally planned for the model application was not completed. Therefore, the present work should be considered a first exploratory application of AquaCitrus to the Villabate orchard rather than a complete validation of the model under Mediterranean SDI conditions.

Future work should first complete the calibration of AquaCitrus using the historical dataset available for the 2018–2021 period and subsequently validate the model with the independent monitoring data collected during the 2022–2024 experimental campaigns. This validation should include not only the FI treatment, but also the deficit irrigation and farmer-managed irrigation treatments, to assess the model performance under contrasting irrigation strategies.

A further priority concerns the refinement of soil parameterization. Since AquaCitrus is sensitive to soil hydraulic properties and root distribution, future applications would benefit from a more complete hydraulic characterization of the soil profile, including direct measurements or well-documented estimates of field capacity, permanent wilting point, saturation water content, and saturated hydraulic conductivity at different depths.

Plant-based measurements collected in this thesis also represent an important future perspective for model evaluation. Continuous stem water potential measurements, Scholander chamber observations, and sap-flow measurements could provide additional information for assessing the physiological consistency of the simulations. Once sapwood area is determined, sap-flow data could be converted into transpiration estimates and used to further evaluate the model's ability to reproduce plant water use.

Once the robustness of the model at the Villabate site has been consolidated and its ability to simulate different irrigation treatments has been verified, future developments could extend the application to other experimental sites characterized by different pedoclimatic conditions, including other citrus-growing areas of Sicily and the Mediterranean basin. This would allow the transferability of the model to be assessed and would support the development of site-specific parameterizations for different soils, climates, and citrus varieties. At a later stage, after a more extensive validation process, simplified user interfaces based on web platforms or applications could also be considered, to make the model more accessible to technicians and agronomists without programming expertise.

In conclusion, the preliminary application of AquaCitrus suggests that a modelling framework explicitly accounting for wet and dry soil fractions can improve the interpretation of soil water status in citrus orchards irrigated with SDI. Nevertheless, additional calibration, validation, and parameter refinement are required before the model can be used as a robust tool for irrigation scheduling or decision support at the Villabate site.

In conclusion, the work presented here represents a first attempt to adapt and apply the AquaCitrus model to the conditions of a Mediterranean citrus orchard irrigated with a subsurface drip irrigation (SDI) system. Although the preliminary results are encouraging and suggest a potential of the model in representing the water dynamics typical of localized irrigation systems, the research path is still at an early stage. Consolidation of the approach requires the completion of multi-annual calibration, independent validation on data not used for calibration, and the extension of simulations to the different irrigation treatments present in the experimental field. Only subsequently can more advanced perspectives be explored, such as the integration of physiological data, application to other pedoclimatic contexts, and the development of operational decision support tools.

REFERENCES

Autovino, D., Rallo, G., & Provenzano, G., 2018. Predicting soil and plant water status dynamic in olive orchards under different irrigation systems with Hydrus-2D: Model performance and scenario analysis. *Agricultural water management*, *203*, 225-235.

Boubakri, N., Garcia-Prats, A., Jimenez-Bello, M. Á., Carricondo-Anton, J. M., & Pulido-Velazquez, M., 2023. Aquacitrus: A Crop Water Model for Citrus Orchards. *Available at SSRN 5139362*.

Foster, T., Brozović, N., Butler, A. P., Neale, C. M. U., Raes, D., Steduto, P., ... & Hsiao, T. C., 2017. AquaCrop-OS: An open source version of FAO's crop water productivity model. *Agricultural water management*, *181*, 18-22.

Friend, A. D., 2001. Modelling canopy CO2 fluxes: are 'big-leaf'simplifications justified?. *Global Ecology and Biogeography*, *10*(6), 603-619.

Knauer, J., El-Madany, T. S., Zaehle, S., & Migliavacca, M., 2018. Bigleaf—An R package for the calculation of physical and physiological ecosystem properties from eddy covariance data. *PloS one*, *13*(8), e0201114.

Monteith, J.L., 1965. Evaporation and environment, in: Symposia of the Society for Experimental Biology. Cambridge University Press (CUP) Cambridge, pp. 205–234.

Pereira, L. S., Paredes, P., & Jovanovic, N., 2020. Soil water balance models for determining crop water and irrigation requirements and irrigation scheduling focusing on the FAO56 method and the dual Kc approach. *Agricultural water management*, *241*, 106357.

Rallo, G., & Provenzano, G., 2016. Modelli di bilancio agro-idrologico per la previsione delle dinamiche di stress idrico di colture arboree Mediterranee. *ITALUS HORTUS*, *22*(3), 31-48.

Steduto, P., C Hsiao, T., Fereres, E., & Raes, D., 2012. *Crop yield response to water*. FAO.

CHAPTER 5: CONCLUSIONS

The research activity presented in this thesis contributed to advancing the understanding and management of irrigation water in Mediterranean citrus orchards by integrating three complementary pillars: soil hydraulic characterization, continuous monitoring of the SPAc, and agro-hydrological modelling. These components were not addressed as independent topics, but as interconnected elements of a broader methodological framework aimed at supporting more precise and resilient irrigation management under conditions of increasing water scarcity and climatic variability.

The experimental site of Villabate (Sicily, Italy), represented the common thread of the thesis. The site represents an open-air laboratory where soil characterisation, innovative monitoring technologies, different irrigation methods and strategies, and modelling tools were combined under real field conditions. This integrated approach made it possible to analyse irrigation management from different but complementary perspectives: the hydraulic behaviour of the soil, the physiological response of the crop, and the capacity of models to reproduce SWC dynamics. The main added value of the thesis lies precisely in this integration, which provides a more complete interpretation of water movement and plant response than could be obtained from isolated measurements or single-method studies.

The first pillar of the thesis concerned **Soil Hydraulic Characterisation**. The comparative analyses of laboratory and field methods confirmed that the estimation of saturated and near-saturated hydraulic conductivity is strongly affected by the measurement technique, the experimental configuration, and the assumptions adopted during data interpretation. The comparison between the BEST method, mini-disk infiltrometer, and constant-head permeameter showed that different approaches may provide substantially different hydraulic conductivity functions, especially in the near-saturated range. These results highlight the need for caution when using simplified or indirect methods for soil hydraulic characterisation, particularly when the objective is to parameterise models or interpret water flow processes under localized irrigation.

The comparison between the pressure infiltrometer and the automated SATURO device further showed that simplified field methods can provide useful estimates of soil hydraulic properties, but their applicability depends on soil conditions and measurement objectives. In relatively homogeneous soils, SATURO may represent a practical alternative for field characterisation, whereas in highly heterogeneous soils or in the presence of preferential flow, more flexible methods such as the pressure infiltrometer may still be preferable. The analysis also suggested that the use of literature-based estimates of the α^* parameter may be acceptable in some cases, potentially reducing field measurement time and operational complexity.

The two laboratory studies on repacked soil columns provided additional methodological contributions. The low-cost compaction apparatus developed during the research proved to be a simple and reproducible tool for preparing soil columns under controlled compaction conditions. The experiments demonstrated that compaction energy, aggregate stability, sieving duration, and packing produced can influence hydraulic continuity. These findings are relevant not only from a laboratory perspective, but also for the broader issue of standardising soil hydraulic measurements and improving the comparability of results obtained by different operators and laboratories.

The second major component of the thesis was the continuous **monitoring of the SPA continuum** during the 2022-2024 irrigation seasons. This activity represented one of the most original aspects of the research, because it combined SWC measurements, atmospheric data, continuous stem water potential monitoring, Scholander chamber measurements, and sap-flow observations. The integration of these measurements allowed the response of mandarin trees to be interpreted not only in terms of soil water status, but also in terms of plant hydraulic behaviour and atmospheric demand. The monitoring results clearly showed that irrigation system and irrigation strategy strongly affect SWC dynamics. Subsurface drip irrigation systems maintained relatively stable soil moisture conditions through frequent and low-volume irrigation events, whereas deficit irrigation induced progressive soil drying during the stress period. The shift to sprinkler irrigation produced more pronounced wetting-drying cycles, reflecting the lower frequency and higher volume of irrigation events. These differences were mirrored by the plant-based measurements, confirming the importance of combining soil and plant indicators when evaluating irrigation management strategies.

Continuous stem water monitoring with FloraPulse microtensiometers provided valuable information on the temporal dynamics of plant water status. The sensors captured clear diurnal patterns, seasonal responses to irrigation management, and the impact of extreme atmospheric events. In particular, the 2023 heat wave demonstrated that high evaporative demand could impair plant water status even when soil water status is not severely limiting. The incomplete overnight recovery of plant water status observed during extreme heat conditions underlines the importance of considering both soil water status and atmospheric demand when designing irrigation strategies under climate change scenarios.

The validation of FloraPulse microtensiometers against Scholander pressure chamber measurements represented an important methodological step. The two methods were significantly correlated, confirming the potential of microtensiometers for continuous monitoring of stem water potential in mandarin orchards. At the same time, systematic differences were observed, including an offset between the two methods and a time lag in the response of the microtensiometers. These results indicate that continuous microtensiometer readings should not be interpreted as direct replacements of pressure chamber measurements without appropriate correction or calibration. Rather, they should be considered as complementary tools capable of providing high-frequency information on plant water status dynamics.

Sap flow measurements provided complementary physiological information into crop water use. Although the data were not converted into whole-tree transpiration because sapwood area was not determined, the observed sap flux dynamics were consistent with changes in evaporative demand, irrigation regime, and soil water s. Under well-watered conditions, sap flux closely followed atmospheric demand, whereas under deficit irrigation the plants maintained relatively sustained sap flow despite more negative stem water potential values, suggesting physiological adjustment to moderate water stress. These results confirm the value of sap-flow measurements as part of an integrated monitoring framework and highlight the importance of determining sapwood area in future studies to convert sap flow into transpiration estimates. The third pillar of the thesis concerned **Agro-hydrological Modelling**. The preliminary application of the AquaCitrus model to the Villabate experimental site allowed the potential of a citrus-specific model to be evaluated under subsurface drip irrigation. The comparison with the FAO-56 soil water balance approach highlighted the conceptual differences between the two modelling frameworks. FAO-56 provides a simplified and operational representation of the root zone based on average soil water depletion, whereas AquaCitrus explicitly distinguishes wet and dry soil fractions and simulates SWC at different depths.

The preliminary results obtained for the Full Irrigation treatment during the 2018 irrigation season showed that AquaCitrus was able to reproduce the main temporal patterns of SWC within the wetted soil volume. The model performed particularly well in the deeper layers, where soil water status was more stable and less affected by the steep gradients generated near the buried drip line. Larger discrepancies were observed close to the emitter depth, where the spatial heterogeneity of the wetted bulb makes simulation more challenging. Overall, the results suggest that the conceptual structure of AquaCitrus is more suitable than a single-reservoir approach for representing soil water status under subsurface drip irrigation.

However, the modelling results must be interpreted as preliminary. The application was limited to one irrigation treatment and one irrigation season, and the full calibration and independent validation strategy originally planned for the Villabate dataset was not completed. Therefore, AquaCitrus cannot yet be considered an operational tool for irrigation scheduling at the site. Future work should complete the calibration using the historical dataset available for the 2018–2021 period and validate the model with the independent monitoring data collected during the 2022–2024 experimental campaigns. The model should also be extended to the deficit irrigation and farmer-managed irrigation treatments in order to assess its performance under contrasting irrigation strategies.

Overall, **this thesis contributes** to demonstrating that sustainable irrigation management in Mediterranean citrus orchards cannot rely on a single source of information. Soil hydraulic characterization is needed to understand water storage and movement in the root zone; continuous SPAc monitoring allows the physiological response of the crop to be observed under different irrigation regimes and climatic conditions; agro-hydrological modelling provides a framework for integrating these data and testing the response of the system to irrigation management. The main contribution of the thesis is therefore not only the development or application of individual methods, but their integration within a common experimental framework at the Villabate site.

Several limitations should be acknowledged. The hydraulic characterisation of the soil profile should be strengthened, particularly for the parameters required by agro-hydrological models at different depths. The SPAc monitoring network was limited to a small number of representative trees and should be expanded in future studies to better capture spatial variability within the orchard. Sap-flow measurements should be completed by determining sapwood area, allowing the conversion of sap flux into transpiration estimates. The interpretation of FloraPulse microtensiometer data also requires further work to account for sensor dynamics, time lag, and possible offsets with respect to Scholander chamber measurements. Finally, the AquaCitrus application should be completed through calibration with the 2018–2021 historical dataset and independent validation with the 2022–2024 monitoring data, extending the analysis to deficit irrigation and farmer-managed irrigation treatments.

Future research should build on this integrated framework by improving soil hydraulic parameterization, strengthening plant-based monitoring, and completing the validation of AquaCitrus under contrasting irrigation strategies. Once the robustness of the modelling framework has been verified at Villabate, its application could be extended to other citrus orchards, soil types, and pedoclimatic conditions in Sicily and the Mediterranean basin. This would allow the transferability of the approach to be assessed and would support the development of site-specific irrigation management strategies.

The increasing frequency of drought periods, heat waves, and water restrictions in Mediterranean agriculture makes the development of adaptive irrigation strategies increasingly urgent. The Villabate experimental site demonstrated how field characterisation, continuous monitoring, and modelling can be combined to improve the interpretation of SPAc interactions and to support more resilient irrigation management. Although further validation and operational development are still required, the results of **this thesis provide a solid basis for future applications** aimed at improving water use efficiency, reducing non-beneficial water losses, and sustaining citrus production in water-limited environments.

Appendix A: Effects of Soil Compaction on Its Physical and Hydraulic Properties

Background

Repacked soil columns are commonly employed for determining soil hydrodynamic properties in laboratory settings, as they provide a controlled and replicable experimental environment that offers several advantages over the use of undisturbed soil samples (Starrett et al., 1996; Leuther and Schlüter, 2021; Bagarello et al., 2024). One of the primary benefits of using repacked columns is the ability to isolate and manipulate specific physical variables, such as bulk density, porosity, and also initial water content, allowing researchers to examine their individual effects on water retention and flow dynamics (Ikoyi and Schmalenberger, 2021; Nakhli et al., 2021). This level of control is often difficult to achieve with undisturbed samples, which can exhibit natural heterogeneity and variability in structure due to biotic and abiotic factors. Additionally, repacked columns facilitate the definition of standardized experimental conditions, ensuring consistency across different trials and research settings. This standardization is particularly valuable for comparative studies and model calibration, as it reduces the uncertainty associated with natural soil variability. Moreover, the enhanced repeatability of measurements obtained from repacked samples makes the testing process more efficient and manageable, particularly when multiple replications are required or when evaluating the effects of specific treatments (Comegna et al., 2023; Bondì et al., 2024, Castellini et al., 2025). Despite these advantages, it is important to acknowledge that repacking may alter the natural soil structure, potentially affecting the representativeness of the results in relation to field conditions (Bondì et al., 2022).

Repacked soil samples can be used for various experimental purposes that include: I) testing theories, devices and procedures for determining saturated hydraulic conductivity (K_s) (Reynolds and Elrick, 1987); II) assessing the influence of specific factors on K_s values in different soil types (Moutier et al., 1998); III) analyzing the effects of wastewater reuse on K_s (Viviani and Iovino, 2004); IV) investigating the relationships between K_s (or unsaturated hydraulic conductivity, K) and macroscopic soil physical properties (Assouline, 2006); V) evaluating the impact of surface seal formation on K (Armenise et al., 2018); and VI) analysing the effects of organic and inorganic amendments on soil hydraulic properties (Bondì et al., 2024; Castellini et al., 2025). Although the use of repacked soil samples offers several experimental advantages, the determination of K_s or K, as well as other physical and hydraulic soil properties, requires careful selection of an appropriate packing method. In fact, the chosen procedure for assembling the soil column significantly affects the reliability and accuracy of the obtained experimental results (Lewis and Sjöstrom, 2010).

Over the years, several packing methods have been applied in different investigations. Reicovsky et al. (1980) used a laboratory press with pistons that compressed moist soil samples from both ends simultaneously. Laliberte et al. (1966) achieved varying densities by vibrating soil columns after filling them with air-dried soil. Alternative packing methods use a series of wetting and drying cycles to assist compaction (Bowman, 1988; Corwin, 2000; Jones et al., 1974; Shih and Rosen, 1985). For example, Corwin (2000) introduced soil in thin layers, each less than 0.5 cm thick, and subjected them to multiple wet-dry cycles to improve packing uniformity. Bagarello et al. (2004), on the other hand, proposed a manual method of progressive 1 cm layers compacted sequentially. However, operator-to-operator variability is an inherent feature of all experimental procedures (Griffiths and Rosenfeld, 1954), and it can significantly affect the replicability of results and, consequently, the scientific robustness of an experiment. Such variability may arise both during sample preparation and during subsequent measurements, and can be influenced by several factors, including the operator's level of experience (Bagarello et al., 2025). Using non-mechanized tools, such as pestles or manual instruments, is particularly critical and introduces operator-dependent error, which is difficult to quantify and compromises comparability between studies. Furthermore, different sample preparation methods applied to the same soil type can yield significantly different results (Gunaratnam et al., 2020; Bagarello et al., 2022).

Despite at least 300 years of experience in the use of soil columns, no standardization of experimental methods on column preparation has occurred, which complicates comparison between investigations (Lewis and Sjöstrom, 2010). Moving towards standardized methods requires considering that many factors could influence experimental results. For example, some of these factors concerned with the preliminary sample preparation steps, before performing the K_s experiment, include the use of sieved air-dried soil, the duration of sieving time and the surface scraping between layers. Mechanical sieving duration is rarely reported in scientific papers. The lack of this information is justified if sieving duration does not influence the particle size distribution of the soil used for the experiment. However, sieving, typically carried out to remove particles larger than 2 mm, can significantly alter particle size distribution and aggregate structure, especially when prolonged. Recent studies (Díaz-Zorita et al. 2007; Bartley et al. 2019) demonstrate that sieving duration alters the distribution of fine particles, thereby modifying soil porosity. Fomin et al. (2021) recommend that sieving follow well-defined protocols, specifying duration, mesh size, and soil moisture conditions, as these factors influence the final soil microstructure and hence its hydraulic conductivity.

In some investigations, the soil samples were prepared with a step-by-step procedure, pouring at each step a known soil mass. For example, Moody et al. (2009) prepared the column by introducing soil in 5–10 increments. Zhang et al. (2017) prepared the column by pouring 5 cm of soil followed by compaction. Ghosh and Pekkat (2019), packed the soil in three layers and imparted an equal number of blows on each layer, depending on the desired state of compaction.

Another, often overlooked, but equally important practice when preparing the soil column by adding subsequent layers of soil is the scraping of exposed surfaces between compacted layers, which is necessary to ensure vertical hydraulic continuity within the column. Lewis and Sjöstrom, (2010) showed that untreated surfaces can form partially impermeable interfaces that hinder water percolation. The importance of lightly scarifying the soil surface after compaction and before adding another soil mass to ensure hydraulic connectivity between layers has been reported in a few studies (Plummer et al., 2004; Seol and Lee, 2001).

To investigate the influence of these factors on the preparation of repacked soil columns, it is essential to adopt measurement techniques that are not only sensitive to microstructural changes but also reproducible and easy to apply. Among the infiltrometric techniques available today, the Simplified Falling Head (SFH) technique proposed by Bagarello et al. (2004) stands out for its effectiveness in assessing saturated hydraulic conductivity, both in the field and the laboratory. This makes it particularly useful for evaluating the impact of soil sample preparation methods on the soil's hydrodynamic properties. The SFH method enables precise monitoring of permeability variations induced by compaction, texture, and sample preparation. Its versatility and sensitivity make it ideal for comparative studies and for evaluating the systematic effects of different preparation practices (Teng et al., 2019; Concialdi et al., 2019). Recent studies have further validated the SFH method's capabilities by testing how resulting K_s values depend on various factors involved in preparing initially air-dry soil columns. Research conducted primarily on loamy soils has examined key variables including the specific manual packing method employed (Bagarello et al., 2022) and the effects of reusing the same soil mass for repeated K_s determinations (Bagarello et al., 2024). Further investigation of additional factors is essential to improve the prediction of how laboratory preparation methods of initially air-dry soil columns influence the determination of saturated hydraulic conductivity using the SFH technique. Such insights could also serve as a valuable reference for studies involving different soil types, initial moisture conditions, and alternative K_s measurement methods.

In this context, to address these knowledge gaps and provide a solid empirical basis for the development of standardized protocols, this appendix presents the results of two sequential and complementary experimental studies. These investigations were specifically designed to quantify the impact of critical preparatory factors, often overlooked or inconsistently reported in the literature, on the final hydraulic response of the soil. The systematic approach adopted aims to identify and evaluate the individual and combined influence of key operational parameters, paving the way for a more robust and reproducible preparation procedure. Both investigations employed the Simplified Falling Head (SFH) technique (Bagarello et al., 2004) as the common and sensitive method to detect the induced hydraulic changes. Therefore, to ensure a clear and independent presentation, Appendix **A.1** first delineates the theoretical foundations, standardized procedure, and governing equation of this core methodology. With this shared experimental framework established, the two studies presented in this Appendix **A.2** and **A.3** offer complementary experimental insights into how sample preparation affects soil hydraulic properties.

Specifically, Appendix **A.2** evaluated the effects of controlled mechanical compaction on three different soils using a custom-designed soil compaction apparatus (SCA). The SCA consisted of a Teflon pestle that slides within a Plexiglas guide cylinder and compacts soil inside a lower Plexiglas container cylinder, where the soil column is formed. Compaction is achieved through successive drops of the pestle from a fixed height. The gravitational potential energy imparted to the soil per drop can be calculated based on the known mass of the pestle and the fall height.

Appendix **A.3** examined the effects of sieving duration (5 and 30 minutes) and surface scraping between successive layers of compacted soil columns. The soil was air-dried, sieved, and then used to prepare 24 columns with two methods: a one-step procedure (12 columns) and a three-step procedure (12 columns). The columns were compacted by the SCA apparatus. For each method, the surface of six randomly chosen columns were scraped with a rigid brush before the addition of any new soil layer.

In conclusion, the two papers contained in this Appendix examined how soil preparation methods can influence some of its key properties such as porosity and saturated hydraulic conductivity. The findings highlight the critical role of consistent and standardized sample preparation methods in ensuring the reproducibility of measurements, regardless of geographic location or operator influence, and improving our understanding of how different methods influence soil hydraulic behaviour.

Therefore, the experimental results from these studies provide a basis for developing unified guidelines. These future protocols must explicitly address the critical parameters investigated, specifically compaction methods, sieving duration, layering, and surface preparation, to mitigate systematic errors and enable robust, comparable measurements of soil hydrodynamic properties across the scientific community.

A.1: Simplified Falling Head (SFH)

The Simplified Falling Head (SFH) technique proposed by Bagarello et al. (2004) enables the estimation of the field-saturated hydraulic conductivity, K_{fs} (L T^{-1}), using data collected during a variable-head infiltration test. This method relies on a one-dimensional cumulative infiltration model under falling head conditions, described using the Green and Ampt (1911) approach as reformulated by Philip (1992):

$$t = \frac{\Delta\theta}{K_{fs}(1-\Delta\theta)} \times \left[\frac{I(t)}{\Delta\theta} - \frac{H_0 - h_f}{1-\Delta\theta} ln\left(1 + \frac{(1-\Delta\theta)I(t)}{\Delta\theta(H_0 - h_f)}\right)\right] \tag{1.0}$$

Where t (T) is the time, $\Delta\theta$ (L^3 L^{-3}) is the difference between the water content of the saturated soil, I (L) is the cumulative infiltration, H_0 (L) is the height of surface head at time $t = 0$ and h_f (L) is the pressure potential at the wetting front, with h negative. The equation accounts for gravitational forces and is valid until the surface load drops to zero. The pressure potential h_f can be replaced by the parameter $\alpha*$ (L^{-1}), as proposed by Elrik et al. (2002):

$$\alpha^* = \frac{K_{fs}}{\phi_m} = -\frac{1}{h_f} \tag{1.1}$$

where ϕ_m is the matrix flow potential (Gardner, 1958). Thus obtaining:

$$t = \frac{\Delta\theta}{K_{fs}(1-\Delta\theta)} \times \left[\frac{I(t)}{\Delta\theta} - \frac{H_0 - \frac{1}{\alpha^*}}{1-\Delta\theta} ln\left(1 + \frac{(1-\Delta\theta)I(t)}{\Delta\theta\left(H_0 - \frac{1}{\alpha^*}\right)}\right)\right] \tag{1.2}$$

The technique (**Fig. 1**) proposed by Bagarello et al. (2004) involves applying a known volume of water, V (L^3), to the surface of the soil within a cylinder inserted at a fixed depth, d (L), into the soil.

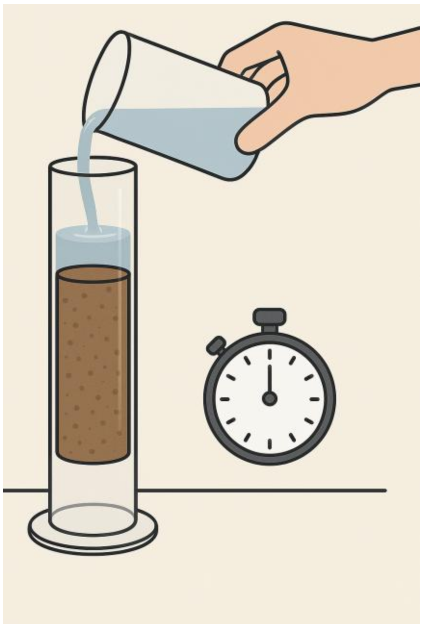

Fig. 1 Simplified Falling Head (SFH)

The time interval from the water application to the moment t_a when the water has fully infiltrated and the soil surface is exposed to the atmosphere is measured. The saturated hydraulic conductivity of the soil, K_s (L T^{-1}), can be calculated using the following equation (Bagarello et al., 2004):

$$K_s = \frac{\Delta\theta}{t_a(1-\Delta\theta)}\left[\frac{D}{\Delta\theta} - \frac{\left(D+\frac{1}{\alpha^*}\right)}{1-\Delta\theta} ln\left(1+\frac{(1-\Delta\theta)D}{\Delta\theta\left(D+\frac{1}{\alpha^*}\right)}\right)\right] \quad (1.3)$$

in which t_a (T) is the time for the applied water volume to infiltrate, D = V/A (L) is the height of the ponded head of water at t= 0, A (L^2) is the infiltration surface, and $\alpha*$ (L^{-1}) is a parameter that accounts for the contribution to the total flux of the unsaturated matrix. The SFH technique can be applied both in field conditions and in laboratory settings, such as for determining the hydraulic conductivity of repacked soil columns or undisturbed soil samples.

REFERENCES

Armenise, E., Simmons, R.W., Ahn, S., Garbout, A., Doerr, S.H., Mooney, S.J., Sturrock, C.J., Ritz, K., 2018. Soil seal development under simulated rainfall: Structural, physical and hydrological dynamics. Journal of Hydrology 556, 211–219. https://doi.org/10.1016/j.jhydrol.2017.10.073

Assouline, S., 2006. Modeling the Relationship between Soil Bulk Density and the Hydraulic Conductivity Function. Vadose Zone Journal 5, 697–705. https://doi.org/10.2136/vzj2005.0084

Bagarello, V., Iovino, M., Elrick, D., 2004. A simplified falling head technique for rapid determination of field-saturated hydraulic conductivity. Soil Sci. Soc. Am. J., 68: 66-73.

Bagarello, V., Barone, S., Caltabellotta, G., Varadi, F.K., Zanna, F., Autovino, D., 2025. A Test of Factors Influencing One-Dimensional Mini-Disk Infiltrometer Experiments on Repacked Loam Soil Columns. Hydrology 12, 85. https://doi.org/10.3390/hydrology12040085

Bagarello, V., Caltabellotta, G., Iovino, M., 2024. Soil reuse effects on determination of saturated hydraulic conductivity of different loamy soils. European J Soil Science 75, e13454. https://doi.org/10.1111/ejss.13454

Bagarello, V., Caltabellotta, G., Iovino, M., 2022. Manual packing and soil reuse effects on determination of saturated hydraulic conductivity of a loam soil. Geoderma 405, 115465. https://doi.org/10.1016/j.geoderma.2021.115465

Bartley, P.C., Jackson, B.E., Fonteno, W.C., 2019. Effect of particle length to width ratio on sieving accuracy and precision. Powder Technology 355, 349–354. https://doi.org/10.1016/j.powtec.2019.07.016

Bondì, C., Castellini, M., Iovino, M., 2024. Temporal variability of physical quality of a sandy loam soil amended with compost. Biologia. https://doi.org/10.1007/s11756-024-01637-1

Bondì, C., Castellini, M., Iovino, M., 2022. Compost Amendment Impact on Soil Physical Quality Estimated from Hysteretic Water Retention Curve. Water 14, 1002. https://doi.org/10.3390/w14071002

Castellini, M., Bondì, C., Leogrande, R., Giglio, L., Vitti, C., Mastrangelo, M., Bagarello, V., 2025. Evaluating the Effects of Compost, Vermicompost, and Biochar on Physical Quality of Sandy-Loam Soils. Applied Sciences 15, 3392. https://doi.org/10.3390/app15063392

Comegna, A., Belviso, C., Rivelli, A.R., Coppola, A., Dragonetti, G., Sobhani, A., Di Prima, S., Satriani, A., Cavalcante, F., Lovelli, S., 2023. Analysis of critical water flow and solute transport parameters in different soils mixed with a synthetic zeolite. CATENA 228, 107150. https://doi.org/10.1016/j.catena.2023.107150

Concialdi, P., Bagarello, V., Alagna, V., Iovino, M., 2019. Laboratory evaluation of falling-head infiltration for saturated soil hydraulic conductivity determination. J Agricult Engineer 51, 27–35. https://doi.org/10.4081/jae.2019.1003

Corwin, D.L., 2000. Evaluation of a simple lysimeter-design modification to minimize sidewall flow. Journal of Contaminant Hydrology 42, 35–49. https://doi.org/10.1016/S0169-7722(99)00088-1

Díaz-Zorita, M., Grove, J.H., Perfect, E., 2007. Sieving duration and sieve loading impacts on dry soil fragment size distributions. Soil and Tillage Research 94, 15–20. https://doi.org/10.1016/j.still.2006.06.006

Elrick, D.E., Angulo-Jaramillo, R., Fallow, D.J., Reynolds, W.D., Parkin, G.W., 2002. Infiltration under constant head and falling head conditions. Wash. DC Am. Geophys. Union Geophys. Monogr. Ser. 129, 47–53.

Fomin, D., Timofeeva, M., Ovchinnikova, O., Valdes-Korovkin, I., Holub, A., Yudina, A., 2021. Energy-based indicators of soil structure by automatic dry sieving. Soil and Tillage Research 214, 105183. https://doi.org/10.1016/j.still.2021.105183

Gardner, W.R., 1958. Some Steady State Solutions of the Unsaturated Moisture Flow Equation with Application to Evaporation from a Water Table. Soil Science, 85, 228-232

Ghosh, B., Pekkat, S., 2019. Effect of initial compaction state on near-saturated hydraulic conductivity. J. Irrig. Drain. Eng. 145 (12), 04019028. https://doi.org/10.1061/ (ASCE)IR.1943-4774.0001428

Green, W.H. and Ampt, G.A., 1911. Studies on Soil Physics, 1: The Flow of Air and Water through Soils. The Journal of Agricultural Science, 4, 1-24. https://doi.org/10.1017/S0021859600001441.

Griffiths, J.C., Rosenfeld, M.A., 1954. Operator Variation in Experimental Research. The Journal of Geology 62, 74–91. https://doi.org/10.1086/626134

Gunaratnam, A., Grafton, M., Jeyakumar, P., Bishop, P., Davies, C.E., 2020. Study the influence of soil moisture and packing incremental level on soil physical and hydraulic properties.

Ikoyi, I., & Schmalenberger, A. 2021. Design and Construction of Repacked Soil Columns for Measuring Solute Transport, Plant Growth and Soil Biota. Bio-protocol, 11(2), e3884-e3884.

Laliberte, G.E., Corey, A.T., Brooks, R.H., 1966. Properties of unsaturated porous media.

Leuther, F., Schlüter, S., 2021. Impact of freeze–thaw cycles on soil structure and soil hydraulic properties. SOIL 7, 179–191. https://doi.org/10.5194/soil-7-179-2021

Lewis, J., Sjöstrom, J., 2010. Optimizing the experimental design of soil columns in saturated and unsaturated transport experiments. Journal of Contaminant Hydrology 115, 1–13. https://doi.org/10.1016/j.jconhyd.2010.04.001

Moutier, M., Shainberg, I., Levy, G.J., 1998. Hydraulic Gradient, Aging, and Water Quality Effects on Hydraulic Conductivity of a Vertisol. Soil Science Soc of Amer J 62, 1488–1496. https://doi.org/10.2136/sssaj1998.03615995006200060003x

Moody, J.A., Kinner, D.A., Úbeda, X., 2009. Linking hydraulic properties of fire-affected soils to infiltration and water repellency. J. Hydrol. 379 (3-4), 291–303. https://doi. org/10.1016/j.jhydrol.2009.10.015.

Nakhli, S.A.A., Tian, J., Imhoff, P.T., 2021. Preparing and characterizing repacked columns for experiments in biochar-amended soils. MethodsX 8, 101205. https://doi.org/10.1016/j.mex.2020.101205

Philip JR, 1992. Falling head ponded infiltration. Water Resour. Res. 28, 2147-2148. DOI: https://doi.org/10.1029/92WR00704

S. F. Shih, M. Rosen, 1985. Water Table Effects on Nutrient Contents of Celery, Lettuce and Sweet Corn. Transactions of the ASAE 28, 1867–1870. https://doi.org/10.13031/2013.32533

Seol, Y., Lee, L.S., 2001. Coupled Effects of Treated Effluent Irrigation and Wetting–Drying Cycles on Transport of Triazines through Unsaturated Soil Columns. J of Env Quality 30, 1644–1652. https://doi.org/10.2134/jeq2001.3051644x

Starrett, S.K., Christians, N.E., Austin, T.A., 1996. Comparing dispersivities and soil chloride concentrations of turfgrass-covered undisturbed and disturbed soil columns. Journal of Hydrology 180, 21–29. https://doi.org/10.1016/0022-1694(95)02897-8

Teng, J., Kou, J., Zhang, S., Sheng, D., 2019. Evaluating the Influence of Specimen Preparation on Saturated Hydraulic Conductivity Using Nuclear Magnetic Resonance Technology. Vadose Zone Journal 18, 1–7. https://doi.org/10.2136/vzj2018.09.0179

Viviani G., Iovino M. 2004. Wastewater reuse effects on soil hydraulic conductivity. Journal of Irrigation and Drainage Engineering, 130: 476-484.

Zhang, J., Lei, T., Yin, Z., Hu, Y., Yang, X., 2017. Effects of time step length and positioning location on ring-measured infiltration rate. Catena 157, 344–356. https://doi.org/10.1016/j.catena.2017.05.013.

A.2: Investigating Soil Compaction and Its Impact on Physical and Hydraulic Properties Using a Simple Testing Apparatus

Vincenzo Bagarello [1], Gaetano Caltabellotta [1], Mariachiara Fusco [1], Girolamo Vaccaro [1] and Dario Autovino [1]*

[1] Department of Agricultural Food and Forest Sciences, University of Palermo, Viale delle Scienze, 90128 Palermo, Italy; vincenzo.bagarello@unipa.it (V.B.); gaetano.caltabellotta@unipa.it (G.A.); mariachiara.fusco@unipa.it (M.F.); girolamo.vaccaro@unipa.it (G.V.)

* Correspondence: dario.autovino@unipa.it; Tel.: +39-091-238-97082

Abstract

Various laboratory methods are used for packing sieved soil, influencing determination of soil properties. This study tested a simple packing method and determined compaction effects on dry bulk density, ρ_b, and saturated hydraulic conductivity, K_s, of three sieved loamy soils (AR, LE, OR). For compaction energies, E_p, of 1 to 100 kJ/m^2, the LE soil, with a similar content of large (> 0.25 mm; 53%) and small (< 0.25 mm; 47%) undispersed soil particles, yielded higher ρ_b (1.43 g/cm^3) and lower K_s (23 mm/h) values as compared with the AR and OR soils (ρ_b = 1.12-1.14 g/cm^3; K_s = 166-167 mm/h), having a larger percentage of undispersed coarse particles (65-68%). Higher E_p values induced a decrease of K_s by 10.0, 2.5 and 16.4 times for the AR, LE and OR soils, respectively. Significant K_s vs. ρ_b relationships (coefficient of determination, $R^2 \geq 0.62$) were observed for each soil. A loamy soil with a small K_s value in little compacted conditions can be less affected by E_p than a similar soil with a high K_s value. The packing method should be reported in investigations on physical and hydraulic properties of sieved and repacked soil.

Keywords: soil physical and hydraulic properties; laboratory experiments; repacked soil; soil compaction apparatus; simplified falling head technique

A.2.1. Introduction

Determining in the laboratory the saturated, K_s, or near-saturated, K, hydraulic conductivity of repacked soil samples connects the studies dealing with ideal data, such as those generated numerically, with the laboratory or field investigations on real soils. Repacked soil samples can be used with different objectives, such as testing theories, devices and procedures to determine K_s (Reynolds and Elrick, 1987), evaluating factors that influence the K_s values of specific soil types (Moutier et al., 1998), determining wastewater reuse effects on K_s (Viviani and Iovino, 2004), relating K_s or K with the bulk soil physical properties (Assouline, 2006), testing soil seal development effects on K (Armenise et al., 2018).

Determining K_s or K, along with other soil physical and hydraulic properties, on repacked samples implies preliminary choosing a packing method. This choice is complex and to some extent arbitrary, also because standard experimental methods are still lacking despite at least 300 years of experience in the use of soil columns (Lewis and Sjöstrom, 2010). Consequently, different packing methods have been applied in different investigations.

For example, Laliberte et al. (Laliberte et al., 1966) obtained different densities by filling cylinders with air-dry soil and then vibrating the soil columns. Reicosky et al. (Reicosky et al., 1981) slightly pressed moist soil samples from both ends simultaneously by a standard laboratory press with pistons. Bagarello et al. (Bagarello et al., 2004) prepared samples of 5 cm in diameter and 4 or 5 cm in height by pouring in subsequent steps 1 cm of soil that was then manually compacted. The samples used by Bagarello et al. (Bagarello et al., 2006) and Concialdi et al. (Concialdi et al., 2020), having a diameter of nearly 9 cm and a height of 32 cm or more, were prepared by filling a column with 40 cm of soil. This column was dropped repeatedly from a height of 5 cm until compaction ceased. In the investigation performed by Stock and Downes (Stock and Downes, 2008), the soil was poured into a cylinder with a 5.6 cm diameter to form a 7.5 cm high column and then it was subjected to an external load of 0.6 kg using a metal weight with a diameter of 5.4 cm. Soil was added in 5-10 increments by Moody et al. (Moody et al., 2009) to prepare samples of 5.1 cm × 20 cm and 10 cm × 12 cm. Petersen et al. (Petersen et al., 2016) used a 200 cm^3 cylinder filled with nearly 200 g of soil that was loaded statically at 12.5 kg for four minutes. The 30 cm × 60 cm samples by Zhang et al. (Zhang et al., 2017) were prepared with a step-by-step procedure, by pouring at each step 5 cm of soil followed by compaction. Ghosh et al. (Ghosh and Pekkat, 2019) prepared samples of 20 cm in diameter × 30 cm in height by packing the soil in three layers and imparting an equal number of blows on each layer. In some investigations, however, the applied packing method was not described (Assouline and Narkis, 2011; Botyanszká et al., 2022; Moutier et al., 1998). Indeed, the lack of information on packing methods appears to be rather common in repacked soil column investigations. In a report on organic micropollutants (EOCs) by the EU (Gibert et al., 2014), it was explicitly stated that <*Although the repacking of soil columns significantly influences the resulting EOCs behavior and fate within the column, it has received little attention, and details on it are rarely explicitly reported or explained in published studies*>. Lack of detailed reporting of experimental conditions impedes taking into account packing effects in the interpretation of the data collected by the experiment (Bromly et al., 2007).

The large variety of applied packing methods has not encouraged the development of many investigations into the effects of the used method on the determination of soil physical and hydraulic properties. This circumstance, together with the lack of any information about the used packing method in several cases, seems to implicitly suggest that the packing method is generally considered a not very relevant factor affecting laboratory determination of soil physical and hydraulic properties.

Instead, the limited available information indicates that determination of these properties should be expected to vary with the applied method to prepare a soil sample.

For example, Oliviera et al. (Oliviera et al., 1996) suggested that preparing homogeneous samples of sandy soils requires depositing layers of a few millimeters followed by compaction with a metal pestle since packing by vibration can cause lateral segregation of soil particles and uniformity of packing can decrease as the thickness of the soil layer increases. Nimmo et al. (Nimmo and Akstin, 1988) reported a fivefold variation of unsaturated soil hydraulic conductivity for samples prepared by different packing methods. Teng et al. (Teng et al., 2019) recognized that K_s can vary by even an order of magnitude due to the dependence of the pore size distribution on the applied packing method. Regarding loam soil columns of 9.3 cm in diameter × 12.5 cm in height, Bagarello et al. (Bagarello et al., 2022) tested two compaction procedures (dropping from a given height, pestle imparting vertical and radial forces on the pressed soil surface) and they disposed the soil in the cylinder in one to six layers. The means of K_s varied by 2.2 times with the applied packing method. Moreover, using the pestle instead of the dropping method yielded less variable results.

The laboratory determination of a physical or hydraulic soil property depends on the packing method used, meaning that two identical investigations differing only in their packing methods may yield inconsistent results. Therefore, it seems necessary to collect more data on the packing method effects, in the perspective of developing, in the near future, standardized experimental methods, also considering that standardized compaction methods are more common in other contexts such as the geotechnical and engineering sectors (American Society for Testing and Materials, 2021; ASTM International, 2012). Perhaps, in a standard methodology relevant for soil hydrology investigations, manual compaction of the soil with a pestle should be avoided since the effectiveness of compaction can be expected to be related to the ability of the operator that prepares the soil sample. On the other hand, using more or less complex, automatized and perhaps expensive equipment does not seem a good choice since this equipment could not be available in many laboratories. Instead, it appears necessary to obtain reproducible results using a simple and cheap methodology.

The simplified falling head (SFH) technique appears a good candidate method to test K_s dependence on the applied packing method since, with this technique, an initially nearly dry soil generally remains in contact with flowing water for a rather short time period after starting the run (Bagarello et al., 2004). Therefore, it can be presumed that the collected data are representative of the pore system formed by the applied packing method.

The general objective of this investigation was to test, for three loamy soils packed by a simple and reproducible method, soil compaction effects on dry bulk density and saturated hydraulic conductivity. The specific objectives were to i) test a new soil compaction apparatus; ii) determine compaction energy effects on both dry soil bulk density and saturated soil hydraulic conductivity; and iii) establish a comparison between the saturated soil hydraulic conductivity values obtained in this investigation and those obtained in the past on the same soils, packed with other methods.

A.2.2. Materials and Methods

A.2.2.1 Soil compaction apparatus

The soil compaction apparatus (SCA) consists of a Teflon pestle sliding inside a Plexiglas guide cylinder and an underlying Plexiglas container cylinder, where the soil column is prepared (**Fig. 1**). The pestle has a diameter of 5 cm, a height of 30 cm and a mass of 0.89 kg. At its upper end, a screw eyelet is installed to connect a rope with a handle. The rope can slide through a fixed pulley, positioned about 2 m above the ground. The guide cylinder, having an internal diameter d_c = 5.3 cm and a height of 50 cm, is aligned with the fixed pulley and secured with metal supports. The distance between the lower end of the guide cylinder and the floor is 85 cm. The container cylinder, also having d_c = 5.3 cm and a height of 25 cm, aligned with the guide cylinder, is equipped at the lower end with a sock and a mesh fixed with a metal band. This configuration allows the pestle to slide inside the two cylinders without encountering obstacles. To ensure greater stability for the container cylinder, a metal bench is positioned underneath it. The compaction procedure involves successive drops of the pestle from a predetermined height. Initially, the container cylinder is filled with a certain amount of soil and connected to the guide cylinder.

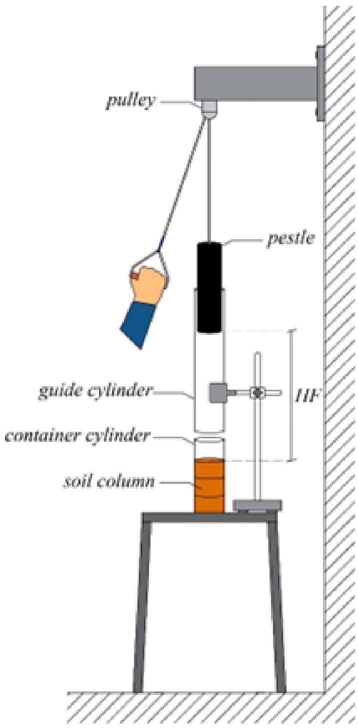

Fig. 1. Schematic view of the soil compaction apparatus.

Subsequently, an operator, by pulling the rope with the handle, places the pestle at the desired fall height and installs an end-stop clamp as a reference. Then, the operator suddenly releases the handle, dropping the pestle inside the container cylinder to compact the soil. The predetermined number of drops of the pestle determines the desired degree of compaction.

A.2.2.2 Soils

Three field sites were sampled for this investigation. Two sites (AR and OR sites) were located at the Department of Agricultural, Food and Forest Sciences of the Palermo (Italy) University, at a mutual distance of about 200 m. Another site (LE site) was located around the town of Lercara, about 45 km south of Palermo. An orchard with trees spaced 4 m × 4 m apart was established at the AR site, a tilled and non-seeded soil was sampled at the LE site and a meadow was considered at the OR site. The soil was collected from zones close to those sampled for other investigations (Bagarello et al., 2024). According to the USDA classification system, the soil used in this investigation was sandy-loam at the AR and LE sites and loam at the OR site (Table 1). The three soils had a relatively similar organic carbon content, ranging from 20.3 (LE) to 27.1 (AR) g/kg (Bagarello et al., 2024).

At each site, approximately 80 kg of soil were collected from the surface layer of nearly 100-150 m^2 areas. The soil was transported to the laboratory and it was spread on plastic sheets for natural drying at room temperature. This process took place for about 40 days, during which the soil was manually mixed every few days to facilitate drying. Once the condition of air-dry soil was reached, the soil was sieved through a 2 mm mesh sieve and the fine fraction was stored to perform the experiment.

The particle size distribution (PSD) of the undispersed soil was determined by mechanical sieving of soil samples without H_2O_2 or sodium hexametaphosphate treatment. At this aim, the percentages by weight of particles of 2-0.86, 0.86-0.425, 0.425-0.25, 0.25-0.106, 0.106-0.075 and <0.075 mm were determined. This analysis was carried out because the fine soil used in this investigation was expected to contain aggregates of elementary particles (Bagarello et al., 2024).

Different loamy soils were considered since a single soil cannot be expected to yield a generally valid information for soils with a given texture. Multiple soils do not offer a guarantee in this sense but certainly provide more information than a single soil. The soils considered in this investigation were already used to test effects of manual packing, soil mass reuse, sieving duration and scraping of exposed soil surfaces on determination of soil physical and hydraulic properties (Autovino et al., 2024; Bagarello et al., 2024, 2022).

Table 1. Mean and coefficient of variation (%, in parenthesis) of the clay, silt and sand content and USDA textural classification of the surface soil at the three sampled field sites (sample size, N = 4 at each site).

Parameter	AR	LE	OR
Clay (< 0.002 mm) (%)	16.5 (2.9)	19.6 (9.4)	20.5 (20.1)
Silt (0.002 – 0.05 mm) (%)	30.3 (12.1)	26.1 (8.9)	31.2 (8.7)
Sand (0.05 – 2 mm) (%)	53.3 (7.5)	54.3 (2.1)	48.3 (3.4)
Textural classification	Sandy-loam	Sandy-loam	Loam

A.2.2.3 Experiment

Soil columns were prepared with a three-step procedure in the container Plexiglas cylinders. In particular, a constant amount of air-dry soil, equal to 480 g, was used to prepare a sample. Air-dry soil was used since dry packing is a common way to prepare soil columns (Lewis and Sjöstrom, 2010; Oliviera et al., 1996) and also considering that the SFH technique yields the K_s value of an initially unsaturated soil (Bagarello et al., 2004). One third of the soil mass was poured into the cylinder and the soil was compacted by an established number of blows of the pestle (NB = 5, 10, 20, 35 or 50) falling from a fixed height (HF = 0.05, 0.1, 0.2, 0.35 or 0.5 m). The second third was then added and the same compaction procedure was applied again. Finally, the last third of the soil was poured and compacted in the same manner. The final height, h_f (cm), of each soil column was measured after compaction to determine the bulk volume of the soil column, V_t (cm^3). All possible combinations between NB and HF were considered, yielding, for each soil, a total of 50 soil columns (5 NB values × 5 HF values × 2 cylinders). Each soil column was filled with a soil mass that had not been used before. The gravitational potential energy, E_p, dissipated on a soil layer was calculated taking into account that both the mass of the pestle (m_p = 0.89 kg) and the height of fall were known. In particular, for a single blow, E_p is equal to $m_p g$ (HF)/A, g (m/s^2) being the acceleration due to gravity and A (m^2) being the exposed surface of the soil sample. For example, with NB = 10, HF = 0.35 m and A = 0.0022 m^2, the dissipated energy to compact a layer was equal to E_p = 10 × 0.89 × 9.81 × 0.35/(1000 × 0.0022) = 14.0 kJ/m^2. A similar soil compaction method, i.e. load of 1.5 kg allowed to freely fall from a height of 1 m for five to 20 times, was applied in another test of compaction energy effects on soil physical and hydraulic properties (Abdulkareem et al., 2023). More in general, the method applied in this investigation takes into account that dry soil can be packed by loading small discrete amounts of soil into a cylinder and then mechanically packing it in some manner (Gibert et al., 2014; Lewis and Sjöstrom, 2010).

Before applying the SFH technique (Bagarello et al., 2004) to determine the saturated hydraulic conductivity, K_s, of a given soil column, the gravimetric soil water content, w (g/g), was determined by placing a few replicated samples of nearly 30 g of air-dry soil in an oven at 105 °C for 24 h. The measured w value was considered representative of the antecedent gravimetric soil water content, w_i (g/g), for the SFH experiments that were performed the day after measuring w. Taking into account that the SFH technique requires establishing a one-dimensional infiltration process, free water should not appear at the bottom of the column by the end of the infiltration run. For this reason, a water volume, V_w (cm^3), equal to the empty pore volume in the upper 2/3 of the soil column was used to perform each SFH run:

$$V_w = \left(\frac{2}{3} \times h_f\right) \times \pi \times \frac{d_c^2}{4} \times (\theta_s - \theta_i) \tag{1.0}$$

in which θ_s (cm^3/cm^3) is the volumetric water content of the saturated soil and θ_i (cm^3/cm^3) is the antecedent volumetric soil water content. In this investigation, θ_i and θ_s were determined using w_i and the dry soil bulk density, ρ_b (g/cm^3), assuming that θ_s coincided with the porosity obtained from the ρ_b data (Mubarak et al., 2009). A direct measurement of ρ_b was not available since the soil used to fill the cylinder was air-dry and not oven-dry. Therefore, ρ_b was determined by the following relationship (Bagarello et al., 2022):

$$\rho_b = \frac{m_s}{V_t} = \frac{m_{ad}}{V_t(1 + w_i)} \tag{1.1}$$

where m_s (g) is the mass of the oven-dry soil and m_{ad} (g) is the mass of the air-dry soil. For each run, the infiltration time, t_a (h), of the applied water volume was determined as the time from the application of water to the instant when all free water disappeared from the soil surface. In no case did the wetting front reach the bottom of the soil column nor were preferential flow zones observed during the SFH run at the contact zone between the soil and the cylinder.

A.2.2.4 Calculations and data analysis

The mean weight diameter (MWD) of the undispersed soil particles was calculated by assuming that all particles of a given size range had a diameter equal to the average between the two extremes (e.g., 1.43 mm for the 2-0.86 mm range).

The saturated soil hydraulic conductivity, K_s (mm/h), was calculated by the SFH equation (Bagarello et al., 2004):

$$K_s = \frac{\Delta\theta}{t_a(1-\Delta\theta)}\left[\frac{D}{\Delta\theta} - \frac{\left(D+\frac{1}{\alpha^*}\right)}{1-\Delta\theta} ln\left(1+\frac{(1-\Delta\theta)D}{\Delta\theta\left(D+\frac{1}{\alpha^*}\right)}\right)\right] \tag{1.2}$$

in which $\Delta\theta = \theta_s - \theta_i$, $D = V_w/A$ (mm) is the height of the ponded head of water at $t = 0$ and α^* (1/mm) is a soil texture/structure parameter that was fixed at 0.012 1/mm in this investigation (Concialdi et al., 2020; Elrick and Reynolds, 1992).

The data were analyzed as follows: i) comparison among the soil textural characteristics of the three undispersed soils; ii) comparison among the means of the ρ_b and K_s values overall obtained for each soil (sample size, N = 50 for each dataset); iii) test of the effect of E_p on both ρ_b and K_s for the three soils; iv) determination of the relationship between K_s and ρ_b; and v) comparison between the K_s vs. ρ_b relationships determined in this investigation and the means of K_s obtained with the SFH technique on the AR, LE and OR soils in some previous investigations (Bagarello et al., 2024, 2022).

Taking into account that sieved soil was used, a given dataset was summarized by the arithmetic mean and the associated coefficient of variation (CV). To compare two datasets, F and two-tailed t tests at $p = 0.05$ were performed. Comparing two datasets at a time was preferred over performing a simultaneous comparison among the three soils since establishing differences between, e.g., the AR and OR soils does not depend on the information collected on the LE soil. Statistical significance of the fitted relationships to the data was tested by a two-tailed t test at $p = 0.05$ (Glantz, 2012).

To establish if two K_s values differed appreciably or not, in addition to the statistical analysis it was considered that literature provides some suggestion on the similarity between two K_s values depending on their mutual deviation. In investigations on undisturbed field soils, K_s values differing by two or three times could be considered relatively similar given the wide range of possible K_s values and the extreme variability of this soil hydrodynamic parameter found in the field (Elrick and Reynolds, 1992). In the absence of any perturbation embedded in field and laboratory measurements (measurement error, random noise, natural variability), such as when numerically simulated data are used, two K_s values can be considered practically equal if they differ by no more than 1.25 times (Reynolds, 2013). Adapting these suggestions to this investigation, differences by < 1.25, 1.25 – 3 and > 3 times were considered negligible, moderate and appreciable, respectively.

A.2.3. Results

A.2.3.1 Soil textural characteristics

The AR and LE soils used in this investigation had a similar mean weight diameter, MWD, equal to 0.53 mm in the former case and 0.57 mm in the latter one (**Fig. 2**). A higher MWD value was obtained for the OR soil (0.70 mm). Therefore, in an undispersed status, this last soil was overall a little coarser (higher MWD value by 22-30%) than the other two soils. Undispersed particles larger than 0.25 mm represented the 64.6% of all particles for the AR soil, the 52.7% for the LE soil and the 67.9% for the OR soil. Therefore, the LE soil had a similar content of relatively large (> 0.25 mm) and relatively small (< 0.25 mm) particles. Instead, the coarser particles prevailed over the finer ones in both the AR and OR soils.

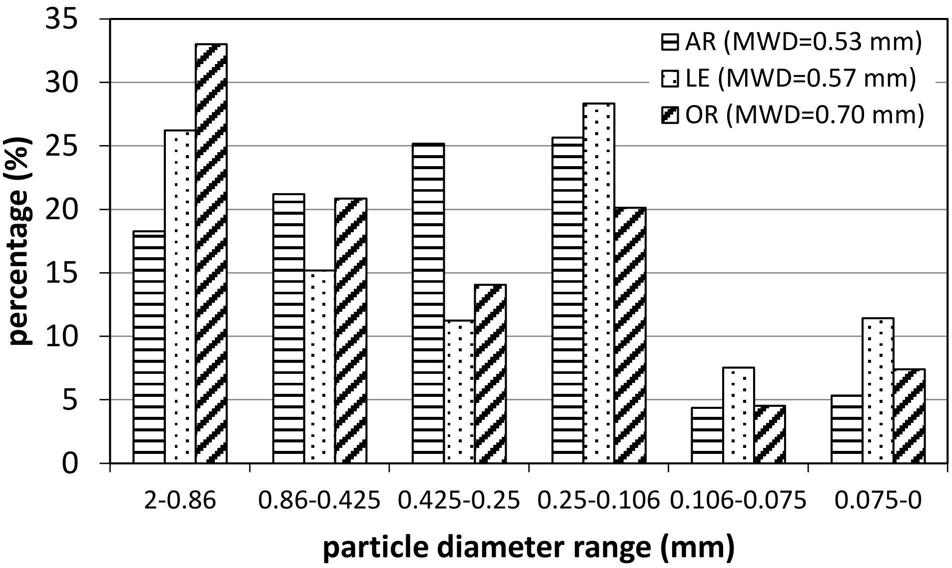

Fig. 2. Percentage by weight of the undispersed soil particles of given size ranges for the three sampled soils (AR, LE, OR).

However, the distribution of the coarser particles differed between these two soils. The AR soil was relatively poor in 2-0.86 mm particles (18.3%) and relatively rich in 0.425-0.25 mm particles (25.2%). Instead, the OR soil was richer in 2-0.86 mm particles (33.0%) and poorer in 0.425-0.25 mm particles (14.1%). The content of 0.86-0.425 mm particles was similar for these two soils (21.2% and 20.8% for the AR and OR soils, respectively).

A.2.3.2 Soil compaction experiment

Using the SCA with different combinations between the number of blows (NB) and the height of fall (HF) of the compacting pestle yielded gravitational potential energy, E_p, values varying from a minimum of 1 kJ/m^2 (NB = 5; HF = 5 cm) to a maximum of 100 kJ/m^2 (NB = 50; HF = 50 cm). Therefore, depending on the run, a soil layer received a widely different energy since E_p varied by two orders of magnitude.

Depending on the E_p value, the final height, h_f, of the N = 50 air-dry soil columns ranged from 17.0 to 20.2 cm for the AR soil, 14.3 to 16.7 cm for the LE soil and 17.2 to 21.5 cm for the OR soil. Therefore, compaction was more effective in the LE soil than in the AR and OR soils.

The means of θ_i were similar among the three tested soils since they varied between 0.03 (LE and OR soils) and 0.04 (AR soil) cm^3/cm^3 with CV values ranging from 4% to 6%, depending on the soil.

The means of the 50 ρ_b values for the AR and OR soils differed by a non-significant 1.0% (Table 2). A significantly higher ρ_b value was obtained with the LE soil. In particular, the mean of ρ_b of this last soil was 25.8% higher than that of the AR soil and 27.1% higher as compared with the OR soil. Variability of ρ_b decreased according to the OR (CV = 5.3%) > AR (4.6%) > LE (3.7%) sequence. Therefore, in the tested range of E_p values, the ρ_b values for the LE soil were overall higher and less variable than those of the other two soils.

The means of K_s for the AR and OR soils differed by a non-significant 0.8% but they differed significantly from the LE soil, yielding a 7.3-7.4 times smaller value (Table 2). Even the variability of K_s decreased according to the OR (CV = 105%) > AR (73%) > LE (29%) sequence. Therefore, the K_s values for the LE soil were appreciably smaller and less variable than those of the other two soils.

Table 2. Summary statistics of the dry soil bulk density, ρ_b, and saturated soil hydraulic conductivity, K_s, values obtained for the AR, LE and OR soils with different combinations between number of blows and height of fall of the compacting pestle (sample size, N = 50 for each dataset).

Parameter	Statistic	AR	LE	OR
ρ_b (g/cm^3)	Min	1.030	1.325	0.976
	Max	1.249	1.564	1.220
	Mean	1.136 (a)b	1.429 (a)(c)	1.124 b(c)
	CV (%)	4.6	3.7	5.3
K_s (mm/h)	Min	45.6	12.5	26.0
	Max	629.4	41.9	743.7
	Mean	167.0 (a)b	22.6 (a)(c)	165.7 b(c)
	CV (%)	73.2	29.0	105.0

For a given parameter, values followed by the same lowercase letter enclosed in parenthesis were significantly different according to an F test and a two-tailed t test at p = 0.05. Values followed by the same lowercase letter not enclosed in parenthesis were not significantly different.

For all soils, the dry bulk density increased with E_p according to a statistically significant (coefficients of determination, $R^2 \geq 0.76$) power relationship (**Fig. 3a**). There was a clear similarity between the ρ_b vs. E_p curves for the AR and OR soils even if the ρ_b vs. E_p relationship was more scattered for the latter soil ($R^2 = 0.76$) than the former one ($R^2 = 0.84$). The relationship for the LE soil was placed above those obtained with the other two soils and it had an R^2 value of 0.88, rather similar to that of the AR soil. Therefore, more dissipated energy at the surface of a soil layer implied more compaction, as expected. Moreover, all factors of the experiment being equal, a given E_p value determined a soil-dependent ρ_b value.

The three ρ_b vs. E_p relationships appeared nearly parallel, suggesting that, for the three tested soils, a given increase of E_p induced a similar increase of ρ_b in absolute value. For example, ρ_b was predicted to vary between 1.02 and 1.33 g/cm^3 for E_p = 1 kJ/m^2, depending on the soil, and it increased by 0.18-0.20 g/cm^3 with E_p = 100 kJ/m^2, regardless of the soil. In all cases, most of the increase of ρ_b was detected in the range of the smaller E_p values. For example, the 63-64% of the increase of ρ_b predicted for an increase of E_p from 1 to 100 kJ/m^2 occurred as E_p increased from 1 to 20 kJ/m^2.

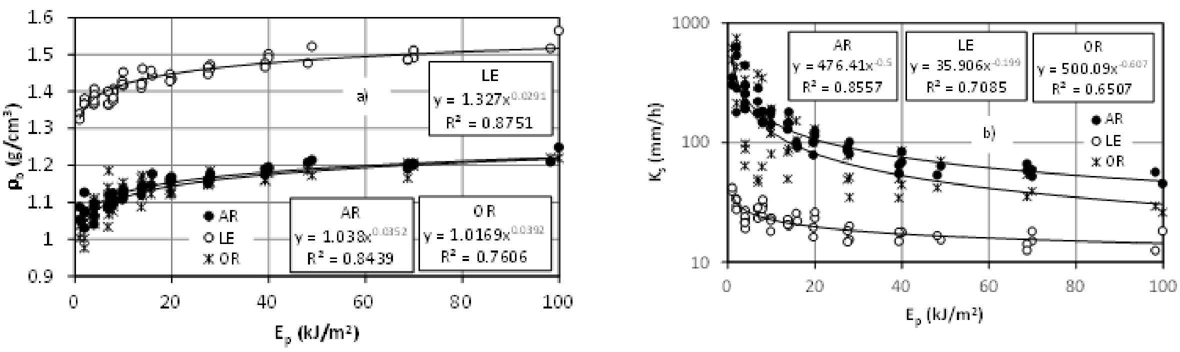

(a) **(b)**

Fig. 3. Dry soil bulk density, ρ_b (**a**), and saturated soil hydraulic conductivity, K_s (**b**), against the gravitational potential energy, E_p, for the three tested soils (AR, LE, OR).

The saturated soil hydraulic conductivity decreased with E_p for all soils according to a statistically significant power relationship yielding the highest and the lowest R^2 values for the AR ($R^2 = 0.86$) and OR ($R^2 = 0.65$) soils, respectively (**Fig. 3b**). According to the fitted relationships, a difference was noticed between the LE soil on one side and the AR and OR soils on the other side.

In the case of the LE soil, the K_s value corresponding to the lowest compaction energy was relatively small (K_s = 35.9 mm/h for E_p = 1 kJ/m^2) and an increase of E_p up to 100 kJ/m^2 induced a decrease of K_s by 2.5 times. An appreciable percentage of this decrease occurred in a range of relatively small E_p values. For example, K_s decreased by 1.8 times as E_p increased from 1 to 20 kJ/m^2. This decrease represented the 73% of the decrease occurring by considering a fivefold wider range of E_p values (from 1 to 100 kJ/m^2).

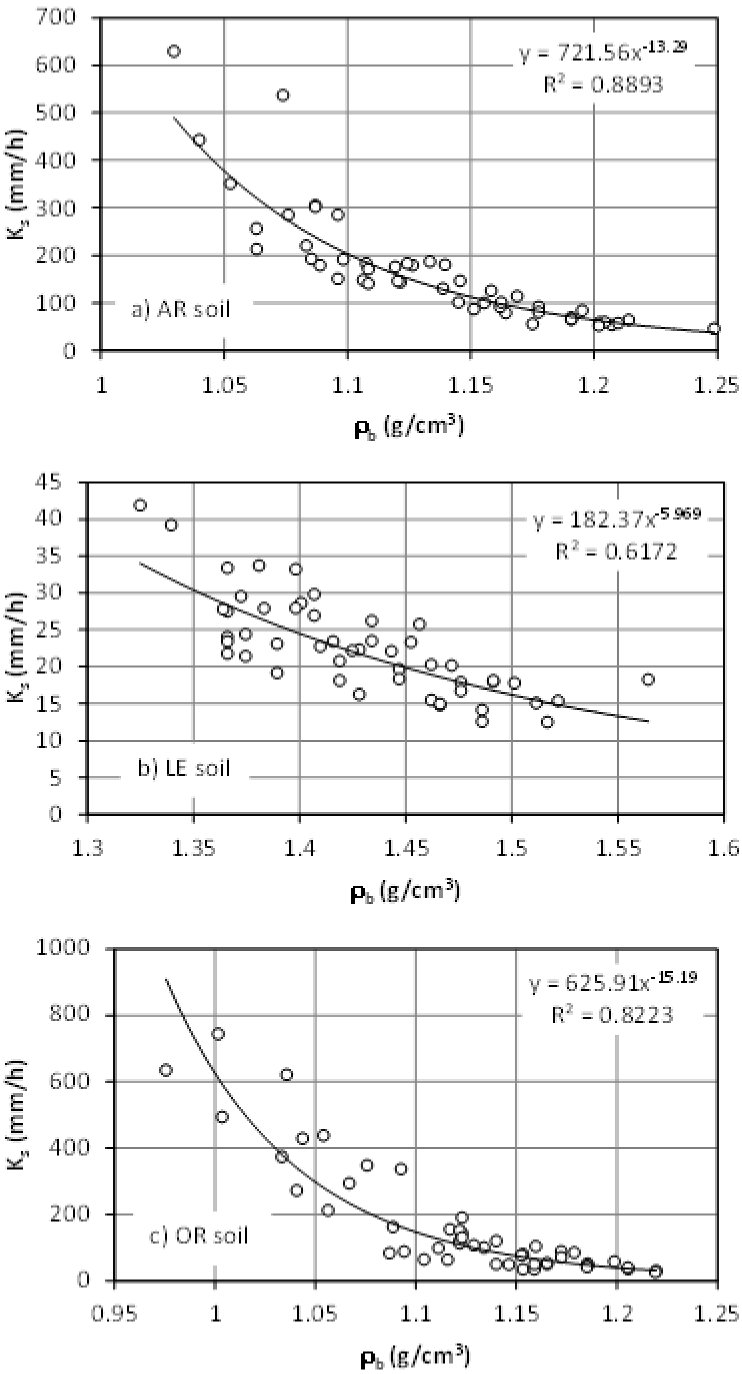

(a) (b) (c)

Fig. 4. Relationship between the saturated soil hydraulic conductivity, K_s, and the dry soil bulk density, ρ_b, for the AR (**a**), LE (**b**) and OR (**c**) soils.

Instead, with the AR and OR soils, a much higher K_s value was obtained for E_p = 1 kJ/m^2 (476.4 and 500.1 mm/h, respectively) and the overall decrease of K_s in the 1 < E_p < 100 kJ/m^2 range was noticeable, since K_s was predicted to decrease by exactly an order of magnitude for the former soil and by 16.4 times for the latter one. In these two soils, even a relatively limited increase of E_p induced an appreciable decrease of K_s but this decrease represented a relatively small percentage of the total decrease for a wider range of E_p values. For example, the increase of E_p from 1 to 20 kJ/m^2 induced a decrease of K_s by 4.5 (AR soil) or 6.2 (OR soil) times and these reductions represented the 45%

(AR soil) and the 38% (OR soil) of those occurring with a fivefold wider range of E_p values (from 1 to 100 kJ/m^2).

Regardless of the soil, K_s decreased as ρ_b increased (**Fig. 4**), in accordance with many other investigations (Assouline, 2006; Gao et al., 2018; Ma et al., 2023; Tian et al., 2019; Xu et al., 2021; Zhang and Wang, 2023). All fitted relationships were statistically significant, since $R^2 \geq 0.62$ was obtained, but the K_s vs. ρ_b relationship for the LE soil was weaker than those for the AR and OR soils. All K_s vs. ρ_b relationships appeared physically plausible taking into account that they should theoretically yield $K_s = 0$ when ρ_b coincides with the soil particle density, ρ_s, since, in this limiting case, the soil porosity is null. In particular, the predicted K_s values for $\rho_b = \rho_s = 2.65$ g/cm^3 were equal to 0.002 (AR soil), 0.54 (LE soil) and 0.0002 (OR soil) mm/h and hence close or very close to zero.

A.2.3.3 Comparison with other datasets

For all soils (AR, LE, OR), the K_s vs. ρ_b relationships obtained in this investigation yielded smaller predictions of K_s as compared with the measured values by Bagarello et al. (Bagarello et al., 2024, 2022) (**Fig. 5**). In particular, two corresponding values of K_s differed by 1.3 times for the AR soil considered by Bagarello et al. (Bagarello et al., 2022) and by 1.8 (AR soil), 1.6 (LE soil) and 3.6 (OR soil) times as compared with the data by Bagarello et al. (Bagarello et al., 2024). Therefore, differences between the previous K_s data (Bagarello et al., 2024, 2022) and those predicted by the developed K_s vs. ρ_b relationships were moderate in three cases and appreciable in a case. In this last case, however, the threshold discriminating between moderate and appreciable differences was exceeded by only a little (3.6 against 3.0).

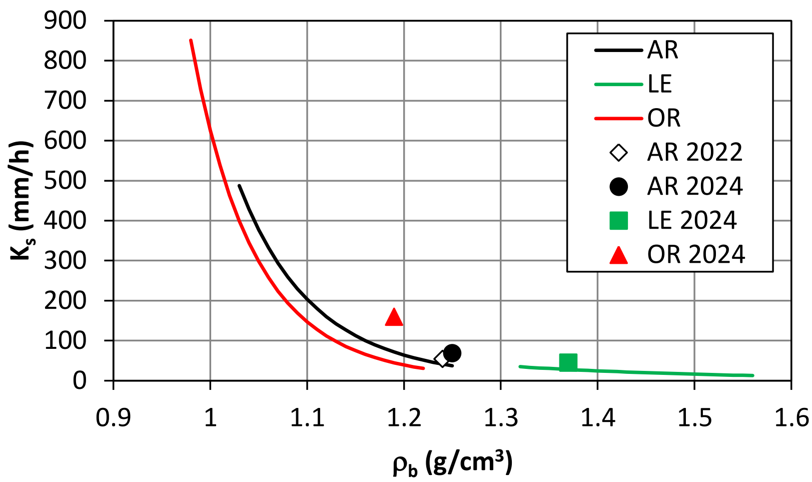

Fig. 5. Comparison between the saturated soil hydraulic conductivity, K_s, against dry soil bulk density, ρ_b, relationships obtained in this investigation for three soils (AR, LE, OR) and the (K_s, ρ_b) data pairs obtained for the same soils in other investigations (Bagarello et al., 2024, 2022).

A.2.4. Discussion

A.2.4.1 Soil compaction effects

This investigation suggested that the K_s vs. E_p relationship (**Fig. 3b**) varied with the textural characteristics of the undispersed soil (**Fig. 2**). In particular, under a low compaction force (small E_p value), K_s was greater for the AR and OR soils (476 and 500 mm/h for E_p = 1 kJ/m^2, respectively) than the LE soil (36 mm/h) probably because the coarser particles (> 0.25 mm) predominated over the finer ones in the former two soils (65-68%) but not in the latter one (53%). Therefore, the AR and OR soils had more of a coarse soil response while the LE soil behaved more like a finer soil.

The functionally finer soil was affected by the dissipated compaction energy less than a coarser soil, as suggested by the higher (closer to zero) exponent of the K_s vs. E_p relationship for the LE soil as compared with the other two soils. In the former case, it appeared that the arrangement of the soil particles constituting the sampled porous medium stabilized early, that is in response to a relatively limited compaction energy, and the increase in this energy modified the arrangement of the soil particles only a little. The more negative exponents of the K_s vs. E_p relationships obtained for the AR and OR soils suggested that, for these soils, a more effective breakdown of soil aggregates, the breakdown of more aggregates and a closer contact between particles occurred as compaction energy increased.

The difference ($P_{d0.25}$) between the percentage of undispersed particles > 0.25 mm and the corresponding percentage for the dispersed soil is indicative of the presence of large, and presumably unstable (Márquez et al., 2004), aggregates. In this investigation, $P_{d0.25}$ was equal to 44.7%, 40.5% and 50.4% for the AR, LE and OR soils, respectively. Taking into account that the exponent of the K_s vs. E_p relationship (**Fig. 3b**) became more negative from the LE soil (-0.20) to the OR soil (-0.61), the calculation of $P_{d0.25}$ suggested that the sensitivity of K_s to the applied compaction energy increased as the percentage of unstable aggregates increased.

The circumstance that the effect of the compaction energy on K_s increased from the LE soil (decrease of K_s by 2.5 times for E_p increasing from 1 to 100 kJ/m^2) to the OR soil (corresponding decrease of K_s by 16.4 times) was consistent with the detected changes in dry soil bulk density as E_p increased from 1 to 100 kJ/m^2 (**Fig. 3a**) since ρ_b was predicted to increase by 14.3% for the LE soil, 17.6% for the AR soil and 19.8% for the OR soil. In other words, the more reactive soil to E_p in terms of K_s was also the more reactive soil with reference to ρ_b.

The investigation also suggested that, if the K_s value of the little compacted soil is small, the expectation could be that the largest part of the overall limited decrease of K_s will occur in a relatively narrow range of rather small E_p values. Instead, if the K_s value of a little compacted soil is relatively high, the decrease of K_s associated with a relatively narrow range of rather small E_p values can be appreciable but it can only represent a relatively small percentage of the possible decrease with a wider range of E_p values.

Trying to generalize these results, it seems that soil compaction effects on the determination of K_s with the SFH technique could be expected to depend on the characteristics of the undispersed fine soil particles (< 2 mm) used for the experiment. If the soil mass is mainly composed by elementary particles, the soil compaction energy should have a relatively limited effect on the determination of K_s since even a small or relatively small compaction force is enough to induce a nearly stable arrangement of the particles that constitute the soil sample. If, instead, the fine fraction includes aggregates of smaller particles, it is plausible to believe that compaction effects will be influenced by the stability of these aggregates (Levy and Miller, 1997) and hence on the factors that can influence this stability, such as their size or the clay and soil organic matter content (Le Bissonnais and Arrouays, 1997; Levy and Mamedov, 2002; Márquez et al., 2004; Tanner et al., 2021). Consequently, it appears plausible to suggest that the shape of the relationship between K_s and E_p should be expected to change from soil to soil.

In particular, K_s could decrease only slowly as E_p increases if a small compaction energy is enough to prepare a stable soil sample in which the internal arrangement of the soil particles does not vary much as a consequence of more compaction energy. This could be the case, for example, of a soil essentially made up of elementary particles.

If the soil has a high percentage of unstable aggregates, the K_s vs. E_p relationship could present an initial sharply decreasing trend followed by a nearly stable or slowly decreasing branch. Initially, a small increase in the dissipated energy promotes a noticeable alteration of the soil sample. However, a stabilization is reached relatively soon and then the relationship becomes nearly horizontal or decreases slowly because almost all possible alterations have occurred.

If, instead, the soil contains aggregates differing by their stability, the decrease of K_s with E_p could be more gradual since a small energy destroys only some aggregates but a larger energy is necessary to also destroy more stable aggregates.

Experimentally determining the K_s vs. E_p relationships for other soils is necessary to verify if, and to what extent, the suggested reasoning finds any support.

According to the fitted K_s vs. E_p relationships of **Figure 3b**, the ratio between the highest and the lowest estimate of K_s for the three soils decreased monotonically from 13.9 for E_p = 1 kJ/m^2 to 3.3 for E_p = 100 kJ/m^2. This result yielded some support to the suggestion that the saturated hydraulic conductivity of different disturbed soils could tend to collapse towards a rather narrow range of small values (Bagarello et al., 2024; Bagarello and David, 2020).

Detecting differences among the three soils that varied with E_p (large for small compaction energies but relatively small for large compaction energies) also confirmed the importance of describing, in the investigations on sieved and repacked soil samples, the compaction methodologies also with reference to the energy transferred to the soil. Although this is not the first time that this suggestion has been given (e.g., (Sridharan and Sivapullaiah, 2005)), information on the applied energy is rarely reported. A consequence is that, without this information, two investigations methodologically identical in several aspects but not detailed with reference to the sample preparation method cannot be confidently compared with each other.

This investigation only considered air-dry soil to prepare the soil columns. This circumstance on the one hand implies the need to carry out further experiments with different initial soil water content values (Blanco-Canqui et al., 2009; Huo et al., 2022) also adapting, if necessary, the K_s determination method, given that the SFH technique cannot be applied on an initially saturated soil column. On the other hand, however, it is believed that the data reported in this study may have a general interest to the scientific community since preparation of initially air-dry soil columns is common in hydrologically relevant investigations (Assouline, 2006; Assouline and Narkis, 2011; Gupta and Staple, 1964; Miyazaki et al., 1984; Smettem et al., 1995; Zhang and Wang, 2023).

A.2.4.2 Comparison with other datasets

The K_s vs. ρ_b relationships developed in this investigation consistently predicted moderately or, in a case, appreciably smaller K_s values than those obtained by Bagarello et al. (Bagarello et al., 2024, 2022) (**Fig. 5**). This result was not surprising since the comparison was established between two experiments differing by several factors including the point where the soil was collected at the field sites, the applied packing method (SCA in this investigation vs. manual packing in (Bagarello et al., 2024, 2022)) and the diameter of the soil column (5.3 cm in this investigation vs. 9.3 cm in the other investigations).

Packing may be expected to induce the formation of longitudinally and laterally non-uniform soil volumes (Gao et al., 2018; Oliviera et al., 1996) as well as the development of relatively large voids in the contact zone between the soil aggregates and the wall of the column (Assouline and Narkis, 2011). Perhaps, the SCA apparatus compacted the soil more effectively as compared with a manual packing procedure. Nor can it be ruled out that the effectiveness of the compaction method did not change appreciably but soil compaction was overall more effective in this investigation since the pressed surface was smaller. It would not be the first time that this interpretation is proposed since, for example, Lewis and Sjöstrom (Lewis and Sjöstrom, 2010) reported that uniformly packing larger columns may be expected to be more difficult. These suggestions should be tested in the future by establishing comparisons between the two packing methods (SCA, manual packing) all other experimental factors being equal.

A.2.4.3 Soil compaction apparatus

With reference to soil compaction, much more sophisticated equipment and investigation methods than those applied in this investigation can be found in the literature (Matthews et al., 2010; Watabe et al., 2000; Whalley et al., 2012). On the one hand, this approach allows to obtain specific information, such as consolidation and shear deformation effects on saturated soil hydraulic conductivity, which cannot likely be obtained with simpler methodologies. On the other hand, however, the experiment is poorly reproducible not because of a lack of information but rather since the costs are high and there is the need of highly specialized personnel. Therefore, investigations such as those mentioned above have a great scientific relevance but simpler experimental methods can help to reduce subjectivity in preparation of disturbed soil columns.

Realization of the SCA does not require any particular manual skills or non-routine construction tools. The cost of the necessary material to produce the device does not exceed a few dozen euros and its construction requires just a few hours of work. Therefore, the apparatus is characterized by a remarkable simplicity of construction and also by its low cost. Further, soil compaction requires choosing a height of falling and a number of blows. Therefore, exactly the same, simple methodology could be applied by different research teams and it could be described with respect to any relevant detail.

Further testing, and perhaps improving, the SCA in a perspective of its common use, at least in certain research area, could help to counteract the tendency not to provide adequate information on the used packed methods (Bromly et al., 2007; Gibert et al., 2014).

A.2.5. Conclusions

An experiment with a nearly homogeneous porous medium is expected to generally yield almost stable values of soil physical and hydraulic properties between replicates since the variability typical of the real soils is purposely removed or minimized. If a single packing method is applied, this expectation has some basis. If the packing method varies, the expectation that the determined soil properties remain nearly constant may lose its foundation since the limited available information about packing method effects suggests that soil properties can change with the applied packing method.

The soil compaction apparatus developed in this investigation seems usable to apply exactly the same packing method in different circumstances and laboratories since it is composed by cheap and easy to assemble components. Moreover, operating the device is simple. The soil compaction energy, E_p, can be determined, taking into account that the mass of the pestle and its height of fall are known.

For three loamy soils, the saturated soil hydraulic conductivity, K_s, determined by a transient infiltration method is expected to decrease as the dry bulk density, ρ_b, of the compacted soil increases. An advantage of the applied methodology is that both K_s and ρ_b can be expressed as a function of the dissipated energy to prepare the soil sample.

A soil having a relatively small value of K_s for small E_p values can be expected to be affected by the dissipated compaction energy less than a soil yielding a relatively high K_s value under the same compaction conditions.

If the saturated hydraulic conductivity of the little compacted soil is small, the largest part of the overall limited decrease of K_s will occur in a relatively narrow range of rather small E_p values. Instead, if the K_s value of a little compacted soil is relatively high, the decrease of K_s associated with a relatively narrow range of rather small E_p values can be appreciable but it can only represent a relatively small percentage of the possible decrease with a wider range of E_p values.

These findings apply to initially air-dry loam soils that remain in contact with flowing water for a short time after being suddenly wetted. Therefore, they cannot be generalized to any soil, antecedent soil water content or laboratory measurement method. In the future, additional experiments on packing effects on the determination of ρ_b and K_s should therefore be carried out in different experimental conditions and on different soils, including the sandy and clayey ones. Describing in more detail than usual the applied packing method, including the applied compaction energy, in the investigations dealing with physical and hydraulic properties of sieved and repacked soil appears necessary both to interpret the results of an investigation with greater confidence and to make it possible to replicate them in other laboratories. The soil compaction apparatus and the packing procedure applied in this investigation appear a good candidate method to prepare repacked soil samples and to describe in detail the soil compaction stage. Hopefully, the results of this investigation could contribute to the development of accepted guidelines to standardize packing procedures even in the awareness that different types of experiments may require different experimental approaches.

Potentially, the suggested methodology to prepare a soil column has a wider field of use than the one tested in this investigation. For example, it could be used without any adaption with a miniaturized tension infiltrometer to also study unsaturated soil flow processes. These investigations could be of interest to test water quality or soil amendment effects on the soil hydrodynamic response in both the saturated and the close to saturation regions.

REFERENCES

Abdulkareem, J.H., Abdulkadir, A., James, T.T., 2023. Effect of Compaction Energy on Selected Physical and Hydraulic Properties of Soils Amended With Different Sources of Organic Matter. Diyala Agricultural Sciences Journal 15. https://doi.org/10.52951/dasj.23150209

American Society for Testing and Materials, 2021. ASTM D698 - 12: Standard Test Methods for Laboratory Compaction Characteristics of Soil Using Standard Effort (12,400 ft-lbf/ft 3 (600 kN-m/m 3)) 1. ASTM International D698 − 12.

Armenise, E., Simmons, R.W., Ahn, S., Garbout, A., Doerr, S.H., Mooney, S.J., Sturrock, C.J., Ritz, K., 2018. Soil seal development under simulated rainfall: Structural, physical and hydrological dynamics. J Hydrol (Amst) 556, 211–219. https://doi.org/10.1016/j.jhydrol.2017.10.073

Assouline, S., 2006. Modeling the Relationship between Soil Bulk Density and the Hydraulic Conductivity Function. Vadose Zone Journal 5. https://doi.org/10.2136/vzj2005.0084

Assouline, S., Narkis, K., 2011. Effects of long-term irrigation with treated wastewater on the hydraulic properties of a clayey soil. Water Resour Res 47. https://doi.org/10.1029/2011WR010498

ASTM International, 2012. ASTM, D1557-12, Standard Test Methods for Laboratory Compaction Characteristics of Soil Using Modified Effort, ASTM International, West Conshohocken, PA, 2012. ASTM Standard Guide 91.

Autovino, D., Bagarello, V., Caltabellotta, G., Varadi, F.K., Zanna, F., 2024. One-dimensional infiltration in a layered soil measured in the laboratory with the mini-disk infiltrometer. Journal of Hydrology and Hydromechanics 72, 149–157. https://doi.org/10.2478/johh-2024-0001

Bagarello, V., Caltabellotta, G., Iovino, M., 2024. Soil reuse effects on determination of saturated hydraulic conductivity of different loamy soils. Eur J Soil Sci 75. https://doi.org/10.1111/ejss.13454

Bagarello, V., Caltabellotta, G., Iovino, M., 2022. Manual packing and soil reuse effects on determination of saturated hydraulic conductivity of a loam soil. Geoderma 405. https://doi.org/10.1016/j.geoderma.2021.115465

Bagarello, V., David, S.M., 2020. Run duration effects on the hydrodynamic properties of a loam soil estimated by steady-state infiltration methods. Journal of Agricultural Engineering 51. https://doi.org/10.4081/jae.2020.1075

Bagarello, V., Elrick, D.E., Iovino, M., Sgroi, A., 2006. A laboratory analysis of falling head infiltration procedures for estimating the hydraulic conductivity of soils. Geoderma 135. https://doi.org/10.1016/j.geoderma.2005.12.008

Bagarello, V., Iovino, M., Elrick, D., 2004. A Simplified Falling-Head Technique for Rapid Determination of Field-Saturated Hydraulic Conductivity. Soil Science Society of America Journal 68, 66–73. https://doi.org/10.2136/sssaj2004.6600

Blanco-Canqui, H., Stone, L.R., Schlegel, A.J., Lyon, D.J., Vigil, M.F., Mikha, M.M., Stahlman, P.W., Rice, C.W., 2009. No-till Induced Increase in Organic Carbon Reduces Maximum Bulk Density of Soils. Soil Science Society of America Journal 73. https://doi.org/10.2136/sssaj2008.0353

Botyanszká, L., Šurda, P., Vitková, J., Lichner, Igaz, D., 2022. Effect of microplastics on silty loam soil properties and radish growth. Journal of Hydrology and Hydromechanics 70. https://doi.org/10.2478/johh-2022-0018

Bromly, M., Hinz, C., Aylmore, L.A.G., 2007. Relation of dispersivity to properties of homogeneous saturated repacked soil columns. Eur J Soil Sci 58, 293–301. https://doi.org/10.1111/j.1365-2389.2006.00839.x

Concialdi, P., Bagarello, V., Alagna, V., Iovino, M., 2020. Laboratory evaluation of falling-head infiltration for saturated soil hydraulic conductivity determination. Journal of Agricultural Engineering 51. https://doi.org/10.4081/jae.2019.1003

Elrick, D.E., Reynolds, W.D., 1992. Methods for Analyzing Constant-Head Well Permeameter Data. Soil Science Society of America Journal 56. https://doi.org/10.2136/sssaj1992.03615995005600010052x

Gao, Y., Qian, H., Li, X., Chen, J., Jia, H., 2018. Effects of lime treatment on the hydraulic conductivity and microstructure of loess. Environ Earth Sci 77. https://doi.org/10.1007/s12665-018-7715-9

Ghosh, B., Pekkat, S., 2019. Effect of Initial Compaction State on Near-Saturated Hydraulic Conductivity. Journal of Irrigation and Drainage Engineering 145. https://doi.org/10.1061/(asce)ir.1943-4774.0001428

Gibert, O., Hernández, M., Vilanova, E., Cornellà, O., 2014. Guidelining protocol for soil-column experiments assessing fate and transport of trace organics, Demeau. European Union, Brussels, Belgium, Demeau.

Glantz, S.A., 2012. Primer of biostatistics. McGraw-Hill, New York.

Gupta, R.P., Staple, W.J., 1964. Infiltration into Vertical Columns of Soil under a Small Positive Head. Soil Science Society of America Journal 28. https://doi.org/10.2136/sssaj1964.03615995002800060016x

Huo, L., Liu, J., Abbas, A., Ding, Q., Wang, H., Zhou, Z., Meng, L., Bai, Z., 2022. Effects of dry bulk density and water content on compressive characteristics of wet clayey paddy soil. Agron J 114. https://doi.org/10.1002/agj2.21057

Laliberte, G.E., Corey, A.T., Brooks, R.H., 1966. Properties of Unsaturated Porous Media. Hydrology Papers.

Le Bissonnais, Y., Arrouays, D., 1997. Aggregate stability and assessment of soil crustability and erodibility: II. Application to humic loamy soils with various organic carbon contents. Eur J Soil Sci 48. https://doi.org/10.1111/j.1365-2389.1997.tb00183.x

Levy, G.J., Mamedov, A.I., 2002. High-Energy-Moisture-Characteristic Aggregate Stability as a Predictor for Seal Formation. Soil Science Society of America Journal 66. https://doi.org/10.2136/sssaj2002.1603

Levy, G.J., Miller, W.P., 1997. Aggregate Stabilities of Some Southeastern U.S. Soils. Soil Science Society of America Journal 61. https://doi.org/10.2136/sssaj1997.03615995006100040024x

Lewis, J., Sjöstrom, J., 2010. Optimizing the experimental design of soil columns in saturated and unsaturated transport experiments. J Contam Hydrol 115, 1–13. https://doi.org/10.1016/j.jconhyd.2010.04.001

Ma, J., Qiu, Y., Gao, Y., An, Y., Duan, Z., Li, S., 2023. Effects of Sample Preparation Methods on Permeability and Microstructure of Remolded Loess. Water (Switzerland) 15. https://doi.org/10.3390/w15193469

Márquez, C.O., Garcia, V.J., Cambardella, C.A., Schultz, R.C., Isenhart, T.M., 2004. Aggregate-Size Stability Distribution and Soil Stability. Soil Science Society of America Journal 68. https://doi.org/10.2136/sssaj2004.7250

Matthews, G.P., Laudone, G.M., Gregory, A.S., Bird, N.R.A., De, A.G., Whalley, W.R., 2010. Measurement and simulation of the effect of compaction on the pore structure and saturated hydraulic conductivity of grassland and arable soil. Water Resour Res 46. https://doi.org/10.1029/2009WR007720

Miyazaki, T., Nielsen, D.R., MacIntyre, J.L., 1984. Early stage infiltration of water into horizontal and vertical soil columns. Hilgardia 52. https://doi.org/10.3733/hilg.v52n06p024

Moody, J.A., Kinner, D.A., Úbeda, X., 2009. Linking hydraulic properties of fire-affected soils to infiltration and water repellency. J Hydrol (Amst) 379. https://doi.org/10.1016/j.jhydrol.2009.10.015

Moutier, M., Shainberg, I., Levy, G.J., 1998. Hydraulic Gradient, Aging, and Water Quality Effects on Hydraulic Conductivity of a Vertisol. Soil Science Society of America Journal 62. https://doi.org/10.2136/sssaj1998.03615995006200060003x

Mubarak, I., Mailhol, J.C., Angulo-Jaramillo, R., Ruelle, P., Boivin, P., Khaledian, M., 2009. Temporal variability in soil hydraulic properties under drip irrigation. Geoderma 150, 158–165. https://doi.org/10.1016/j.geoderma.2009.01.022

Nimmo, J.R., Akstin, K.C., 1988. Hydraulic Conductivity of a Sandy Soil at Low Water Content After Compaction by Various Methods. Soil Science Society of America Journal 52. https://doi.org/10.2136/sssaj1988.03615995005200020001x

Oliviera, I.B., Demond, A.H., Salehzadeh, A., 1996. Packing of Sands for the Production of Homogeneous Porous Media. Soil Science Society of America Journal 60, 49–53. https://doi.org/10.2136/sssaj1996.03615995006000010010x

Petersen, C.T., Hansen, E., Larsen, H.H., Hansen, L. V., Ahrenfeldt, J., Hauggaard-Nielsen, H., 2016. Pore-size distribution and compressibility of coarse sandy subsoil with added biochar. Eur J Soil Sci 67. https://doi.org/10.1111/ejss.12383

Reicosky, D.C., Voorhees, W.B., Radke, J.K., 1981. Unsaturated Water Flow Through a Simulated Wheel Track. Soil Science Society of America Journal 45, 3–8. https://doi.org/10.2136/sssaj1981.03615995004500010001x

Reynolds, W.D., 2013. An assessment of borehole infiltration analyses for measuring field-saturated hydraulic conductivity in the vadose zone. Eng Geol 159, 119–130. https://doi.org/10.1016/j.enggeo.2013.02.006

Reynolds, W.D., Elrick, D.E., 1987. A laboratory and numerical assessment of the guelph permeameter method. Soil Sci 144. https://doi.org/10.1097/00010694-198710000-00008

Smettem, K.R.J., Ross, P.J., Haverkamp, R., Parlange, J.Y., 1995. Three-Dimensional Analysis of Infiltration from the Disk Infiltrometer: 3. Parameter Estimation Using a Double-Disk Tension Infiltrometer. Water Resour Res 31. https://doi.org/10.1029/95WR01722

Sridharan, A., Sivapullaiah, P.V., 2005. Mini compaction test apparatus for fine grained soils. Geotechnical Testing Journal 28. https://doi.org/10.1520/gtj12542

Stock, O., Downes, N.K., 2008. Effects of additions of organic matter on the penetration resistance of glacial till for the entire water tension range. Soil Tillage Res 99. https://doi.org/10.1016/j.still.2008.02.002

Tanner, S., Katra, I., Argaman, E., Ben-Hur, M., 2021. Mechanisms and processes affecting aggregate stability and saturated hydraulic conductivity of top and sublayers in semi-arid soils. Geoderma 404. https://doi.org/10.1016/j.geoderma.2021.115304

Teng, J., Kou, J., Zhang, S., Sheng, D., 2019. Evaluating the Influence of Specimen Preparation on Saturated Hydraulic Conductivity Using Nuclear Magnetic Resonance Technology. Vadose Zone Journal 18. https://doi.org/10.2136/vzj2018.09.0179

Tian, Z., Kool, D., Ren, T., Horton, R., Heitman, J.L., 2019. Approaches for estimating unsaturated soil hydraulic conductivities at various bulk densities with the extended Mualem-van Genuchten model. J Hydrol (Amst) 572. https://doi.org/10.1016/j.jhydrol.2019.03.027

Viviani, G., Iovino, M., 2004. Wastewater Reuse Effects on Soil Hydraulic Conductivity. Journal of Irrigation and Drainage Engineering 130, 476–484. https://doi.org/10.1061/(asce)0733-9437(2004)130:6(476)

Watabe, Y., Leroueil, S., Le Bihan, J.P., 2000. Influence of compaction conditions on pore-size distribution and saturated hydraulic conductivity of a glacial till. Canadian Geotechnical Journal 37. https://doi.org/10.1139/t00-053

Whalley, W.R., Matthews, G.P., Ferraris, S., 2012. The effect of compaction and shear deformation of saturated soil on hydraulic conductivity. Soil Tillage Res 125. https://doi.org/10.1016/j.still.2012.05.020

Xu, P., Zhang, Q., Qian, H., Li, M., Yang, F., 2021. An investigation into the relationship between saturated permeability and microstructure of remolded loess: A case study from Chinese Loess Plateau. Geoderma 382. https://doi.org/10.1016/j.geoderma.2020.114774

Zhang, J., Lei, T., Yin, Z., Hu, Y., Yang, X., 2017. Effects of time step length and positioning location on ring-measured infiltration rate. Catena (Amst) 157, 344–356. https://doi.org/10.1016/j.catena.2017.05.013

Zhang, L., Wang, J., 2023. Prediction of the soil saturated hydraulic conductivity in a mining area based on CT scanning technology. J Clean Prod 383. https://doi.org/10.1016/j.jclepro.2022.135364

A.3: Determining saturated hydraulic conductivity of a repacked loam soil by the simplified falling-head technique: impact of sieving duration and scraping of exposed surfaces

Dario Autovino[1*], Vincenzo Bagarello[1], Gaetano Caltabellotta[1], Mariachiara Fusco[1], Massimo Iovino[1]

[1] Department of Agricultural, Food and Forest Sciences, University of Palermo, Viale delle Scienze, 90128, Palermo, Italy.
*Corresponding author: dario.autovino@unipa.it

Abstract: Many methods are used in laboratory for packing sieved soil. Determination of soil properties is expected to vary with the applied packing method. The objective of this investigation was to test the impact of initial soil sieving duration and scraping of exposed soil surfaces on saturated hydraulic conductivity, K_s, of an initially air-dry loam soil determined by the simplified falling-head technique. Two sieving durations (5 and 30 min) were considered. A brush was used to scrape exposed surfaces for half of the tested soil columns. A long sieving yielded a finer soil than a short sieving and 9-22% smaller values of K_s. Scraping the exposed soil surfaces yielded 4-17% smaller K_s values than those obtained on the not scraped columns. None of the observed differences was statistically significant. Therefore, sieving duration and treatment of the exposed soil surfaces were minor factors influencing determination of K_s. Reaching general conclusions about sieving duration and scraping effects requires testing these factors with other soils, initial soil water conditions and K_s measurement techniques.

Keywords: Soil column preparation method; saturated soil hydraulic conductivity; undispersed particle size distribution; hydraulic continuity.

A.3.1 INTRODUCTION

Determining the saturated hydraulic conductivity, K_s, of undisturbed field soils is necessary for many agronomic, engineering and environmental activities, such as understanding and predicting water movement or seepage in soils, that can also be expected to depend on the flow direction (Nam et al., 2021; Woessner et al., 2020). Obtaining appropriate K_s values for an intended use is very difficult since this parameter is extremely sensitive to sample size, flow geometry, sample collection procedures and various soil physical-hydrological characteristics (Reynolds et al. 2000). Repacked soil does not represent an alternative to undisturbed soil since repacking alters the characteristics of the porous medium. Nevertheless, saturated conductivity of sieved and repacked soil columns is determined for many reasons such as testing theories (Reynolds & Elrick 1987) or establishing the effects of wastewater (Viviani & Iovino 2004), organic amendment (Bondì et al. 2024), wildfire (Šurda et al. 2023) or rock fragments (Wu et al. 2021) on the soil hydrodynamic behavior as well as serving as input data for numerical simulations (Ghazouani et al. 2015). Working with homogeneous soil columns favors reproducibility of the experiment and hence it makes collaboration between different research teams easier. Despite at least 300 years of experience in the use of soil columns, no standardization of experimental methods has occurred, which complicates comparison between investigations (Lewis & Sjöstrom 2010). Moving towards standardized methods requires considering that many factors could influence experimental results. Sieving duration of an air-dry soil mass and treatment of any exposed soil surface before performing the K_s experiment are two of these factors.

Before preparing a soil column, the porous medium is generally passed through a sieve to include in the sample particles smaller than a given size, frequently fixed at 2 mm, but mechanical sieving duration is rarely reported in scientific papers. The lack of this information is justified if sieving duration does not influence the particle size distribution of the soil used for the experiment. However, Díaz-Zorita et al. (2007) reported that the probability of discriminating between soils increased with a longer sieving duration. According to Bartley et al. (2019), sieving duration influences the probability of a particle to pass through a given sieve. Fomin et al. (2021) suggested that sieving duration is a factor to be considered to define an optimal sieving method. Therefore, it is still necessary to verify if sieving duration is a practically negligible experimental factor.

In some investigations it is explicitly reported that, when the soil sample is prepared by layers, the interface is, and should be, scraped before addition of another soil mass to ensure hydraulic connectivity between the layers since, after compaction, the exposed soil surface could act as a layer with different properties from those of the other portion of the soil column (Lewis & Sjöstrom 2010). We did not find in the literature specific laboratory comparisons between K_s values of scraped and not scraped soil columns. However, the effects of even a thin smeared or compacted soil layer on hydrological processes (Assouline & Mualem, 2006) or field measurement of K_s (Bagarello 1997) are documented. Therefore, scraping impact on laboratory K_s determination should be investigated.

The saturated hydraulic conductivity of an initially unsaturated repacked soil column can be determined in the laboratory from an early-time falling-head infiltration process with the simplified falling-head (SFH) technique, which is also usable in the field (Bagarello et al. 2004). Recently, the dependence of the K_s values obtained by this technique on several factors related with laboratory preparation of an initially air-dry soil column was tested. Investigations were mainly performed on loamy soils and the tested factors included the applied manual method for packing the soil (Bagarello et al. 2022), the reuse of the same soil mass for repeated determinations of K_s (Bagarello et al. 2024), and the relationship between K_s and the dissipated soil compaction energy by a simple laboratory apparatus (Autovino et al. 2024), also taking into account that K_s of repacked soil samples is expected to decrease with increasing bulk density as a response of the smaller volume of coarse pores (Dec et al., 2008). Testing other factors is necessary to better predict the impact of the laboratory preparation method of an initially air-dry soil column on determination of K_s by the SFH technique. This information could also represent a reference for investigations with other soils, initial soil water conditions and K_s measurement techniques.

The general objective of this investigation was to determine how different choices that can be made when a soil column has to be prepared influence determination of saturated hydraulic conductivity of an initially air-dry loam soil with the simplified falling-head technique. The specific objectives were to test dependence of the measured K_s values on i) duration of mechanical sieving; and ii) scraping of exposed soil surfaces during preparation of the soil column.

A.3.2 MATERIALS AND METHODS

A.3.2.1 Soil

The soil was collected at the orchard of the Department of Agricultural, Food and Forest Sciences of the University of Palermo (Italy, 38°06'24'' N, 13°21'06'' E). The soil organic carbon content, determined with the Walkley-Black method, was of 27.1 g/kg. According to the USDA classification system, the sand, silt and clay percentages were equal to 50.7%, 30.3% and 19.0%, respectively, and the soil was classified as loam (Bagarello et al. 2024). A soil mass of nearly 80 kg was collected in the field and it was transported to the laboratory and spread on plastic sheets and manually stirred every two or three days for nearly one month to facilitate natural drying. The gravimetric water content, w (g/g), of this soil was periodically measured. The experiment started as w stabilized at the air-dry value, w_i (g/g). Fresh soil, that is a soil mass never used for other K_s determinations, was used to prepare each soil column in this investigation. A 30 cm diameter and 7 cm high sieve filled with 2-3 kg of air-dry soil was used for sieving the air-dry soil.

A.3.2.2 Soil compaction apparatus

The soil compaction apparatus by Bagarello et al. (2025) was used to prepare a soil column. The apparatus consists of a Teflon pestle sliding inside a Plexiglas guide cylinder and an underlying Plexiglas cylinder containing the soil. The pestle has a diameter of 5 cm, a height of 30 cm and a mass, m_p = 0.89 kg. At its upper end, a screw eyelet connects a rope with a handle. The rope slides through a fixed pulley. The guide cylinder, having an internal diameter, d_c, of 5.3 cm and a height of 50 cm, is aligned with the pulley and secured by metal supports. The container cylinder, also having d_c = 5.3 cm and a height of 25 cm, aligned with the guide cylinder, is equipped at the bottom with a sock and a mesh fixed with a metal band. Compaction involves repeated drops of the pestle from a given height, HF (m). The gravitational potential energy, E_p, dissipated to prepare the soil column is calculated since both the mass of the pestle and the height of fall are known. In particular, for a single blow, E_p (J/m^2) is equal to $m_p \times g \times HF/A$, g (m/s^2) being the acceleration due to gravity and A (m^2) the exposed surface of the soil sample.

A.3.2.3 Saturated soil hydraulic conductivity

The saturated hydraulic conductivity, K_s (L/T), of a soil column was determined by the simplified falling-head (SFH) technique (Bagarello et al. 2004). A fixed water volume was used for each K_s test. The infiltration time, t_a (T), was determined as the time from water application to the instant when all free water disappeared from the soil surface. The following equation was used to calculate K_s:

$$K_s = \frac{\Delta\theta}{t_a(1-\Delta\theta)}\left[\frac{D}{\Delta\theta} - \frac{\left(D+\frac{1}{\alpha^*}\right)}{1-\Delta\theta} ln\left(1+\frac{(1-\Delta\theta)D}{\Delta\theta\left(D+\frac{1}{\alpha^*}\right)}\right)\right] \quad (1.0)$$

in which $\Delta\theta$ (L^3/L^3) is the difference between the saturated (θ_s) and the initial (θ_i) volumetric soil water content, $D = V/A$ (L) is the height of the ponded head of water at $t = 0$, V (L^3) is the applied water volume, A (L^2) is the infiltration surface, and α^* (1/L) is a soil texture/structure parameter that was fixed at 0.012 1/mm (Elrick & Reynolds 1992). In this investigation, θ_i and θ_s were determined using the gravimetric soil water content of the air-dry soil, w_i (g/g), and the dry soil bulk density, ρ_b (g/cm^3), assuming that θ_s coincided with the porosity. Since the soil used to fill the cylinder was air-dry and not oven-dry, ρ_b was determined by the following relationship:

$$\rho_b = \frac{m_s}{V_t} = \frac{m_{ad}}{V_t(1+w_i)} \quad (1.1)$$

where m_s (g) is the mass of the dry soil, V_t (cm^3) is the bulk volume of the soil sample, and m_{ad} (g) is the mass of the air-dry soil.

A.3.2.4. Sieving duration

The soil mass was passed through a 2 mm mechanical sieve. Sieving duration, *SD* (T), was equal to 5 min for a part of the soil and 30 min for another part. The particle size distribution, PSD, of the undispersed soil passing through the sieve was determined without initially treating the soil with H_2O_2 or sodium hexametaphosphate to verify if the different sieving durations had a detectable effect on the fine (< 2 mm) soil particle content. At this aim, the percentages by weight of particles of 2-0.86, 0.86-0.425, 0.425-0.25, 0.25-0.106, 0.106-0.075 and < 0.075 mm were determined. For a given *SD* value, the PSD of $N = 8$ soil samples was determined.

The soil passing through the sieve was used to prepare the soil columns for the SFH runs. A column was prepared with a one-step procedure using 580 g of air-dry soil. The soil was poured in the cylinder and then it was compacted by an established number of blows of the pestle, *NB*, falling from a fixed height, *HF*. In particular, three combinations between *NB* and *HF* were used, that is 10 (*NB*) × 0.10 m (*HF*), 30 × 0.30 m and 50 × 0.50 m. The corresponding E_p values were equal to 4.1 (low, L, compaction energy), 37.0 (intermediate, I, energy) and 102.8 kJ/m^2 (high, H, energy), respectively. The final height, h_f (L), of the soil samples varied on average from 21.5 cm for E_p = 4.1 kJ/m^2 to 20.1 cm for E_p = 102.8 kJ/m^2 for a soil sieved for 5 min and from 20.9 cm (E_p = 4.1 kJ/m^2) to 19.6 (E_p = 102.8 kJ/m^2) with *SD* = 30 min. Taking into account that the SFH technique requires establishing a one-dimensional infiltration process, free water should not appear at the bottom of the column by the end of the run. For this reason, a water volume, V_w (cm^3), equal to the empty pore volume in the upper 75% of the soil column was used to perform each SFH run:

$$V_w = 0.75\, h_f \times \pi \times \frac{d_c^2}{4} \times (\theta_s - \theta_i) \qquad (1.2)$$

The V_w values varied from 142 to 172 cm^3, depending on the soil sample, for *SD* = 5 min and from 127 to 154 cm^3 for *SD* = 30 min. Four different soil columns were prepared for each E_p and *SD* value. Therefore, a dataset of *N* = 24 individual determinations of ρ_b and K_s was obtained (3 E_p values × 2 *SD* values × 4 replicates).

The one-step soil column preparation method was adopted to avoid the risk to introduce, in the developed dataset, some noise due to a possible hydraulic discontinuity in the case of a preparation by layers. The experiment was repeated with three E_p values to recognize a possible effect of the dissipated energy on the differences between the two sieving durations.

A.3.2.5. Scraping

In this experiment, the soil mass passing through a 2 mm mechanical sieve for 5 min was used to prepare the soil columns for the SFH runs. A total of 12 soil columns were prepared with a one-step procedure using 580 g of air-dry soil for each column. The soil was poured in the cylinder and then it was compacted by blowing the pestle 48 times from a height of 0.48 m. Consequently, E_p was equal to 94.7 kJ/m^2. After compaction, the exposed soil surface of six randomly chosen columns was scraped by sliding over the surface a small rigid brush, prepared by sticking several needles into a cork connected to a rod. Other 12 soil columns were prepared with a three-step procedure using 193.3 g of air-dry soil at each step. Each of the three layers was compacted by blowing the pestle 16 times from a height of 0.48 m in order not to change the total dissipated energy for a soil column (E_p = 94.7 kJ/m^2). Also in this case, the exposed soil surfaces of six randomly chosen columns were scraped by the brush. In particular, scraping preceded addition of any new soil mass. Even in this case, eq.(3) was used to determine V_w for each infiltration run. The final height of the 24 soil samples was equal on average to 19.9 cm (coefficient of variation, CV = 1.1%) and the mean V_w value was equal to 142 cm^3 (CV = 2.4%).

A three-step procedure was also used in this experiment to verify if the differences between scraped and not scraped soil columns depended on the number of scraped surfaces in a sample.

A.3.2.6. Statistical analysis

F and two-tailed t tests at P = 0.05 were applied in this investigation to establish comparisons between two datasets with reference to both dry soil bulk density and saturated soil hydraulic conductivity.

A.3.3. RESULTS AND DISCUSSION

A.3.3.1 Sieving duration

Undispersed particles having an equivalent diameter ≥ 0.25 mm represented the 66.5% of all particles when the soil was sieved for 5 min and the 63.6% with SD = 30 min (**Fig. 1**). Therefore, the content of coarse particles was smaller by 2.9 percentage units with a longer sieving. More in detail, sieving duration did not influence appreciably the percentages of 0.86-0.425 and 0.106-0.075 mm particles, since two corresponding percentages differed at the most by 0.3 units. With SD = 5 min, there were more particles of 2-0.86 mm (by 1.7 units) and 0.425-0.25 mm (by 1.1 units) and less particles of 0.25-0.106 mm (by 1.4 units) and 0.075-0 mm (by 1.2 units) as compared with SD = 30 min. Therefore, coarseness of the soil decreased as SD increased. The effect of a longer sieving on the undispersed PSD was similar to that detected as a consequence of using repeatedly the same soil mass for preparing soil columns (Bagarello et al. 2024).

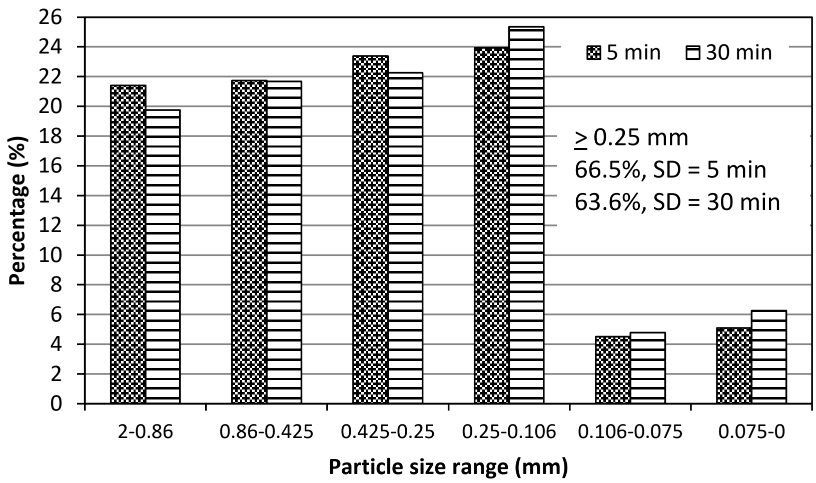

Fig. 1. Percentage by weight of soil particles of a given size range for a sieving duration of 5 and 30 min (each percentage is the mean of eight values)

Regardless of *SD*, the dry soil bulk density, ρ_b, increased as expected (Dec et al., 2008; Shafiq et al. 1994; Autovino et al. 2024) as E_p increased from a L to a H value (**Table 1** and **Fig. 2**). The increase was similar for the two *SD* values (6.6% and 6.0% with *SD* = 5 and 30 min, respectively). For *SD* = 5 min, the largest energy dissipated in this experiment yielded a significantly more compacted soil than that obtained with a small and an intermediate energy but, in this range of relatively small E_p values ($4 \leq E_p \leq 37$ kJ/m^2), the applied energy did not influence significantly ρ_b (Table 1). For *SD* = 30 min, all differences between two means were significant. Regardless of E_p, the ρ_b value obtained with *SD* = 30 min was greater than that obtained with *SD* = 5 min by a percentage varying from 1.0% to 1.9%, depending on E_p. However, the differences between the two *SD* values were not significant.

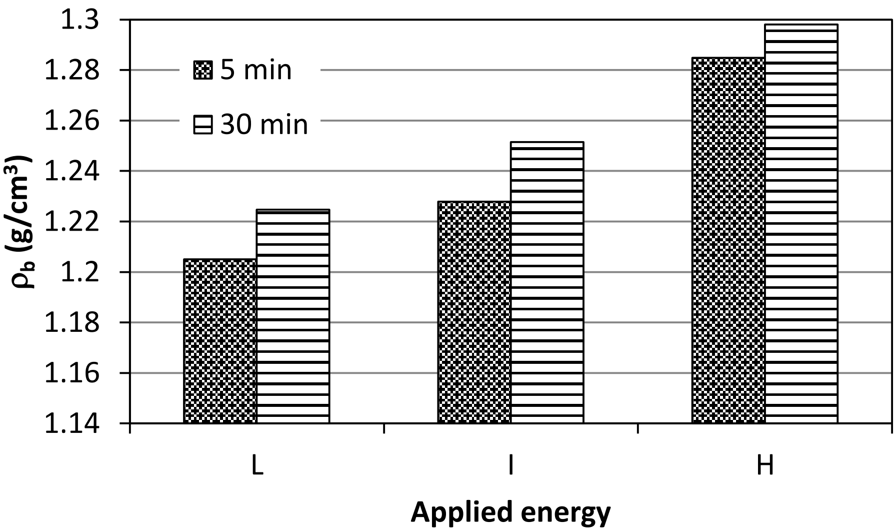

Fig. 2. Mean values of the dry soil bulk density, ρ_b, for two sieving durations, *SD*, and three levels of the applied soil compaction energy, E_p (low, L; intermediate, I; high, H; sample size, $N = 4$ for each *SD* and E_p value)

Table 1. Summary statistics of the dry soil bulk density, ρ_b, and saturated soil hydraulic conductivity, K_s, values obtained for each applied compaction energy, E_p, on soil samples prepared after two different sieving durations (sample size, $N = 4$ for each energy, variable and sieving duration)

E_p	**Statistic**	**ρ_b (g/cm^3)**		**K_s (mm/h)**	
		5 min	**30 min**	**5 min**	**30 min**
Low, L	Min	1.18	1.21	62.4	44.7
(4 kJ/m^2)	Max	1.22	1.25	90.0	67.0
	Mean	1.21 a A (B)	1.22 a (A) (B)	73.4 a (A) (B)	57.5 a (A) (B)
	CV (%)	1.4	1.34	18.1	18.1
Intermediate, I	Min	1.21	1.24	38.6	34.8
(37 kJ/m^2)	Max	1.25	1.26	44.1	43.0
	Mean	1.23 a A (C)	1.25 a (A) (C)	41.4 a (A) (C)	37.7 a (A) (C)
	CV (%)	1.5	0.6	6.6	10.0
High, H	Min	1.26	1.28	25.5	23.3
(103 kJ/m^2)	Max	1.29	1.32	30.2	25.9
	Mean	1.28 a (B) (C)	1.30 a (B) (C)	27.6 a (B) (C)	24.8 a (B) (C)
	CV (%)	1.2	1.2	7.5	4.9

For given compacting energy and variable, values in a row followed by the same lower case letter not enclosed in parenthesis were not significantly different according to an F test and a two-tailed t test at $P = 0.05$. For given variable and sieving duration, values in a column followed by the same upper case letter not enclosed in parenthesis were not significantly different according to an F test and a two-tailed t test at $P = 0.05$. Values followed by the same upper case letter enclosed in parenthesis were significantly different.

The saturated soil hydraulic conductivity, K_s, decreased as E_p increased from L to H for both SD = 5 and 30 min (**Table 1** and **Fig. 3**). In particular, K_s decreased by 62% with SD = 5 min and by 57% with SD = 30 min. For a given SD value, all differences between two means of K_s were significant. Regardless of E_p, the K_s value obtained with SD = 30 min was smaller than that obtained with SD = 5 min by a percentage varying with E_p between 9% and 22%. However, differences between two corresponding means of K_s were not significant.

Differences between the ρ_b and K_s values obtained with the two sieving durations were not so large to be statistically significant. However, sieving duration did not appear to have a totally negligible effect on the tested soil properties since a long sieving yielded numerically larger ρ_b values and smaller K_s values than a short sieving for all applied energies. This last circumstance suggested that the detected differences between the two sieving durations, although small, had a physical explanation and they were not only obtained by chance. A longer sieving implies a larger content of fine particles in the soil used for the experiment (**Fig. 1**). Therefore, there is a greater probability that small particles occupy the empty spaces at the contact zones between the coarser particles. A soil column prepared with a given soil mass will then have a smaller bulk volume and hence a greater ρ_b value (**Fig. 2**). The presence of these small particles makes the pores overall narrower and it induces flow to be more tortuous with the consequence that K_s decreases (**Fig. 3**).

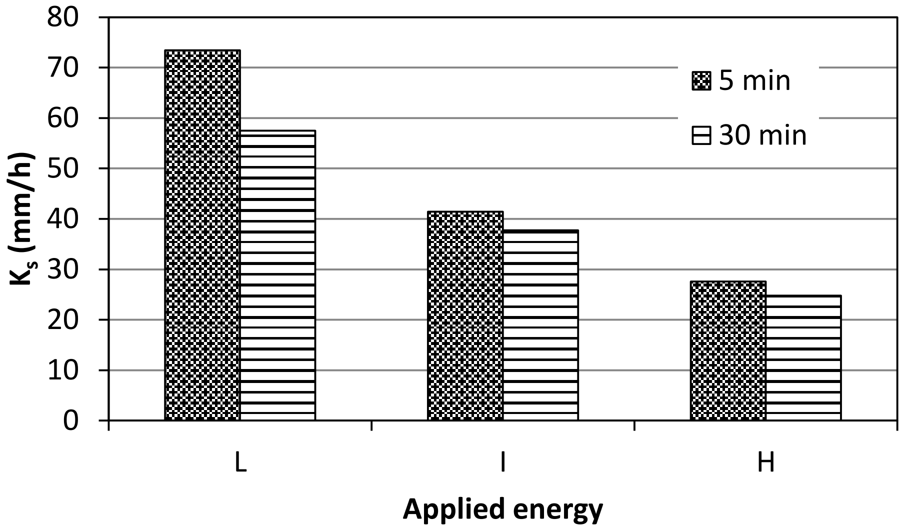

Fig. 3. Mean values of the saturated soil hydraulic conductivity, K_s, for two sieving durations, *SD*, and three levels of the applied soil compaction energy, E_p (low, L; intermediate, I; high, H; sample size, $N = 4$ for each *SD* and E_p value)

According to this investigation, sieving duration was a minor and statistically negligible factor influencing the ρ_b and K_s data. Consequently, two datasets obtained under identical conditions only differing by sieving duration can be considered drawn from the same population. However, the existence of some small differences between the two *SD* values having a plausible physical explanation also suggests that more appreciable effects of sieving duration could be detected in other experimental conditions. In this case, a longer sieving could likely imply preparing a more compacted and less conductive soil column. Sieving duration should be reported in scientific papers (Díaz-Zorita et al. 2007). Two investigations performed with similar sieving durations are comparable with more confidence than two investigations differing appreciably by sieving duration.

A.3.3.2 Scraping

There was not any statistically significant difference between the ρ_b values obtained on the scraped (SC) and the not scraped (NSC) soil columns, regardless of whether the sample was prepared in one or three steps (Table 2). In particular, the percentage difference between two corresponding means, Δ, was equal to 0.6% for the columns prepared in one step and to 0.1% for those prepared in three steps. The SC and NSC columns also yielded statistically similar K_s values for both sample preparation methods. However, the SC and NSC soil columns prepared by a three-step method yielded more similar K_s values than those prepared by a one-step method since Δ was equal to 3.6% in the former case and 16.9% in the latter one.

Regardless of the treatment of the exposed soil surfaces (SC, NSC), preparing the soil sample in three steps yielded significantly higher ρ_b values as compared with those obtained by the one-step method (Δ = 1.5% for the SC columns and 1.0% for the NSC ones). Even K_s was greater with the three- than the one-step method. However, with the SC columns, the difference between the two corresponding means was equal to 26.6% and it was statistically significant. With the NSC columns, the difference was smaller (Δ = 12.2%) and not significant.

The established SC vs. NSC comparisons, yielding not statistically significant and also small differences between corresponding datasets for both sample preparation methods ($\Delta \leq 0.6\%$ for ρ_b and $\Delta \leq 17\%$ for K_s), suggested that scraping the exposed surfaces or not was irrelevant in this investigation. According to this result, two investigations performed on a relatively coarse soil having an initially low water content can be expected to be comparable even if the exposed soil surfaces are scraped in a case but not in the other case.

Table 2. Summary statistics of the dry soil bulk density, ρ_b, and saturated soil hydraulic conductivity, K_s, values obtained by preparing the soil sample in one or three steps and scraping (SC columns) or not scraping (NSC columns) any exposed soil surface (sample size, N = 6 for each step number, variable and scraping treatment)

Steps	Columns	Statistic	ρ_b (g/cm^3)	K_s (mm/h)
1	SC	Min	1.27	19.6
		Max	1.31	27.6
		Mean	1.29 a (c)	24.4 a (c)
		CV (%)	1.3	10.8
	NSC	Min	1.30	21.6
		Max	1.31	32.8
		Mean	1.30 a (d)	28.5 a (d)
		CV (%)	0.3	13.4
3	SC	Min	1.30	26.9
		Max	1.32	33.9
		Mean	1.31 b (c)	30.9 b(c)
		CV (%)	0.8	10.4
	NSC	Min	1.29	28.8
		Max	1.32	34.8
		Mean	1.31 b (d)	32.0 b (d)
		CV (%)	0.9	7.7

For a given variable, values in a column followed by the same lower case letter not enclosed in parenthesis were not significantly different according to an F test and a two-tailed t test at P = 0.05. Values followed by the same lower case letter enclosed in parenthesis were significantly different.

However, for both preparation methods (one- and three-step), the minimum, maximum and mean values of K_s were numerically smaller in the scraped columns than in those in which the soil surface was left intact after compaction. Therefore, scraping appeared to induce a decrease of K_s, although not at a statistically relevant level. Scraping was performed by sliding some needles over the exposed surface. It was unlikely that this operation implied a soil compaction additional to that performed with the compaction apparatus. More likely, sliding the needles induced some mixing of the soil particles at the exposed surface. A consequence of this mixing was that small particles were moved over this surface and they blocked some of the larger pores. This occlusion contributed to impede infiltration through the treated surface. In other terms, scraping the soil surface, rather than favoring hydraulic continuity, hindered it. In any case, the consequences of this phenomenon on K_s determination were small and not statistically significant.

The three-step sample preparation method yielded higher values of both ρ_b and K_s than the one-step method (Table 2). Differences between two datasets were not large ($\Delta \leq 1.5\%$ for ρ_b and $\leq 27\%$ for K_s) even if most of them were statistically significant. Therefore, this investigation also suggested that using, for a given value of total compaction energy, a three-step packing method instead of a one-step method increased global compaction of the soil column (larger ρ_b value) and yielded a larger K_s value. This result, that could appear unexpected (Assouline, 2006), was likely due to the fact that all energy was dissipated on the exposed soil surface with the one-step method whereas it was more evenly distributed along the vertical with the three-step method. Dissipating less energy at the infiltration surface likely produced a vertically more homogeneous soil sample (Oliviera et al. 1996) and it made water entry into the soil easier. This circumstance, determining a smaller t_a value, implied obtaining a larger K_s value. Characterizing in some detail the properties of the top soil layer appears advisable in future research to independently verify the soundness of the suggested explanation with reference to packing method effects on K_s.

A.3.4 CONCLUSIONS

Sieving duration and scraping of exposed surfaces could be expected not to have a statistically relevant effect on saturated hydraulic conductivity, K_s, of a repacked column prepared with an initially air-dry loam soil and determined by the simplified falling-head technique. Therefore, these two factors can be considered as having no more than a minor effect on preparation of these columns. The practical implication is that two datasets only differing by sieving duration or the applied treatment of the exposed surfaces during preparation of the soil column could be considered as belonging to the same population of measurements.

This conclusion is only valid for a specific experiment and it cannot be considered to have a general validity. Therefore, sieving duration and treatment of exposed surfaces effects should be tested in other experimental conditions, that is considering other soils, initial soil water conditions and K_s measurement techniques. In light of the data obtained in this investigation, a prediction that can be made is that a longer sieving duration and the scraping of the exposed surfaces during soil column preparation could yield smaller K_s values.

In the perspective to move towards standardized methods to prepare a repacked soil column, an optimal sieving duration could be the minimum duration beyond which the undispersed particle size distribution does not change further. As regards scraping, an alternative method to the one applied in this investigation could be positioning, and then lifting, a film of adhesive material on the exposed surface of the soil.

Finding an acceptable compromise between complexity of the soil column preparation method and homogeneity of the soil sample requires additional investigations. In particular, it seems necessary trying to support results for some tested factors, such as number of applied layers, soil compaction method or soil water content, in more general contexts and with reference to different soils. In addition, it appears advisable to also consider other factors less or not investigated at all, such as the duration of the storage period before performing the experiment, the operator that prepares the sample, or the actual inner diameter of cylinders having a given nominal diameter.

REFERENCES

Assouline S., 2006. Modeling the relationship between soil bulk density and the hydraulic conductivity function. Vadose Zone Journal, 5: 697-705.

Assouline S., Mualem Y., 2006. Runoff from heterogeneous small bare catchments during soil surface sealing. Water Resources Research, 42: W12405.

Bagarello V., 1997. Influence of well preparation on field saturated hydraulic conductivity measured with the Guelph Permeameter. Geoderma, 80: 169-180.

Bagarello V., Iovino M., Elrick D., 2004. A simplified falling head technique for rapid determination of field-saturated hydraulic conductivity. Soil Science Society of America Journal, 68: 66-73.

Bagarello V., Caltabellotta G., Iovino M., 2022. Manual packing and soil reuse effects on determination of saturated hydraulic conductivity of a loam soil. Geoderma, 405, 115465,

Bagarello V., Caltabellotta G., Iovino M., 2024. Soil reuse effects on determination of saturated hydraulic conductivity of different loamy soils. European Journal of Soil Science, 75: e1345422,

Bagarello, V., Caltabellotta, G., Fusco, M., Vaccaro, G., & Autovino, D., 2025. Investigating Soil Compaction and Its Impact on Physical and Hydraulic Properties Using a Simple Testing Apparatus. Water, 17(5), 723.

Bartley P.C. III, Jackson B.E., Fonteno W.C., 2019. Effect of particle length to width ratio on sieving accuracy and precision. Powder Technology, 355: 349-354.

Bondì, C., Castellini, M., Iovino, M., 2024. Temporal variability of physical quality of a sandy loam soil amended with compost. Biologia.

Dec D., Dörner J., Becker-Fazekas O., Horn, R., 2008. Effect of bulk density on hydraulic properties of homogenised and structured soils, Journal of Soil Science and Plant Nutrition 8(1): 1-13.

Díaz-Zorita M., Grove J.H., Perfect E., 2007. Sieving duration and sieve loading impacts on dry soil fragment size distributions. Soil & Tillage Research, 94: 15-20,

Elrick D.E., Reynolds W.D., 1992. Methods of analyzing constant-head well permeameter data. Soil Science Society of America Journal, 56: 320-323.

Fomin D., Timofeeva M., Ovchinnikova O., Valdes-Korovkin I., Holub A., Yudina A., 2021. Energy-based indicators of soil structure by automatic dry sieving. Soil & Tillage Research, 214, 105183,

Ghazouani H., M'Hamdi B. D., Autovino D., Bel Haj A. M., Rallo G., Provenzano G., Boujelben A., 2015. Optimizing subsurface dripline installation depth with Hydrus 2D/3D to improve irrigation water use efficiency in the central Tunisia. International Journal of Metrology and Quality Engineering, 6.

Lewis J., Sjöstrom J., 2010. Optimizing the experimental design of soil columns in saturated and unsaturated transport experiments. Journal of Contaminant Hydrology, 115: 1-13.

Nam S., Gutierrez M., Diplas P., Petrie J., 2021. Laboratory and in situ determination of hydraulic conductivity and their validity in transient seepage analysis. Water, 13, 1131, https://doi.org/10.3390/w13081131.

Oliviera I.B., Demond A.H., Salehzadeh A., 1996. Packing of sands for the production of homogeneous porous media. Soil Science Society of America Journal, 60: 49-53.

Reynolds W.D., Elrick D.E., 1987. A laboratory and numerical assessment of the Guelph permeameter method. Soil Science, 144: 282-299.

Reynolds W.D., Bowman B.T., Brunke R.R., Drury C.F., Tan C.S., 2000. Comparison of tension infiltrometer, pressure infiltrometer, and soil core estimates of saturated hydraulic conductivity. Soil Science Society of America Journal, 64: 478–484.

Shafiq M., Hassan A., Ahmad S., 1994. Soil physical properties as influenced by induced compaction under laboratory and field conditions. Soil & Tillage Research, 29: 13-22.

Šurda, P., Lichner, Ľ., Iovino, M., Hološ, S., Zvala, A., 2023. The Effect of Heating on Properties of Sandy Soils. Land 12.

Viviani G., Iovino M., 2004. Wastewater reuse effects on soil hydraulic conductivity. Journal of Irrigation and Drainage Engineering, 130: 476-484.

Woessner W.W., Poeter E.P., 2020. Hydrogeologic properties of earth materials and principles of groundwater flow. The Groundwater Project, Guelph, Ontario, Canada, 205 pages, ISBN: 978-1-7770541-2-0.

Wu X., Meng Z., Dang X., Wang J., 2021: Effects of rock fragments on the water infiltration and hydraulic conductivity in the soils of the desert steppes of Inner Mongolia, China. Soil & Water Research, 16.